

UNIVERSITÉ DU QUÉBEC À MONTRÉAL

PRÉPARATION ET CARACTÉRISATION DE NOUVEAUX MATÉRIAUX À
BASE DE GRAPHÈNE POUR L'ENVIRONNEMENT ET LA CONVERSION
D'ÉNERGIE

THÈSE
PRÉSENTÉE
COMME EXIGENCE PARTIELLE
DU DOCTORAT EN CHIMIE

PAR
BENJAMIN DIBY OSSONON

AVRIL 2018

UNIVERSITÉ DU QUÉBEC À MONTRÉAL
Service des bibliothèques

Avertissement

La diffusion de cette thèse se fait dans le respect des droits de son auteur, qui a signé le formulaire *Autorisation de reproduire et de diffuser un travail de recherche de cycles supérieurs* (SDU-522 – Rév.07-2011). Cette autorisation stipule que «conformément à l'article 11 du Règlement no 8 des études de cycles supérieurs, [l'auteur] concède à l'Université du Québec à Montréal une licence non exclusive d'utilisation et de publication de la totalité ou d'une partie importante de [son] travail de recherche pour des fins pédagogiques et non commerciales. Plus précisément, [l'auteur] autorise l'Université du Québec à Montréal à reproduire, diffuser, prêter, distribuer ou vendre des copies de [son] travail de recherche à des fins non commerciales sur quelque support que ce soit, y compris l'Internet. Cette licence et cette autorisation n'entraînent pas une renonciation de [la] part [de l'auteur] à [ses] droits moraux ni à [ses] droits de propriété intellectuelle. Sauf entente contraire, [l'auteur] conserve la liberté de diffuser et de commercialiser ou non ce travail dont [il] possède un exemplaire.»

À l'Éternel des Armées!

« L'imagination est plus importante que la connaissance. »

Albert Einstein.

REMERCIEMENTS

En préambule de cette thèse, je tiens tout d'abord à remercier mon directeur de thèse, le Professeur Daniel Bélanger de l'Université du Québec à Montréal (UQÀM) de m'avoir proposé cette thèse, suite à la maîtrise effectuée sous sa supervision. J'aimerais le remercier pour sa disponibilité, son encadrement scientifique, de haute qualité et pour ses conseils qui m'ont permis de progresser aussi bien scientifiquement que personnellement.

J'aimerais sincèrement remercier le Professeur Mohamed Siaj et le Professeur Ricardo Izquierdo, respectivement de l'Université du Québec à Montréal et de l'École de Technologie Supérieure (ÉTS) d'avoir accepté de m'accompagner tout au long cette thèse de doctorat. J'ai été très heureux de bénéficier de vos commentaires scientifiques et de vos conseils qui m'ont permis de redresser ma pente le plus souvent. Le disciple que je suis, continuera d'apprendre auprès des grands Maîtres que vous êtes. J'adresse mes sincères remerciements à Monsieur Alexis Laforgue, de bien vouloir accepter d'évaluer cette thèse de doctorat.

Le Dr. Gwenael Chamoulaud, que j'appelle la tour de contrôle est vivement à remercier pour toutes les formations de haut niveau reçues sur les équipements de NanoQAM, qui ont permis de valoriser mes matériaux. Ça été pour moi une grâce de te côtoyer, cher Maître.

Je souhaite remercier et saluer l'ensemble de mes collègues, doctorants et post-doctorants pour la bonne ambiance au bureau et au laboratoire Bélanger.

Je suis également très reconnaissant envers tous ceux ou toutes celles qui, de loin ou de près ont contribué à l'aboutissement de ces travaux de doctorat.

Famille Ossonon N'houni! Dieu vous bénisse pour toutes vos prières et vos encouragements.

Et enfin, je remercie tout particulièrement l'élue de mon cœur, Marie-France N'cho pour son soutien défectible depuis le début de cette aventure qui fut semblable à une traversée du désert, qui a toujours été présente dans les bons moments comme dans les moments les plus difficiles pour m'apporter son amour. Mahéva, Priscillia et Yohana, papa vous aime et vous je remercie pour la joie que vous m'avez procurée au cours de toute cette épreuve.

Le graphène apparaît comme un matériau "caméléon", capable de s'adapter et d'apporter des solutions à nos problèmes, juste laisser le chercheur s'épanouir.

RÉSUMÉ

Depuis sa découverte, le graphène et ses dérivés continuent de susciter un grand intérêt en raison de leurs propriétés physico-chimiques exceptionnelles. Le graphène est une nanostructure de carbone hybridé sp^2 dont les propriétés électroniques et optiques font de lui un matériau intéressant pour la conception et le développement d'une nouvelle génération de dispositifs et matériaux innovants pour la microélectronique et l'optique. Cependant, de nombreux défis, tels que la production de masse, la qualité du graphène produit et l'adaptation de sa bande interdite sont à surmonter avant leur utilisation dans des procédés industriels à grande échelle. Alors, pour profiter pleinement des propriétés de ce matériau 2D, il est important de développer des méthodes efficaces de modification de surface. La fonctionnalisation du graphène peut permettre soit d'ajouter une propriété conférée par la molécule greffée ou adsorbée, soit de modifier les propriétés électroniques du substrat graphénique en changeant la structure cristalline des carbones sp^2 .

L'objectif de cette thèse a porté en premier lieu sur l'étude de la modification covalente des dérivés de graphène par différentes approches, faciles à réaliser, en se basant sur des cations diazonium intermédiaires au greffage de molécules organiques. Au cours de cette étude, certains procédés préexistants ont été améliorés ou modifiés dans le but de préparer de l'oxyde de graphène réduit (RGO) avec des propriétés différentes et du graphène (EG) de très haute qualité obtenu par l'exfoliation électrochimique du graphite. Ensuite, la fonctionnalisation avec la molécule d'anthraquinone et la modification par des nanoparticules métalliques des feuillets de graphène lors de l'exfoliation électrochimique du graphite ont été étudiées. Cette méthode plus simple permet de réduire les étapes de préparation des nanocomposites à base de graphène. Finalement, différentes techniques ont été utilisées pour caractériser les matériaux ainsi préparés.

Mots clés: Graphite, matériaux 2D, exfoliation chimique et électrochimique, oxyde de graphène réduit (RGO), graphène (EG), molécules organiques, nanoparticules, fonctionnalisation, électrochimie.

ABSTRACT

Graphene and its derivatives have attracted great interest in the recent years because of their exceptional physical and chemical properties. Graphene is an hybrid sp² carbon nanostructure whose electronic and optical properties make it an interesting material for the design and development of a new generation of innovative devices and materials for microelectronics and optics. However, many challenges such as mass production, quality of graphene and bandgap adaptation must be overcome before their use in large scale industrial processes. Then, to take full advantage of properties of this 2D material, it is important to develop effective methods for surface modification. The functionalization of graphene can make possible either to add a property conferred by the grafted or adsorbed molecule or to modify the electronic properties of the graphene substrate by modifying the structure of the sp² carbons.

In this thesis, we studied the covalent modification of graphene and its derivatives by different approaches, easy to perform, based on diazonium chemistry by grafting organic molecules. During this study, some pre-existing processes have been improved or modified in order to produce reduced graphene oxide (RGO) with different properties and high-quality graphene (EG) obtained by electrochemical exfoliation. Then, the covalent functionalization of graphene sheets by anthraquinone molecules and also their non-covalent modification by nanoparticles from the metal cations during the electrochemical exfoliation of the graphite were studied. A simpler and environmentally friendly method has been proposed, thereby reducing the synthesis steps of graphene-based nanocomposites. Finally, various techniques have been used to characterize the materials prepared.

Keywords: Graphite, 2D materials, chemical and electrochemical exfoliation, reduced graphene oxide (RGO), graphene (EG), organic molecules, nanoparticles, functionalization, electrochemistry.

TABLE DES MATIÈRES

RÉSUMÉ.....	vi
ABSTRACT.....	vii
LISTE DES FIGURES.....	xiii
LISTE DES TABLEAUX.....	xxi
LISTE DES ABRÉVATIONS, SIGLES ET ACRONYMES.....	xxii
INTRODUCTION	1
1.1 Mise en contexte	1
1.1.1 Découverte du graphène.....	2
1.1.2 Structure cristallographique et électronique du graphène.....	4
1.1.3 Propriétés du graphène	6
1.2 Champs d'applications possibles du graphène.....	7
1.2.1 Matériaux composites à base de graphène	8
1.2.2 Capteurs à base de graphène	9
1.2.3 Le graphène pour l'électronique	10
1.2.4 Supercondensateurs électrochimiques au graphène	11
1.2.5 Le graphène dans les batteries.....	13
1.2.6 Le graphène et les panneaux solaires	15
1.2.7 Le graphène dans les peintures et revêtements	17
1.2.8 Conclusions	18
1.3 Méthodes de préparation.....	20
1.3.1 Exfoliation micromécanique	20
1.3.2 Croissance épitaxiale du graphène sur du carbure de silicium (SiC).....	21
1.3.3 Dépôt chimique en phase vapeur (CVD)	22
1.3.4 Exfoliation chimique en phase liquide	25

1.3.5 Méthode de Hummers: préparation du graphène chimiquement modifié.....	28
1.3.5.1 Préparation de l'oxyde de graphène	30
1.3.5.2 Réduction de l'oxyde de graphène	32
1.3.6 Exfoliation électrochimique du graphite	36
1.3.7 Méthodes industrielles de production du graphène	38
1.3.8 Conclusions	38
1.4 Méthodes de fonctionnalisation /modification	39
1.4.1 Méthodes non-covalentes de fonctionnalisation du graphène.....	40
1.4.1.1 Par des groupements organiques	40
1.4.1.2 Par des nanoparticules (NPs)	43
1.4.2 Méthodes covalentes	46
1.4.3 Conclusions	49
1.5 Objectifs de la thèse.....	50

CHAPITRE I	
SYNTHESIS AND CHARACTERIZATION OF SULFOPHENYL-	
FUNCTIONALIZED REDUCED GRAPHENE OXIDE SHEETS.....	53
Résumé de l'article 1	53
1 Introducion.....	56
2 Experimental.....	57
2.1 Preparation of graphene oxide (GO)	57
2.2 Preparation of reduced graphene oxide (RGO)	58
2.3 Covalent attachment of 4-sulfophenyl groups by the chemistry on RGO surface	58
2.4 Morphological and structural characterization.....	59
3 Results and discussion	61
3.1 Morphological characterization of RGO and SRGO	61
3.2 Optical band gap.....	63
3.3 Nitrogen gas adsoption.....	64

3.4	FTIR	67
3.5	Raman Spectroscopy	68
3.6	Electrical conductivity measurements.....	70
3.7	X-ray Photoelectron Spectroscopy (XPS).....	71
3.8	Thermogravimetric analysis coupled to mass spectrometry	76
4	Conclusion	79
5	Acknowledgements.....	79
6	References.....	80
7	Electronic Supplementary information.....	86

CHAPITRE II		
FUNCTIONALIZATION OF GRAPHENE SHEETS BY THE DIAZONIUM CHEMISTRY DURING ELECTROCHEMICAL EXFOLIATION OF GRAPHITE		89
	
	Résumé de l'article 2	89
1	Introducion.....	92
2	Experimental.....	94
2.1	Materials and reagents.....	94
2.2	Electrochemical exfoliation.....	94
2.3	In situ electrochemical grafting.....	96
2.4	Characterization techniques	97
3	Results and discussion	100
3.1	Description of the experimental procedure and observation.....	100
3.2	Characterization of materials	101
4	Mechanism of the exfoliation/functionalization process	114
5	Conclusions	117
6	Acknowledgements.....	118
7	References.....	118
8	Electronic Supplementary information.....	132

CHAPITRE III

A ONE-STEP METHOD TO DECORATE GRAPHENE SHEETS WITH METAL NANOPARTICLES DURING THE ELECTROCHEMICAL EXFOLIATION OF GRAPHITE	136
Résumé de l'article 3	136
1 Introducion.....	138
2 Experimental.....	140
2.1 Materials and chemicals	140
2.2 Synthesis of graphene sheets.....	141
2.3 Synthesis of graphene-Ag, graphene-Au and graphene-Ag/Au	141
2.4 Characterization techniques	142
2.5 Electrochemical measurements	143
3 Results and discussion	144
3.1 Mechanism of the formation of metal nanoparticles on electrochemically exfoliated graphene sheets	144
3.2 Characterization of graphene nanocomposites.....	145
3.3 Thermogravimetric analysis.....	147
3.4 ICP analysis.....	149
3.5 X-ray diffraction (XRD).....	151
3.6 X-ray Photoelectron Spectroscopy (XPS).....	153
3.7 Raman spectroscopy.....	155
3.8 Electrocatalytic behavior for O ₂ reduction	157
4 Conclusion	160
5 Acknowledgements.....	160
6 References.....	161
7 Electronic Supplementary information.....	173
7.1 Dynamic light scattering	173
7.2 Morphology characterization	175
7.3 Thermogravimetric analysis	178
7.4 XPS analysis.....	179

CONCLUSIONS ET PERSPECTIVES.....	181
RÉFÉRENCES.....	186

LISTE DES FIGURES

INTRODUCTION

Figure 1.1 Structure de certains allotropes représentatifs du carbone [2–4].....	1
Figure 1.2 A: Vue atomique de la structure en nid d'abeille à deux dimensions d'atomes de carbone dans le graphène. B: image de la microscopie électronique en transmission (MET) à haute résolution [7].....	2
Figure 1.3 Représentation de la structure du graphène et d'autres formes de nanostructures de carbone sp ² . Le diagramme schématique montre bien que le graphène est l'élément de base de toute forme graphitique [8].....	3
Figure 1.4 (A) Représentation de la structure cristalline du graphène en forme de "nid d'abeille" avec une maille élémentaire formée de deux atomes distincts A et B. (B) Structure de bande du graphène et (C) agrandissement de la structure de bande au voisinage de l'un des points (K) de Dirac et montrant ainsi le cône [1].	5
Figure 1.5 Propriété optique du graphène: Transmittance pour une monocouche et une bicouche de graphène (absorption optique: 2,3% par une monocouche) supportés sur une membrane poreuse [30,32].....	7
Figure 1.6 (A) Étude du comportement mécanique du polystyrène (PS) et des films nanocomposites (PS-graphène) avec des teneurs différentes en feuilles de graphène. (B) Le module de Young et sa résistance à la traction changent avec la teneur croissante en graphène [65].	9
Figure 1.7 Téléphones intelligents à écran tactile (A) [80] et flexible (B) [81]à base de graphène, (C) Capteur transparent représentant une rétine artificielle [82]... ..	10
Figure 1.8 Schéma de base d'un supercondensateur électrochimique basé sur un matériau carboné [89].	11
Figure 1.9 (A) Courbes de charge et de décharge galvanostatique de différents composés de molybdate de manganèse ($MnMoO_4$) à densité de courant de 2 A g ⁻¹ et (B) variation de la capacité spécifique en fonction du nombre de cycle pour le composé $MnMoO_4$ (courbe en bleu) et le composite Gr- $MnMoO_4$ à 8 A g ⁻¹ [93].	13

Figure 1.10 (A) Profils des premières courbes de lithiation et de délithiation de différentes électrodes préparées à partir du silicium (Si) et différents matériaux conducteurs tels le graphène (Gr) et le carbone amorphe (AC). (B) Capacité de rétention en fonction du nombre de cycles [95].	14
Figure 1.11 (A) Courbes courant-tension (J-V) obtenues avec une source d'illumination simulant le spectre solaire. (AM1.5) de différents matériaux [102], (B) Cellule solaire flexible basée sur l'oxyde de graphène réduit (RGO), (C) Structure d'une cellule solaire flexible biexcitée par la lumière du soleil et de pluie [100].	16
Figure 1.12 (A) Étude du comportement hydrofuge de l'eau sur une feuille revêtue par le nanocomposite de graphène (DE/TiO ₂ /RGO). (B) Étude électrochimique de la corrosion de différents échantillons de cuivre (nu et revêtus) [108].	18
Figure 1.13 Schéma montrant les méthodes classiques couramment utilisées pour la synthèse du graphène ainsi que les applications actuelles et futures [111].	19
Figure 1.14 Exfoliation mécanique du graphène par du ruban adhésif à partir du graphite [8].	21
Figure 1.15 Croissance du graphène par décomposition thermique du SiC, ainsi que le modèle structurel du graphène bicouche sur SiC. La ligne bleue brisée représente la couche tampon pour prévenir la déchirure possible des feuillets de graphène formés [113].	22
Figure 1.16 (A) Processus schématisé de la croissance du graphène sur du nickel à partir du méthane [135]. (B): Croissance du graphène à partir du polyméthacrylate de méthyle (PMMA) [127].	23
Figure 1.17 (A) Spectres Raman obtenus des films de graphène préparés par CVD à partir de différents précurseurs hydrocarbonés. (B) Microscopie électronique à balayage des films de graphène obtenus à partir du (a) méthanol (b), éthanol, (c) propan-1-ol et (d) méthane sur un substrat de Cu. (C) Large feutrage de graphène obtenu par CVD transféré sur un substrat de SiO ₂ /Si [114].	24
Figure 1.18 Schéma illustratif pour la préparation de graphène à partir de la décomposition de (NH ₄) ₂ CO ₃ [144].	25
Figure 1.19 (A) Schéma du processus d'exfoliation du graphène. Le bain ultrasons permet d'exfolier le graphite en quelques feuillets de graphène, qui sont ensuite encapsulés par les micelles de cholate de sodium. (B) Photographie d'une dispersion de graphène de 90 µg mL ⁻¹ dans le cholate de sodium (CS), six semaines après sa préparation. (C) Schéma illustrant une monocouche de cholate de sodium ordonnée sur le graphène [152].	26

- Figure 1.20 Image AFM de graphène préparé par exfoliation chimique et le profil en épaisseur correspondant. L'épaisseur de l'ordre de 10 nm traduit l'empilement de plusieurs feuillets de graphène [147]. 28
- Figure 1.21 Processus de préparation de l'oxyde de graphène réduit (graphène chimiquement converti) à partir de la trilogie "oxydation-exfoliation-réduction". Un traitement oxydant est initialement réalisé pour générer de l'oxyde de graphite, qui est suivie par une exfoliation pour produire de l'oxyde de graphène. Enfin, une réduction produit l'oxyde de graphène réduit communément noté RGO [75,164]..... 29
- Figure 1.22 Représentation schématique des procédures suivies à partir du graphite pour la préparation de l'oxyde de graphène basée sur la méthode initiale de Hummers [164]. La méthode améliorée de Hummers permet d'éviter le dégagement des gaz (NO_x) hautement toxiques [171] et produire un matériau moins oxygéné [165]. 31
- Figure 1.23 A: Équation schématisée de la déoxygénation de l'oxyde de graphène (GO), B: Images des suspensions de GO et de l'oxyde de graphène réduit (RGO) en milieux NaOH et KOH aqueux. Au cours du processus de réduction, la couleur jaune brillant de la dispersion de l'oxyde de graphène dans l'eau devient noire une fois le RGO formé [180]. C: Microscopie électronique en transmission d'un mono-feuillet RGO teintée de couleurs par endroits pour mettre en exergue les différentes zones caractéristiques graphène préparé. La zone de graphène cristalline sans défauts est affichée dans la couleur gris clair d'origine. Les régions contaminées sont en gris foncé. Les régions bleues sont les réseaux de carbone monocouche désordonnés, ou défauts topologiques étendus, que nous identifions comme des restes du processus d'oxydoréduction. Les zones rouges mettent en évidence des atomes ou des substitutions individuelles. Les zones vertes indiquent des défauts topologiques isolés, c'est-à-dire des rotations à liaison simple ou des noyaux de dislocation. Les trous et leurs reconstructions de bord sont colorés en jaune [75]. 33
- Figure 1.24 Spectres XPS d'oxydes de graphène (GO) traité sous H_2 à différentes températures sous une pression de 2 Torr [185]. 34
- Figure 1.25 Evaluation des capacités spécifiques de différentes électrodes préparées à partir des échantillons de RGO (ou GNS), cyclées dans du KOH 6 M avec des densités de courant différentes [189]. 36

Figure 1.26 Schéma des mécanismes d'exfoliation cathodique et anodique. Une charge négative (A) ou positive (B) est créée sur une électrode de graphite en imposant un potentiel approprié, attirant des ions intercalants de charge opposée. Des molécules co-intercalantes (ex. H ₂ O) peuvent éventuellement être présentes au cours du processus. Des flocons de graphène sont spontanément produits lors de l'évolution de gaz ou aussi par sonication. La contre électrode peut être en platine ou en graphite [198].	37
Figure 1.27 Illustration des méthodes de préparation actuelles pour le graphène et les matériaux de graphène [112].	39
Figure 1.28 Mécanisme proposé pour la préparation d'une dispersion aqueuse stable de graphène par empilement des molécules d'anthracène sur les feuillets du graphène [210].	41
Figure 1.29 (A) Image AFM d'un feuillet de graphène fonctionnalisé [210]. (B) Images de l'oxyde de graphène réduit (r-GO) et du graphène fonctionnalisé par les groupements pyrène-butyrat (PB ⁻ -G) dispersés dans l'eau (0,1 mg mL ⁻¹) [213]. (C) Voltammogrammes cycliques des électrodes modifiées de la polyaniline sulfonée (SPANI) (en pointillé) et le graphène modifié (SPANI/r-G) (ligne pleine) dans 1.0 M H ₂ SO ₄ à une vitesse de balayage de 50 mV s ⁻¹ [214].	42
Figure 1.30 Images SEM d'un matériau nanocomposite (A) RGO et (B) RGO-AuNPs [222].	44
Figure 1.31 (A) Synthèse de l'oxyde métallique encapsulé dans le graphène (GE-MO) avec différentes étapes: 1- Modification de l'oxyde métallique par greffage d'aminopropyltriméthoxysilane (APS) pour rendre la surface d'oxyde chargée positivement; 2- Assemblage hybride entre les nanoparticules d'oxyde métallique chargé positivement et l'oxyde de graphène chargé négativement par des interactions électrostatiques; 3- Réduction chimique. Images (B) MEB et (C) MET des particules d'oxyde de graphène encapsulées [225]....	45
Figure 1.32 Schéma général du greffage à partir d'un sel de diazonium avec un groupe fonctionnel R et de son contre-ion X ⁻ sur une feuille de graphène [235].	46
Figure 1.33 (A) Schéma du greffage du cation KMoSn[N ₂ ⁺] avec le graphène mettant en exergue la liaison C-C (en rouge) [238]. (B) Spectres Raman ($\lambda = 532$ nm) des feuillets de graphène non modifié (pristine) et modifié par le nitrophényle (NP-functionalized). En inséré, image optique d'un échantillon de graphène attaché (mono-couche) à un flocon de graphène plus épais [240].	48

Figure 1.34 Représentation schématique des densités d'états occupés et inoccupés du graphène et d'un sel de diazonium [235].	49
Figure 1.35 A) Processus général du greffage des chlorotétriazines substituées (Tz) sur l'oxyde de graphène (FGS) [227], (B) Représentation schématique de la réaction de Diels-Alder entre un dérivé dihydronaphalène (D1) et le graphène [248].....	50

CHAPITRE I

Figure 1. Optical images of GO, RGO and SRGO dispersed in water at the concentration of 0.5 mg mL^{-1}	59
Figure 2. EDX spectra and TEM images of (a) RGO and (b) SRGO	61
Figure 3. Visible/near-infrared spectra of (a) RGO, (b) SRGO and the plot of $(\alpha h\nu)^2$ as a function of $h\nu$ for (c) RGO and (d) SRGO (see Supporting Information, Figure S9 for complete absorption spectra)	64
Figure 4. a) N ₂ adsorption isotherms of graphene oxide, reduced graphene oxide before (RGO) and after reaction with in situ-generated 4-sulfophenyl diazonium cations (SRGO), b) Cumulated surface area vs. pore width of GO, RGO and SRGO, c) Pore size distribution of GO, RGO and SRGO. The insets present the data for GO at a more sensitive scale.	65
Figure 5. FTIR curves of graphene oxide, reduced graphene oxide and sulfophenyl acid groups modified RGO.	68
Figure 6. Raman spectra of GO, RGO and SRGO recorded using 532 nm laser excitation.....	69
Figure 7. (a) XPS survey spectra of graphene oxide (GO), reduced graphene oxide (RGO) and sulfophenyl-modified RGO (SRGO); XPS C 1s spectra of (b) GO, (c) RGO and (d) SRGO, (f) S 2p core level spectrum of SRGO and XPS O 1s spectra of (f) GO, (g) RGO and (h) SRGO	73
Figure 8. TGA and TGA-MS profiles under helium for the graphene oxide (GO), reduced graphene oxide (RGO) and RGO modified by sulfophenyl groups (SRGO) between 30 and 900 °C at a heating rate of 5 °C/min. (a, c and d) Mass variation with (a) OH, H ₂ O, CO and CO ₂ MS profiles, (c) CO ₂ MS profile and (d) SO ₂ MS and C ₆ H ₁₂ profiles	78
Figure S1. UV-Vis/NIR spectra of RGO and SRGO.....	87
Figure S2. Raman spectrum of natural graphite powder.....	87

CHAPITRE II

Figure 1 Spontaneous functionalization of electrochemically exfoliated graphene sheets (EG) anthraquinone during electrochemical exfoliation of graphite in a one-pot process.	95
Figure 2 Photographic images of: (a) the electrochemical cell used for electrochemical exfoliation of graphite and graphene flakes floating at the surface of the electrolyte, (b) as prepared graphene, (c) graphene in DMF (10 mg mL^{-1}), (d) a self-supporting film, (e) the electrochemical cell used after electrochemical exfoliation and production of anthraquinone modified graphene flakes, (f) graphene sheets functionalized by anthraquinone groups. (A colour version of this figure can be viewed online.)	100
Figure 3 High-magnification SEM images of electrochemically exfoliated graphene (EG) (a) and anthraquinone-modified graphene sheets (EG-AQ) (b); TEM images of EG (c) and EGAQ (d); HRTEM of single and bilayer of EG (e) and EG-AQ (f); AFM images of EG (g) and EG-AQ (h). (A colour version of this figure can be viewed online.)	104
Figure 4 (a) N_2 adsorption isotherms of unmodified and AQ-modified graphene. The inset shows the pore size distribution of EG and EG-AQ. (b) FTIR spectra for electrochemically exfoliated graphene sheets (EG), 2-aminoanthraquinone (AAQ) and functionalized graphene sheets by anthraquinone groups (EG-AQ). (c) XPS survey spectrum of EG-AQ and (d) core level C 1s spectra of EG and EG-AQ. The inset shows the subtracted signal obtained by difference between C 1s spectra of EG and EG-AQ. (e) Raman spectra with a 532 nm excitation laser wavelength of the electrochemically exfoliated graphene sheets (EG) and for anthraquinone-modified graphene sheets (EG-AQ). (f) Raman spectrum of graphite with the 2D spectra of EG and EG-AQ as inset. (g) TGA curves of (inserted) EG in air and under He flow (inset), and EG, EG-AQ' and EG-AQ under He atmosphere. Heating rate: 5 °C/min. (h) Cyclic voltammograms for unmodified (full curve) and anthraquinone-grafted graphene (dashed curve) in a 0.5 M H_2SO_4 solution at a scan rate of 10 mV s^{-1}	108
Figure 5 Main steps of the mechanism of electrochemical exfoliation/functionalization of graphene sheets. (A colour version of this figure can be viewed online).....	115
Figure S1 Optical photographs of unmodified (EG) and modified (EG-AQ) graphene dispersed at 0.5 mg mL^{-1} in water by bath sonication immediately after preparation (0 min) and after 2, 15, 40 and 60 min.	133

Figure S2 Plot of A/L (absorbance/path length (600 nm)) vs. exfoliated graphene concentration : (a) EG and (b) EG-AQ.....	133
Figure S3 XPS survey spectrum of EG.....	134
Figure S4 Redox reaction of covalently bound anthraquinone in acid electrolyte ..	134
CHAPITRE III	
Figure 1. Schematic of the formation of EG-metal nanoparticles hybrids..	145
Figure 2. TEM images (left hand side) of graphene nanocomposites A (EG-Ag), B (EG-Au) and C (EG-Ag _{0.5} /Au _{0.5}), histogram for the metal particles (center) and EDX profile (right hand side). The Cu and Ni peaks are attributed to the substrates.....	147
Figure 3. TGA profiles of graphene-AgNPs (EG-Ag), graphene-AuNPs (EG-Au) and graphene-Ag/Au nanocomposites (EG-Ag _{0.5} /Au _{0.5}) recorded with a temperature ramp of 5 °C/min under air.....	148
Figure 4. XRD patterns of (A) graphite and graphene (EG) samples at various temperature and (B) EG-Ag, EG-Au and EG-Ag _{0.5} /Au _{0.5} nanocomposites.	152
Figure 5. XPS (A) survey spectrum of EG-Ag _{0.5} /Au _{0.5} , and core level spectra of (B) EG-Au and EG-Ag/Au and (C) EG-Ag and EG-Ag _{0.5} /Au _{0.5} nanocomposites.	154
Figure 6. Raman spectra of (A) EG, (B) EG-Ag, (C) EG-Au and (D) EG-Ag _{0.5} /Au _{0.5} nanocomposites.....	156
Figure 7. Cyclic voltammograms of EG-Ag, EG-Au and EG-Ag _{0.5} /Au _{0.5} in (A) O ₂ and (B) N ₂ -saturated, (C) Cyclic voltammograms of EG-Ag _x /Au _x (x= 0.5, 1, 5 and 10) catalysts in O ₂ -saturated 0.1 M KOH solution. Scan rate is 10 mV s ⁻¹ .	159
Figure S1. Photograph of typical electrochemical cell for graphene nanocomposites synthesis.....	173
Figure S2. DLS of (A) EG-Ag, (B) EG-Au and (C) EG-Ag/Au.....	174
Figure S3. SEM images of (A) EG, (B) EG-Ag _{0.5} /Au _{0.5} , (C) EG-Ag ₁ /Au ₁ , (D) EG-Ag ₅ /Au ₅ , and (E) EG-Ag ₁₀ /Au ₁₀	176
Figure S4. TEM images at different magnifications of EG-Ag _{0.5} /Au _{0.5} and EDX spectra.	177

Figure S5. TGA profiles of graphene-Ag/Au nanocomposites with different metal concentrations (EG-Ag _{0.5} /Au _{0.5} , EG-Ag ₁ /Au ₁ , EG-Ag ₅ /Au ₅ , and EG-Ag ₁₀ /Au ₁₀) recorded with a temperature ramp of 5 °C/min under air.	178
Figure S6. XPS survey spectrum of EG, EG-Ag and EG-Au, and C 1s level of EG-Ag, EG-Au and EG-Ag _{0.5} /Au _{0.5}	179
Figure S7. Raman spectra of EG-Ag _x /Au _x nanocomposites (x = 0.5, 1, 5 and 10)...	181

LISTE DES TABLEAUX

CHAPITRE I

Table 1 Specific surface areas and electronic conductivity of graphene oxide (GO), reduced graphene oxide (RGO) and sulfophenyl-modified reduced graphene oxide (SRGO)	67
Table S1 Atomic concentration and curve-fitting parameters obtained from the XPS spectra	86
Table S2 Elemental analysis of RGO modified with sulfophenyl groups	86

CHAPITRE II

Table 1 Experimental conditions used for the electrochemical exfoliation of graphite electrode and functionalization by spontaneous reduction of anthraquinone diazonium ions together with relevant parameters for the process and resulting materials	99
---	----

CHAPITRE III

Table 1 Results of TGA and ICP analysis of EG/metal hybrids	150
Table S1 XPS elements concentration (at.%) of the surface graphene nanocomposites samples	179

LISTE DES ABRÉVIATIONS, SIGLES ET ACRONYMES

Ag	Argent
Al	Aluminium
AgNO ₃	Nitrate d'argent
AgCl	Chlorure d'argent
at	atomique (atomic)
AQ	Anthraquinone
Au	Or
CV	Voltammetrie cyclique (cyclic voltammetry)
DLS	Diffusion dynamique de la lumière (Dynamic light scattering)
EDX	Spectroscopie à rayons X à dispersion d'énergie (energy-dispersive X-ray)
EG	Graphène exfolié (exfoliated graphene)
GO	Oxyde de graphène (graphene oxide)
GC	Carbone vitreux (glassy carbon)
Mg	Magnésium
SEM	Microscopie électronique en balayage (scanning electron microscopy)
RGO	Oxyde de graphène réduit (reduced graphene oxide)

ORR	Réaction de réduction de l'oxygène (oxygen reduction reaction)
TEM	Microscopie électronique en transmission (transmission electron microscopy)
UV	Ultra violet
XRD	Diffraction des rayons X (X-ray diffraction)
XPS	Spectroscopie du photoélectron X (X-ray photoelectron spectroscopy)
h	heure (hour)
M	Mole par litre
MΩ	MégaOhm
mM	Millimole par litre
mW	Milliwatt
mA	Milliampère
min	Minute
mL	Millilitre
mV	Millivolt
nm	Nanomètre
µg/L	Microgramme par litre
µm	Micromètre
nm	Nanomètre
mm	Millimètre
mVs ⁻¹	Millivolt par seconde
V	Volt
D	Dimension
s	Seconde
%	Pourcentage
g	Gramme

E	potentiel
eV	Électron-volt
vs	Versus
°C	Degré Celsius

INTRODUCTION

1.1 Mise en contexte

Le carbone naturel se présente sous de nombreuses formes différentes les unes des autres et les propriétés de chaque forme dépendent de sa structure spécifique (Figure 1.1) [1]. Cela fait du carbone un bloc de construction véritablement unique pour les nanomatériaux [2–4]. C'est pour cette raison que le carbone a été étudié depuis plusieurs décennies avec beaucoup d'intérêt, et continue de susciter plus d'enthousiasme pour la communauté scientifique. En particulier, avec la nanoscience qui connaît un formidable essor depuis plusieurs années, de nouvelles propriétés pour les nanostructures de carbone sont encore découvertes, offrant ainsi de nouvelles opportunités qui conduisent à de nouvelles applications pour ces matériaux, suscitant parfois de nouveaux débats scientifiques et sociaux. Une forme particulière de carbone qui a bouleversé de nombreuses théories scientifiques, telle que la stabilité d'une monocouche atomique [11–14] au fil des années nous intéresse dans cette étude, à savoir, le carbone hybridé sp^2 , à deux dimensions.

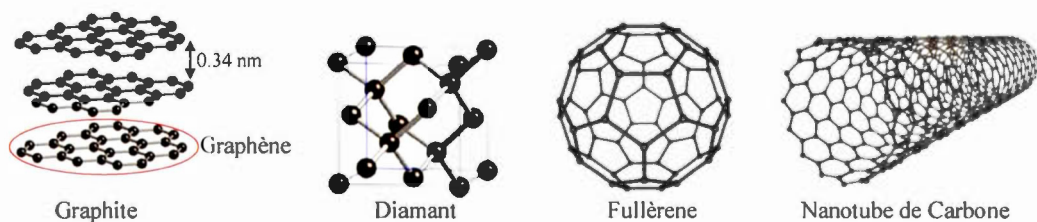


Figure 1.1 Structure de certains allotropes représentatifs du carbone [2–4].

1.1.1 Découverte du graphène

Le graphène est un matériau naturel, composé d'une monocouche bidimensionnelle formée d'atomes de carbone, organisés selon un motif hexagonal, en forme de nid d'abeilles (Figure 1.2) [5–7]. Ce feuillet de carbone hybridé sp^2 , avec son motif 2D constitue la base de toutes les formes graphitiques (Figure 1.3) [8]. Elle peut être enveloppée sous la forme de molécules C_{60} , de la famille des fullerènes (système 0-D) [9], elle peut aussi être enroulée en spirale pour prendre la forme des nanotubes de carbone à une dimension (1-D) [10], et peut aussi être empilée sous forme de matériau tridimensionnel (3-D) comme le graphite [8].

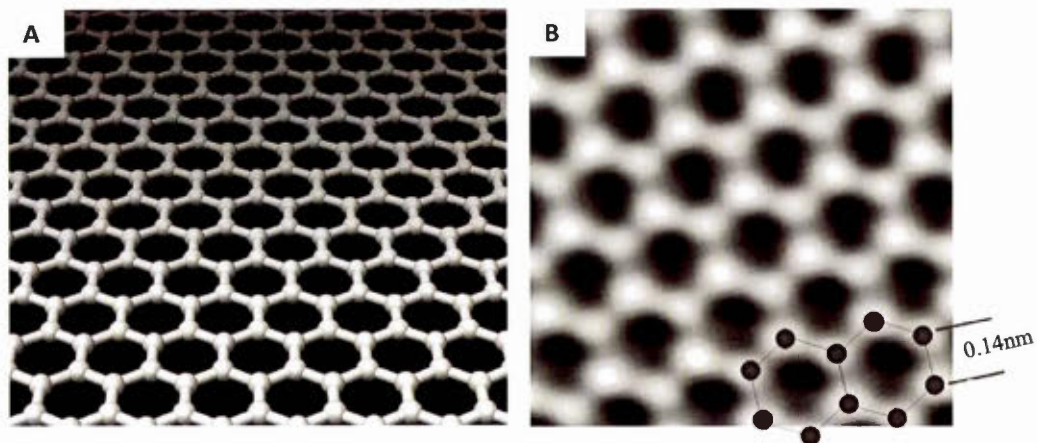


Figure 1.2 A: Vue atomique de la structure en nid d'abeille à deux dimensions d'atomes de carbone dans le graphène. B: image de la microscopie électronique en transmission (MET) à haute résolution [7].

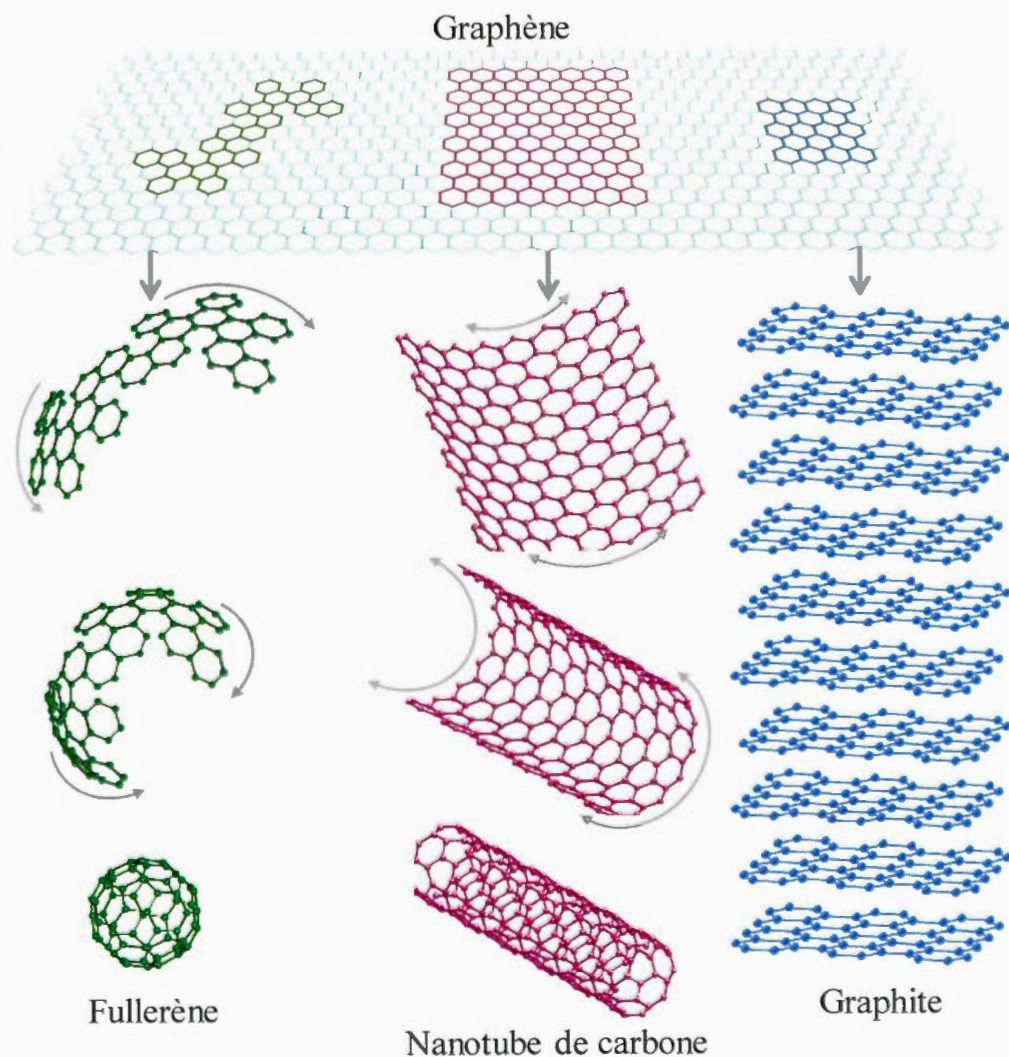


Figure 1.3 Représentation de la structure du graphène et d'autres formes de nanostructures de carbone sp^2 . Le diagramme schématique montre bien que le graphène est l'élément de base de toute forme graphitique [8].

Dans les années 40, le graphène (ou le "2D-graphite") a déjà fait l'objet de plusieurs études théoriques basées sur le calcul des bandes d'énergie, mais tous ces travaux se contredisent puisque ce matériau de type 2D serait thermodynamiquement instable donc ne pouvant pas être isolé [11,12]. Certains travaux, dont celui portant sur la théorie de Landau et Peierls ont même nié même l'existence d'un tel matériau à deux dimensions possédant un réseau cristallin [13,14]. Ce n'est qu'en 2004, qu'une seule couche de graphène a pu être isolée dans son état stable par clivage micromécanique du graphite pyrolytique hautement orienté (HOPG) en utilisant un ruban adhésif, par Geim et Novoselov [15]. Cette découverte leur a valu le Prix Nobel de Physique en 2010 [16] et a permis de stimuler la recherche scientifique tant dans l'industrie que dans les universités.

1.1.2 Structure cristallographique et électronique du graphène

Le graphène se présente sous forme d'un réseau hexagonal et bidimensionnel d'atomes de carbone hybridés en sp^2 . L'hybridation sp^2 formée à partir d'une orbitale s et deux orbitales p conduit à une structure planaire trigonale avec une base de deux atomes distincts A et B (Figure 1.4A). Les atomes de carbone les plus proches sont liés par une liaison σ , avec une distance interatomique $d_{C-C} = a \approx 1,42 \text{ \AA}$ [1]. La bande σ , qui est une liaison covalente est responsable de la solidité de la structure du réseau bidimensionnel du graphène. La maille élémentaire (Figure 1.4A) est constituée de deux atomes de carbone distincts (A et B) et caractérisée par les vecteurs de base \vec{a}_1 et \vec{a}_2 où $a_1 = a_2 = \sqrt{3}a$ (Équation 1.1). Dans cette configuration, chaque atome de carbone va former avec ses trois plus proches voisins trois liaisons σ avec un angle de 120° , et dispose en plus d'une orbitale p_z non hybridée, perpendiculaire à la structure planaire. Ces orbitales, disposant chacune d'un électron supplémentaire (bande à moitié pleine) peuvent se recouvrir en se chevauchant pour créer les bandes π (bande de valence) et π^* (bande conduction).

$$\mathbf{a}_1 = \frac{\mathbf{a}}{2}(3, \sqrt{3}), \mathbf{a}_2 = \frac{\mathbf{a}}{2}(3, -\sqrt{3}) \quad (1.1)$$

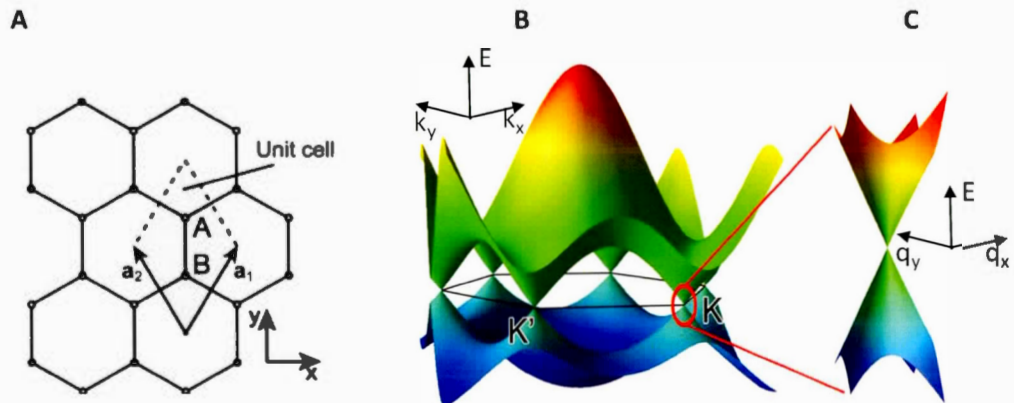


Figure 1.4 (A) Représentation de la structure cristalline du graphène en forme de "nid d'abeille" avec une maille élémentaire formée de deux atomes distincts A et B. (B) Structure de bande du graphène et (C) agrandissement de la structure de bande au voisinage de l'un des points (K) de Dirac et montrant ainsi le cône [1].

Il a été démontré lors de l'étude de bande du graphène [11], que la présence de deux atomes par maille élémentaire conduit à l'existence de deux points non équivalents K et K' situés aux extrémités de la zone de Brillouin (Figure 1.4B et C). Ces deux points de Dirac sont d'une importance capitale pour la physique du graphène. Leurs coordonnées dans l'espace sont données par les équations suivantes [1]:

$$\mathbf{K} = \left(\frac{2\pi}{3a}, \frac{2\pi}{3\sqrt{3}a} \right), \mathbf{K}' = \left(\frac{2\pi}{3a}, -\frac{2\pi}{3\sqrt{3}a} \right) \quad (1.2)$$

Au voisinage du point K (ou K'), l'énergie est nulle. Ceci confère au graphène ses propriétés électroniques très intéressantes.

1.1.3 Propriétés du graphène

Jusqu'à ce jour, le graphène est connu comme étant le matériau le plus fin, à un atome de carbone d'épaisseur et le plus résistant. Il possède des propriétés physico-chimiques uniques et exceptionnelles qui suscitent un vif engouement tant pour les chimistes, les physiciens que pour le monde industriel. Il a une très grande surface spécifique de l'ordre de $2630 \text{ m}^2/\text{g}$ [15,17], largement supérieure à celle des nanotubes de carbone [18,19] et des carbones activés [7,20–24]. Malgré sa très grande flexibilité [25–27], il possède une force mécanique intrinsèque de haute résistance à la rupture de 42 N/m [28], 100 fois supérieure à celle de l'acier [29]. Pourtant le graphène demeure transparent, puisqu'un feuillet de graphène n'absorbe que 2.3 % de la lumière infrarouge (Figure 1.5) [30–32] et très léger (0.77 mg/m^2) [33]. Il possède une excellente conductivité thermique (5300 W/Km) [34] et électrique due à sa structure sp^2 planaire [7,12,31,35]. La mobilité électronique dépasse largement $100\,000 \text{ cm}^2 \text{ V}^{-1} \text{ s}^{-1}$, même à température ambiante [32]. Le graphène parfait est considéré comme un matériau semi-métallique à cause de sa bande interdite énergétique nulle [35–37]. Cette nature semi-métallique fait de lui un conducteur transparent idéal où la transparence et la faible résistance sont nécessaires [25,26,38].

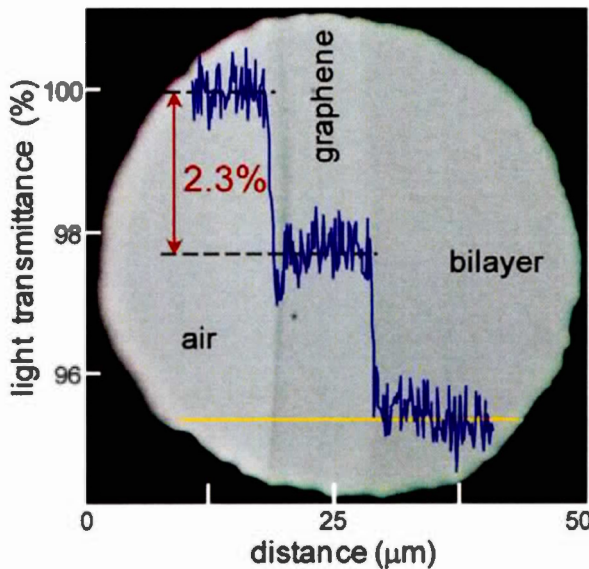


Figure 1.5 Propriété optique du graphène: Transmittance pour une monocouche et une bicouche de graphène (absorption optique: 2,3% par une monocouche) supportés sur une membrane poreuse [30,32].

1.2 Champs d'applications possibles du graphène

Le graphène est un matériau de base avec des propriétés mécaniques et électriques étonnantes. En tant que tel, il offre de nouvelles possibilités pour la recherche fondamentale et pour une utilisation dans un large éventail d'applications dans des domaines différents [39]. Les prédictions basées sur les propriétés que possèdent le graphène ont ouvert plusieurs voies d'applications potentielles notamment dans le domaine des batteries [40–42], des supercondensateurs électrochimiques [12,41,43], des cellules solaires [44–47], des piles à combustible [44], du stockage de l'hydrogène [48,49], la capture et le stockage du CO₂ [50,51], la récupération des métaux [52], la désalinisation des eaux [53], les écrans flexibles

[54], les capteurs et biocapteurs [55,56] et aussi dans la conception et l'élaboration de systèmes et dispositifs pour la photodétection, le spintronique et l'optoélectronique [12,57,58]. Ainsi, dans ce chapitre nous ferons l'état des lieux des domaines les plus prometteurs et populaires.

1.2.1 Matériaux composites à base de graphène

Le graphène peut être donc combiné à d'autres éléments (polymères, métaux, oxydes métalliques, céramiques ou gaz), à très faible quantité pour produire différents types de matériaux (matériaux composites) ayant des propriétés supérieures et très intéressantes [59]. La recherche sur les matériaux composites à base de graphène (graphène/plastique, graphène/fibres de carbone, graphène/polyépoxydes, graphène/nanoparticules) est en forte croissance dans l'optique d'une utilisation très prochaine dans l'industrie automobile et aéronautique [60]. Ces matériaux deviennent plus légers, solides et plus résistants à l'érosion [61] et la corrosion [62] en raison des propriétés qu'ils acquièrent en se combinant au graphène, même à très faible quantité [39,63,64]. À l'ajout de 0.9% en poids de graphène dans le polystyrène, des chercheurs ont montré que la résistance à la rupture et le module de Young augmentaient respectivement de 70 et 57% (Figure 1.6) [65]. La compagnie Vorbeck a pu améliorer les propriétés des thermoplastiques, des élastomères et des époxydes en les rendant plus solides, plus conducteurs et plus performants en y ajoutant moins 1% de graphène [66]. En décorant le graphène avec des nanoparticules (Ag, Pt, Au) ou des oxydes métalliques telles MoS₂, Co, CoO, il est possible d'augmenter l'activité électrocatalytique pour la réduction de l'oxygène [67,68]. Une solution pour surmonter certains défis tels que la non-conductivité et la rigidité de certains matériaux (S, Si) est soit de développer un composite de soufre à base de graphène capable d'adsorber le polysulfure, augmenter la conductivité électrique et s'adapter au changement structurel, lorsque ces éléments sont utilisés dans les batterie au lithium [69–71].

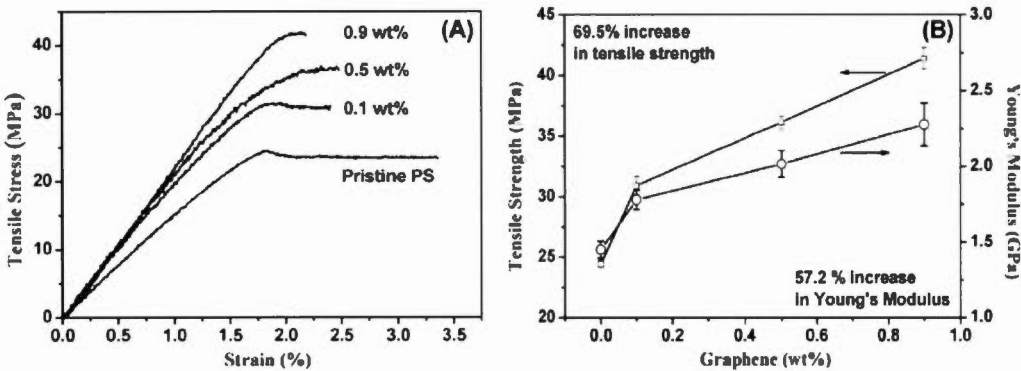


Figure 1.6 (A) Étude du comportement mécanique du polystyrène (PS) et des films nanocomposites (PS-graphène) avec des teneurs différentes en feuilles de graphène. (B) Le module de Young et sa résistance à la traction changent avec la teneur croissante en graphène [65].

1.2.2 Capteurs à base de graphène

Une application intéressante du graphène est la conception des biocapteurs et des capteurs chimiques de très petite taille et plus économique. À cause de sa grande surface spécifique, le graphène est capable d'augmenter la quantité de biomolécules qu'il peut détecter en solution au cours d'une analyse. L'excellente conductivité électrique du graphène et sa bande interdite presque nulle favorisent le transfert rapide des électrons entre l'analyte et la surface de l'électrode [55,56]. Ces propriétés peuvent favoriser la conception d'équipements miniaturisés à très haute sensibilité. Une fois en contact avec l'analyte (exemple: un brin d'ADN), le graphène change ses propriétés électriques. Les électrodes à base de graphène ont montré leur utilité pour la détection des molécules gazeuses (exemples: CO_2 , NO_2) [72,73], des métaux lourds en solution aqueuse [74,75], des contaminants, des anticorps et bien d'autres éléments [76–78].

1.2.3 Le graphène pour l'électronique

Alliant flexibilité, résistance, transparence et conductivité, le graphène tend à révolutionner l'industrie de l'électronique. À partir de ce nanofeuillet d'atomes de carbone en nid d'abeilles, il est possible de concevoir des transistors tels que ceux fabriqués à partir du silicium, de téléphones intelligents souples et très résistants et aussi des fenêtres intelligentes [79]. La conception de nouveaux appareils électroniques avec des écrans tactiles (Figure 1.7A) [80], des écrans flexibles (Figure 1.7B) [81] avec des circuits souples, transparents et résistants et des diodes électroluminescentes organiques (OLED) est en forte croissance [38].



Figure 1.7 Téléphones intelligents à écran tactile (A) [80] et flexible (B) [81] à base de graphène, (C) Capteur transparent représentant une rétine artificielle [82].

De plus, des chercheurs ont pu développer une rétine artificielle basée sur le graphène (Figure 1.7C) dans le but de servir de prothèse optique pour les personnes ayant un handicap à l'oeil [82]. Plusieurs autres travaux ont montré l'importance du graphène dans la nanoélectronique qui pourrait révolutionner ce domaine [32,83–86].

1.2.4 Supercondensateurs électrochimiques au graphène

Les supercondensateurs, également appelés condensateurs électrochimiques, sont des dispositifs capables de stocker une certaine quantité de charge électrique. Ils

se rechargent très rapidement et ont une longue durée de vie grâce à leur système de charge et décharge très rapides sur plusieurs cycles [87]. Les supercondensateurs peuvent être classés comme des condensateurs électriques à double couche (en anglais: Electrical double-layer capacitor, EDLC) dans lesquels des charges électrostatiques sont accumulées aux interfaces électrode/électrolyte pour stocker l'énergie [87]. Il est typiquement composé de deux électrodes, un électrolyte et un séparateur (Figure 1.8) [88–90].

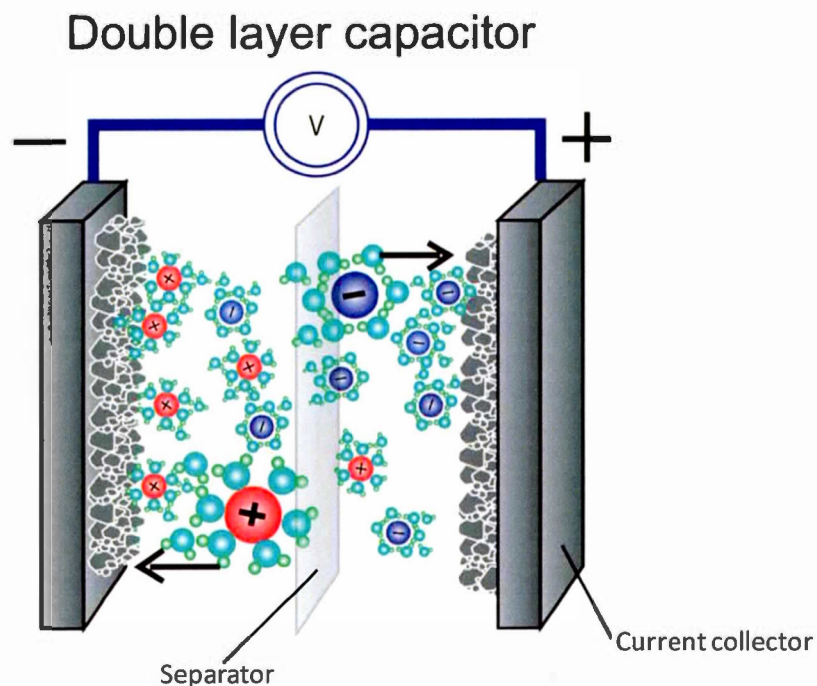


Figure 1.8 Schéma de base d'un supercondensateur électrochimique basé sur un matériau carboné [89].

La puissance et la densité d'énergie d'un supercondensateur sont intimement liées aux propriétés électrique et structurale du matériau carboné. Une grande surface spécifique est l'un des paramètres les plus importants conduisant à une grande capacité gravimétrique et donc à une grande densité de stockage d'énergie [91,92]. Bien que des progrès considérables aient été réalisés avec les matériaux carbonés usuels (exemples: noir de carbone, charbon actif, noir d'acétylène) à structure poreuse, la capacité expérimentale obtenue reste en dessous des valeurs théoriques attendues. La découverte du graphène avec sa grande surface spécifique ($2630\text{ m}^2/\text{g}$) [15] offre de nouvelles possibilités pour améliorer la densité énergétique des supercondensateurs à base de carbone.

Le molybdate de manganèse démontre une très bonne performance électrochimique lorsqu'on y ajoute une faible quantité de graphène (6.7 % p/p), comme additif lors de la préparation des matériaux hybrides composites graphène-MnMoO₄ (Figure 1.9A) [93]. Ces résultats (Figure 1.9B) proviennent en partie du composé pseudocapacitif MnMoO₄ (II) et surtout à l'effet synergique entre le graphène et le MnMoO₄, lié aux avantages apportés par le graphène incluant sa flexibilité, sa grande surface spécifique et sa haute conductivité électrique. L'oxyde de nickel a été combiné au graphène 3D pour améliorer les performances et la stabilité de Ni(OH)₂, car le graphène 3D peut agrandir la surface de l'électrode, améliorant ainsi la conductivité des ions et des électrons [94]. Un certain nombre d'oxydes métalliques (MO), tels que ZnO, SnO₂, Co₃O₄, MnO₂ et RuO₂, ont été combinés avec des dérivés de graphène pour préparer des électrodes pour des supercondensateurs [12]. À partir de l'électrode hybride graphène/MO, les NPs MO vont contribuer au stockage d'énergie via la réaction redox entre les différents états d'oxydation du métal.

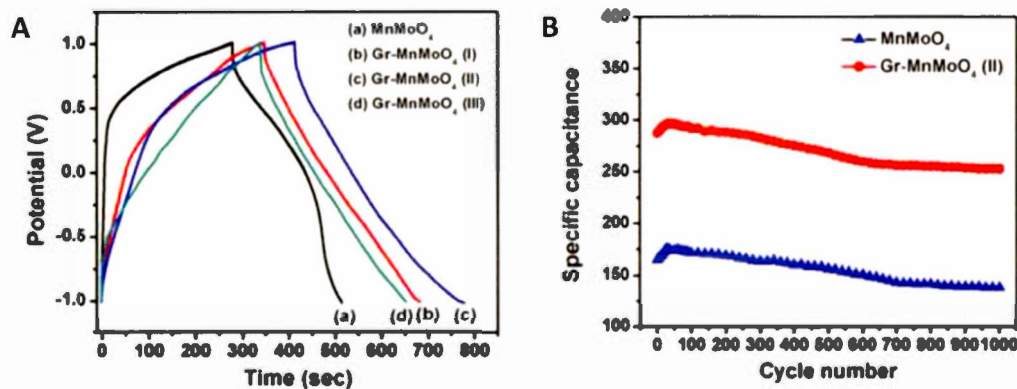


Figure 1.9 (A) Courbes de charge et de décharge galvanostatique de différents composés de molybdate de manganèse (MnMoO_4) à densité de courant de 2 A g^{-1} et (B) variation de la capacité spécifique en fonction du nombre de cycle pour le composé MnMoO_4 (courbe en bleu) et le composite Gr-MnMoO_4 à 8 A g^{-1} [93].

1.2.5 Le graphène dans les batteries

Les batteries lithium-ion (Li-ion) sont largement utilisées dans les dispositifs électroniques portables tels les téléphones intelligents et les véhicules électriques. Cependant, la durée de vie de la batterie est un défis majeur, c'est pourquoi beaucoup d'efforts sont déployés dans le but de pallier à ce problème majeur. L'utilisation du graphène dans les matériaux d'électrode pour les batteries lithium-ion (Li-ion) pourrait améliorer leur capacité de stockage (Figure 1.10) [95]. La densité d'énergie et la performance des batteries Li-ion dépendent largement des propriétés physiques et chimiques des matériaux de cathode et d'anode [96,70].

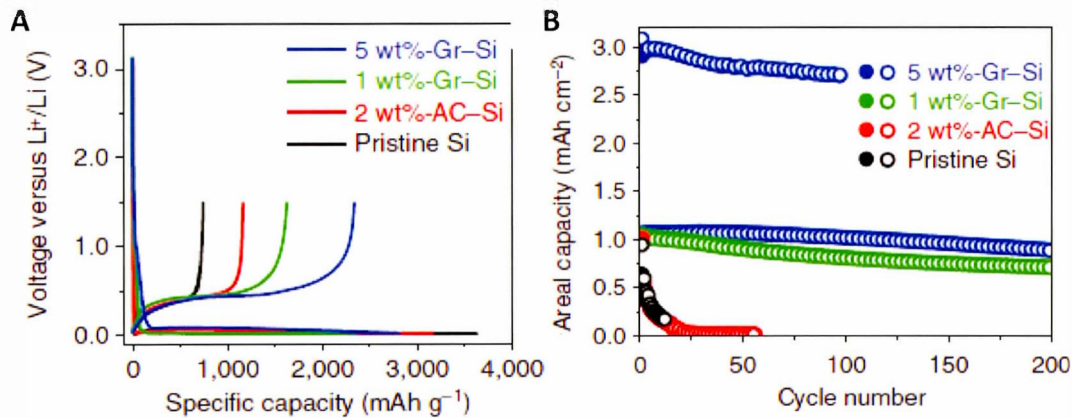


Figure 1.10 (A) Profils des premières courbes de lithiation et de délithiation de différentes électrodes préparées à partir du silicium (Si) et différents matériaux conducteurs tels le graphène (Gr) et le carbone amorphe (AC). (B) Capacité de rétention en fonction du nombre de cycles [95].

Les travaux de Son et *coll.* mettent en exergue l'effet du graphène sur les performances électrochimiques des particules de silicium enrobées de feuillets de graphène [95]. En effet, le graphène avec sa grande flexibilité couplée à sa conductivité électrique permet de contenir les phénomènes de dilatation et de contraction répétées lors de la charge et de la décharge de l'anode. Ce sont en fait ces contraintes mécaniques qui impactent négativement la durée de vie des batteries. De plus, comme le graphène est très conducteur, il permet aussi de maintenir un transfert électronique rapide entre les particules de Si. Toutes ces propriétés permettent de pratiquement doubler la capacité spécifique de l'anode au graphène ($\sim 760 \text{ mAh g}^{-1}$) [71] comparée à celle du graphite (372 mAh g^{-1}) [97]. Plusieurs autres nanostructures d'oxyde métallique, comme SnO_2 , Co_3O_4 , MnO_2 , TiO_2 , Fe_3O_4 et Cu_2O , ont été composées avec du graphène pour les batteries au lithium [63,98]. La désintégration rapide de la capacité est habituellement observée dans les anodes à base d'oxyde de métal pur, en raison de la mauvaise conductivité, de la dégradation, d'une expansion

structurelle et une agglomération entre particules. L'utilisation de matériaux à base de graphène comme matrices des nanostructures d'oxyde métallique permet de résoudre ces problèmes [99].

1.2.6 Le graphène et les panneaux solaires

Dû à son coût élevé, sa fragilité, sa quantité limitée et sa perte de conductivité lors de la flexion, l'oxyde d'indium dopé à l'étain, appelé ITO (de l'anglais Indium Tin Oxide) utilisé pour les cellules photovoltaïques [32] peut être remplacé par le graphène. Le graphène est un candidat potentiel parce qu'il possède de très bonnes propriétés électroniques [8]. Il est flexible, hautement conducteur, transparent et capable de convertir efficacement la lumière en énergie [38]. Plusieurs travaux ont montré l'efficacité du graphène lorsqu'il est combiné à d'autres matériaux ou dopé par des nanoparticules [32,39,100,101]. La figure 1.11A montre la courbe photocourant-voltage obtenue en dopant le graphène au soufre et l'azote. La performance obtenue est légèrement supérieure à celle du platine dans les mêmes conditions d'analyse. Récemment, beaucoup plus d'efforts ont été consacrés au développement de ces nouveaux matériaux pour répondre à la demande croissante dans des zones géographiques plus pluvieuses où le soleil est moins présent à cause du changement climatique. Alors, ces phénomènes météorologiques vont très souvent affecter le rendement des panneaux solaires.

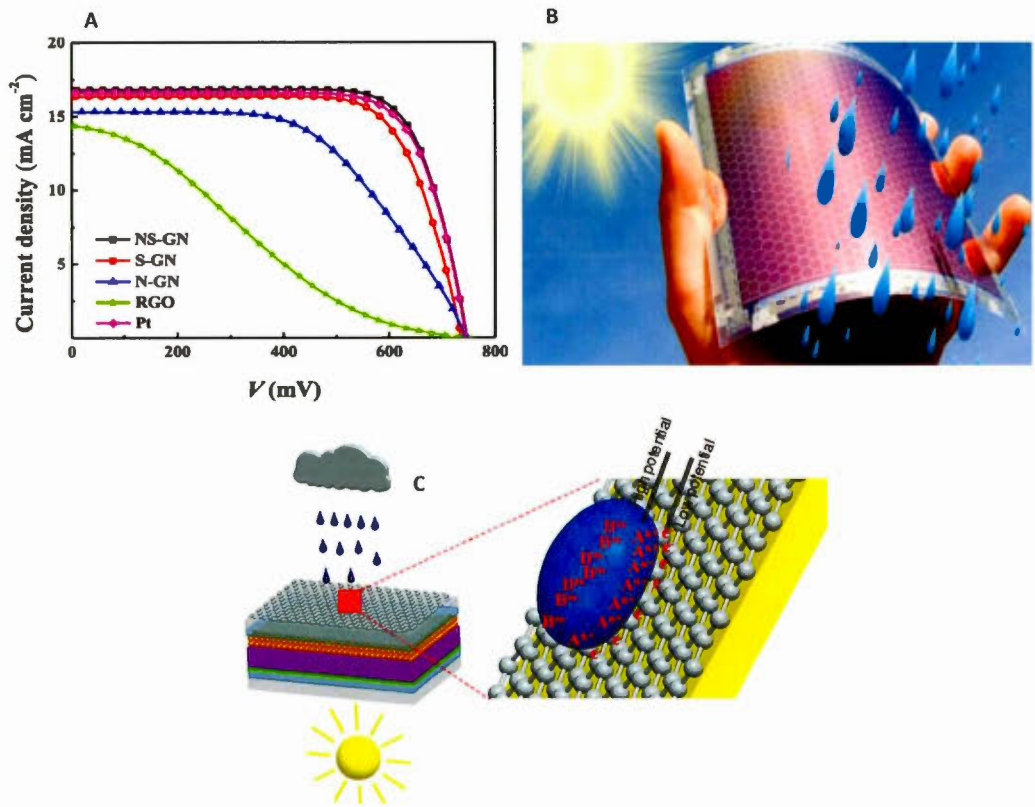


Figure 1.11 (A) Courbes courant-tension (J-V) obtenues avec une source d'illumination simulant le spectre solaire (AM1.5) de différents matériaux [102], (B) Cellule solaire flexible basée sur l'oxyde de graphène réduit (RGO), (C) Structure d'une cellule solaire flexible biexcitée par la lumière du soleil et de pluie [100].

Alors, dans le but de s'adapter à la météo, des chercheurs ont conçu des panneaux photovoltaïques bifonctionnels capables de capter l'énergie du soleil, mais aussi à partir de l'eau de pluie à partir d'une cellule solaire basée sur le graphène (Figure 1.11B et C) [100]. Ils ont proposé un mécanisme selon lequel lorsque la pluie entre en contact avec la cellule solaire, le graphène lie ses électrons aux cations (Na^+ ,

Ca^{2+} et NH_4^+) contenus dans les gouttes d'eau. Précisément, chaque fois qu'une goutte d'eau atteint la couche d'oxyde de graphène réduit (RGO), cela engendre un mouvement d'électrons π qui induit ensuite une pseudocapacité électrique à double-couche entre l'électron π et le cation (Figure 1.11C). Ce phénomène donne naissance à un courant et à un potentiel [103,104]. Même si le taux de conversion de l'énergie reste encore faible (6.53%), comparé aux valeurs actuelles (15-33%) [105], ces panneaux de future génération restent très prometteurs pour répondre à la crise énergétique.

1.2.7 Le graphène dans les peintures et revêtements

La corrosion des métaux est l'un des problèmes auxquels les industries de la métallurgie et électronique sont le plus souvent confrontées. De nombreuses méthodes de lutte contre la corrosion utilisent des revêtements de polymères conducteurs et des couches de conversion qui contiennent des matières toxiques et dangereuses pour l'environnement, en particulier des composés de chrome, de phosphore et de zinc [106,107]. Alors, le graphène apparaît comme un choix intéressant et nécessaire.

Le graphène dispose de propriétés très particulières qui ouvrent la porte à de nombreux types intéressants de revêtements, de peintures et d'encre. L'excellente résistance mécanique du graphène peut rendre les revêtements durables, qui ne craquent pas et peuvent résister aux agressions environnementales de l'eau, l'huile et la poussière. Par exemple, un revêtement composite superhydrophobe et robuste à base de graphène qui permet de lutter efficacement contre la corrosion et toutes sortes d'intempéries a été préparé par le groupe de Losic [108]. Ce revêtement a des propriétés d'une couche autonettoyante et résiste l'oxydation et l'infiltration d'eau (Figure 1.12) [108]. Des films d'oxyde de graphène réduit (RGO) obtenu par

réduction chimique de l'oxyde de graphène dans la vitamine C et aussi dans l'acide iodhydrique ont montré une grande résistance à l'humidité, à la diffusion des molécules d'eau et aussi à la diffusion des agents corrosifs tels les ions Cl^- et F^- à travers les films [109].

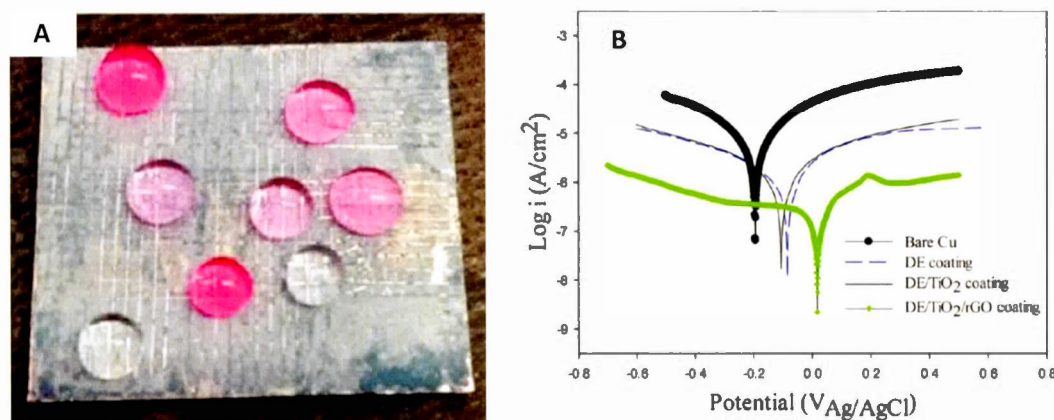


Figure 1.12 (A) Étude du comportement hydrofuge de l'eau sur une feuille revêtue par le nanocomposite de graphène (DE/TiO₂/RGO). (B) Étude électrochimique de la corrosion de différents échantillons de cuivre (nu et revêtus) [108].

Parce que le graphène est conducteur et transparent, il peut être utile pour préparer diverses peintures conductrices et dans autres types de revêtements [60,110].

1.2.8 Conclusions

Les propriétés étonnantes du graphène peuvent permettre des applications polyvalentes allant des appareils électroniques aux matériaux d'électrodes en passant par les revêtements et les peintures conductrices. Le graphène présente des propriétés électroniques exceptionnelles, permettant à l'électricité de circuler rapidement à travers les matériaux. En fait, il a été démontré que les électrons dans le graphène se

comportent comme des particules sans masse semblables aux photons, passant à travers une couche de graphène sans diffuser. Cette propriété électronique exceptionnelle est d'une importance capitale pour de nombreuses applications dans les appareils électroniques, et l'on s'attend à ce que le graphène puisse éventuellement remplacer le silicium pour rendre les ordinateurs et les téléphones intelligents plus performants. La figure 1.13 résume brièvement certaines applications actuelles et futures du graphène [111].

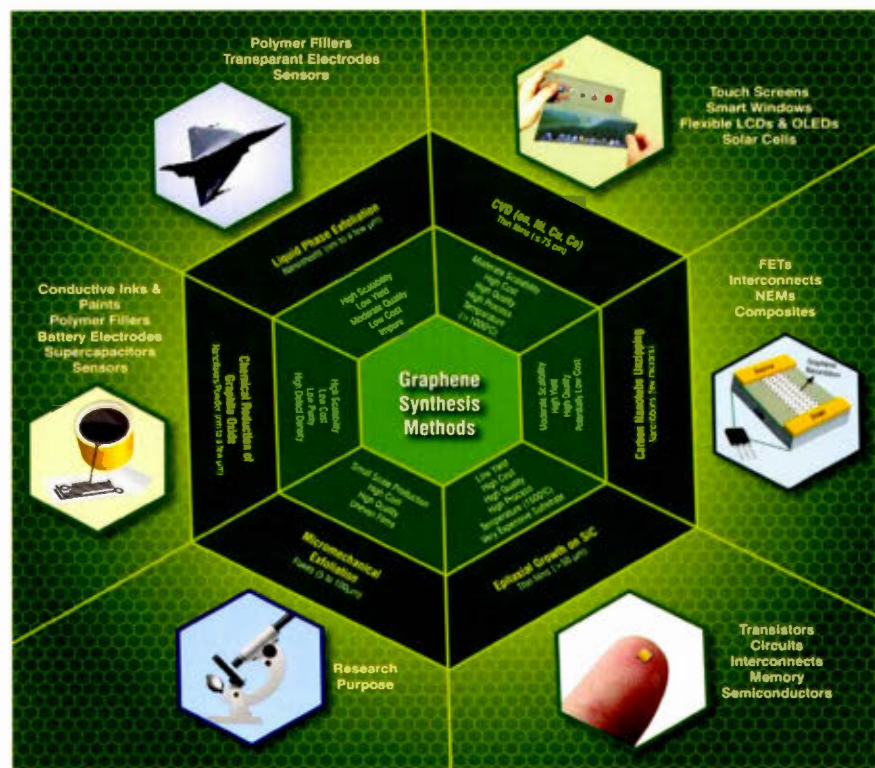


Figure 1.13 Schéma montrant les méthodes classiques couramment utilisées pour la synthèse du graphène ainsi que les applications actuelles et futures [111].

Cependant, l'application la plus importante pour le graphène est probablement son utilisation dans les matériaux composites. En effet, il a été démontré qu'en ajoutant une petite quantité de graphène dans presque tous les polymères, il est possible de concevoir des matériaux légers et très résistants. Les composites conduisent de l'électricité et peuvent résister à des températures beaucoup plus élevées que les polymères [7,112].

1.3 Méthodes de préparation

La recherche sur le graphène est en constante progression depuis sa découverte en 2004 [15]. De plus en plus, les chercheurs s'intéressent à la production du graphène à grande échelle avec moins de défauts. Ainsi, afin de préparer du graphène de meilleure qualité, plusieurs méthodes telles que l'exfoliation mécanique[15], la croissance par épitaxie sur du carbure de silicium[113], le dépôt chimique en phase vapeur[114], l'exfoliation chimique en phase liquide[115], l'oxydation chimique/exfoliation suivie d'une réduction[116,117], l'exfoliation électrochimique[118], la méthode à l'arc électrique[117] et d'autres formes de préparation du graphène telles que les méthodes de production industrielle[119] ont été développées et continuent de voir le jour. Chaque méthode de synthèse présente des avantages et aussi des inconvénients [7].

1.3.1 Exfoliation micromécanique

L'exfoliation micromécanique du graphite pyrolytique hautement orienté (HOPG) est la méthode qui a permis à Geim et Novoselov d'isoler, pour la première fois un feutre de graphène dans sa forme stable en 2004 [15]. Cette méthode est basée sur un clivage répétitif du graphite à l'aide d'un ruban adhésif (en anglais: Scotch-tape method) pour obtenir finalement une monocouche ou quelques couches de graphène (Figure 1.14) [10]. Elle est très facile à réaliser pour obtenir du graphène

de très bonne qualité, presque sans défaut avec la taille des cristaux qui varie du nanomètre à plusieurs dizaines de micromètres [120]. Par contre, le rendement demeure très faible.

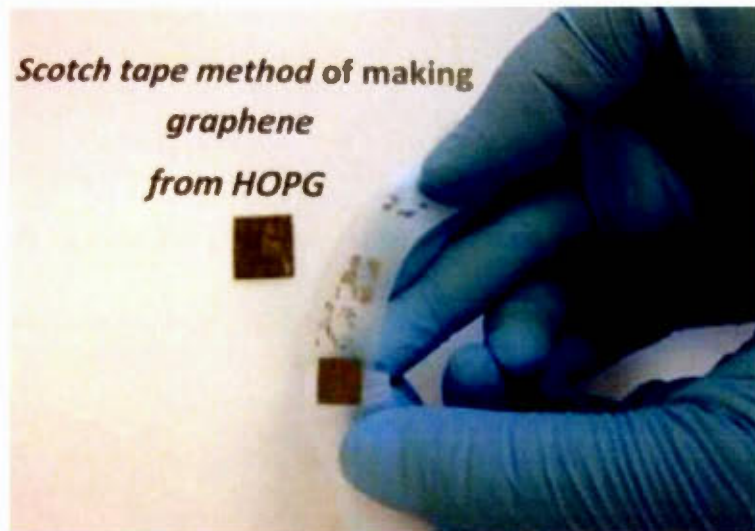


Figure 1.14 Exfoliation mécanique du graphène par du ruban adhésif à partir du graphite [8].

1.3.2 Croissance épitaxiale du graphène sur du carbure de silicium (SiC)

La croissance des films de graphène de haute qualité par cette méthode est motivée par l'utilisation du graphène dans l'électronique moderne. La méthode de croissance des feuillets de graphène consiste à chauffer à très haute température (environ 1300 °C) [121], sous un vide très poussé ou sous pression atmosphérique d'argon un substrat de carbure de silicium (SiC) jusqu'à la sublimation des atomes de Si en surface (Figure 1.15) [113,122]. Les atomes de carbone restant se réorganisent en graphène. Le graphène formé est majoritairement de plusieurs couches à cause de la grande réactivité des feuillets de graphène adjacents [113,123] mais il est possible

d'obtenir localement une monocouche de graphène en contrôlant la température [113]. C'est un procédé très prometteur car le graphène obtenu a une structure bien définie qui peut être ainsi utile autant pour la recherche fondamentale que dans l'industrie pour la fabrication de systèmes en microélectronique tels que des transistors de hautes fréquences [113,124].

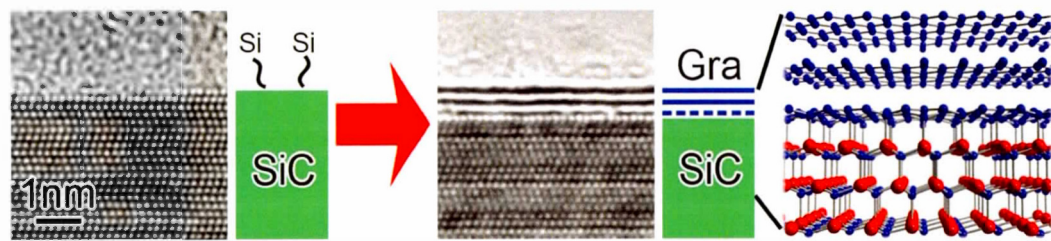


Figure 1.15 Croissance du graphène par décomposition thermique du SiC, ainsi que le modèle structurel du graphène bicouche sur SiC. La ligne bleue brisée représente la couche tampon pour prévenir la déchirure possible des feuillets de graphène formés [113].

Cependant, le coût élevé du SiC, les températures de synthèse élevées et la taille des feuillets de graphène produit limitent l'intérêt de la croissance sur SiC pour une production à grande échelle sans ignorer l'intercalation des certains éléments tels que Si, H, Li, Au, O et aussi Na qui peuvent affecter la qualité du graphène en changer ses propriétés électroniques [121,125].

1.3.3 Dépôt chimique en phase vapeur (CVD)

Le dépôt chimique en phase vapeur (CVD) est une méthode prometteuse et une alternative à l'exfoliation mécanique pour produire une monocouche de graphène ($> 95\%$) et quelques feuillets ($< 5\%$) [126] de graphène de très haute qualité et à grande échelle, sur des susbtrats métalliques tels que le cuivre [126] et le nickel dans

une chambre fermée [114,127–129]. D'autres métaux de transition tels que le platine [130], le cobalt [37,131] ont été déjà utilisés pour la croissance du graphène [132]. Cependant, ceux-ci ont été abandonnés à cause des plis formés lors de la croissance des feuillets de graphène qui rendent les films de graphène discontinus. Cette technique a pour but de faire croître un film de graphène à partir d'une source gazeuse (méthane, propane, éthane) (Figure 1.16A) [129,133], liquide (le méthanol, l'éthanol, le propanol) [114] ou d'un précurseur solide contenant le carbone telle que le polyméthacrylate de méthyle (Figure 1.16B) [127,134].

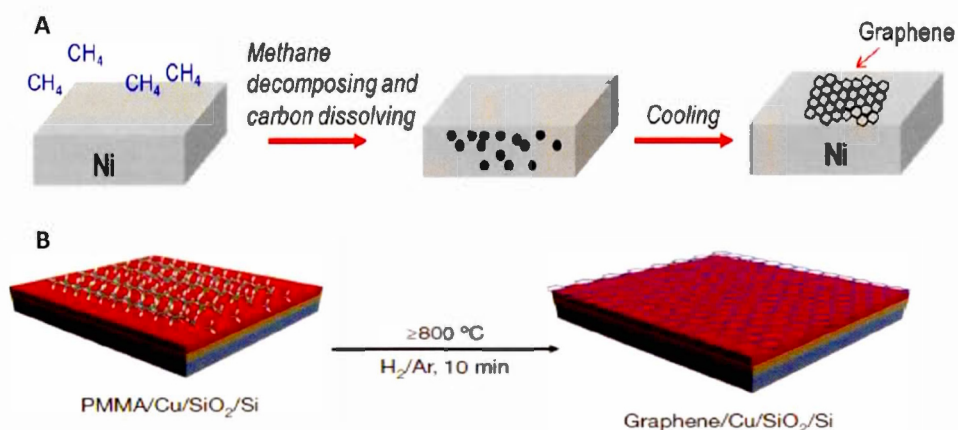


Figure 1.16 (A) Processus schématisé de la croissance du graphène sur du nickel à partir du méthane [135]. (B): Croissance du graphène à partir du polyméthacrylate de méthyle (PMMA) [127].

En général, la croissance en phase vapeur consiste à introduire des sources de carbone couplées à l'hydrogène dans un four maintenu à très haute température (environ 1000 °C). Au cours de la réaction, la source hydrocarbonée se décompose pour produire des espèces de carbone actif (Figure 1.16A) sur un substrat métallique (ex. Cu, Ni) ou semi-conducteur (ex. Ge/Si) [133,136]. Ensuite les espèces peuvent se

nucléer pour recouvrir la surface du substrat avec ou sans catalyseur pour former le graphène. Cependant, il est important de noter que plusieurs facteurs tels que la température, la pression, la source de carbone, le gaz tampon et le substrat peuvent influencer qualitativement la formation du graphène. Il a été démontré que les précurseurs liquides, à basse température ($800\text{ }^{\circ}\text{C}$) sur des substrats de Cu permettent d'obtenir de larges films uniformes de graphène de très haute qualité, comme le démontrent les spectres Raman avec un ratio des pics $I_{2D}/I_G \geq 2$ et les images de la microscopie électronique à balayage à la figure 117 [114].

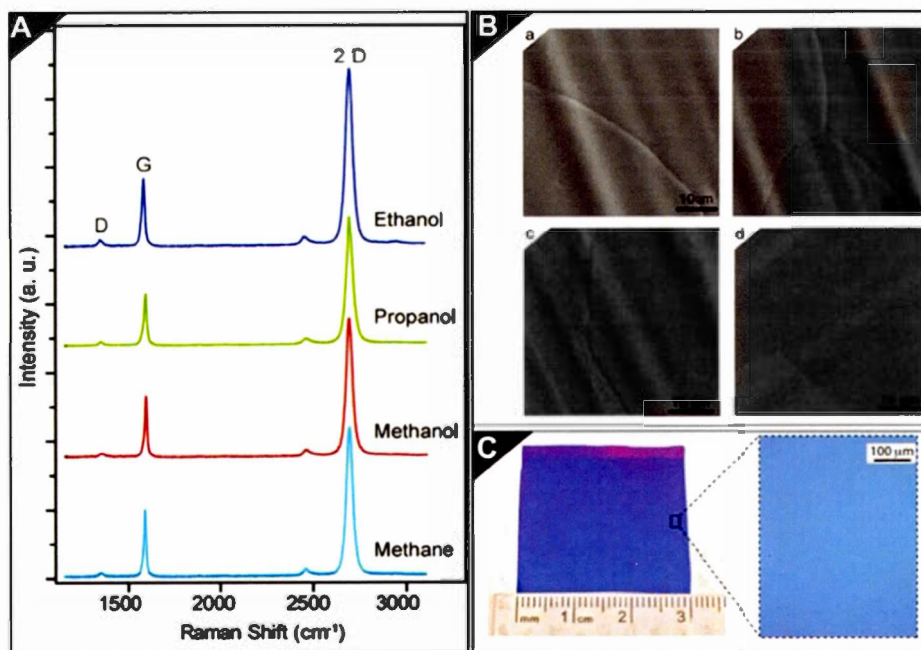


Figure 1.17 (A) Spectres Raman obtenus des films de graphène préparés par CVD à partir de différents précurseurs hydrocarbonés. (B) Microscopie électronique à balayage des films de graphène obtenus à partir du (a) méthanol (b), éthanol, (c) propan-1-ol et (d) méthane sur un substrat de Cu. (C) Large feuillet de graphène obtenu par CVD transféré sur un substrat de SiO_2/Si [114].

Cette technique permet d'obtenir des films de graphène possédant une mobilité des porteurs de charge largement supérieure à $10000 \text{ cm}^2 \text{V}^{-1} \text{S}^{-1}$ [37,137], très utiles pour des applications dans le domaine électronique, des capteurs, de l'optoélectronique flexible et bien plus d'autres mais elle reste toutefois limitée par le coût pour la production industrielle [132,137].

1.3.4 Exfoliation chimique en phase liquide

Comme l'exfoliation mécanique, l'exfoliation chimique en phase liquide consiste à briser les forces de van der Waals entre les feuillets de graphite pour produire du graphène. L'intercalation de molécules organique ou gazeuse (Figure 1.18) entre les feuillets de graphite facilite la séparation et permet une bonne dispersion de ces feuillets une fois le milieu réactionnel soumis aux ultrasons. Cependant, cette méthode utilisant un solvant aqueux, requiert souvent l'ajout d'un surfactant (ex. dodécylbenzènesulfonate de sodium) pour minimiser la tension de surface [138,139], d'un polymère [140,141] ou d'un solvant organique [142] pour exfolier le graphite [138,139,143–146].

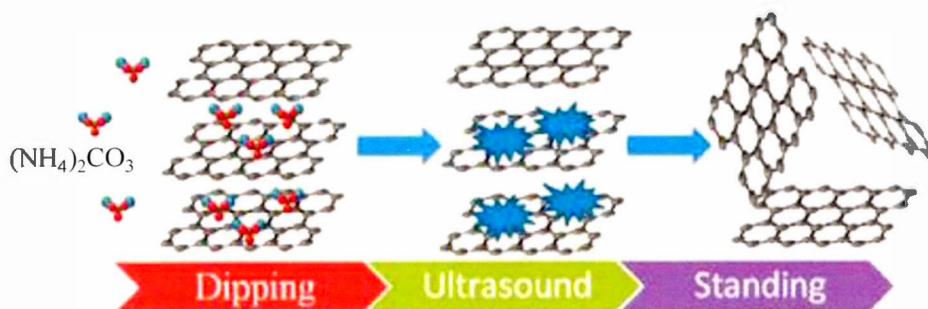


Figure 1.18 Schéma illustratif pour la préparation de graphène à partir de la décomposition de $(\text{NH}_4)_2\text{CO}_3$ [144].

Les solvants couramment utilisés sont l'eau avec l'ajout de certains acides sulfatés tels que le persulfate d'ammonium, l'acide sulfurique [138,141,147], la N-méthyl-2-pyrrolidone (NMP) [146,148,115], le *N,N*-diméthylformamide l'acide (DMF) [148,115,149], le diméthylsulfoxyde (DMSO) [148], le peroxyde d'hydrogène (H_2O_2) [150] et aussi certains composés aromatiques [151]. Les solvants organiques, les surfactants et les polymères utilisés permettent de préparer des suspensions colloïdales de graphène avec une très grande stabilité (Figure 1.19) [149,152].

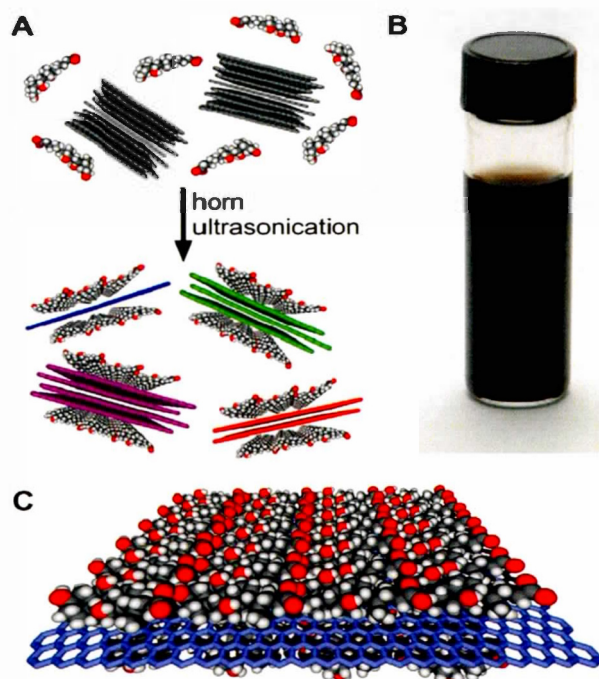


Figure 1.19 (A) Schéma du processus d'exfoliation du graphène. Le bain ultrasons permet d'exfolier le graphite en quelques feuillets de graphène, qui sont ensuite encapsulés par les micelles de cholate de sodium. (B) Photographie d'une dispersion de graphène de $90 \mu\text{g mL}^{-1}$ dans le cholate de sodium (CS), six semaines après sa préparation. (C) Schéma illustrant une monocouche de cholate de sodium ordonnée sur le graphène [152].

Bien que l'exfoliation chimique permet de produire du graphène avec un bon rendement [147], elle est limitée par la qualité du graphène dont le nombre de couches reste très variable comme le montre la figure 1.20 [147]. Ceci influence considérablement les propriétés mécaniques et électroniques du matériau préparé. De plus, un temps de sonication plus long peut générer des défauts à la surface des feuillets de graphène et aussi peut conduire à la réduction de leur taille même si cela permet de réduire le nombre de couches de graphène [153,154].

Certains solvants utilisés pour l'exfoliation ont été démontrés toxiques pour l'environnement [155,116]. Mais, malgré ce désavantage, elle demeure encore l'une des voies largement explorées pour une production économique et en masse du graphène [151].

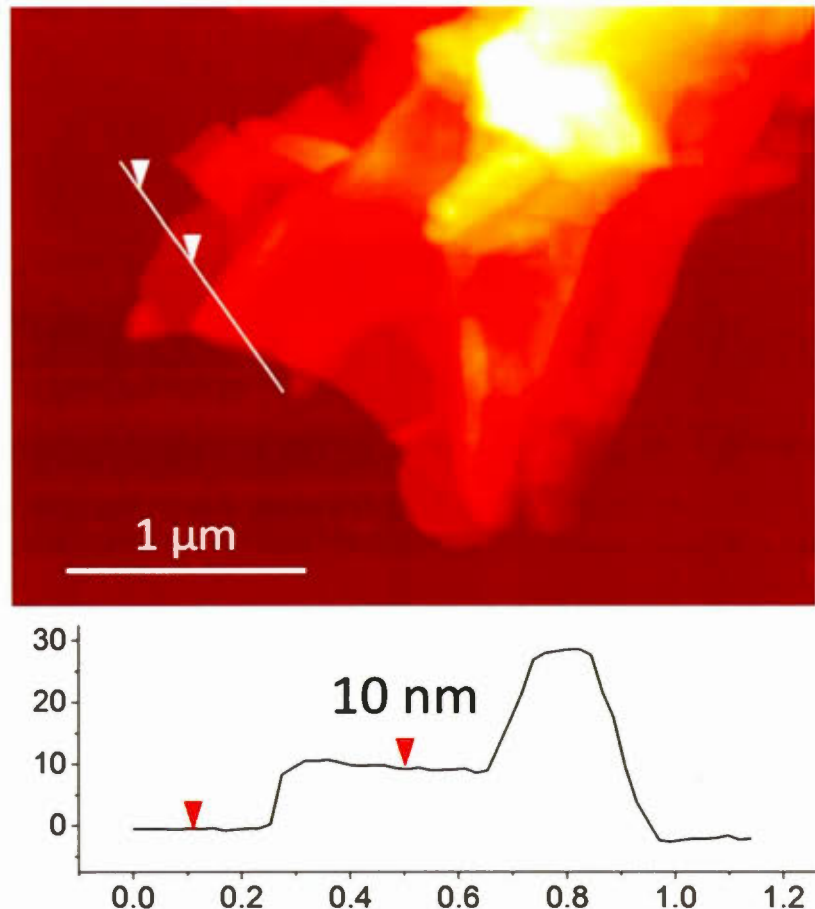


Figure 1.20 Image AFM de graphène préparé par exfoliation chimique et le profil en épaisseur correspondant. L'épaisseur de l'ordre de 10 nm traduit l'empilement de plusieurs feuillets de graphène [147].

1.3.5 Méthode de Hummers: préparation du graphène chimiquement modifié.

La conversion chimique du graphite en oxyde de graphène est l'une des méthodes les plus connues et répandues pour produire du graphène avec très peu de feuillets et en grande quantité. D'une manière générale, la méthode consiste à initialement oxyder le graphite en oxyde de graphite, suivie d'une exfoliation en

oxyde de graphène (GO) avant d'être réduit thermiquement [156–158], chimiquement [158–160] ou électrochimiquement [161–163] pour enfin obtenir l'oxyde de graphène réduit (RGO) ou du graphène chimiquement transformé (CCG) (Figure 1.21) [75].

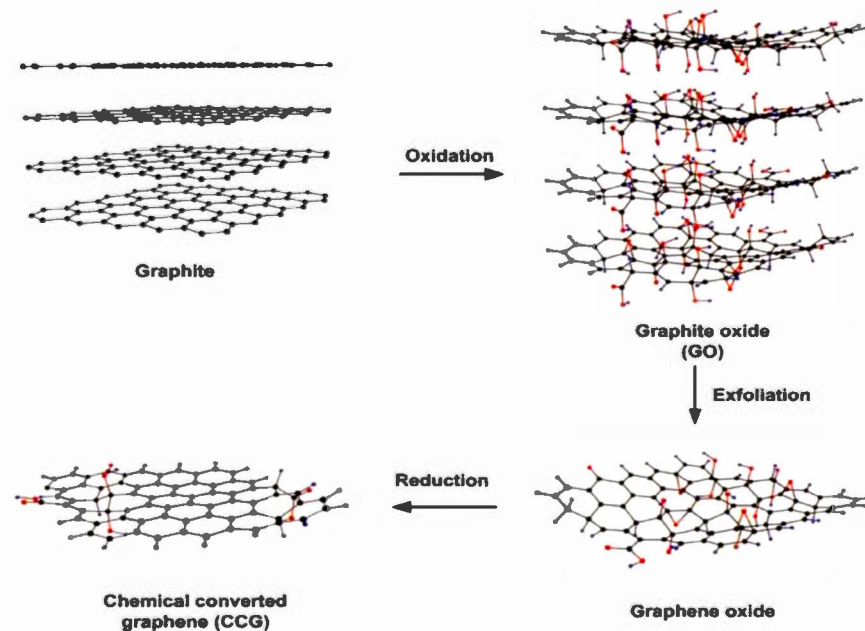


Figure 1.21 Processus de préparation de l'oxyde de graphène réduit (graphène chimiquement converti) à partir de la trilogie "oxydation-exfoliation-réduction". Un traitement oxydant est initialement réalisé pour générer de l'oxyde de graphite, qui est suivie par une exfoliation pour produire de l'oxyde de graphène. Enfin, une réduction produit l'oxyde de graphène réduit communément noté RGO [75,164].

1.3.5.1 Préparation de l'oxyde de graphène (GO)

Dans la plupart des cas, l'oxyde de graphène est produit à partir de la méthode développée par Hummers et Offeman en 1958 [164] qui consiste à traiter le graphite en utilisant un acide très concentré tel que l'acide sulfurique, le nitrate de sodium et en présence d'un oxydant fort comme le permanangate de potassium (Figure 1.22), à des températures variables [165,166]. L'oxyde de graphène peut être aussi préparé par la méthode de Brodie ou de Staudenmaier mais chacun des procédés est jugé dangereux puisque des gaz toxiques (ex. NO_2 , N_2O_4) sont produits au cours de la réaction [167–169]. C'est dans le but de respecter l'environnement que la méthode de Hummers a été plusieurs fois modifiée et améliorée (Figure 1.22) [165,170]. Cette amélioration consiste à préoxyder le graphite avec une solution de H_2SO_4 , le persulfate de potassium et le pentoxyde de phosphore dans un premier temps. Cette méthode exclue l'utilisation du NaNO_3 jugé aussi toxique et une augmentation de la quantité de KMnO_4 est de mise. Ensuite, le graphite préoxydé est mélangé avec H_2SO_4 et l'acide phosphorique dans un ratio 9:1 comme le décrit la procédure adoptée par Marcano et *coll.* [165].

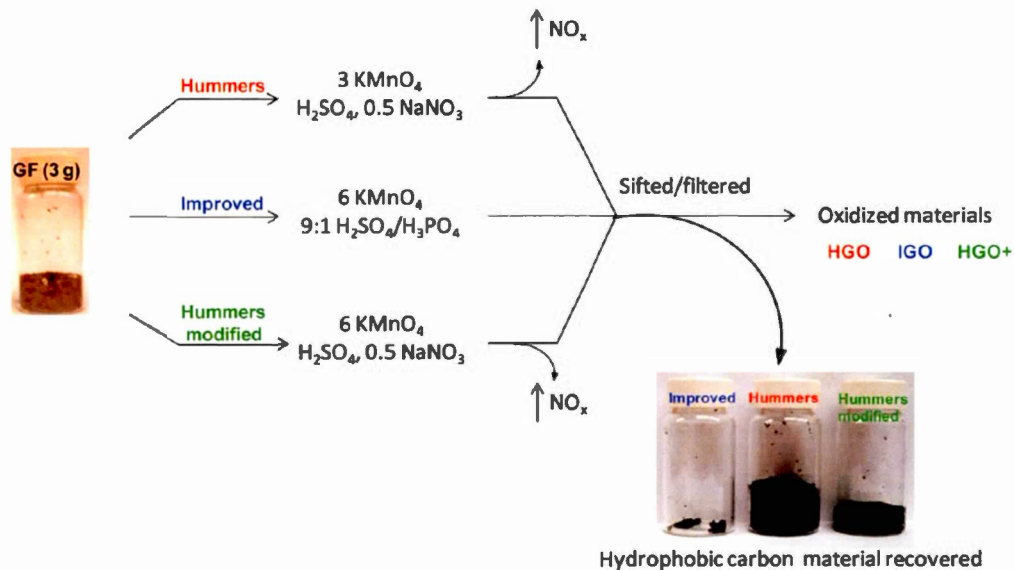


Figure 1.22 Représentation schématique des procédures suivies à partir du graphite pour la préparation de l'oxyde de graphène basée sur la méthode initiale de Hummers [164]. La méthode améliorée de Hummers permet d'éviter le dégagement des gaz (NO_x) hautement toxiques [171] et produire un matériau moins oxygéné [165].

L'ajout du peroxyde d'hydrogène à la toute fin de la réaction, dans cette méthode permet de réduire le permanganate et le dioxyde de permanganate résiduels en sulfate de manganèse soluble et incolore [172]. Une fois traitée au H_2O_2 , la coloration de la suspension passe progressivement du brun foncé au jaune vif. Ensuite, le mélange est filtré, lavé avec du HCl pour éliminer les ions métalliques résiduels et abondamment avec de l'eau Nanopure jusqu'à ce que le pH du filtrat soit proche de 7 [172,173]. L'oxyde de graphite est alors exfolié complètement dans l'eau par ultrasonication pour obtenir l'oxyde de graphène. Le produit final est ensuite obtenu par séchage à l'air ou séchage au four sous vide [174].

1.3.5.2 Réduction de l'oxyde de graphène

La réduction de l'oxyde de graphène pour l'obtention du graphène ou plus précisement de l'oxyde de graphène réduit (RGO) est une étape très importante dans le processus de synthèse de certains matériaux graphéniques. L'oxyde de graphène est initialement considéré comme un isolant électrique à cause de la perturbation de sa structure sp^2 . Cependant, il est possible de partiellement restaurer son réseau $\pi-\pi$ par un traitement thermique ou via une réduction chimique par un agent réducteur en milieu humide [158,175]. Plusieurs types de réducteurs tels que l'hydrazine [159,165,176], l'iodure de potassium [177], le borohydrure de potassium ou de sodium [178], l'hydroquinone [179], les composés soufrés [160], les bases fortes (Figure 1.23A) [180], les amines et certains acides [175] sont couramment utilisés pour réduire le GO [12]. Parmi tous ces réducteurs, l'hydrazine fut largement utilisée à cause de sa forte réaction de déoxygénéation des groupements fonctionnels du GO. Cependant, il demeure sous forme de traces dans le RGO, ce qui affecte les performances des dispositifs à base de RGO. En plus, il est hautement toxique [166]. Pour remédier à ces inconvénients, plusieurs agents non-toxiques et ayant un pouvoir réducteur fort tels que l'acide L-ascorbique, la vitamine C, le D-glucose, des alcools et l'acide acétique ont été développés dans le but de préparer le RGO [12,175,181,182]. Cependant, tous ces agents réducteurs produisent des RGO contenant un niveau élevé de défauts (Figure 1.23C) [75] qui réduisent les propriétés thermiques et électriques du matériau. Tout récemment, Mohandoss et *coll.* ont développé une approche alternative aux méthodes conventionnelles, qui est très économique, douce et très respectueuse de l'environnement et qui consiste à utiliser la lumière visible fournie par un simulateur solaire pour restorer la structure graphitique de l'oxyde de graphène en RGO [183]. La réduction de GO affecte très peu les propriétés électroniques du matériau avec une conductivité électrique de 166 S/m et un ratio $I_D/I_G = 1.016$. De plus, la réduction de l'état colloïdal de GO n'entraîne pas

l'agrégation de feuillets de RGO produits [183], ce qui peut être bénéfique pour certaines applications.

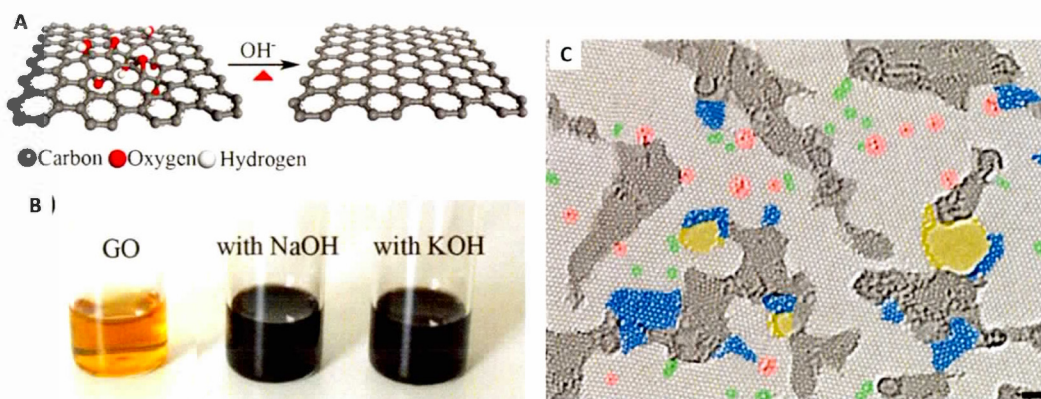


Figure 1.23 A: Équation schématisée de la déoxygénéation de l'oxyde de graphène (GO), B: Images des suspensions de GO et de l'oxyde de graphène réduit (RGO) en milieux NaOH et KOH aqueux. Au cours du processus de réduction, la couleur jaune brillant de la dispersion de l'oxyde de graphène dans l'eau devient noire une fois le RGO formé [180]. C: Microscopie électronique en transmission d'un mono-feuillet RGO teintée de couleurs par endroits pour mettre en exergue les différentes zones caractéristiques graphène préparé. La zone de graphène cristalline sans défauts est affichée dans la couleur gris clair d'origine. Les régions contaminées sont en gris foncé. Les régions bleues sont les réseaux de carbone monocouche désordonnés, ou défauts topologiques étendus, que nous identifions comme des restes du processus d'oxydoréduction. Les zones rouges mettent en évidence des atomes ou des substitutions individuelles. Les zones vertes indiquent des défauts topologiques isolés, c'est-à-dire des rotations à liaison simple ou des noyaux de dislocation. Les trous et leurs reconstructions de bord sont colorés en jaune [75].

La réduction chimique de GO en RGO par un agent réducteur est probablement la méthode la plus employée pour restaurer le réseau sp^2 de l'oxyde de graphène. La réduction thermique est une méthode rapide qui permet également de déoxygénérer le GO et de restaurer la structure graphitique de l'oxyde de graphène [176,184]. Elle est le plus souvent opérée sous un gaz inerte soit l'argon ou l'hélium avec un certain pourcentage d'hydrogène ($\sim 5\%$) soit sous hydrogène pur. Au fur et à mesure que la température de recuit augmente, le taux d'oxygène dans la structure diminue (Figure 1.24) [184,185]. La conductivité électronique augmente avec une élévation de la température due à la graphitisation progressive de l'oxyde de graphène [12,158,186].

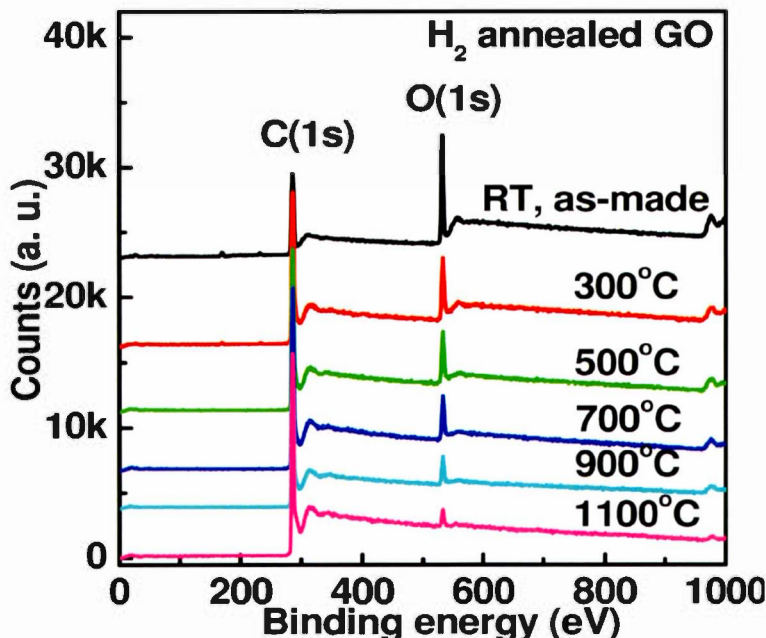


Figure 1.24 Spectres XPS d'oxydes de graphène (GO) traité sous H_2 à différentes températures sous une pression de 2 Torr [185].

Bien que l'oxydation chimique du graphite et l'exfoliation subséquente au bain ultrasons fournissent une grande quantité de monocouches d'oxyde de graphène, la réduction par voie chimique ou thermique entraîne inévitablement des défauts dans la structure du matériau comme le montrent les images obtenues par microscopie électronique en transmission (Figure 1.23C). Cependant, le procédé d'oxydation expose également un grand nombre de défauts dans la structure des feuillets de graphène qui compromettent plus ou moins les propriétés physico-chimiques du matériau bidimensionnel. Malgré les insuffisances révélées, les oxydes de graphène réduits continuent de susciter un intérêt considérable dans la communauté scientifique, compte tenu de leurs applications potentielles dans des dispositifs de stockage d'énergie tels que les supercondensateurs électrochimiques et les batteries rechargeables (Figure 1.25) [17,166,187–189].

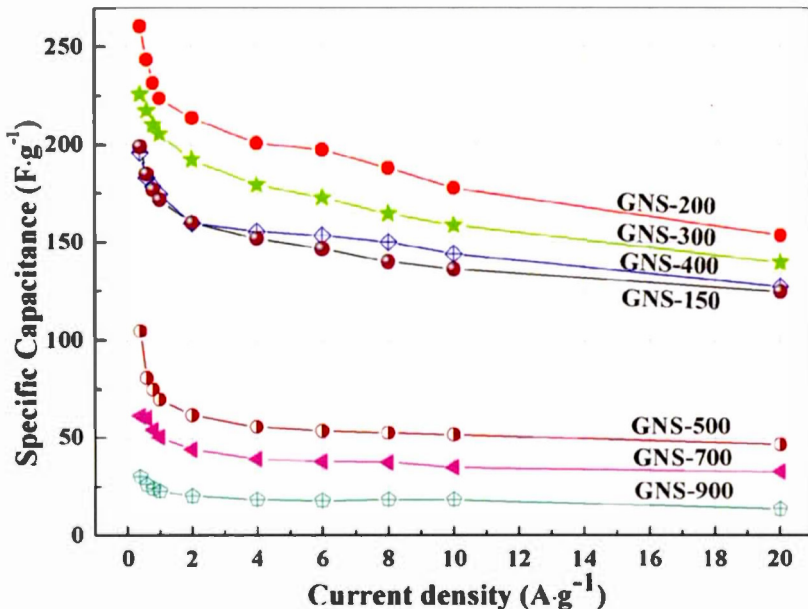


Figure 1.25 Evaluation des capacités spécifiques de différentes électrodes préparées à partir des échantillons de RGO (ou GNS), cyclées dans du KOH 6 M avec des densités de courant différentes [189].

1.3.6 Exfoliation électrochimique du graphite

L'électrochimie pour la production du graphène est apparue dans un contexte où les réactifs et les solvants organiques utilisés pour la synthèse de GO sont néfastes pour l'environnement [148,181] et que cela pose un réel problème pour une production industrielle. En revanche, l'exfoliation électrochimique du graphite présente une méthode plus verte, plus simple et capable de produire du graphène de bonne qualité et à grande échelle [143,189–193]. L'utilisation de l'électrochimie pour l'intercalation de certains ions tels que Li^+ [194], F^- [195], Ni^{2+} [196] et des composés de l'acide sulfurique [197] dans la structure du graphite est bien connue dans la

littérature. Mais, la nature du solvant est un paramètre très important pour permettre une exfoliation efficace du graphite [190].

L'exfoliation électrochimique se résume en deux principales étapes: i) une fois soumis à un potentiel, l'électrode de graphite gonfle macroscopiquement suite à l'intercalation des molécules ou ions, issus ou non de la décomposition de l'électrolyte et, ii) les feuillets exfoliés sont ensuite détachés du solide à cause de l'évolution gazeuse, et dispersés en solution (Figure 1.26) [198].

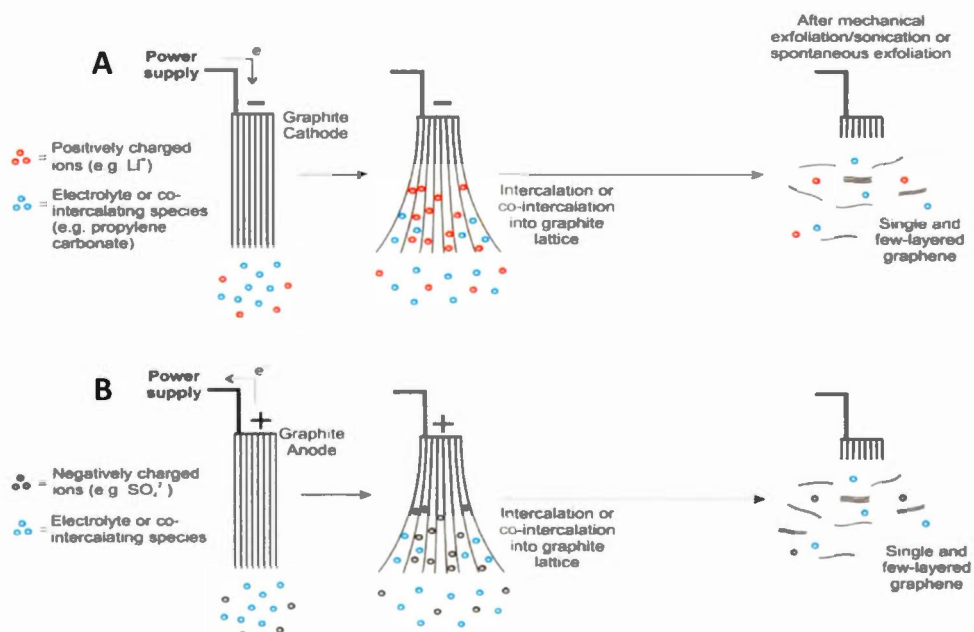


Figure 1.26 Schéma des mécanismes d'exfoliation cathodique et anodique. Une charge négative (A) ou positive (B) est créée sur une électrode de graphite en imposant un potentiel approprié, attirant des ions intercalants de charge opposée. Des molécules co-intercalantes (ex. H_2O) peuvent éventuellement être présentes au cours du processus. Des flocons de graphène sont spontanément produits lors de l'évolution de gaz ou aussi par sonication. La contre-électrode peut être en platine ou en graphite [198].

Plusieurs différents solvants et différents potentiels continuent d'être étudiés dans le but d'améliorer la technique électrochimique pour produire du graphène avec un bon rendement [192,193,198–202].

1.3.7 Méthodes industrielles de production du graphène

Le défi majeur, depuis que le graphène a été isolé pour la première fois en 2004 était d'augmenter la production à un niveau industriel. Vue les limites des méthodes académiques préexistantes, d'autres technologies ont été développées par certaines compagnies afin de produire le graphène à l'échelle industrielle. La compagnie cambridge Nanosystems a mise en place une technologie basée sur le craquage du gaz naturel (CH_4) et du dioxyde de carbone (CO_2) à partir d'une torche à plasma. Cette technique permet de produire du graphène de très haute qualité et en masse [203]. En collaboration avec l'université de Princeton, la compagnie Vorbeck Materials Corp (USA) prépare du graphène à grande échelle en soumettant l'oxyde de graphite soit à une élévation rapide (2 à 5 min) de la température (700 à 3000 °C) soit à un temps prolongé (15 à 150 min) [119,204]. En revanche, les start-up telles que Nanotech Instruments (Angstron Materials), Nanoxplore, Raymor, XG Sciences orientent leurs efforts vers le développement de procédés tels que l'exfoliation, la synthèse chimique, etc. pour la production à grande échelle de nanoplaquettes de graphène [205].

1.3.8 Conclusions

La figure 1.27 dévoile les différentes méthodes actuelles et usuelles pour la préparation du graphène et de ses dérivés. Le défi commun est de pouvoir préparer des mono-feuilles de graphène et en quantité industrielle pour pouvoir tirer profit de toutes ses propriétés.

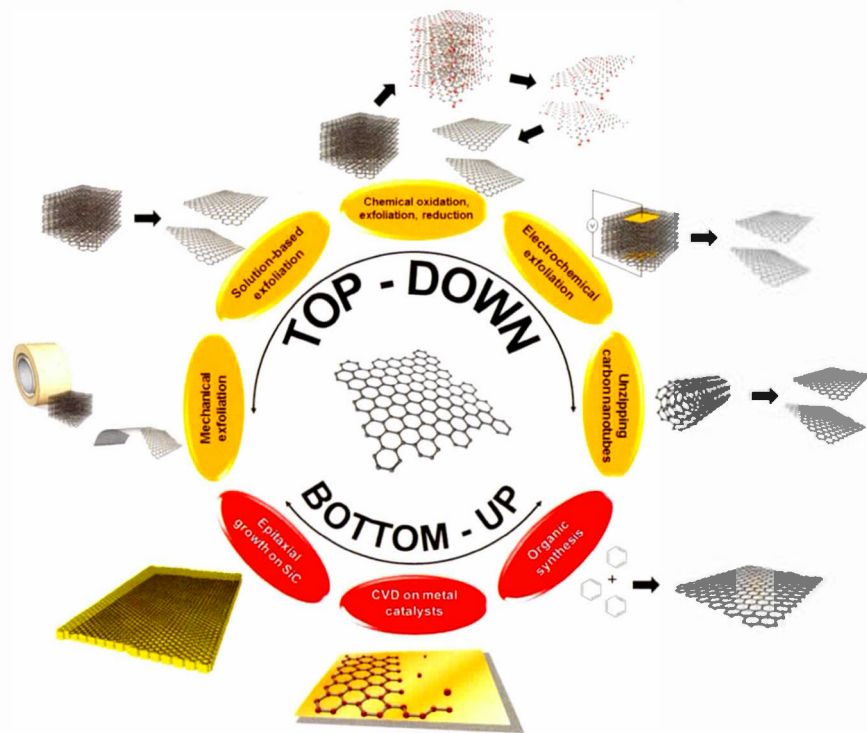


Figure 1.27 Illustration des méthodes de préparation actuelles pour le graphène et les matériaux de graphène [112].

1.4 Méthodes de fonctionnalisation /modification

Au cours des dernières années, plusieurs approches ont été développées dans le but de produire du graphène sans aucun défaut. Comme précédemment énuméré, les méthodes les plus usuelles incluent l'exfoliation du graphite, la réduction de l'oxyde de graphène (GO) et le dépôt chimique en phase vapeur (CVD). Cependant, la stabilité chimique du graphène limite ses applications. En outre, sa faible dispersibilité dans les solvants organiques et inorganiques courants ne favorise pas son interaction avec d'autres matériaux. Or dans certains cas, une bonne dispersion du graphène dans les solvants communs est requis pour la formation de nanocomposites

homogènes. Aussi, la plupart des applications électroniques sont limitées par l'absence d'une bande interdite (caractéristique d'un semiconducteur) dans le graphène parfait. Ce qui le rend moins compétitif dans le domaine des semiconducteurs et des capteurs. Par conséquent, la fonctionnalisation apparaît comme un moyen efficace pour adapter les propriétés du graphène à un large domaine d'applications [206,207]. Généralement, le graphène et ses dérivés sont modifiés par deux principales approches: la fonctionnalisation covalente et non covalente.

1.4.1 Méthodes non-covalentes de fonctionnalisation du graphène

1.4.1.1 Par des groupements organiques

La fonctionnalisation non-covalente de l'oxyde de graphène (GO), de l'oxyde de graphène réduit (RGO) et du graphène est basée sur des interactions faibles de van der Waals, les interactions π - π et les interactions électrostatiques entre le graphène les composés aromatiques cibles ou les polymères conjugués [208,209]. Cette combinaison peut produire des matériaux composites fonctionnels à base de graphène. Il est nécessaire qu'un chevauchement puisse exister entre les deux composants pour avoir une interaction notable. Généralement, la structure planaire du graphène et de la molécule cible est fortement favorisée. Les molécules aromatiques et polymères conjugués ont un grand plan aromatique et peuvent s'adsorber à la surface du graphène sans trop perturber sa conjugaison électronique sp^2 [210,211].

Bose et *coll.* ont montré qu'il est possible de fonctionnaliser les feuillets de graphène par l'acide 9-anthracène carboxylique (9-ACA) tel que montré à la figure 1.28. Ils ont pu exfolier le graphite en graphène en phase liquide, en ajoutant le 9-ACA à la solution sous ultrasons. Après l'exfoliation, les molécules d'anthracène

restent fortement attachées à la surface du graphène via les interactions π - π et facilitent ainsi la stabilisation de la suspension de graphène [145,210,212].

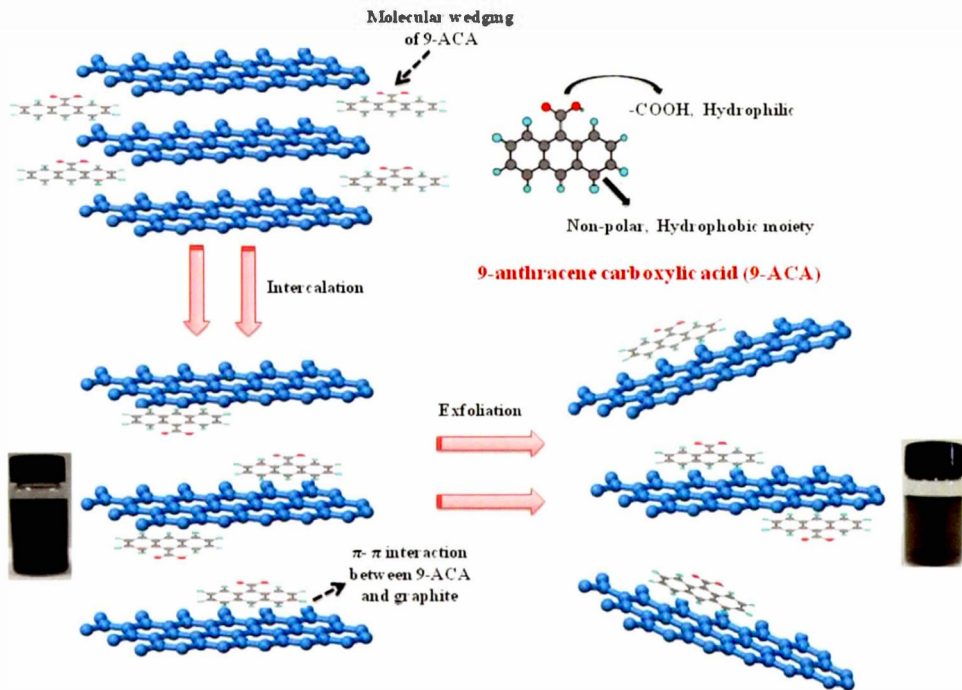


Figure 1.28 Mécanisme proposé pour la préparation d'une dispersion aqueuse stable de graphène par empilement des molécules d'anthracène sur les feuillets du graphène [210].

L'image AFM (Figure 1.29A) indique que l'épaisseur du matériau hybride graphène-anthracène est de 1,25 nm alors que l'épaisseur d'une couche unique de graphène s'avère être d'environ 0.35 nm. Par conséquent, l'image AFM confirme la liaison moléculaire non-covalente de l'anthracène au plan de base du graphène par les interactions π - π [210].

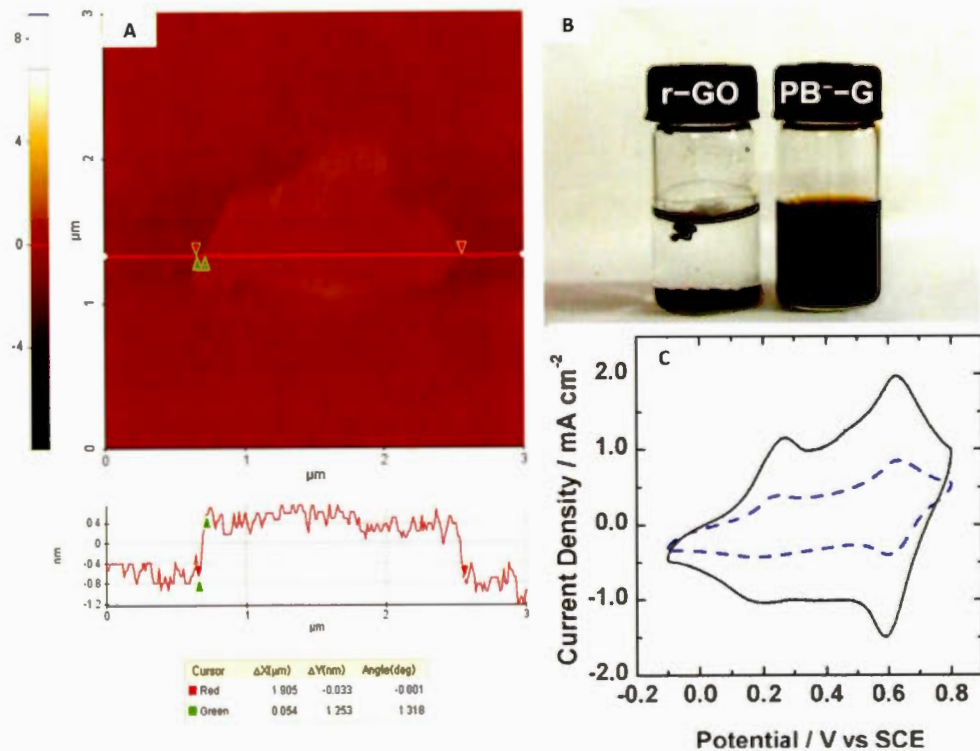


Figure 1.29 (A) Image AFM d'un feuillet de graphène fonctionnalisé [210]. (B) Images de l'oxyde de graphène réduit (r-GO) et du graphène founctionnalisé par les groupements pyrine-butyrat (PB⁻-G) dispersés dans l'eau ($0,1 \text{ mg mL}^{-1}$) [213]. (C) Voltammogrammes cycliques des électrodes modifiées de la polyaniline sulfonée (SPANI) (en pointillé) et le graphène modifié (SPANI/r-G) (ligne pleine) dans $1.0 \text{ M H}_2\text{SO}_4$ à une vitesse de balayage de 50 mV s^{-1} [214].

Les travaux réalisés par l'équipe de Shi [213], en fonctionnant le graphène par des dérivés de pyrine (pyrine-1-butyrat, PB⁻) ont permis de solubiliser le graphène dans l'eau (Figure 1.29B) [213]. La procédure adoptée est simple et facile à réaliser en une seule étape. Elle se résume par l'ajout de l'acide pyrinebutyrique et de l'hydrazine directement à la suspension de GO à 80°C . La figure 1.29C décrit

l'activité électrochimique (ligne pleine) de l'électrode composite, préparée via l'adsorption de la polyaniline sulfonée sur le graphène par les interactions π - π . On remarque un perte de densité de courant pour l'électrode non-composite SPANI [214]. Dans cette même étude, Il a été aussi démontré que la fonctionnalisation non-covalente permet d'améliorer la tenue mécanique du film en milieu aqueux, possiblement due aux fortes interactions entre les chaînes de SPANI et les plans de base du graphène.

1.4.1.2 Par des nanoparticules (NPs)

L'addition des nanoparticules métalliques ou des oxydes métalliques au graphène est aussi une autre approche non-covalente pour fonctionnaliser le graphène et ses dérivés (GO, RGO) [215,216]. Cette approche fait l'objet d'étude d'un chapitre dans cette thèse. L'inclusion des nano-matériaux métalliques tels que Au, Ag, Pt, Pd, et Cu produit des matériaux nanocomposites hybrides graphène-NPs et peut améliorer certaines limitations du graphène tout en fournissant des propriétés supplémentaires et nouvelles pour plusieurs types applications dans le domaine des biocapteurs, de la réduction du CO₂ ou O₂, des batteries, de l'optoélectronique et autres [215,217–220]. Deux principales méthodologies sont utilisées pour l'inclusion des nanoparticules dans la structure du graphène.

L'approche par réduction électrochimique est une technique simple, rapide et verte pour la préparation de matériaux hybrides graphène-NPs. Le procédé classique de dépôt électrochimique consiste en trois étapes: Dans un premier temps, on prépare le dépôt de feuilles de graphène sur une électrode (carbone vitreux, ITO), la deuxième consiste à immerger l'électrode revêtue de graphène dans une solution électrolytique contenant des précurseurs métalliques, et enfin on applique un potentiel adéquat pour réduire les cations métalliques et réaliser la déposition [216,219,221,222]. Par

exemple, Yu et *coll.* ont pu électrodepositer des nanoparticules d'or (AuNPs) sur une électrode d'oxyde d'indium et d'étain (ITO), préalablement revêtue d'une couche d'oxyde de graphène (GO). La couche de GO a aussi subi une réduction électrochimique lors du dépôt (Figure 1.30) [217,222]. La stratégie est simple et bien adaptée pour préparer des matériaux composites à grande échelle [215].

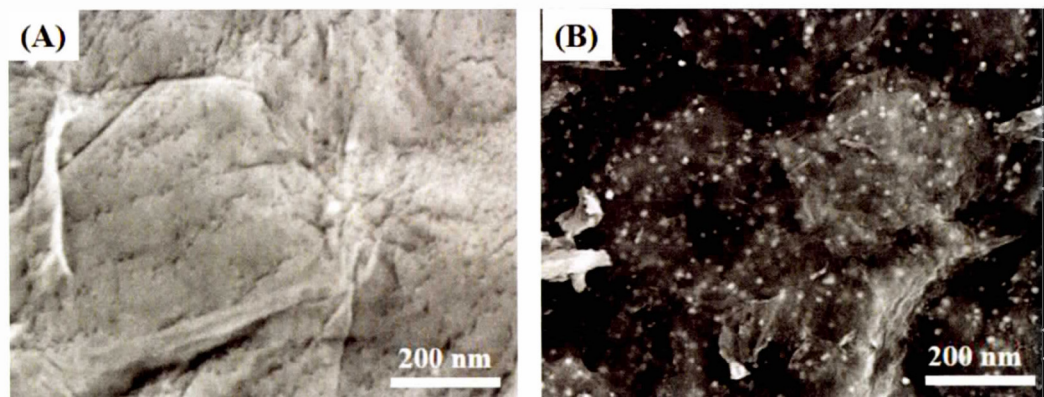


Figure 1.30 Images SEM d'un matériau nanocomposite (A) RGO et (B) RGO-AuNPs [222].

L'autre voie communément employée pour décorer le graphène, le GO ou le RGO par des nanoparticules est la méthode chimique. Elle permet d'encapsuler les nanoparticules à l'intérieur des feuillets de graphène, à cause de leur flexibilité ou d'immobiliser les nanoparticules à la surface du graphène par des interactions d'empilement π - π , des interactions de van der Waals ou surtout par des interactions électrostatiques [223,224]. L'approche principale implique la formation de nanocrystallites en solution, en présence du graphène fonctionnalisé ou non suivie de la croissance directe des nanostructures à la surface du graphène. Souvent, l'ajout d'un réducteur dans le milieu réactionnel est nécessaire. Cette méthode a fait l'objet de plusieurs travaux [218]. Par exemple, Yang et *coll.* [225] ont rapporté une stratégie

nouvelle pour la synthèse d'oxyde métallique encapsulé dans le graphène (GE-MO), par coassemblage entre l'oxyde de graphène (GO) chargé négativement et les nanoparticules d'oxyde chargées positivement (Figure 1.31). Le but de cette étude était de préparer des matériaux d'anode à haute performance pour le stockage du lithium.

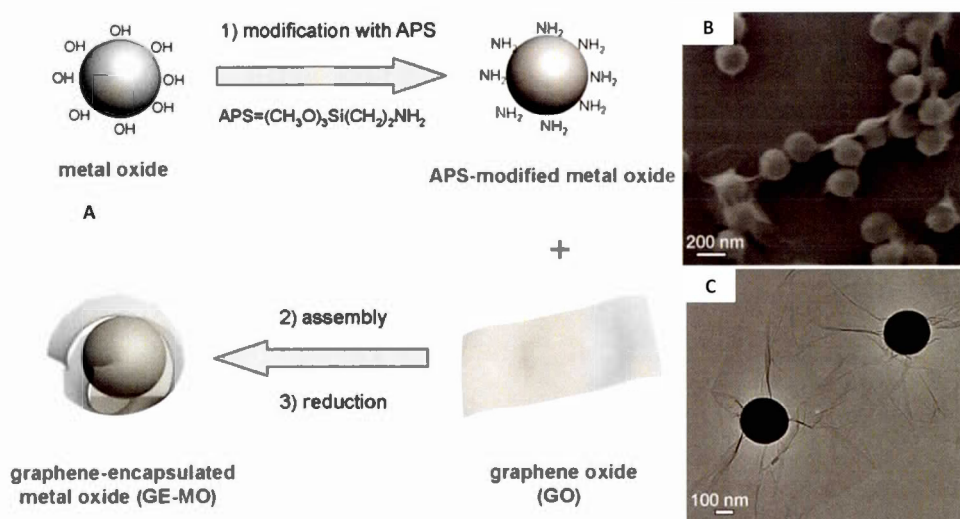


Figure 1.31 (A) Synthèse de l'oxyde métallique encapsulé dans le graphène (GE-MO) avec différentes étapes: 1- Modification de l'oxyde métallique par greffage d'aminopropyltriméthoxysilane (APS) pour rendre la surface d'oxyde chargée positivement; 2- Assemblage hybride entre les nanoparticules d'oxyde métallique chargé positivement et l'oxyde de graphène chargé négativement par des interactions électrostatiques; 3- Réduction chimique. Images (B) MEB et (C) MET des particules d'oxyde de graphène encapsulées [225].

1.4.2 Méthodes covalentes

Les réactions de fonctionnalisation covalente du graphène avec les composés organiques comprennent principalement deux voies. La formation d'une liaison covalente entre un radical libre et un atome de carbone du graphène [226] ou par l'intermédiaire des groupements fonctionnels oxygénés présents à la surface du graphène (GO, RGO) [227]. Les groupements oxygénés sont généralement localisés au bord des feuillets (COOH, OH) et dans les plans de base (C-O-C, OH) [228,229].

Une approche prometteuse de fonctionnalisation du graphène est la chimie du diazonium, largement utilisée pour modifier les propriétés de divers matériaux par greffage [230–233]. Le greffage par réduction des sels de diazonium a été rapporté dans la littérature pour la modification des feuillets de graphène [226,234–237]. L'intérêt de la méthode repose sur la facilité de préparation, la réduction rapide des sels de diazonium qui conduit aux radicaux aryles hautement réactifs et la formation d'une liaison covalente entre le composé aryle et un atomes de surface du substrat.

Le mécanisme du greffage est principalement basé sur un transfert électronique à partir du graphène, puisque riche en électrons avec sa structure sp^2 , comme le décrit bien la figure 1.32 [235]. Il s'en suit une réduction de l'ion aryle diazonium avec un dégagement gazeux d'azote (N_2) suivie de la formation de la liaison covalente entre le groupement aryle et le graphène.

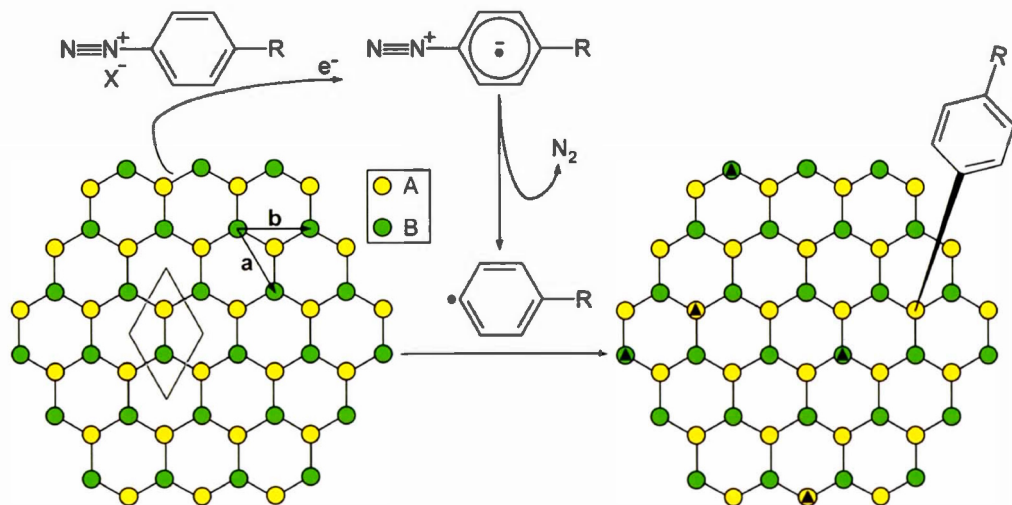


Figure 1.32 Schéma général du greffage à partir d'un sel de diazonium avec un groupe fonctionnel R et de son contre-ion X^- sur une feuille de graphène [235].

Au cours de l'attachement des groupements phényles, les atomes de carbone hybridés sp^2 se transforment en carbone sp^3 (Figure 1.33A) [238], créant ainsi des défauts dans la structure du graphène. Les défauts créés dans la structure du matériau sont confirmés par l'apparition du pic D (spectre du graphène modifié) qui, initialement est absent dans le spectre Raman du graphène non modifié (Figure 1.33B). La présence des bandes D^* et $\text{D}+\text{D}^*$ sont aussi des signes de la rupture de la symétrie du graphène due au greffage [239].

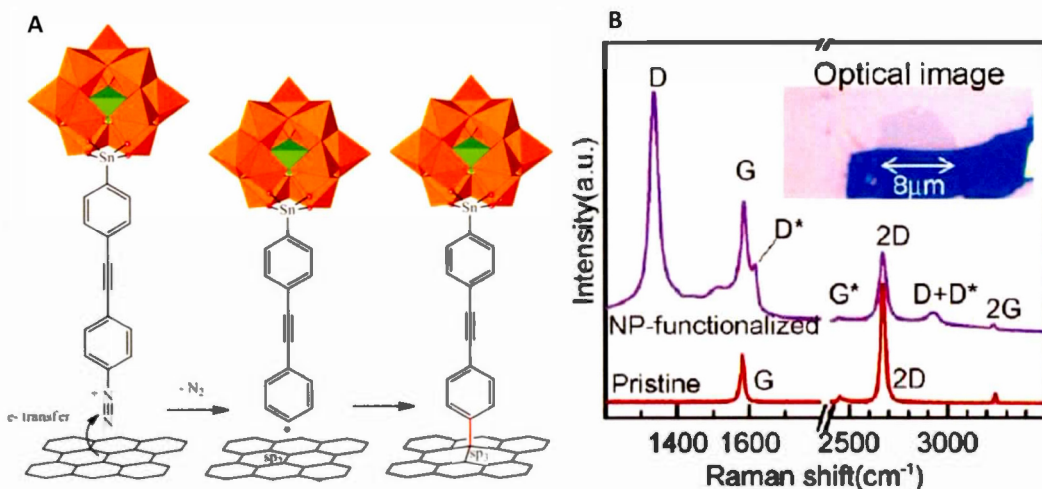


Figure 1.33 (A) Schéma du greffage du cation $\text{KMoSn}[\text{N}_2^+]$ avec le graphène mettant en exergue la liaison C-C (en rouge) [238]. (B) Spectres Raman ($\lambda = 532 \text{ nm}$) des feuillets de graphène non modifié (pristine) et modifié par le nitrophényle (NP-functionalized). En inséré, image optique d'un échantillon de graphène attaché (mono-couche) à un flocon de graphène plus épais [240].

La possibilité du transfert électronique lors du processus du greffage a été étudiée par plusieurs groupes de recherche [240–243]. La réduction de l'ion diazonium est principalement liée à la densité d'état électronique (DOS: Density of State en anglais) du graphène et du cation diazonium, mais aussi à la cinétique de réaction [241,243]. Dans ces études, il a été montré que le graphène ($E_F = -4.6 \text{ eV}$, énergie de Fermi du graphène non dopé) [244] dispose d'états occupés, donc capable d'enclencher spontanément un transfert d'électrons vers les états inoccupés des cations diazonium, ayant un potentiel redox $\sim 5.15 \text{ eV}$ (Figure 1.35) [235,245].

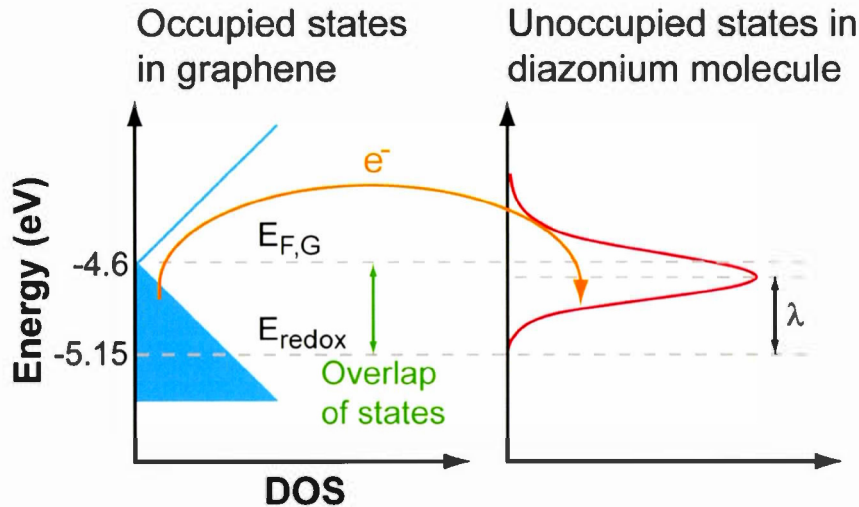


Figure 1.34 Représentation schématique des densités d'états occupés et inoccupés du graphène et d'un sel de diazonium [235].

Plusieurs autres stratégies existantes ont été adaptées au graphène, à l'oxyde de graphène et à l'oxyde de graphène réduit dans le but de les fonctionnaliser [224,227,246,247]. Les travaux réalisés par Li et *coll.* ont montré qu'il est possible de modifier le GO à partir des sites oxygénés à la surface en formant des liens covalents entre la molécule cible et les groupements hydroxyles (OH) (Figure 1.35A) [227]. La Figure 1.35B résume le processus de décoration de la surface du graphène par des dérivés dihydronaphtalène via la réaction de Diels-Alder [248].

1.4.3 Conclusions

La fonctionnalisation covalente ou non-covalente permet en général, de moduler les propriétés de surface du graphène et ses dérivés afin de les rendre plus compétitif en améliorant ses capacités pour différents types d'applications. Le graphène, ayant une structure planaire sp^2 est aussi prédisposé à s'aggrégger

rapidement lors de la préparation. Alors l'un des rôles, non le moindre de la modification est de prévenir efficacement ce phénomène.

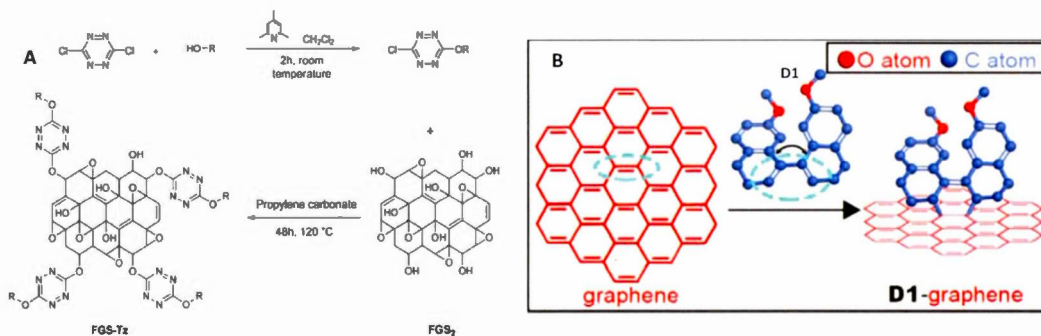


Figure 1.35 A) Processus général du greffage des chlorotétrazines substituées (Tz) sur l'oxyde de graphène (FGS) [227], (B) Représentation schématique de la réaction de Diels-Alder entre un dérivé dihydronaphalène (D1) et le graphène [248].

1.5 Objectifs de la thèse

Ce projet de recherche vise principalement à préparer des matériaux hybrides à base de graphène, à partir de nouvelles méthodes ou celles préexistantes dans le but d'améliorer ou de modifier les propriétés électroniques et optiques du matériau en variant certains paramètres de synthèse. L'une des principales difficultés, qui se présente comme un défis majeur pour l'industrie et la recherche académique est de produire du graphène de haute qualité et en grande quantité. Un autre objectif est de réaliser la fonctionnalisation du graphène, de manière covalente avec des molécules organiques ou non-covalente via un dépôt de nanoparticules métalliques à leur surface, se basant sur des procédures améliorées, ce qui rendrait le graphène plus concurrentiel dans plusieurs domaines d'applications.

Cette thèse s'articule autour de trois principaux chapitres, présentés sous forme d'articles scientifiques.

Dans le chapitre I du manuscrit, nous nous sommes intéressés à la préparation de certains dérivés du graphène. L'oxyde de graphène réduit, communément nommé RGO (reduced graphene oxide, en anglais) est obtenu par réduction thermique de l'oxyde de graphène (GO: graphene oxide, en anglais). Les propriétés optiques et électroniques du RGO ont été ensuite comparées à celui modifié via la chimie du diazonium, par réaction spontanée. Ces travaux ont fait l'objet d'une publication dans le journal scientifique, RSC Advances.

La synthèse du graphène par exfoliation électrochimique et sa modification subséquente par greffage covalent a été étudiée dans le chapitre II. D'une part, cette étude a conduit à la mise en place d'une voie de fonctionnalisation innovante en utilisant les cations diazonium. Les résultats obtenus dans ce chapitre ont été publiés, dans le périodique Carbon.

Enfin, le dernier chapitre est consacré à la synthèse des matériaux nanocomposites graphène/nanoparticules métalliques. Ainsi, l'argent et l'or ont servi de matériaux modèles pour cette étude. Les feuillets de graphène ont été décorés par Ag, Au et Ag-Au de manière non-covalente, contrairement à la fonctionnalisation (covalente) utilisée dans les deux chapitres précédents. Du point de vue de l'application, l'intégration des nanoparticules dans une matrice de graphène doit permettre d'obtenir des matériaux présentant une activité électrocatalytique pour la réduction de l'oxygène.

En conclusion de ces travaux de thèse, nous proposons des pistes de réflexion pour des projets futurs à la suite d'une brève discussion.

CHAPITRE I

SYNTHESIS AND CHARACTERIZATION OF SULFOPHENYL-FUNCTIONALIZED REDUCED GRAPHENE OXIDE SHEETS

Résumé de l'article

L'oxyde de graphène réduit (RGO), préparé par la méthode de Hummers et réduction thermique a montré une très grande surface BET ($900 \text{ m}^2/\text{g}$) avec une bande interdite relativement faible de 0.95 eV. Suite à la modification chimique par greffage spontané de groupements sulfophényles, le SRGO présente une surface spécifique de plus petite valeur ($300 \text{ m}^2/\text{g}$), avec une légère augmentation de la bande interdite (1.18 eV). Le greffage des groupements sulfophényles à la surface du RGO, a causé une diminution de la conductivité électronique et de la porosité du matériau. La spectroscopie Raman, la microscopie électronique en transmission, la mesure de la surface BET, l'analyse de la bande interdite et la conductivité électronique ont permis de confirmer le greffage covalent à la surface du RGO. Les résultats de ces travaux ont été publiés dans le périodique RSC Advances (*RSC Adv.*, 2017, 7, 27224-27234; DOI:10.1039/C6RA2831J).

Contribution des auteurs:**Benjamin Diby Ossonon**

L'auteur principal a effectué toutes les manipulations, toutes les expériences au laboratoire. Il a également proposé un plan et a écrit l'article en faisant les figures et les recherches bibliographiques appropriées. Benjamin a participé à la correction de l'article avant sa soumission finale.

Daniel Bélanger

Le co-auteur a supervisé le projet de recherche et les expériences en laboratoire, il a donné de nombreux conseils et des directives. Il a également contribué à la rédaction et aux corrections de l'article avant sa soumission.

Article 1. Synthesis and Characterization of Sulfophenyl-functionalized Reduced Graphene Oxide Sheets

B. D. Ossonon and D. Bélanger

Département Chimie, Université du Québec à Montréal, CP8888, Succ. Centre Ville, Montréal, Québec, Canada H3C 3P8

Paru dans **RSC Adv.**, 2017, 7, 27224-27234

Abstract

We report the modification of graphene oxide (GO) by thermal reduction to obtain reduced graphene oxide (RGO) and subsequent modification by sulfophenyl groups as well as the characterization of these materials by thermogravimetric analysis coupled with mass spectroscopy (TGA-MS). The chemical modification of RGO was carried out by spontaneous reaction of RGO with in situ generated sulfophenyl diazonium ions. The three different types of materials were also characterized by elemental analysis, Fourier transform infrared spectroscopy (FTIR), Raman spectroscopy and X-ray photoelectron spectroscopy (XPS). The characteristic absorption band at 1034 and 1160 cm⁻¹ in the FTIR spectrum of the sulfophenyl-modified RGO (SRGO), as well as Raman spectroscopy and TGA-MS data indicated that sulfophenyl groups were successfully grafted on RGO. The presence of organic molecules at the SRGO surface was also demonstrated by elemental analysis, transmission electron microscopy, energy dispersive X-ray spectroscopy and XPS. TGA data and elemental analysis results showed that the loading of sulfophenyl groups was about 12 wt.% and UV-visible-near IR spectroscopy confirms the slight increase of the optical band gap of RGO after covalent grafting of sulfophenyl groups on its surface.

1 Introduction

Graphene is a two-dimensional carbon material consisting in a single-atom-thick graphitic layer that has been used in electronic devices^{1,2}, composite materials^{3,4} and energy storage systems⁵⁻⁹. Graphene is commonly produced from natural graphite that is widely available at low cost¹⁰. However, graphene is not directly prepared from graphite. Instead it is obtained by reduction of graphene oxide (GO), previously produced by the Hummers' method¹¹. The reduction of GO to graphene restores the electronic properties of graphene and has been performed by using reducing agents such as hydrazine (N_2H_4)^{12,13}, sodium borohydride ($NaBH_4$)^{14,15}, dimethyl hydrazine³ and hydriodic acid (HI)^{16,17}. However, these reducing agents may be harmful for the environment or too expensive when used for mass production of graphene. Also, the quality of the reduced GO, RGO, strongly depends on the reducing agent and other experimental conditions¹⁸. Alternatively, thermal reduction, which is considered a green method because no hazardous chemicals are required, can also afford RGO.

Graphene possesses a zero band gap that severely limits its applications due to its chemical inertness^{4,19}. Opening the band gap of graphene and its derivative by doping, intercalation or grafting by organic molecules would be useful for applications mentioned above^{6,8}. Importantly, functionalization with organic molecules led to a good dispersion of graphene in common organic solvents²⁰. For several large-scale applications, RGO is a more widely used and attractive material than graphene. Similarly, its functionalization is important to modify its properties and open up its applications to the areas.

Here we report, a detailed investigation of graphene oxide (GO), reduced graphene oxide (RGO) and sulfophenyl-modified RGO (SRGO) by

thermogravimetric analysis coupled with mass spectrometry (TGA-MS) analysis. The TGA-MS data confirmed the covalent grafting of sulfophenyl groups on RGO. The three materials were also characterized by nitrogen gas adsorption, FTIR, four-point probe measurements as well as by Raman and X-ray photoelectron spectroscopy.

2 Experimental

2.1 Preparation of graphene oxide (GO)

Graphene oxide was synthesized from natural graphite (<44 μ m, 99.99%, supplied by Sigma-Aldrich) through the Hummers' method¹¹ which has been improved to be more environmentally friendly and produce graphene in good yield (95%). The graphite is first pre-oxidized by mixing graphite powder (5 g) with concentrated sulfuric acid (H₂SO₄, 12.5 mL), potassium persulfate (K₂S₂O₈, 2.5 g) and phosphorus pentoxide (P₂O₅, 2.5 g). The mixture was heated at 80 °C for 6 hours. After dilution with 500 mL of H₂O, the mixture was stirred at room temperature overnight. After that, the product is recovered by centrifugation and washed thoroughly with Nanopure water until the filtrate has a pH close to 7 (neutral). The product obtained is then dried at room temperature for one day. Then, the pre-oxidized graphite is dispersed in H₂SO₄ (0 °C, 115 mL). The temperature of the mixture is carefully controlled to not exceed 10 °C. Subsequently, potassium permanganate (KMnO₄, 15 g) is gradually added with constant stirring for 1 hour. The dispersion is then incubated at 35 °C for 2h and this is followed by the addition of Nanopure water (225 mL) in small portions (15 mL) to control the temperature of the mixture, which must remain below 50 °C. In order to completely dissolve the KMnO₄ remaining, hydrogen peroxide (H₂O₂ 30%, 12.5 mL) was immediately added at the end of a second dilution (H₂O, 700 mL), and the mixture is stirred for 48 hours. Finally, the suspension is filtered, washed first with HCl (10%) to remove residual

metal ions, and repeatedly with Nanopure water until the pH of filtrate becomes neutral. The filtrate is quickly tested by adding a few drops of 1 M NaOH to verify the presence of metal ions in GO. The product obtained (graphite oxide) is then dried in air. The resultant graphite oxide was dispersed in Nanopure water kept in the ultrasonic bath for 24 hours to maximize exfoliation. A homogeneous and stable colloidal suspension for several months is obtained (Figure 1, GO).

2.2 Preparation of reduced graphene oxide (RGO)

The reduced graphene oxide (RGO) is obtained by thermal reduction of GO in Ar/5% H₂ at various temperatures for 2h. The resulting RGO can be dispersed in water and the dispersion stayed stable for few hours, as shown in Figure 1.

2.3 Covalent attachment of 4-sulfophenyl groups by the diazonium chemistry on RGO surface

Typically, a mass of 100 mg of RGO is dispersed in 100 mL of an acetonitrile/H₂O (50:50, v/v) mixture and a homogeneous and stable colloidal suspension was obtained after sonication, for 30 min. Then, 15 mmol of amine (4-aminobenzenesulfonic acid) and an excess of sodium nitrite (22.5 mmol; 1.5 equiv. compared to the amine) was directly added to the dispersion. The mixture was dispersed by sonication during an additional 30 min to completely dissolve the reagents and this was followed by the addition of 10 mL of concentrated HCl. The reaction mixture remained under agitation for 24 hours at room temperature. The dispersion was finally vacuum filtered on a nylon filtration membrane having a pore size diameter of 0.47 µm (Pall) and the resulting powder was successively washed with a mixture acetonitrile/Nanopure water, acetonitrile, DMF, methanol and acetone. Finally, the resulting modified-RGO (SRGO) was dried under vacuum at 80 °C overnight before being subjected to thermal annealing under Ar atmosphere at 250 °C

for 1 h. The resulting powder is dispersible in water and remains stable for several days (Figure 1, SRGO).



Figure 1. Optical images of GO, RGO and SRGO dispersed in water at the concentration of 0.5 mg mL^{-1}

2.4 Morphological and structural characterization

The morphology of the graphene materials was investigated by transmission electron microscopy (TEM) using a 200 keV JOEL JEM-2100F model transmission electron microscope operated with a bright field image. The energy band gap of reduced graphene oxide (RGO) and sulfophenyl-modified reduced graphene oxide (SRGO) was determined at room temperature using UV/VIS/NIR Spectrophotometer Lambda 750. For these analyses, the graphene samples were dispersed in NMP (N-methyl-2-pyrrolidone) to form colloidal suspensions (0.03 mg mL^{-1}). The optical band gap (E_g) of RGO and SRGO were estimated using the Tauc-David Mott equation (Eq. 1)²¹⁻²⁵.

$$(\alpha h\nu)^n = A(h\nu - E_g) \quad (1)$$

where $h\nu$ is the photon energy (h is Planck's constant, ν is the light frequency), α the absorption coefficient, E_g is the optical gap, the nature of band transition characterized by $n = 1/2, 2, 3/2$ and 3 and the constant ,which is different for each transition²⁵. Fourier Transform Infrared (FTIR) spectroscopy was employed to characterize the graphene materials using the Nicolet 6700 FTIR in the 3800–700 cm⁻¹ region. XPS spectra were collected using the spectrophotometer PHI 5600-ci (Physical Electronics, Eden Prairie, MN, USA). The excitation source used for survey spectra was by standard Al K_α (1486.6 eV) X-rays at 400 W and for core level spectra, by Mg K_α (1253.6 eV) X-rays at 150 W. The analyses were performed without charge compensation at an angle of 45° with the surface. The detector aperture was set at 5 and the surface area analyzed was 0.016 cm². The core level spectra were curve-fitted with the Casa XPS software by using mixed Gaussian-Lorentzian product function (70% Gaussian). Each spectrum was corrected with respect to C 1s at 284.5 eV (C sp² graphite like carbon) and a Shirley type background subtraction was performed before curve-fitting. Thermogravimetric analysis coupled with mass spectroscopy (TGA-MS) was carried out with a thermal gravimetric analyzer (TA Instruments TGA (Q500) / Discovery MS). Samples of typically 2 mg were placed in Pt pans and heated from 30 to 900°C with a temperature ramp of 5°C/min, under flowing helium (He) atmosphere. Raman spectroscopy measurements were performed using a micro-Raman system (UHTS300) with excitation from an argon ion laser beam (532 nm) at low power level (2 mW) in order to avoid damaging the organic functional groups. The surface area and pore volume were quantified using the Brunauer–Emmett–Teller (BET) method from the adsorption branch data set recorded for P/P₀ values between 3×10^{-1} and 5×10^{-2} . The volume of nitrogen adsorbed was recorded for relative

pressures (P/P_0) ranging from 1×10^{-6} to 1. The density functional theory (DFT) was used to provide a much more accurate approach to pore size analysis²⁶. Prior to measurements, the sample was degassed for 4 h under vacuum. Electronic conductivity of GO, RGO and SRGO films was obtained at room temperature by using a 4-point probe measurement by using a Keithley 6220 DC precision current source (US). The GO, RGO and SRGO films were obtained as follows. The samples were dispersed in water by ultrasonication for 30 min and the resulting suspensions were filtered through a polytetrafluoroethylene (PTFE) membrane filter by vacuum filtration and dried under vacuum at 70 °C overnight. The electrical conductivities were calculated by using the following equation²⁷:

$$(\sigma, \text{ S. cm}^{-1}) = \frac{1}{\rho} = \frac{\ln 2}{\pi d R} = \frac{1}{4.53 d R} \quad (2)$$

where ρ (Ω cm) is the resistivity, d (cm) is the sample thickness and R (Ω) is the resistance.

3 Results and discussion

3.1 Morphological characterization of RGO and SRGO

TEM images were employed to study the morphology of RGO and SRGO. Figure 2a clearly shows that the RGO sheets are almost transparent, suggesting that they consist of a few layers. The EDX spectrum (Figure 2a) of the RGO sample confirms the presence of only carbon and of a small amount of oxygen (O/C: 0.08). On the other hand, Figure 2b exhibits aggregated and wrinkled sheets. This observation demonstrates that the attachment of organic groups on the surface of graphene sheets favour their overlapping and folding^{20,28-30}. It is an indirect way to confirm the functionalization of RGO sheets with organic molecules. The EDX

spectrum of SRGO (Figure 2b) shows sulfur peaks that confirm the presence of sulfophenyl groups on reduced graphene oxide.

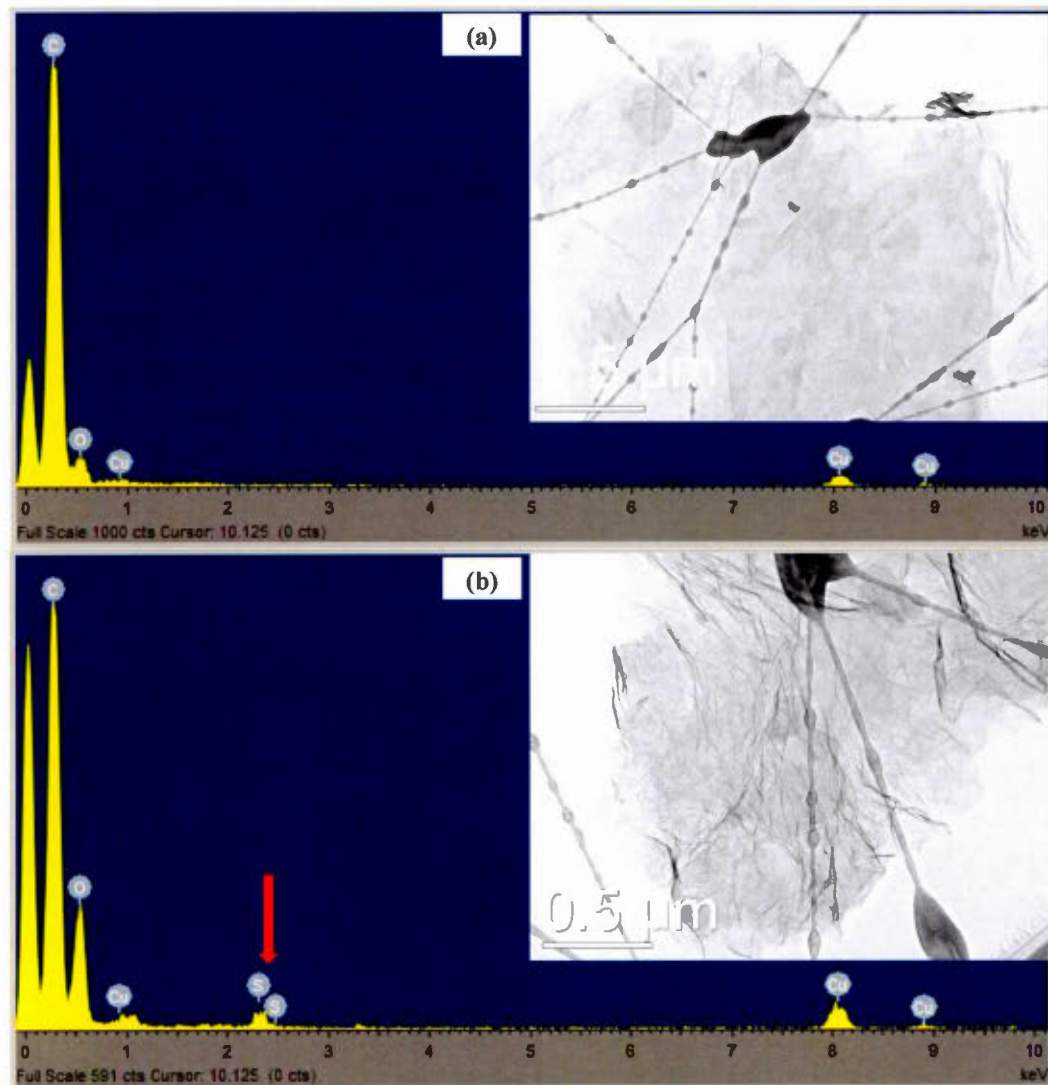


Figure 2. EDX spectra and TEM images of (a) RGO and (b) SRGO.

3.2 Optical band gap

The visible/near-infrared absorption spectra of RGO and SRGO presented in Figures 3a and b were measured to evaluate the optical band gap of graphene materials. The absorption spectra of RGO and SRGO show an absorption band around 1430 nm. The optical band gap (E_g) of the graphene materials was estimated from the absorption spectra (Supporting Information, Figure S9) by plotting $(\alpha h\nu)^2$ versus $h\nu$, as shown in Figure 3c and d, and extrapolating the linear region of the curve to the x-axis³¹. The band gap slightly increased following RGO functionalization, from 0.95³² to 1.18 eV SRGO, indicating that the optical properties of RGO have been changed after chemical modification with sulfophenyl groups³³.

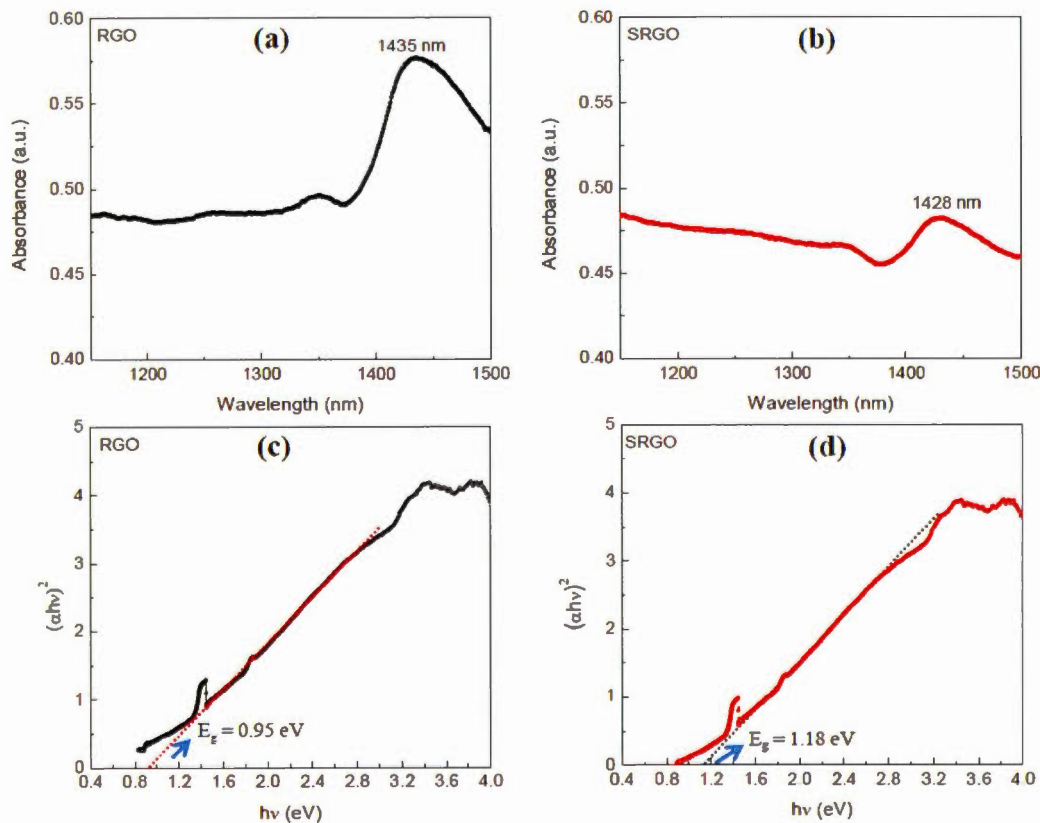


Figure 3. Visible/near-infrared spectra of (a) RGO, (b) SRGO and the plot of $(\alpha h\nu)^2$ as a function of $h\nu$ for (c) RGO and (d) SRGO (see Supporting Information, Figure S9 for complete absorption spectra).

3.3 Nitrogen gas adsorption

Figure 4a shows the nitrogen adsorption/desorption isotherm at 77 K for GO, RGO and SRGO. The adsorption isotherm of GO is featureless and shows a small volume of adsorbed nitrogen gas at low relative pressure (Figure 4a, GO and inset)³⁴.

This translates in a low specific surface areas of 25 and $15 \text{ m}^2 \text{ g}^{-1}$ according to BET and DFT Monte Carlo approaches, respectively (Table 1), which is in agreement with that reported in the literature³⁵. Both unmodified and modified RGO present mixed type I and type II isotherms for low and high relative pressure (P/P_0)^{9,36,37}, respectively. At low P/P_0 (0-0.5), the low adsorbed volume for RGO and SRGO is characteristic of mesoporous-like material, which is confirmed by the plateau and a H3 hysteresis loop^{38,39}. It can be seen that, after modification of RGO, a drop of the adsorbed volume is observed for SRGO at low relative pressure. The effect of organic molecules grafting on graphene sheets can be quantified by BET surface area (Table 1), the cumulated surface area (Figure 4b) as well as the pore size distribution (Figure 4c).

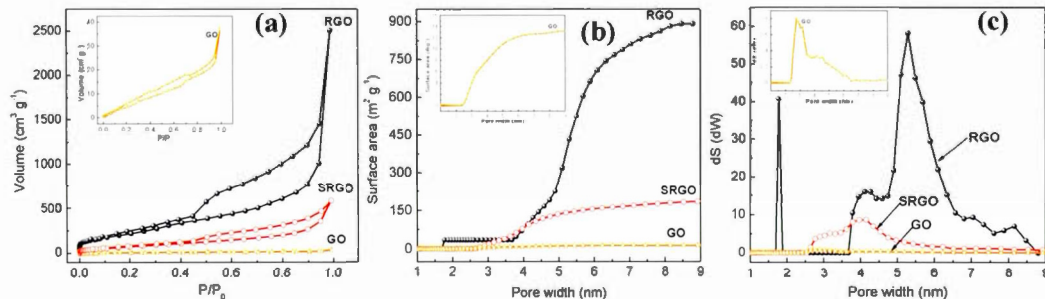


Figure 4. a) N_2 adsorption isotherms of graphene oxide, reduced graphene oxide before (RGO) and after reaction with in situ-generated 4-sulfophenyl diazonium cations (SRGO), b) Cumulated surface area vs. pore width of GO, RGO and SRGO, c) Pore size distribution of GO, RGO and SRGO. The insets present the data for GO at a more sensitive scale.

The BET surface area of RGO is about $900 \text{ m}^2/\text{g}$ and the material consists of small mesopores (2-50 nm) (Figure 4c). The high specific surface area demonstrates that the thermal reduction with loss of oxygen functional groups created porosity.

Although, it is still far below to the theoretical value for completely exfoliated and isolated graphene sheets ($2630\text{ m}^2/\text{g}$)^{4,40,41}, it compares well with those published in the literature^{12,41–43}. The lower value could be due to the agglomeration/precipitation and partial overlapping of reduced sheets during the thermal reduction process, which could lead to inaccessible surface⁴². Following grafting of sulfophenyl groups, the BET surface area decreased to $300\text{ m}^2/\text{g}$ for SRGO (Figure 4b and Table 1). This decrease of the BET surface area provides indirect evidence for grafting. Obviously, the attachment of organic molecules at the RGO surface causes changes in the graphene structure and creates a similar situation to that of the oxides on the surface of the graphene sheets^{44,45}. The grafting block some pores of graphene sheets aggregates which make them inaccessible⁹, which creates a significant decrease of the cumulated surface area (Figure 4b) and a noticeable difference of the pore size distribution (Figure 4c). Interestingly, grafting of sulfophenyl groups lead to smaller pores which might be formed by the decarboxylation of groups present on RGO^{45,46}.

Table 1 Specific surface areas and electronic conductivity of graphene oxide (GO), reduced graphene oxide (RGO) and sulfophenyl-modified reduced graphene oxide (SRGO).

Sample	BET Surface area (m ² /g)	DFT Surface area (m ² /g)	Electronic conductivity, σ (S cm ⁻¹)
GO	25	15	0.5
RGO	900	895	7.7
SRGO	300	200	2.2

3.4 FTIR

Figure 5 shows the Fourier transform infrared spectroscopy (FTIR) spectra of GO, RGO and SRGO. The spectrum of GO (Figure 5a) displays the presence of bands associated to C-O (ν_{C-O} at 1048 cm^{-1}), C-O-C (ν_{C-O-C} at 1223 cm^{-1}), C-OH (ν_{C-O-H} at 1376 cm^{-1}), C=O in carboxylic acid and carbonyl moieties that are present mostly along sheet edges but also on the basal plane of graphene sheets ($\nu_{C=O}$ at 1725 cm^{-1}) and a broad peak between 3000 and 3500 cm^{-1} corresponding to O-H vibration^{13,43,47}. The RGO spectrum exhibits only two peaks at 1160 cm^{-1} (ν_{C-O-H}) and 1550 cm^{-1} ($\nu_{C=C}$), which suggests that the GO has been effectively reduced during the process. The slight shift of these two bands to higher energy indicates the restoration of the π -network⁴³. The SRGO spectrum shows new bands at 1034 and 1160 cm^{-1} , which fall within the range of the symmetric and asymmetric stretching modes of $-SO_3H$ functional groups and demonstrate the presence of sulfophenyl groups on RGO^{48–50}.

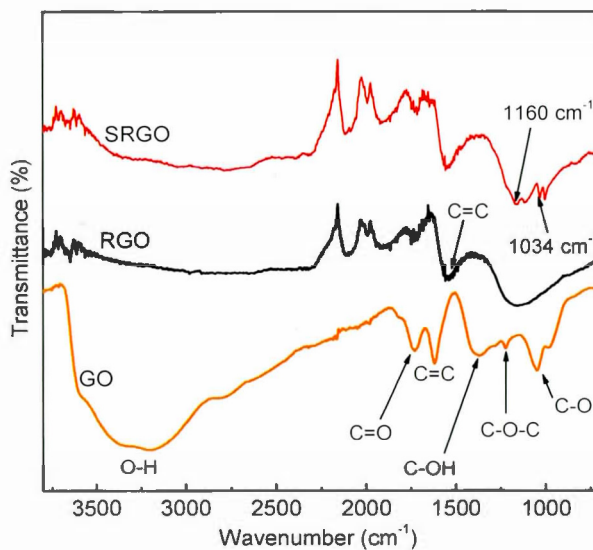


Figure 5. FTIR curves of graphene oxide, reduced graphene oxide and sulfophenyl acid groups modified RGO

3.5 Raman Spectroscopy

Raman spectroscopy provides valuable information for graphene and its derivates because it is very sensitive to the electronic structure of the carbon nanostructures, therefore the degree of hybridization, the crystal disorder and the extent of chemical modification^{20,51}. Figure 6 shows the Raman spectra obtained for GO, RGO and SRGO. Each spectrum exhibits a G band corresponding to the first-order scattering of the E_{2g} mode⁴² around 1600 cm^{-1} and a D band arising from the doubly resonant disorder-induced mode at $\sim 1350\text{ cm}^{-1}$ ⁵²⁻⁵⁶. The ratio of the intensity of these two bands (I_D/I_G) is included on the figure.

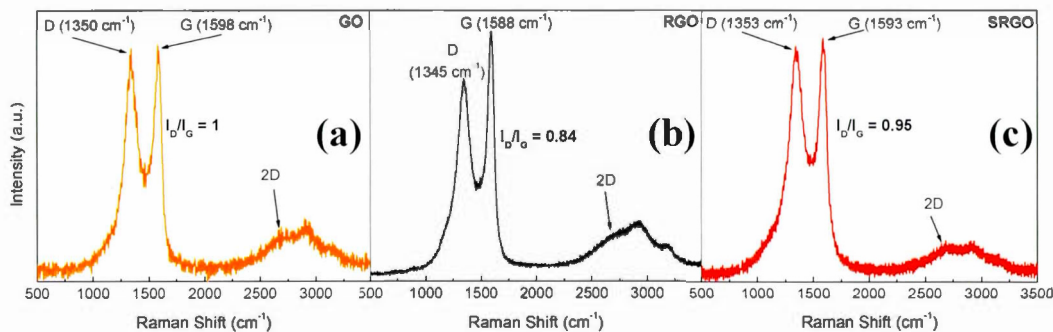


Figure 6. Raman spectra of GO, RGO and SRGO recorded using 532 nm laser excitation.

The GO sample shows a prominent D peak with a I_D/I_G of 1 indicative of significant structural disorder created due to the presence of oxygen functional groups^{57,58}. Consequently, the sharp increase of the I_D/I_G ratio from ~0.09 for pristine graphite (Supporting Information, Figure S10) indicates a decrease in the in-plane crystal and a partial amorphization of graphite, by conversion of sp^2 to sp^3 carbon bonds. The G peak of GO is shifted to higher energy (~19 cm⁻¹) and broadened significantly compared to that of pristine graphite (Supporting Information, Figure S10)^{52,56,57,59}. Following thermal reduction of graphene oxide, the vibration frequency of the G band decreases to 1588 cm⁻¹ (Figure 6b), a value still slightly higher than that of pristine graphite. This phenomenon could be attributed to the influence of residual defects and isolated double bonds in RGO^{56,60}. Nevertheless, the I_D/I_G ratio in this case decreases to 0.84, indicating that there were some structural changes occurring during the thermal reduction process, which did not much alter the structure of RGO but partially restored the graphitic (sp^2) network⁵⁸. Figure 6c shows the Raman spectrum of functionalized RGO (SRGO) by sulfophenyl groups. The increase of the I_D/I_G ratio from 0.84 to 0.95 reflects the enhancement of disorder after grafting which is due to the transformation of sp^2 carbon to sp^3 during the covalent attachment

of organic molecules on graphene sheets²⁰. The slight shift of G-band ($\sim 5 \text{ cm}^{-1}$) to higher energy confirms the covalent grafting of organic molecules, which often isolates sp^2 C atoms^{13,53,61}.

The shape and the position of 2D band of GO, RGO and SRGO spectra around 2680 cm^{-1} indicate that these graphene materials consist of few layers^{62,63}. Also, it provides information on the quality of graphene oxide initially synthesized. Typically, the low intensity of 2D peak and the profile recorded in this region are the signature of graphene oxide and its derivatives^{58,64}. This low intensity and broad 2D peak for GO compared with those of electrochemically exfoliated graphene (EG)^{20,54} or prepared by chemical vapor deposition (CVD)⁵⁵⁻⁵⁷ reflects the more important contribution of the steric effects of oxygen functionalities on the stacked layers as well as the partial amorphization and reduction in sp^2 domains^{43,52}.

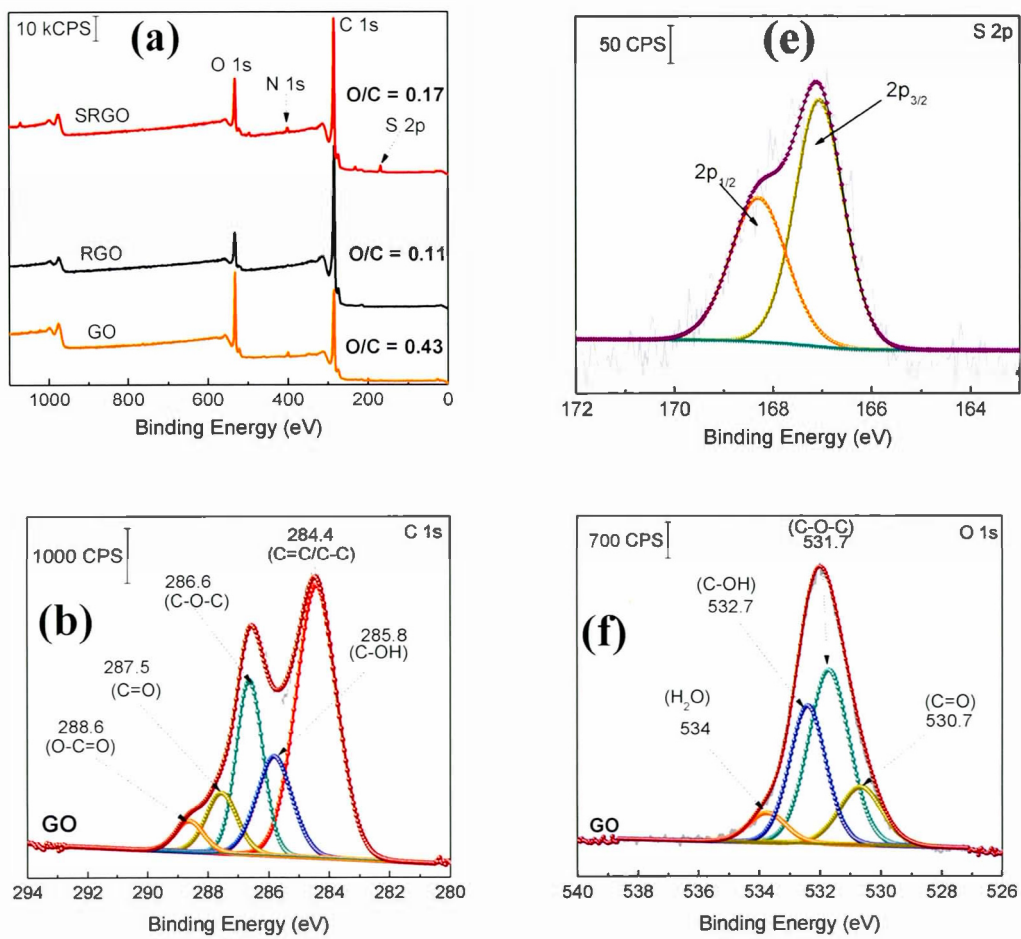
3.6 Electrical conductivity measurements

The electronic conductivities of GO, RGO and SRGO films are collected in Table 1. The low conductivity of graphene oxide (0.5 S cm^{-1}) is due to the lack of π -electronic conjugation caused by the extensive oxidation of graphite during the Hummers process¹¹. The thermal reduction increases the conductivity^{68,69} to 7.7 S cm^{-1} . Theoretically, the reduction of GO should firstly remove the oxygen functionalities groups, secondly rehybridize the sp^3 carbon atoms to sp^2 C and finally leave the material defects free like pristine graphene. However, no reduction method could totally restore the sp^2 structure of graphene. Then, the residual defects will affect the properties especially the electrical conductivity of RGO^{17,69-71}. The higher conductivity of RGO is in good agreement with its lower I_D/I_G ratio relative to that of GO. The significant decrease of electrical conductivity of SRGO (Table 1) is related to the covalent grafting of organic molecules that converts some sp^2 C atoms to sp^3 C

atoms resulting in the increase of the I_D/I_G ratio (Figure 6c) and disruption of the π -network.

3.7 X-ray Photoelectron Spectroscopy (XPS)

XPS is a valuable tool for the surface chemical analysis of carbon nanostructure materials and to confirm the immobilization of the different functional groups at the graphene surface during the synthesis or its functionalization^{45,72,73}. Figure 7 shows a set of XPS spectra for GO, RGO and SRGO. The survey spectra of GO and RGO exhibit the characteristic C 1s peak at 285 eV and O 1s at 533 eV and for GO an additional small N 1s peak at 400 eV which could be related the trapping of molecular nitrogen⁶². The decrease of the O/C ratio from 0.43 to 0.11 after GO reduction to RGO demonstrates that thermal annealing eliminates most of the oxygen functionalities of graphene oxide^{18,69,75}. A decrease of the intensity of N 1s peak is also noticeable. Following RGO functionalization by sulfophenyl groups, the O/C ratio increases from 0.11 to 0.17 due to the sulfonate groups ($-\text{SO}_3^-$) immobilized on graphene sheets. In addition, the SRGO survey spectrum (Figure 7a) displays additional peaks at 230 and 167.7 eV assigned to the sulfonate groups (S 2s and S 2p, respectively)^{76,77}. The N 1s signal observed at 400 eV indicates the formation of azo bridges (C–N=N–C) that are commonly present in grafted modified carbon materials by using diazonium cations^{46,78–82}. Their presence could be used as an indirect proof of grafting⁸³. Furthermore, core level spectra were recorded for the three samples (GO, RGO and SRGO) and curve-fitted spectra are shown in Figure 7b-h.



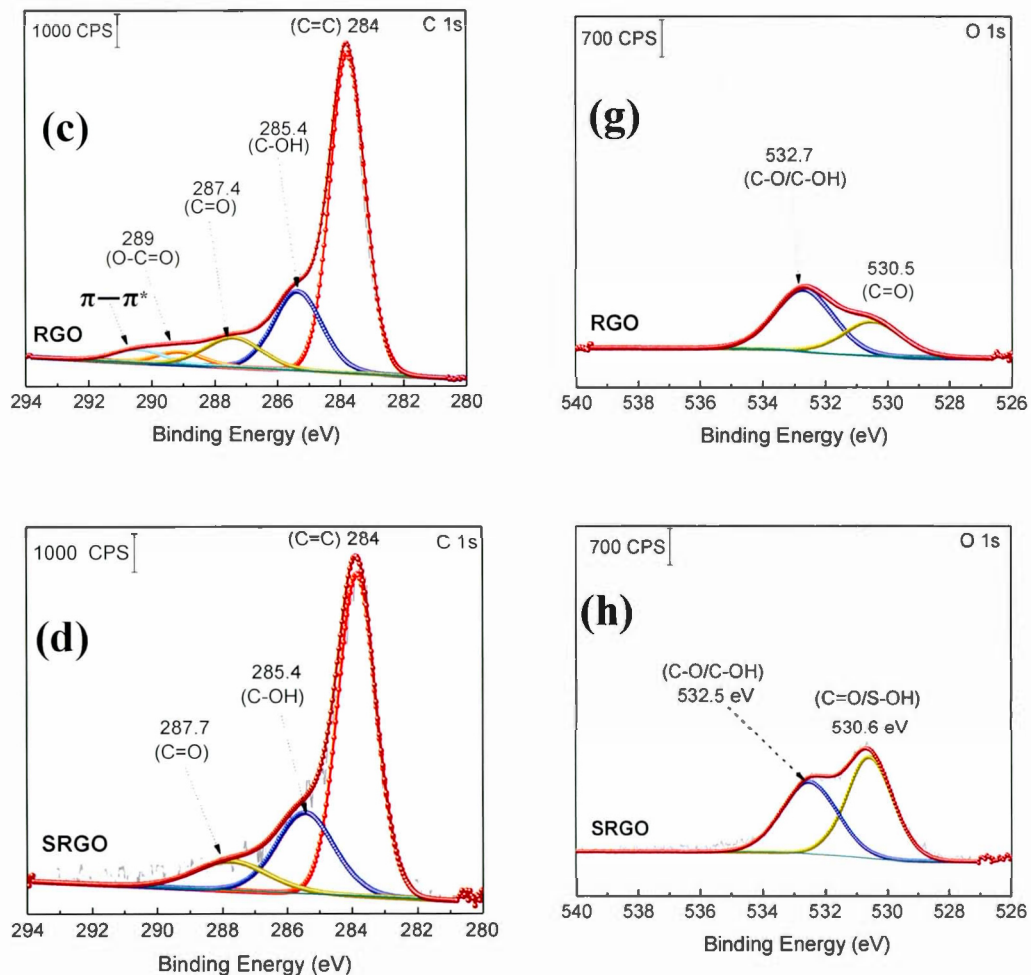


Figure 7. (a) XPS survey spectra of graphene oxide (GO), reduced graphene oxide (RGO) and sulfophenyl-modified RGO (SRGO); XPS C 1s spectra of (b) GO, (c) RGO and (d) SRGO, (f) S 2p core level spectrum of SRGO and XPS O 1s spectra of (f) GO, (g) RGO and (h) SRGO.

C Is Region. The C 1s core level spectrum of GO (Figure 7b) shows a sp^2 component ($C=C/C-C$) in aromatic rings at 284.4 eV, followed by the surface oxides components (sp^3) C-OH (285.8 eV), C-O-C (286.6 eV), C=O (287.5 eV), and the carboxylate carbon (O-C=O) at 288.6 eV. Their atomic concentration (at. %) are given in Supporting Information, Table S1^{17,42}. The relative atomic concentration for different oxygenated carbon functional (C sp^3) groups is also included in Table 2.2 together with their counter parts from the O 1s core level spectra. The C-O species represent 50 % of the total carbon atoms (Supporting Information, Table S1). The high oxygen content of GO is essentially related to the use of KMnO₄ as oxidizing agent during its preparation⁸⁴. For RGO, its C 1s core level spectrum was fitted with five components (Figure 7c). The contribution at 284 eV, attributed to non-oxygenated ring C, shows a significant increase of its relative area and a decrease of the FWHM (supporting Information, Table S1). This suggests that the thermal treatment partially restored the π -electron network by removing most of oxygen functional groups on graphene sheets⁸⁵. Indeed, the component observed at 286.6 eV (C-O-C) in GO spectrum (Figure 7b), significantly decreased after thermal reduction as well as the one of C-OH at 285.8 eV (Supporting Information, Table 2)^{64,69,85,86}. This result is in good agreement with the FTIR spectra of these two materials. The C Is XPS spectrum of RGO (Figure 7c) also exhibits the carbonyl (C=O, 287.4 eV) and the carboxylate carbon (O-C=O, 289 eV) with peak intensities noticeably reduced in comparison to GO. However, their relative atomic concentration in terms of oxygenated carbon species (Supporting Information, Table S1) slightly increased, probably due to CO₂ blisters (especially from epoxy groups)⁸⁵ which could be trapped between graphene sheets during the annealing^{87,88}. In addition, there is an additional component at 290.5 eV corresponding to shake-up satellite ($\pi-\pi^*$) peak or to π -electrons delocalized in the aromatic network⁸⁹. Figure 7d displays the C 1s core level spectrum of modified RGO (SRGO) with sulfophenyl groups. The spectrum can be

fitted with 3 major components. It can be seen that, after graphene functionalization the relative atomic concentration of C-OH (peak at 285.4 eV) increased from 66 to 78% (Supporting Information, Table S1), suggesting an increase of the contribution of graphene derived sp^3 carbon (the C in C-N/C-O) bonds^{27,90,91} due to the reaction with sulfophenyl diazonium ions. It is also noted that the relative area of the peak around 287.7 eV decreased and the carboxylate component (O-C=O) at 289 eV in RGO spectrum (Figure 7c) disappeared after grafting of sulfophenyl groups. The departure of the carboxylic (COOH) groups can be attributed to the decarboxylation of the carboxylic functionalities present at the RGO surface during the reduction of the diazonium cations and subsequent grafting^{45,46}.

S 2p Region. The core level spectrum of S 2p peak displayed in Figure 7a can be curve-fitted with a doublet at 168.3 and 167 eV for S 2p_{1/2} and S 2p_{3/2}, respectively (Figure 7e). This confirms the presence of sulfonate groups ($-SO_3^-$) on the graphene sheets surface^{92,93}.

O 1s Region. The O 1s core level spectrum of graphene oxide (GO) shown in Figure 7f can be curve-fitted with two main contributions at 531.7 and 532.7 eV corresponding to C-O-C (46%)^{74,94,95} and C-O (37%), (Supporting Information, Table S1)^{72,74,85,95,96} bonds^{85,97}, respectively. A third component, located at 530.7 eV can be assigned to the ketone and quinone functionalities (C=O) in lesser amount (16%, Supporting Information, Table S1), which arise at the edge or bonded to the basal plane of GO as carbonyl groups^{85,98,99}. The additional weaker contribution observed at 534 eV is related to water intercalation^{43,85,89,95,96,99–102}. After thermal reduction of GO, two components related to C=O (530.5 eV) and C-OH (532.7 eV) became clearly visible with very low intensities (Figure 7g)^{85,89} and a noticeable decrease of the relative areas (Supporting Information, Table S1) because of complete loss/conversion of C-O-C groups¹⁰³. Water molecules trapped between graphene

layers, were removed during GO thermal reduction^{85,104}. Following RGO functionalization, the atomic concentration (Supporting Information, Table S1) and the peak intensity (Figure 7g) of the component at 530.6 eV considerably increase. This observation is in good agreement with the introduction of the oxygenated groups attributed to S-O bonds⁷³.

3.8 Thermogravimetric analysis coupled to mass spectrometry

The novelty of our work relative the vast literature existing on functionalized graphene lies in the use of TGA-MS to characterize the sulfophenyl-modified RGO. Figure 8 shows the TGA-MS profiles of GO, RGO and SRGO under He flow. The thermogram of graphene oxide (GO) (Figure 8a) shows a major weight loss of 35% between 170 and 300 °C, with an inflection point at 200 °C. The thermogravimetric analysis simultaneously coupled with mass spectroscopy (TGA-MS) allowed to show that the mass loss is originating from OH (*m/z* 17), water (*m/z* 18), CO (*m/z* 28) and CO₂ (*m/z* 44) release. This sudden mass loss is attributed to the removal of labile oxygen functional groups on GO sheets⁴². A weaker mass loss occurs when the temperature is increased between 300 and 900 °C and is related to the gradual removal of more stable oxygen functionalities. The TGA-MS data of GO (Figure 8a and b) indicate that the weight loss above 300 °C can essentially be assigned to CO (*m/z* 28) release. The significant mass loss (~50 wt.%) observed in the TGA analysis reflects the extent of the defects in the GO, which make the material thermally unstable. In contrast, RGO (obtained by thermal reduction of GO at 200 or at 800 °C) show only a 5 wt.% mass loss up to 500 °C, which suggests that a significant amount of labile oxygen groups were removed during heat treatment (Figure 7c and d). Finally, the weight loss (20 %) observed between 500 and 900 °C (Figure 8c and d) is

mostly associated to the departure of the carbonyl groups (CO_2 , m/z 44), that have not been removed during the heat treatment of the GO as shown on the mass spectrum in Figure 8c. The elimination of oxygen functionalities from GO during the thermal annealing enhances the van der Waals forces attraction between graphene layers, which makes RGO thermally more stable¹⁷.

However, after sulfophenyl functionalization of RGO, SRGO displays a different profile compared to RGO (Figure 8d). The onset of weight loss (~ 12 wt.%) observed at about 350 °C is attributed to the thermal removal of organic functional groups and the weight loss is greater than that caused by the departure of only labile oxygen functionalities groups in this range of temperature. Two relevant fragments m/z = 64 (SO_2) and m/z = 78 (C_6H_{12}) are detected between 250 and 550 °C and correlate with the mass loss (Figure 8e and f). The maximum of the SO_2 and C_6H_{12} peaks is around 350 - 400 °C, confirming the chemical bonding between graphene sheets and aryl groups⁸¹. The signal with *m/z* 44, attributed to CO_2 , showed a different profile compared to unmodified RGO, with a maximum at 600 °C. The grafting of sulfophenyl groups on RGO surface is confirmed by elemental analysis (Supporting Information, Table S2). Their mass loading was calculated to be 12 wt.% from the data in Table 2, by considering the presence of a sulfur atom per grafted group.

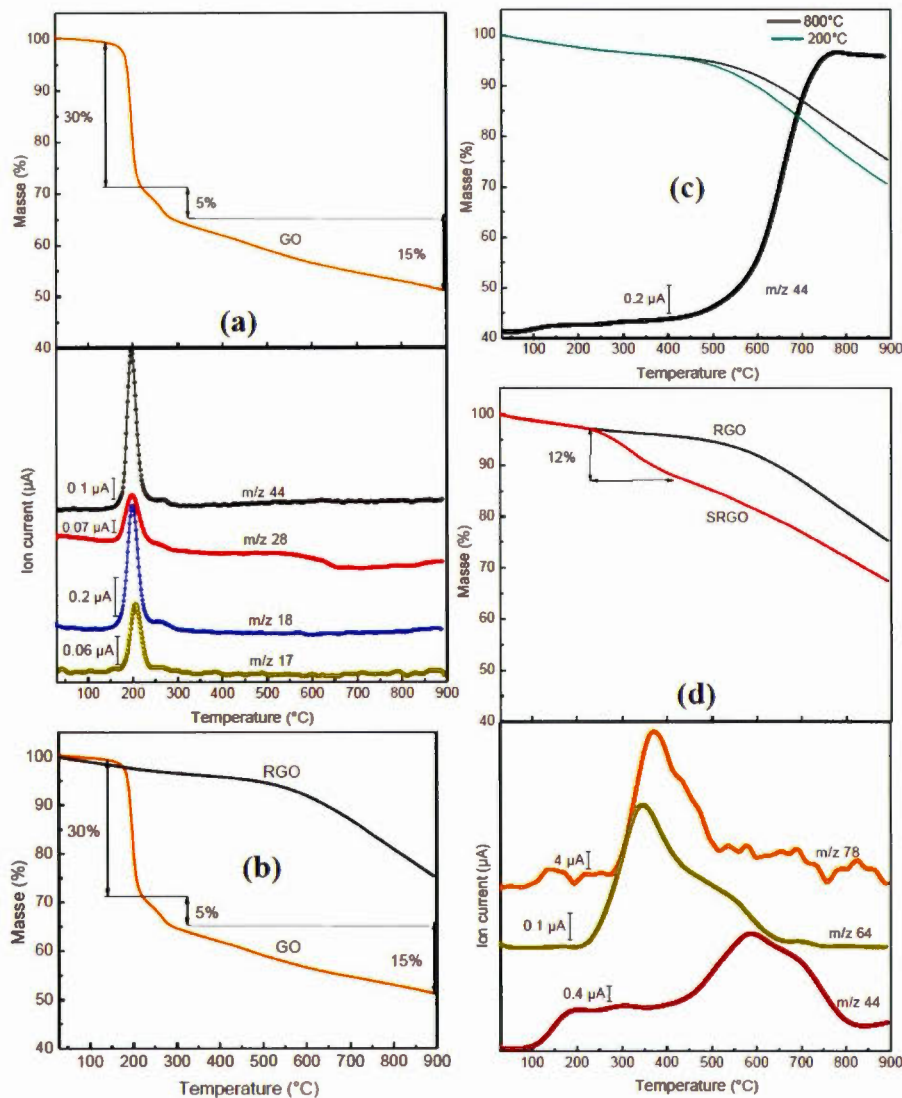


Figure 8. TGA and TGA-MS profiles under helium for the graphene oxide (GO), reduced graphene oxide (RGO) and RGO modified by sulfophenyl groups (SRGO) between 30 and 900 °C at a heating rate of 5 °C/min. (a, c and d) Mass variation with (a) OH, H₂O, CO and CO₂ MS profiles, (c) CO₂ MS profile and (d) SO₂ MS and C₆H₁₂ profiles.

4 Conclusion

Reduced graphene oxide (RGO) was synthesized via thermal reduction of GO under argon/hydrogen between 200 and 800 °C. Thermogravimetric analysis coupled with mass spectra analysis was firstly used to examine oxygen functionalities of GO and secondly to confirm the presence of sulfophenyl groups on the surface of chemically modified RGO. The immobilization of organic molecules on the graphene sheets was demonstrated by TEM, FTIR, XPS and nitrogen gas adsorption. Electronic conductivity measurements and Raman spectroscopy confirmed the covalent bonds between the graphene sheets and the organic molecules. The optical band gap of RGO was found to decrease following grafting of sulfophenyl groups. Finally, sulfophenyl and other aryl modified-graphene have a wide variety of potential applications. Similarly to modified carbons, SRGO and more general aryl-modified graphene could be employed in proton exchange membrane fuel cells, electrochemical capacitors, batteries, inks for printing, sensors as well as automotive and biomedical coatings^{105,106}.

5 Acknowledgements

This work was financially supported by the Natural Sciences and Engineering Research Council of Canada (NSERC). The research infrastructure of NanoQAM was used during this work.

6 References

- 1 Z.-S. Wu, K. Parvez, X. Feng and K. Müllen, *Nat. Commun.*, 2013, **4**, 2487–3487.
- 2 J. H. Seol, I. Jo, A. L. Moore, L. Lindsay, Z. H. Aitken, M. T. Pettes, X. Li, Z. Yao, R. Huang, D. Broido, N. Mingo, R. S. Ruoff and L. Shi, *Science*, 2010, **328**, 213–236.
- 3 S. Stankovich, D. A. Dikin, G. H. B. Dommett, K. M. Kohlhaas, E. J. Zimney, E. A. Stach, R. D. Piner, S. T. Nguyen and R. S. Ruoff, *Nature*, 2006, **442**, 282–286.
- 4 K. S. Novoselov, A. K. Geim, S. V Morozov, D. Jiang, Y. Zhang, S. V Dubonos, I. V Grigorieva and A. . Firsov, *Science*, 2004, **306**, 666–669.
- 5 X. Zhou, Y. Li, G. Ma, Q. Ma and Z. Lei, *J. Alloys Compd.*, 2016, **685**, 216–221.
- 6 Q. Li, Y. Chen, J. He, F. Fu, J. Lin and W. Zhang, *J. Alloys Compd.*, 2016, **685**, 294–299.
- 7 D. Wei, L. Grande, V. Chundi, R. White, C. Bower, P. Andrew and T. Ryhänen, *Chem. Commun.*, 2012, **48**, 1239–1241.
- 8 R. Raccichini, A. Varzi, S. Passerini and B. Scrosati, *Nat. Mater.*, 2015, **14**, 271–279.
- 9 G. Pognon, T. Brousse and D. Bélanger, *Carbon*, 2011, **49**, 1340–1348.
- 10 A. Ambrosi, C. K. Chua, B. Khezri, Z. Sofer, R. D. Webster and M. Pumera, *Proc. Natl. Acad. Sci.*, 2012, **109**, 12899–12904.
- 11 W. S. Hummers and R. E. Offeman, *J. Am. Chem. Soc.*, 1958, **80**, 1339–1339.
- 12 S. Park, J. An, J. R. Potts, A. Velamakanni, S. Murali and R. S. Ruoff, *Carbon*, 2011, **49**, 3019–3023.
- 13 J. R. Lomeda, C. D. Doyle, D. V Kosynkin, W.-F. Hwang and J. M. Tour, *J. Am. Chem. Soc.*, 2008, **130**, 16201–16206.
- 14 T. Kuila, A. K. Mishra, P. Khanra, N. H. Kim and J. H. Lee, *Nanoscale*, 2013, **5**, 52–71.
- 15 H. J. Shin, K. K. Kim, A. Benayad, S. M. Yoon, H. K. Park, I. S. Jung, M. H. Jin, H. K. Jeong, J. M. Kim, J. Y. Choi and Y. H. Lee, *Adv. Funct. Mater.*, 2009, **19**, 1987–1992.
- 16 S. Pei, J. Zhao, J. Du, W. Ren and H. M. Cheng, *Carbon*, 2010, **48**, 4466–4474.

- 17 A. K. Das, M. Srivastav, R. K. Layek, M. E. Uddin, D. Jung, N. H. Kim and J. H. Lee, *J. Mater. Chem. A*, 2014, **2**, 1332–1340.
- 18 R. S. Park, S.; Ruoff, *Nat. Nanotechnol.*, 2009, **4**, 217–224.
- 19 J. Park, S. B. Jo, Y. J. Yu, Y. Kim, J. W. Yang, W. H. Lee, H. H. Kim, B. H. Hong, P. Kim, K. Cho and K. S. Kim, *Adv. Mater.*, 2012, **24**, 407–411.
- 20 B. D. Ossonon and D. Bélanger, *Carbon*, 2017, **111**, 83–93.
- 21 S. Umrao, S. Abraham, F. Theil, S. Pandey, V. Ciobota, P. K. Shukla, C. J. Rupp, S. Chakraborty, R. Ahuja, J. Popp, B. Dietzek and A. Srivastava, *RSC Adv.*, 2014, **4**, 59890–59901.
- 22 L. Song, L. Ci, H. Lu, P. B. Sorokin, C. Jin, J. Ni, A. G. Kvashnin, D. G. Kvashnin, J. Lou, B. I. Yakobson and P. M. Ajayan, *Nano Lett.*, 2010, **10**, 3209–3215.
- 23 M. Saranya, R. Ramachandran, P. Kollu, S. K. Jeong and A. N. Grace, *RSC Adv.*, 2015, **5**, 15831–15840.
- 24 Y. N. Singhbabu, K. K. Sahu, D. Dadhich, a K. Pramanick, T. Mishra and R. K. Sahu, *J. Mater. Chem. C*, 2013, **1**, 958–966.
- 25 X. Li, H. Zhu, J. Wei, K. Wang, E. Xu, Z. Li and D. Wu, *Appl. Phys. A Mater. Sci. Process.*, 2009, **97**, 341–344.
- 26 J. Landers, G. Y. Gor and A. V. Neimark, *Colloids Surfaces A Physicochem. Eng. Asp.*, 2013, **437**, 3–32.
- 27 D. S. Yu, T. Kuila, N. H. Kim, P. Khanra and J. H. Lee, *Carbon*, 2013, **54**, 310–322.
- 28 G. Wang, B. Wang, J. Park, Y. Wang, B. Sun and J. Yao, *Carbon*, 2009, **47**, 3242–3246.
- 29 Y. Zhu, M. D. Stoller, W. Cai, A. Velamakanni, R. D. Piner, D. Chen and R. S. Ruoff, *ACS Nano*, 2010, **4**, 1227–1233.
- 30 Y. Wang, X. Tong, X. Guo, Y. Wang, G. Jin and X. Guo, *Nanotechnology*, 2013, **24**, 1–5.
- 31 S. Umrao, S. Abraham, F. Theil, S. Pandey, V. Ciobota, P. K. Shukla, C. J. Rupp, S. Chakraborty, R. Ahuja, J. Popp, B. Dietzek and A. Srivastava, *RSC Adv.*, 2014, **4**, 59890–59901.
- 32 A. Mathkar, D. Tozier, P. Cox, P. Ong, C. Galande, K. Balakrishnan, A. Leela Mohana Reddy and P. M. Ajayan, *J. Phys. Chem. Lett.*, 2012, **3**, 986–991.
- 33 J. M. Englert, C. Dotzer, G. Yang, M. Schmid, C. Papp, J. M. Gottfried, H.-P. Steinrück, E. Spiecker, F. Hauke and A. Hirsch, *Nat. Chem.*, 2011, **3**, 279–286.

- 34 K. T. Shruthi, M. S. Kumar, A. Pratap and N. Chandrasekaran, *RSC Adv.*, 2015, **5**, 93423–93432.
- 35 Y. Gao, D. Ma, C. Wang, J. Guan and X. Bao, *Chem. Commun.*, 2011, **47**, 2432–2434.
- 36 S. Brunauer, L. S. Deming, W. E. Deming and E. Teller, *J. Am. Chem. Soc.*, 1940, **62**, 1723–1732.
- 37 A. Gambou-Bosca and D. Belanger, *J. Electrochem. Soc.*, 2015, **162**, A5115–A5123.
- 38 K. S. W. Sing and R. T. Williams, *Adsorpt. Sci. Technol.*, 2004, **22**, 773–782.
- 39 T. Ohkubo, J. Miyawaki, K. Kaneko, R. Ryoo and N. A. Seaton, *J. Phys. Chem. B*, 2002, **106**, 6523–6528.
- 40 R. F. Bruinsma, P. G. De Gennes, J. B. Freund and D. Levine, *Nature*, 2004, **427**, 523–527.
- 41 M. D. Stoller, S. Park, Y. Zhu, J. An and R. S. Ruoff, *Nano lett.*, 2008, **8**, 3498–3502.
- 42 S. Stankovich, D. a. Dikin, R. D. Piner, K. a. Kohlhaas, A. Kleinhammes, Y. Jia, Y. Wu, S. T. Nguyen and R. S. Ruoff, *Carbon*, 2007, **45**, 1558–1565.
- 43 D. R. Dreyer, S. Park, C. W. Bielawski and R. S. Ruoff, *Chem. Soc. Rev.*, 2010, **39**, 228–240.
- 44 C. Moreno-Castilla, M. A. Ferro-Garcia, J. P. Joly, I. Bautista-Toledo, F. Carrasco-Marín and J. Rivera-Utrilla, *Langmuir*, 1995, **11**, 4386–4392.
- 45 M. Toupin and D. Bélanger, *Langmuir*, 2008, **24**, 1910–1917.
- 46 A. Le Comte, D. Chhin, A. Gagnon, R. Retoux, T. Brousse and D. Bélanger, *J. Mater. Chem. A*, 2015, **3**, 6146–6156.
- 47 H. Li, Y. Wang, Y. Shi, J. Li, L. H. Yang and H. Ying, *RSC Adv.*, 2013, **35**, 14839–15492.
- 48 D. D. Jiang, Q. Yao, M. A. McKinney and C. A. Wilkie, *Polym. Degrad. Stab.*, 1999, **63**, 423–434.
- 49 J. Lu, Y. Li, S. Li and S. P. Jiang, *Sci. Rep.*, 2016, **6**, 21530–21542.
- 50 D. H. Johnston and D. F. Shriver, *Inorg. Chem.*, 1993, **32**, 1045–1047.
- 51 Z. Xia, F. Leonardi, M. Gobbi, Y. Liu, V. Bellani, A. Liscio, A. Kovtun, R. Li, X. Feng, E. Orgiu, P. Samorì, E. Treossi and V. Palermo, *ACS Nano*, 2016, **10**, 7125–7134.
- 52 A. C. Ferrari and J. Robertson, *Phys. Rev. B*, 2000, **61**, 14095–14107.

- 53 A. C. Ferrari and D. M. Basko, *Nat. Nanotechnol.*, 2013, **8**, 235–246.
- 54 A. C. Ferrari, J. C. Meyer, V. Scardaci, C. Casiraghi, M. Lazzeri, F. Mauri, S. Piscanec, D. Jiang, K. S. Novoselov, S. Roth and A. K. Geim, *Phys. Rev. Lett.*, 2006, **97**, 187401–187405.
- 55 W. Gao, M. Majumder, L. B. Alemany, T. N. Narayanan, M. A. Ibarra, B. K. Pradhan and P. M. Ajayan, *ACS Appl. Mater. Interfaces*, 2011, **3**, 1821–1826.
- 56 M. Fang, K. Wang, H. Lu, Y. Yang and S. Nutt, *J. Mater. Chem.*, 2009, **19**, 7098–7105.
- 57 M. A. Pimenta, G. Dresselhaus, M. S. Dresselhaus, L. G. Cançado, A. Jorio and R. Saito, *Phys. Chem. Chem. Phys.*, 2007, **9**, 1276–1291.
- 58 W. Chen and L. Yan, *Nanoscale*, 2010, **2**, 559–563.
- 59 Y. Wang, D. C. Alsmeyer and R. L. McCreery, *Carbon*, 1990, **2**, 557–563.
- 60 K. N. Kudin, B. Ozbas, H. C. Schniepp, R. K. Prud'homme, I. A. Aksay and R. Car, *Nano lett.*, 2008, **8**, 36–41.
- 61 G. Wei, M. Yan, R. Dong, D. Wang, X. Zhou, J. Chen and J. Hao, *Chem. Eur. J.*, 2012, **18**, 14708–14716.
- 62 H. Lim, J. S. Lee, H. J. Shin, H. S. Shin and H. C. Choi, *Langmuir*, 2010, **26**, 12278–12284.
- 63 M. S. Dresselhaus, A. Jorio, M. Hofmann, G. Dresselhaus and R. Saito, *Nano Lett.*, 2010, **10**, 751–758.
- 64 A. Ganguly, S. Sharma, P. Papakonstantinou and J. Hamilton, *J. Phys. Chem.*, 2011, **115**, 17009–17019.
- 65 A. Guermoune, T. Chari, F. Popescu, S. S. Sabri, J. Guillemette, H. S. Skulason, T. Szkopek and M. Siaj, *Carbon*, 2011, **49**, 4204–4210.
- 66 Z. Jin, T. P. McNicholas, C. J. Shih, Q. H. Wang, G. L. C. Paulus, A. J. Hilmer, S. Shimizu and M. S. Strano, *Chem. Mater.*, 2011, **23**, 3362–3370.
- 67 Y. I. Zhang, L. Zhang and C. Zhou, *Acc. Chem. Res.*, 2013, **46**, 2329–2339.
- 68 K. Parvez, S. Yang, X. Feng and K. Müllen, *Synth. Met.*, 2015, **210**, 123–132.
- 69 S. Pei and H. M. Cheng, *Carbon*, 2012, **50**, 3210–3228.
- 70 C. Singh, A. K. Mishra and A. Paul, *J. Mater. Chem. A*, 2015, **3**, 18557–18463.
- 71 J. Wang, T. Zhou, H. Deng, F. Chen, K. Wang, Q. Zhang and Q. Fu, *Colloids Surf. B: Biointerfaces*, 2013, **101**, 171–176.

- 72 J. Guan, X. Chen, T. Wei, F. Liu, S. Wang, Q. Yang, Y. Lu and S. Yang, *J. Mater. Chem. A*, 2015, **3**, 4139–4146.
- 73 G. Gao, D. Liu, S. Tang, C. Huang, M. He, Y. Guo, X. Sun and B. Gao, *Sci. Rep.*, 2016, **6**, 1–8.
- 74 X. Fan, W. Peng, Y. Li, X. Li, S. Wang, G. Zhang and F. Zhang, *Adv. Mater.*, 2008, **20**, 4490–4493.
- 75 C.-Y. Su, A.-Y. Lu, Y. Xu, F.-R. Chen, A. N. Khlobystov and L.-J. Li, *ACS Nano*, 2011, **5**, 2332–2339.
- 76 S. Baranton and D. Bélanger, *J Phys. Chem. B*, 2005, **109**, 24406–24410.
- 77 E. Lebègue, T. Brousse, J. Gaubicher and C. Cougnon, *Electrochim. Acta*, 2013, **88**, 680–687.
- 78 F. Hauquier, N. Debou, S. Palacin and B. Jousselme, *J. Electroanal. Chem.*, 2012, **677–680**, 127–132.
- 79 J. Lyskawa, A. Grondein and D. Bélanger, *Carbon*, 2010, **48**, 1271–1278.
- 80 D. B. Ossonon, M. Weissmann and D. Bélanger, *Electrochim. Acta*, 2014, **122**, 210–217.
- 81 M. Toupin and D. Bélangeer, *J. Phys. Chem. C*, 2007, **111**, 5394–5401.
- 82 L. Madec, K. A. Seid, J.-C. Badot, B. Humbert, P. Moreau, O. Dubrunfaut, B. Lestriez, D. Guyomard and J. Gaubicher, *Phys. Chem. Chem. Phys.*, 2014, **16**, 22745–22753.
- 83 C. Saby, B. Ortiz, G. Y. Champagne and D. Bélanger, *Langmuir*, 1997, **7463**, 6805–6813.
- 84 T. S. Sreeprasad, S. M. Maliyekkal, K. P. Lisha and T. Pradeep, *J. Hazard. Mater.*, 2011, **186**, 921–931.
- 85 C. Mattevi, G. Eda, S. Agnoli, S. Miller, K. A. Mkhoyan, O. Celik, D. Mastrogiovanni, C. Cranozzi, E. Carfunkel and M. Chhowalla, *Adv. Funct. Mater.*, 2009, **19**, 2577–2583.
- 86 S. Park, K.-S. Lee, G. Bozoklu, W. Cai, S. T. Nguyen and R. S. Ruoff, *ACS Nano*, 2008, **2**, 572–578.
- 87 K. Hu, X. Xie, T. Szkopek and M. Cerruti, *Chem. Mater.*, 2016, **28**, 1756–1768.
- 88 S. Eigler, C. Dotzer, A. Hirsch, M. Enzelberger and P. Müller, *Chem. Mater.*, 2012, **24**, 1276–1282.

- 89 C. Hontoria-Lucas, A. J. López-Peinado, J. de D. López-González, M. L. Rojas-Cervantes and R. M. Martín-Aranda, *Carbon*, 1995, **33**, 1585–1592.
- 90 A. Sinitskii, A. Dimiev, D. A. Corley, A. A. Fursina, D. V. Kosynkin and J. M. Tour, *ACS Nano*, 2010, **4**, 1949–1954.
- 91 A. Mesnage, X. Lefe, P. Je, G. Deniau and S. Palacin, *Langmuir*, 2012, **28**, 11767–11778.
- 92 J. Marwan, T. Addou and D. Bélanger, *Chem. Mater.*, 2005, **17**, 2395–2403.
- 93 A. L. Gui, G. Liu, M. Chockalingam, G. Le Saux, J. B. Harper and J. J. Gooding, *Electroanalysis*, 2010, **22**, 1283–1289.
- 94 A. Y. Romanchuk, A. S. Slesarev, S. N. Kalmykov, D. V Kosynkin and J. M. Tour, *Phys. Chem. Chem. Phys.*, 2013, **15**, 2321–2327.
- 95 H. Dai, Z. Xu and X. Yang, *J. Phys. Chem. C*, 2016, **120**, 22585–22596.
- 96 V. Shubina, L. Gaillet, S. Ababou-Girard, V. Gaudefroy, T. Chaussadent, F. Farças, T. Meylheuc, C. Dagbert and J. Creus, *Appl. Surf. Sci.*, 2015, **351**, 1174–1183.
- 97 A. Ganguly, S. Sharma, P. Papakonstantinou and J. Hamilton, *J. Phys. Chem. C*, 2011, **115**, 17009–17019.
- 98 Y. Ishii, D. Yang, A. Velamakanni, S. J. An and M. Stoller, 2008, **321**, 1815–1818.
- 99 T. Szabo, O. Berkesi, P. Forgo, K. Josepovits, Y. Sanakis, D. Petridis and I. Dékany, *Chem. Mater.*, 2006, **18**, 2740–2749.
- 100 G. Gunasekaran and L. R. Chauhan, *Electrochim. Acta*, 2004, **49**, 4387–4395.
- 101 Y. Xiong, Y. Xie, Z. Li and C. Wu, *Chem. - A Eur. J.*, 2003, **9**, 1645–1651.
- 102 A. Buchsteiner, A. Lerf and J. Pieper, *J. Phys. Chem. B*, 2006, **110**, 22328–22338.
- 103 L. B. Casabianca, M. A. Shaibat, W. W. Cai, S. Park, R. Piner, R. S. Ruoff and Y. Ishii, *J. Am. Chem. Soc.*, 2010, **132**, 5672–5676.
- 104 C. Zhao, H. Gao, C. Chen and H. Wu, *J. Mater. Chem. A*, 2015, **3**, 18360–18364.
- 105 B. Desalegn, T. Brousse and D. Be, *Carbon*, 2015, **92**, 362–381.
- 106 D. Bélanger and J. Pinson, *Chem. Soc. Rev.*, 2011, **40**, 3995–4048.

7 Electronic Supplementary information

Table S1 Atomic concentration and curve-fitting parameters obtained from the XPS spectra

Samples		C sp ²	C sp ³				O 1s			
		C=C/C-C	C-OH	C-O-C	C=O	C(O)-O	C-OH	C-O-C	C=O	H ₂ O
GO	B.E. (eV)	284.4	285.8	286.6	287.5	288.6	532.7	531.7	530.7	534
	FWHM (eV)	1.6	1.4	1.2	1.2	1.1	1.4	1.5	1.6	1.45
	Peak area (a.u.)	8333	2652	3436	1421	662	4067	5768	2020	900
	Relative atomic concentration (%)	-	33	42	17	8	37	46	16	-
RGO	B.E. (eV)	284	285.4	287.4	289	532.7	530.5	nd		
	FWHM (eV)	1.4	2.1	2.1	1.74	2.2	2.1			
	Peak area (a.u.)	12815	5450	2054	715	2727	1550			
	Relative atomic concentration (%)	-	66	25	9	64	36			
SRGO	B.E. (eV)	284	285.4	287.7	532.5	530.6	nd			
	FWHM (eV)	1.4	2.1	2.3	2.1	2				
	Peak area (a.u.)	10524	4002	1108	2864	3935				
	Relative atomic concentration (%)	-	78	22	42	58				

B.E.: Binding Energy

FWHM: full width at half maximum

nd: not determined.

The relative atomic concentration (in %) for different functional groups is calculated with respect to the total area of the oxygenated carbon peaks.

Table S2 Elemental analysis of RGO modified with sulfophenyl groups

SRGO	% wt. N	% wt. S
	1.4	2.5

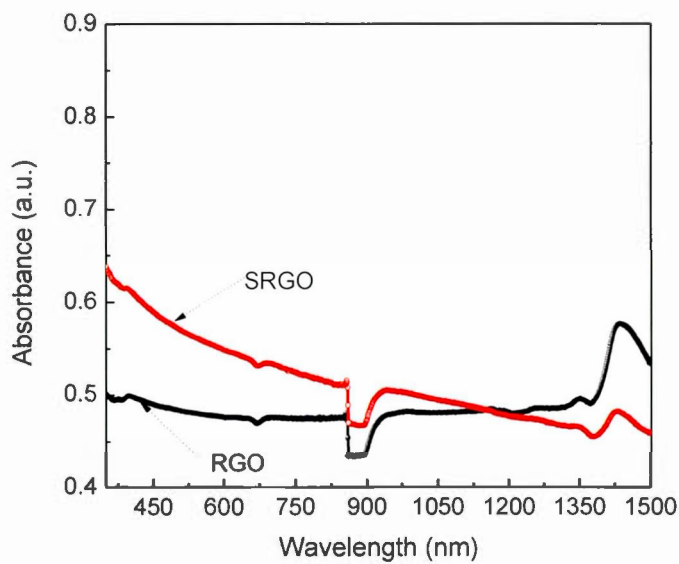


Figure S1. UV-Vis/NIR spectra of RGO and SRGO

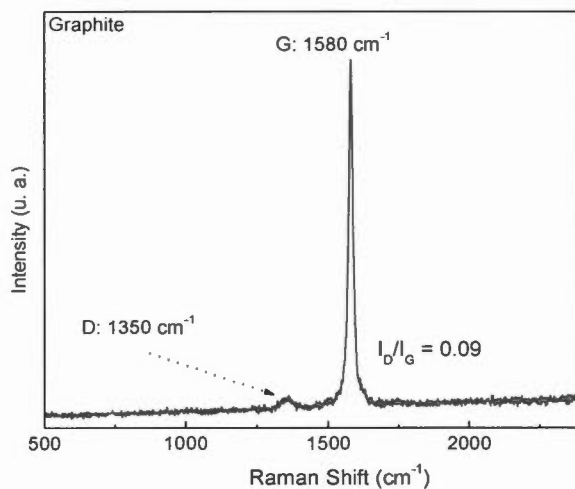


Figure S2. Raman spectrum of natural graphite powder

CHAPITRE II

FUNCTIONALIZATION OF GRAPHENE SHEETS BY THE DIAZONIUM CHEMISTRY DURING ELECTROCHEMICAL EXFOLIATION OF GRAPHITE

Résumé de l'article 2

Ce deuxième article traite de la fonctionnalisation spontanée du graphène lors de sa synthèse électrochimique dans une solution 0,1 M H₂SO₄ contenant des ions anthraquinone diazonium. Cette approche a été adoptée dans l'intérêt de réduire les étapes de la fonctionnalisation en une seule, et de permettre une bonne dispersion du graphène dans différents solvants. Le greffage *in-situ* au cours de l'exfoliation électrochimique du graphite en graphène permet d'empêcher le réempilement des feuillets de graphène exfoliés. Cette technique a permis d'accroître la surface BET du matériau greffé (EG-AQ), contrairement aux méthodes conventionnelles de greffage. Le choix est porté sur la molécule d'anthraquinone pour cette étude parce qu'elle est électrochimiquement active. Ainsi, le taux de greffage des molécules greffées a été évalué par voltammetrie cyclique et par analyse thermogravimétrique. La microscopie électronique à balayage et en transmission (MET) ont permis d'étudier la morphologie et la qualité des feuillets de graphène modifiés et non-modifiés (EG). Le MET a aussi permis d'évaluer le nombre de feuillets du graphène (EG). Les propriétés électroniques des matériaux préparés (EG et EG-AQ) ont finalement été évaluées par spectroscopie Raman, XPS et mesure de conductivité électronique. Ce travail a été publié dans le périodique Carbon. (Carbon 111(2017) 83-93, 10.1016/j.carbon.20109.063).

Contribution des auteurs:

Benjamin Diby Ossonon

L'auteur principal a effectué toutes les expériences en laboratoire relatives à l'article. L'article a été écrit par lui-même. L'intégralité des figures ainsi que la bibliographie ont été à sa charge. Il a révisé le contenu de l'article avant la soumission finale.

Daniel Bélanger

Le co-auteur Daniel Bélanger a supervisé le projet et les expériences en laboratoire du début à la fin. Il a donné de nombreux conseils, des pistes à explorer et a également contribué à la rédaction et aux corrections de l'article avant sa soumission finale.

Article 2. Functionalization of graphene sheets by the diazonium chemistry during electrochemical exfoliation of graphite.

B.D. Ossonon and D. Bélanger

Département Chimie, Université du Québec à Montréal, CP8888, Succ. Centre Ville, Montréal, Québec, Canada H3C 3P8

Paru dans *Carbon 111 (2017) 83-93*

<http://dx.doi.org/10.1016/j.carbon.2016.09.063>

Abstract

Graphene sheets were spontaneously functionalized with anthraquinone molecules in a one-pot process, during the oxidative electrochemical exfoliation of a graphite electrode in a 0.1 M H₂SO₄ solution containing anthraquinone diazonium ions. This counterintuitive process involves the electrochemical oxidation of graphite and reduction of diazonium ions and functionalization occurs by spontaneous reaction of freshly generated graphene sheets with diazonium ions. This reaction is faster than the common approach based on the reaction of diazonium ions with pre-exfoliated graphene sheets. Indeed, the grafting yield of our one-pot process is higher than that of a two-step procedure based on functionalization of already produced graphene sheets, presumably due to the higher reactivity of freshly generated graphene sheets during electrochemical exfoliation. As a result of functionalization, the water dispersibility of graphene sheets was improved and an increase of the BET specific surface area was observed. The presence of anthraquinone molecules was confirmed by Fourier transform infrared spectroscopy, electron microscopy, X-ray photoelectron spectroscopy and cyclic voltammetry. Thermogravimetric analysis, Raman spectroscopy and electronic conductivity measurements are consistent with the

covalent bonding of anthraquinone on the graphene sheets. Thermogravimetric analysis and cyclic voltammetry data allowed the evaluation of the loading of anthraquinone groups on the graphene sheets.

1. Introduction

Graphene, a two-dimensional honeycomb sp^2 lattice with exceptionally high electrical conductivity, elasticity, electron mobility [1], thermal conductivity [2], high specific surface area [3] and mechanical strength [4,5] has received a great deal of attention for its potential application in the future generation of nanoelectronic devices [6,7], composite materials [8] and energy storage systems [6,9]. The production of high-quality graphene has been carried out by, micromechanical cleavage [1], chemical vapor deposition [10] and thermal desorption of Si from a SiC substrate [11]. However, these methods provide high-quality material in relatively small quantity, useful only for selected applications [1,12]. For large-scale production, graphene is obtained by reduction of graphene oxide, itself prepared by the Hummer's method [13], and by either chemical [14–17], thermal [18] or electrochemical [14] techniques [19]. All these methods result in abundant structure defects and surface functional groups on the graphene sheets that significantly affect their electronic properties [2] and their electrochemical behavior [20]. Existing methods to minimize these issues, such as electrochemical expansion [21,22], solvent and surfactant-assisted liquid-phase exfoliation [23] and graphite intercalated compounds [24] required extensive sonication processes which can limit the size and yield of thin graphene layer [6,24]. Finally, the large-scale synthesis of high-quality graphene by electrochemical exfoliation of graphite into graphene sheets has been recently developed by using non-aqueous [21,22] and aqueous electrolytes [6,7,25–

27]. Electrochemical exfoliation from aqueous media is environmentally benign, low-cost in comparison to other procedures and can be used for the large scale production of high-quality and high-purity graphene sheets [25]. Even if graphene itself is an attractive material, its large-scale application usually requires further functionalization to obtain useful material with tailored properties. Functionalization of graphene [28,29] (and its derivatives) with organic molecules by covalent and noncovalent interactions has been reported by using classical chemistries previously used for other carbon materials [30,31]. Among these, modification of graphene by spontaneous reduction of diazonium ions is attracting a lot of interest due to its versatility. Such covalent functionalization of graphene has been already reported for epitaxial graphene [32], graphene nanoribbons [33], chemically converted graphene [34,35] mechanically exfoliated graphene [35,36] as well as chemical vapor deposited graphene [35,37–40]. The functionalization occurred via a spontaneous reduction of diazonium ions that involves the generation of a radical by electron transfer from the carbon substrate to the aryl diazonium ion and subsequent formation of a covalent bond between carbon and the aryl group [41]. Another possible grafting mechanism is based on the spontaneous reaction of a cation generated by heterolytic dediazonation or the reaction of the diazonium cations with the substrate [42]. Noteworthy that in all these previous studies, the grafting was performed on surface deposited graphene-based film [40,43–45] or graphene dispersed in solution [30,38,46].

In this work, we developed a convenient method to functionalize graphene sheets during the oxidative electrochemical exfoliation of graphite in the presence of diazonium cations (Fig. 1). This counterintuitive process, which involves the electrochemical oxidation of graphite and a reduction step, (diazonium ions reduction) occurs by spontaneous reaction of freshly generated graphene sheets with

diazonium ions. To demonstrate the proof-of-concept, electroactive anthraquinone molecules were grafted [47–51]. The resulting materials were characterized by Raman spectroscopy, Fourier transform infrared spectroscopy, thermogravimetric analysis, scanning electron microscopy, transmission electron microscopy and electrochemistry to demonstrate that functionalization by anthraquinone molecules occurred during electrochemical exfoliation.

2. Experimental

2.1. Materials and reagents

Graphite foil (0.5mm thick, 99.8%) was obtained from Alfa Aesar and was natural graphite with crystallite size of 16 nm, determined from the Scherrer equation from the 200 peak of the X-ray diffraction pattern. 2-aminoanthraquinone (2-aminoAQ) (97%) and tert-butyl nitrite (90% solution in acetonitrile) were purchased from Aldrich. Unless otherwise stated, all others reagents were obtained from Aldrich and were used without further purification. Millipore water ($18.2\text{ M}\Omega\text{ cm}$) obtained from a Milli-Q water purification system was used for sample rinsing and preparation of all aqueous solutions.

2.2. Electrochemical exfoliation

For electrochemical exfoliation, a graphite foil ($7.5\text{ cm} \times 2\text{ cm} \times 0.05\text{ cm}$ (thickness)) used as anode (connected to the positive terminal of a DC power supply) with a Pt mesh (4 cm^2) as cathode, were immersed into the $0.1\text{ M H}_2\text{SO}_4$ electrolyte. Table 1 presents experimental conditions used for electrochemical exfoliation. The distance between the graphite foil and the Pt electrode was kept constant ($\approx 4\text{ cm}$). An electrochemical exfoliation was also carried out by using a Nafion membrane to

isolate the negative and positive electrode compartments (Supporting Information). Electrochemical exfoliation starts immediately after applying a DC voltage of 10 V (Fig. 2a). After a 1 h electrolysis, the exfoliated graphene sheets were collected by vacuum filtration through a polytetrafluoroethylene (PTFE) membrane filter with 0.47 mm pore size and washed several times with Nanopure water to remove residual acid. Typically, a mass of 500 mg is obtained in these experimental conditions. The electrochemically exfoliated graphene sheets powder was then dispersed in dimethylformamide (DMF) by ultrasonication for 10 min. The dispersion was left standing still 24 h for the precipitation of some thick graphitic flakes and only the upper part of the dispersion was used thereafter for all characterization. Following vacuum filtration, the obtained powder was dried in vacuum at 70 °C overnight before a heat treatment at 200 °C under an inert atmosphere of argon for 1 h to remove solvent trapped in the material. Graphene sheets flakes (Fig. 2b) are recovered in good yield (70%) and used for characterization. These graphene sheets can form a good dispersion in DMF (Fig. 2c) as well as a self-supporting film (Fig. 2d).

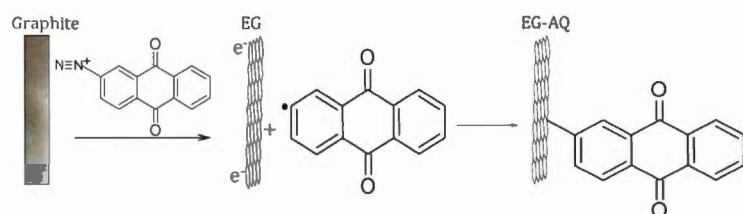


Figure 1 Spontaneous functionalization of electrochemically exfoliated graphene sheets (EG) anthraquinone during electrochemical exfoliation of graphite in a one-pot process.

2.3. In situ electrochemical grafting

The diazonium ions solution was prepared by dispersing 2-aminoanthraquinone (5 mmol) in 100 mL of acetonitrile by strong sonication (Bransonic 3510, Branson) for 30 min and keeping the solution under stirring and heating at 50 °C for about 12 h until complete dissolution of the quinone derivative [52]. Then, the mixture was cooled at room temperature and 5 mmol of tertbutylnitrite was added and the mixture was stirred for 30 min to generate in situ the anthraquinone-2-diazonium cations. In order to functionalize graphene sheets during the exfoliation process, the saturated diazonium ions solution was added to 200 mL of 0.15 M H₂SO₄ to obtain a final H₂SO₄ concentration of 0.1 M (Table 1). A potential (DC voltage) of 10 V was applied for 1 h. The electrolysis also yielded graphene flakes floating at the surface of the initially dark brown solution (Fig. 2e). The dispersion was then collected with a polytetrafluoroethylene (PTFE) membrane filter with 0.47 mm pore size and washed successively with Nanopure water, acetonitrile, methanol, dimethylformamide (DMF) and acetone. Each solvent was used three times to remove ungrafted moieties. Finally, the obtained powder (~ 350 mg) was dried in vacuum at 70 °C overnight before undergoing a thermal treatment at 200 °C under an inert atmosphere (Ar) for 1 h to remove solvent trapped in the materials. The resulting modified graphene sheets exhibited a better dispersibility than unmodified electrochemically exfoliated graphene sheets. This is demonstrated by optical photographs of the anthraquinone-modified graphene sheets dispersion that remains stable over a period of 1 h, unlike the unmodified graphene dispersion for which sedimentation is observed (Supporting Information, Fig. S1). A set of control experiments were also performed and include: i) pre-exfoliation of graphite in 200 mL of 0.1 M H₂SO₄ during 1 h and subsequent reaction with in situ generated diazonium ions (solution same as above) added to the 0.1 M H₂SO₄ solution for 1 h (Table 1); ii) electrochemical exfoliation of graphite in 0.1 M H₂SO₄ containing

anthraquinone (16 mM) for 1 h and iii) electrochemical exfoliation in 0.1 M H₂SO₄ in the presence of 2-aminoanthraquinone (16 mM).

2.4. Characterization techniques

Thermogravimetric analysis was carried out with a thermogravimetric analyzer (TA Instruments TGA (Q500)/Discovery MS). Samples (typically 2 mg) were placed in a Pt pan and heated from 30 to 900 °C with a temperature ramp of 5 °C/min, under flowing helium atmosphere or air. Raman spectroscopy measurements were performed using a micro-Raman system (UHTS300) with excitation from an argon ion laser beam (532 nm) at low power level of 2 mW in order to avoid damaging the organic functional groups. Electronic conductivity of self-supported films (Fig. 2d) was obtained at room temperature by using by a 4-point probe measurement using a Keithley 6220 DC precision current source (US). The morphological studies were performed with a scanning electron microscope (SEM) JSM-840A equipped with a field emission gun (FEG). Transmission Electron Microscopy (TEM) and high resolution transmission electron microscopy (HRTEM) images were taken by using JOEL JEM-2100F model with a 200 keV transmission electron microscope operated with a bright field image. Atomic Force Microscopy (AFM) images were obtained using Veeco/Bruker AFM instrument in ScanAsyst mode. The graphene dispersion (0.5 mg/mL in DMF) was spin-coated onto a mica substrate at 1500 rpm for 60 s and annealed at 400 °C for 30 min under flowing argon atmosphere to evaporate residual solvent before measurements. Nitrogen gas adsorption measurements were performed at 77 K by using an Autosorb-I instrument (Quantachrome Instrument, USA) and controlled by the AS1Win software. The volume of nitrogen adsorbed was recorded for relative pressures (P/P₀) ranging from 1×10^{-6} to 1. Prior to measurements, the sample (50–70 mg) was degassed for 4 h

under vacuum. The specific surface area of the graphene samples was determined by the BrunauereEmmetteTeller (BET) method [53,54] from the adsorption branch data set recorded for P/P₀ values between 3×10^{-1} and 5×10^{-2} . XPS data have been collected with the spectrophotometer PHI 5600-ci (Physical Electronics, Eden Prairie, MN, USA). The excitation source used for survey spectra was by Al (1486.6 eV) Xrays at 300 W and for core level spectra, by Mg Ka (1253.6 eV) Xrays at 150 W. The analyses were performed without charge compensation at an angle of 45° with the surface. The detector aperture was set at 4 and the surface area analyzed was 0.005 cm². Electrochemical measurements were performed at room temperature using a three-electrode configuration in a one-compartment cell. The working electrode consists of a composite electrode prepared by mixing the modified anthraquinone-modified or unmodified graphene sheets and PTFE as binder in a 90:10 wt% ratio in a small volume of ethanol until a homogenized paste-like consistency was obtained. The paste was cold rolled and a square of approximately 0.25 cm² in size and 2.5–3 mg in weight was placed on a stainless steel grid (80 mesh, 0.127 mm, from Alfa Aesar) used as a current collector and was pressed at 0.9 MPa. The counter electrode was a platinum grid placed approximately at 20 mm of the working electrode. All potentials are reported versus a Ag/AgCl reference electrode that was placed at 5 mm of the working electrode. Degassed aqueous 0.5 M sulfuric acid was used as electrolyte. Prior to any measurement, the composite electrode was dipped in the electrolyte for 30 min in order to allow the electrolyte to impregnate the electrode porosity. Cyclic voltammetry was carried out using a potentiostat electrochemical interface SI480 (Solartron Instruments) controlled with DC Corrware software (Scribner Associates, version 2.8d).

Table 1 Experimental conditions used for the electrochemical exfoliation of graphite electrode and functionalization by spontaneous reduction of anthraquinone diazonium ions together with relevant parameters for the process and resulting materials

	Electrochemical exfoliation ^a	Pre-electrochemical exfoliation ^b followed by functionalization ^b	Electrochemical exfoliation and functionalization ^c
Electrolyte ^a	0.1 M H ₂ SO ₄	0.1 M H ₂ SO ₄ (200 mL)	0.1 M H ₂ SO ₄ + 16 mM AQ diazonium ions ^d
Potential ^a , V	10	10	10
Time ^a , h	1	1	1
Electrolyte ^b	—	200 mL of 0.1 M H ₂ SO ₄ + 100 mL of 16 mM AQ diazonium ions ^d	—
Potential ^b , V	—	No applied potential, spontaneous reaction	—
Time ^b , h	—	1	—
Mass of graphene sheets, mg	500	305	350
Yield ^a , %	70	61	52
AQ loading, wt% (TGA ^b)	—	2	7
AQ loading, wt% (Echem ⁱⁱⁱ)	—	0.08	1.7

i.
$$\frac{\text{mass of EG (or EG-AQ)}}{\text{Initial mass of the graphite electrode} - \text{final mass of the electrode}} \times 100.$$

ii. Difference of weight loss at 600 °C for EG-AQ and EG samples

iii. See Experimental section (Section 2.4)

a Experiential conditions used for electrochemical exfoliation, pre-electrochemical exfoliation as well as electrochemical exfoliation and functionalization

b Experiential conditions used for chemical functionalization following pre-electrochemical exfoliation

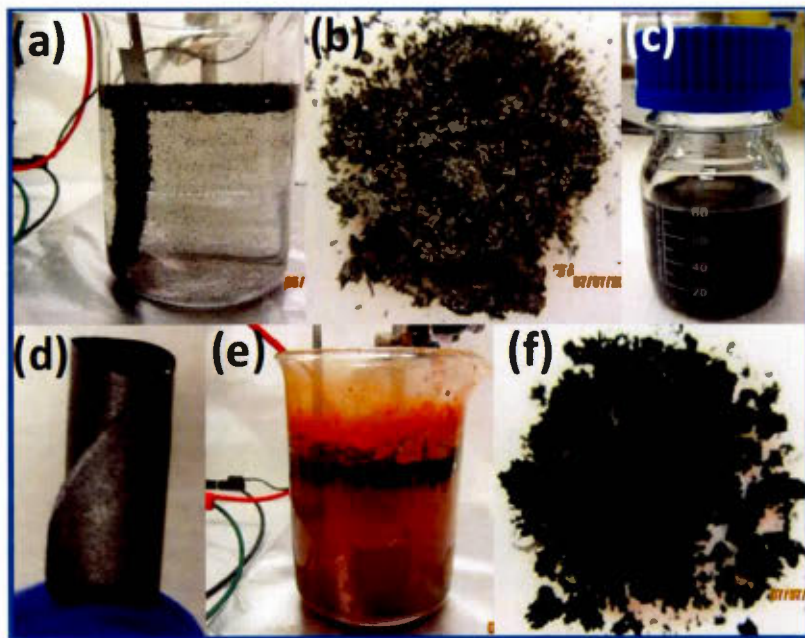


Figure 2 Photographic images of: (a) the electrochemical cell used for electrochemical exfoliation of graphite and graphene flakes floating at the surface of the electrolyte, (b) as prepared graphene, (c) graphene in DMF (10 mg mL^{-1}), (d) a self-supporting film, (e) the electrochemical cell used after electrochemical exfoliation and production of anthraquinone modified graphene flakes, (f) graphene sheets functionalized by anthraquinone groups. (A colour version of this figure can be viewed online.)

3. Results and discussion

3.1. Description of the experimental procedure and observation

A recent report has shown that electrochemical oxidation of graphite in aqueous H_2SO_4 yielded graphene sheets consisting mainly between 1 and 4 layers of

graphene, when appropriate experimental conditions are used [7]. In our work, we have found that a graphite electrode is also electrochemically exfoliated in the presence of diazonium ions in the 0.1 M H₂SO₄ solution. Indeed, following electrolysis of the graphite electrode, the presence of graphene flakes floating at the surface of the solution is observed (Fig. 2e). In this case, the yield for the formation of exfoliated graphene sheets is 52%, thus slightly lower than when the electrochemical exfoliation is performed only in 0.1 M H₂SO₄ (70%) (Table 1). The AQ-modified graphene sheets powder (Fig. 2f) is darker than the unmodified graphene sheets flakes (Fig. 2b). Nonetheless, the extinction coefficient at 660 nm of anthraquinone-modified graphene sheets dispersion determined from UV-visible spectra of dispersions of various concentrations was found to be smaller ($\epsilon_{660\text{nm}} = 1886 \text{ mL mg}^{-1} \text{ m}^{-1}$) than that of unmodified graphene sheets dispersions ($\epsilon_{660\text{nm}} = 3500 \text{ mL mg}^{-1} \text{ m}^{-1}$) (Supporting Information, Fig. S2). During the functionalization, defects created in the graphene structure disrupt its electronic structure, make the material less conductive and lower its extinction coefficient [55]. The lower absorption coefficient might suggest a loss of the graphitic character due to the increase of sp³-hybridized carbons for the anthraquinone modified graphene sheets.

3.2 Characterization of materials

Electron microscopy analysis

Fig. 3a and b shows the SEM images for electrochemically exfoliated graphene sheets (EG) and graphene sheets modified with anthraquinone groups (EG-AQ), respectively. The presence of individual graphene nanosheets with different sizes is clearly visible on Fig. 3a. The graphene sheets appear almost transparent under the electron microscope, indicating that the graphene sheets are composed of a few layers. Close examination of Fig. 3b reveals that the anthraquinone

functionalized graphene sheets are a slightly crumpled. This phenomena has been already observed for graphene sheets functionalized by organic molecules [24,56,57]. The SEM image shows thin and wrinkled flakes transparent to electrons despite the functionalization. The morphological characteristics of exfoliated graphene sheets and anthraquinone-modified graphene sheets were also investigated by transmission electronic microscopy (TEM) and high-resolution TEM (HRTEM). At low magnification, transparent graphene sheets are noticeable in Fig. 3c and d, confirming the SEM analysis that graphene sheets contain only a few layers. By comparing Fig. 3c and d, one can conclude that the functionalization did not damage the structure of the graphene sheets. HRTEM images of as-prepared graphene and anthraquinone-modified graphene shown in Fig. 3e and f, respectively, confirm that the majority of graphene sheets range from a single layer to bilayers.

Atomic force microscopy (AFM)

The number of layers of the graphene sheets was further investigated by AFM and representative images are shown in Fig. 3g and h. Line profiles over graphene flakes indicate thicknesses in the range of 1 nm for electrochemically exfoliated graphene sheets, which correspond to a value slightly higher than a single graphene layer [24,30,58]. The thickness of the anthraquinone-modified graphene sheets is about twice larger at about 2.5 nm. These measured thickness values are in the range reported for electrochemically exfoliated graphene sheets [44,58]. The larger thickness of the EG-AQ sheets could be explained by the presence of the grafted anthraquinone molecules on the surface of the graphene sheets. By considering a perpendicular orientation of the grafted molecule ($0.388 \text{ nm} \times 0.744 \text{ nm} \times 1.165 \text{ nm}$) [47], the anthraquinone molecule should contribute about 1.2 nm to the thickness of a graphene/anthraquinone assembly. However, since it is not possible to clearly image the perpendicularly grafted molecule and that other orientations of the grafted

molecules are possible, it seems plausible to assume that electrochemical exfoliation in the presence of diazonium ions yield graphene sheets with a slightly larger number of graphene layers indicating a less efficient electrochemical exfoliation. In this case, it could be postulated that the edges of the graphene sheets are the most likely grafting sites [59] and that, on the basal plane, a combination of horizontally adsorbed molecules and perpendicularly grafted anthraquinone molecules is occurring. Finally, the size of the graphene sheets observed on the AFM images is in the mm range, in agreement with previous studies on electrochemically exfoliated graphene sheets [6,7].

Nitrogen gas adsorption

Fig. 4a displays the nitrogen gas adsorption isotherms for anthraquinone-functionalized (EG-AQ) and unfunctionalized graphene (EG) sheets, together with the corresponding pore size distribution (Fig. 4a, inset). The adsorption isotherm for EG is characterized by a relatively small volume increase at low relative pressure that is followed by a sloped plateau, which is similar in shape to those seen for low surface area activated carbons [60]. EGAQ displays a completely different type of isotherm with negligible volume uptake at low relative pressure and an hysteresis between the adsorption and desorption branches at higher pressure, slightly resembling that of mesoporous carbon [61]. This clearly demonstrates the effect of the presence of grafted molecules on the pore texture. This is further demonstrated on the pore size distribution plot (Fig. 4a, inset). Unmodified graphene (EG) displays

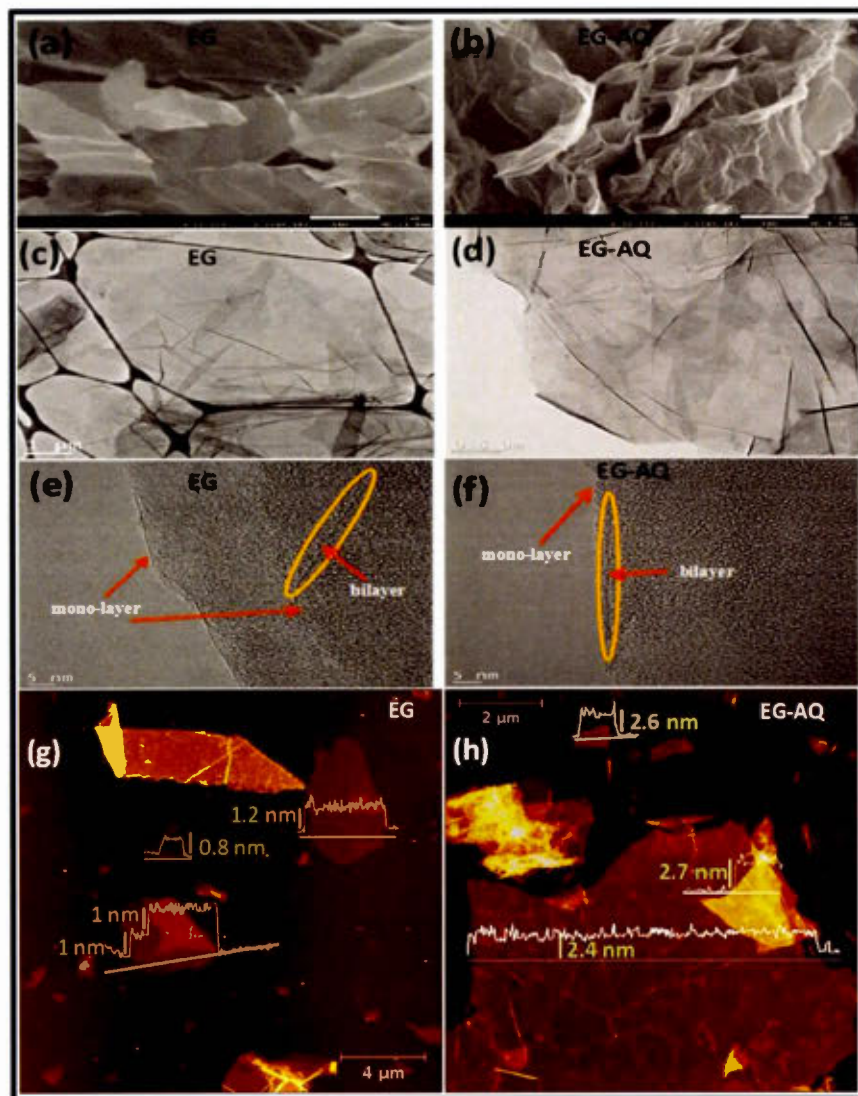


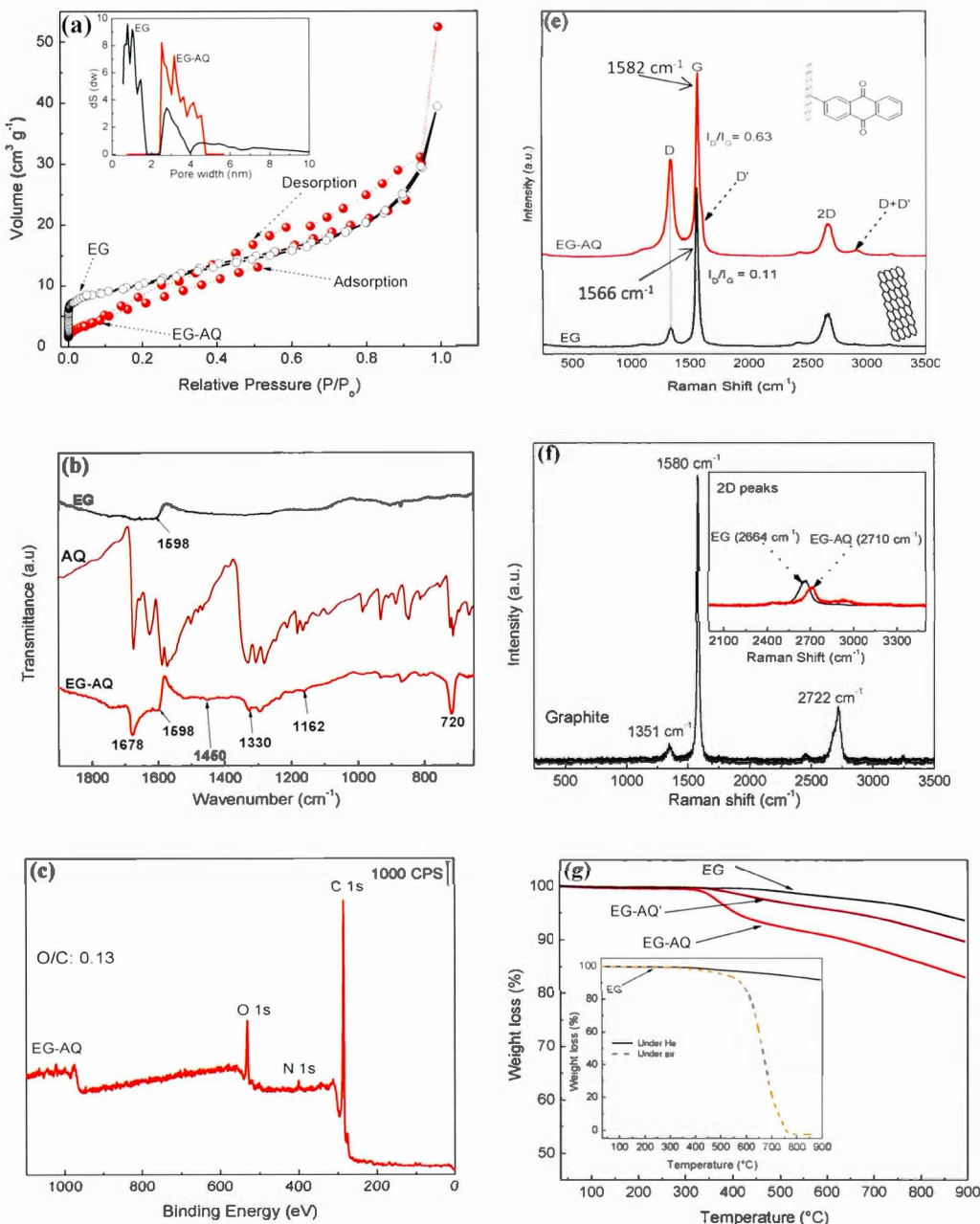
Figure 3 High-magnification SEM images of electrochemically exfoliated graphene (EG) (a) and anthraquinone-modified graphene sheets (EG-AQ) (b); TEM images of EG (c) and EGAQ (d); HRTEM of single and bilayer of EG (e) and EG-AQ (f); AFM images of EG (g) and EG-AQ (h). (A colour version of this figure can be viewed online.)

two kinds of pores with a significant amount of micropores, smaller than 2 nm and a contribution of mesopores between 2 and 5 nm. Following grafting of anthraquinone molecules on graphene sheets, the micropores are blocked, presumably due to the attachment of anthraquinone groups [47,60] and an increase of the contribution of mesopores is observed. These are in agreement with the qualitative trend seen on the adsorption isotherms. The BET specific surface area of the electrochemically exfoliated graphene sheets functionalized with anthraquinone was found to 60 ± 4 m^2/g , which is significantly larger than that (25 ± 4 m^2/g) of the unmodified electrochemically exfoliated graphene sheets. These small values are consistent with a significant restacking of graphene sheets for both materials because they are much smaller than the theoretical surface area of graphene ($2630 \text{ m}^2/\text{g}$) [1]. Indeed, from the measured surface area, the number of graphene layers could be estimated to about 100 and 40 for EG and EG-AQ, respectively [62]. Nonetheless, the larger BET specific surface area of EG-AQ suggests that the presence of grafted anthraquinone molecules slightly prevent the aggregation of the graphene sheets. This observation is consistent with the better dispersibility of EG-AQ powder. The discrepancy in the number of graphene layers deduced from AFM and gas adsorption measurements is due to the different methods (Experimental section) used to prepare the samples for these analyses.

FTIR spectroscopy

FTIR spectra of electrochemically exfoliated graphene sheets (EG) and graphene sheets functionalized by anthraquinone groups (EG-AQ) are presented in Fig. 4a. The spectrum of EG-AQ shows the presence of additional bands, which are absent in the spectrum of EG and that are attributed to the grafted quinone groups. The spectrum of 2-aminoanthraquinone AAQ presented in Fig. 4b shows that most of

these bands are observed for EG-AQ albeit with a lower intensity and a slight shift of the position. The band at 1678 cm^{-1} (C=O) for EG-AQ confirms the presence of anthraquinone groups on the graphene sheets [63]. The one at 1330 cm^{-1} is also observed for AAQ. The band at 1598 cm^{-1} , appearing as shoulder of both EG and EG-AQ spectra is due to the stretching mode of double bond (C=C) in the graphene structure [17]. Furthermore, the band at 720 cm^{-1} is attributed to the grafted quinone as it is observed for the free molecule. Finally, the band located at 1162 cm^{-1} is associated to the (C-OH) stretching mode [64]. Thus, the FTIR data confirm the presence of anthraquinone on the graphene sheets during the electrochemical exfoliation process.



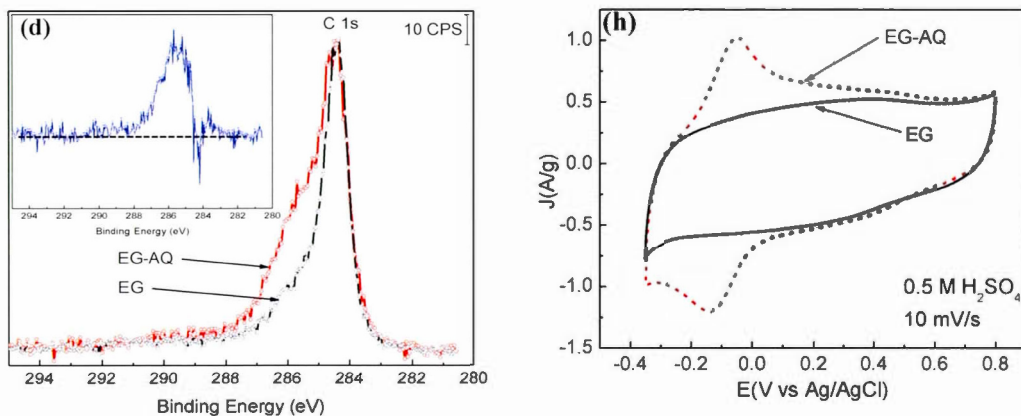


Figure 4 (a) N_2 adsorption isotherms of unmodified and AQ-modified graphene. The inset shows the pore size distribution of EG and EG-AQ. (b) FTIR spectra for electrochemically exfoliated graphene sheets (EG), 2-aminoanthraquinone (AAQ) and functionalized graphene sheets by anthraquinone groups (EG-AQ). (c) XPS survey spectrum of EG-AQ and (d) core level C 1s spectra of EG and EG-AQ. The inset shows the subtracted signal obtained by difference between C 1s spectra of EG and EG-AQ. (e) Raman spectra with a 532 nm excitation laser wavelength of the electrochemically exfoliated graphene sheets (EG) and for anthraquinone-modified graphene sheets (EG-AQ). (f) Raman spectrum of graphite with the 2D spectra of EG and EG-AQ as inset. (g) TGA curves of (inserted) EG in air and under He flow (inset), and EG, EG-AQ' and EG-AQ under He atmosphere. Heating rate: 5 °C/min. (h) Cyclic voltammograms for unmodified (full curve) and anthraquinone-grafted graphene (dashed curve) in a 0.5 M H_2SO_4 solution at a scan rate of 10 mV s⁻¹

X-ray photoelectron spectroscopy

X-ray photoelectron spectroscopy (XPS) was used to investigate the electronic properties of the electrochemically exfoliated materials and to determine the nature of the chemical bonding of the anthraquinone moieties with the graphene surface. The

XPS survey spectrum of electrochemically exfoliated graphene sheets (Supporting Information, Fig. S3) show the expected C 1s and O 1s peaks at 285 and 532 eV, respectively. The presence of a N 1s peak at 400 eV on the spectrum of anthraquinone-modified graphene sheets (Fig. 4c) can be taken as a first indication of the covalent grafting of anthraquinone molecules during the electrochemical exfoliation. This peak is due to the formation of the azo linkage (C-N=N-C) between the carbon substrate and the grafted molecule and is commonly observed during surface functionalization by using the diazonium chemistry [65–67]. Its presence could be explained by either the reaction of diazonium cations with phenol groups present on the graphene sheets [68] or directly with graphene sheets [25]. The O/C atomic ratio evaluated from the survey spectra data revealed an increase from 0.06 to 0.13 for the EG and EG-AQ samples, respectively. This increase is consistent with the presence of anthraquinone molecules at the graphene sheets surface. Fig. 4d shows the core level of C 1s spectra of EG and EG-AQ. The C 1s spectrum of EG-AQ is characterized by a more intense shoulder on the main peak. The additional contribution becomes more obvious in the difference spectra (inset of Fig. 4d) in which the positive peak at 285.5 eV is due to the presence of anthraquinone molecules on graphene nanosheets surface.

Raman spectroscopy

Raman spectroscopy was used for characterization of graphene sheets generated by electrochemical exfoliation of graphite in the absence and the presence of anthraquinone diazonium ions in the electrolyte. Raman analysis is a powerful tool to estimate the number of graphene layers and support the formation of a covalent linkage between the graphene substrate and organic molecules [69,70]. The Raman spectrum of EG shown in Fig. 4e exhibits three prominent Raman Stokes peaks; a D

peak at $\sim 1340 \text{ cm}^{-1}$, a G peak (E_{2g} symmetry of carbon atoms) at $\sim 1566 \text{ cm}^{-1}$ and a single symmetric 2D peak at $\sim 2680 \text{ cm}^{-1}$, that is consistent with the literature [6,7,10,26,70–74]. The appearance of the D peak is caused by the breathing mode of sp^2 carbon atoms and associated with the presence of few sp^3 carbon atoms or defects in the graphene structure [69,70,75]. The intensity of the G band (I_G) is associated with the amount of sp^2 -carbon [17,76,77]. The Raman intensity ratio (I_D/I_G) is used to evaluate the quality of graphitic nanostructures. The low I_D/I_G ratio of 0.11 for EG gives a good indication of the high-quality graphene prepared by electrochemical exfoliation [6,7,78]. In addition, the position and the shape of the 2D band (2664 cm^{-1}) of as-prepared graphene suggests that the graphene sheets consist of 1–2 layers [26,69–71,79,80]. This result confirms the high-resolution TEM data. This represents a significant shift in comparison to the position of the 2D band of graphite (Fig. 4f), which is observed at 2722 cm^{-1} [70]. Interestingly, the spectrum of anthraquinone-modified graphene sheets shows the corresponding band at 2710 cm^{-1} . This slight shift toward higher energy, compared to unmodified graphene sheets is in good agreement with observation made with graphene functionalized by reaction with diazonium ions [36,81]. Another important main feature of the Raman spectrum of the anthraquinone-modified graphene sheets (Fig. 4e, EG-AQ), is the increase of the relative intensity of the D band indicating the conversion of sp^2 -carbons to sp^3 state due to the covalent grafting of anthraquinone groups onto the graphene sheets [30,82]. The I_D/I_G ratio changes significantly from 0.11 to 0.63 due to the generation of defects upon functionalization. Moreover, the G peak position was slightly shifted by 16 cm^{-1} (from 1566 to 1582 cm^{-1}) after graphene functionalization. This shift is attributed to the presence of isolated sp^2 -carbons separated by anthraquinone groups in the carbon network [83]. The spectrum also shows D' and D + D' peaks appearing at ~ 1620 and $\sim 2930 \text{ cm}^{-1}$, respectively and that are practically absent in the graphene spectrum. These changes are attributable to the breaking of translational symmetry of

the honeycomb lattice of sp^2 -carbon bonds on the basal plane of graphene due to the formation of localized C–C sp^3 bonds by the grafting of anthraquinone groups [70,82,84].

Thermogravimetric analysis

Thermogravimetric analysis (TGA) was performed under air to evaluate the loading of AQ molecules on the graphene sheets (Table 1), the thermal stability of graphene sheets and get some insight on the number of graphene layers. TGA measurements performed under helium atmosphere allow to estimate the loading of anthraquinone groups and to evaluate the thermal stability of the grafted layers. All samples were heat treated at 200 °C under argon for 1 h prior to TGA analysis. The thermogram obtained for EG (Fig. 4g) shows clearly that EG is thermally stable under helium. The slight weight loss observed is attributed to the departure of oxygenated groups present on the surface of the graphene sheets. However, under air-flow (Fig. 4g, inset), one can observe an abrupt mass loss around 600 °C due to degradation of the graphene material. This behavior is consistent with that observed for graphene predominantly containing 1 to 2 layers [72]. The anthraquinone modified graphene sheets, investigated under He flow, showed an onset of mass loss at ~300 °C that is significantly larger compared to EG and that corresponds to 7 wt% anthraquinone molecules and attributed to the grafting of the graphene sheets during the electrochemical exfoliation [29,33]. In the case of EG-AQ' obtained by chemical modification of electrochemically exfoliated graphene in two steps: electrochemical exfoliation for 1 h (step 1) and functionalization for 1 h (step 2) (see Table 1 for more details) and which is the common method to functionalize carbon-based powders [30], one can observe a monotonous decrease up to 900 °C. Furthermore, a smaller

mass loss is obtained (2 wt%) in this case (see above). The lower grafting efficiency will be discussed below.

Electrochemical measurements

Cyclic voltammetry was used to investigate and to confirm the presence and loading of anthraquinone groups on functionalized graphene sheets. The cyclic voltammogram of the AQ grafted graphene sheets electrode (Fig. 4h, EG-AQ) shows well-defined cathodic and anodic waves centered at -0.15 and -0.06 V, respectively, that are consistent with values reported for anthraquinone-grafted on carbon powder [47–49,85]. The cyclic voltammogram contrasts with that of the unmodified graphene sheets electrode (Fig. 4h, EG) that shows a nearly rectangular shape similar to those reported for graphene electrode [6,9,17,86]. The redox peaks, observed on the cyclic voltammogram of the EG-AQ are attributed to the well-known 2 protons, 2 electrons quinone redox interconversion in acid media (Supporting Information, Fig. S4) [48,87]. The gravimetric capacitance of the EG electrode was determined to be 53 ± 1 F/g. For the functionalized EG, the contribution of graphene sheets after subtraction of the faradaic charge of the grafted AQ molecules [47] was estimated to 52 ± 2 F/g. By taking into account, the BET surface area, their double layer capacitances are 210 and $86 \mu\text{F}/\text{cm}^2$, respectively. These values are much higher than those computed for graphene from the reported gravimetric capacitance and BET surface area and which range from 20 to $75 \mu\text{F}/\text{cm}^2$ [88]. The highest values found in our work seem to suggest difference in restacking of the graphene sheets samples used for gas adsorption and electrochemistry measurements. The anthraquinone loading for anthraquinone functionalized graphene sheets is determined to be 1.7 wt% from the anodic charge of the cyclic voltammetry [85,89]. Surprisingly, this value is smaller than that determined by thermogravimetric measurements. The observed difference is intriguing and is not fully understood at the moment but possible explanations are

given below. It is important to consider that both EG and EG-AQ samples were heat-treated under Ar prior to measurements. Despite that, it is possible that strongly adsorbed molecules of anthraquinone and solvent remained trapped in the EG-AQ materials. This will led to an overestimation of the 7 wt% mass loss. The difference of the nitrogen gas adsorption isotherms (Fig. 4a) points to a change of pore texture and accessibility to the surface in case of the functionalized EG sheets. Furthermore, this may have the consequence to leave some anthraquinone molecules electrochemically inaccessible. Also, possible leaching of AQ molecules during the cyclic voltammetry measurements can be ruled out because no significant decrease of the AQ redox wave was observed between the first and the fifth cycles. Thus, more work is needed to get a clear understanding of the difference of AQ loading observed by TGA and electrochemistry.

Electrical conductivity measurements

The effect of the electrografting of anthraquinone groups on graphene sheets on the electronic conductivity of the materials was assessed by four-point probe measurements of self-supported films (Fig. 2d) of electrochemically exfoliated graphene sheets and anthraquinone modified graphene sheets. Electrochemically exfoliated graphene exhibited a high electrical conductivity to 124 S/cm, in the range of those reported in the literature [3,74,90,91]. However, a significant decrease of conductivity (20 S/cm) is observed for the anthraquinone functionalized graphene sheets. This decrease is attributed to the transformation of sp^2 -hybridized carbons, necessary for electronic conductivity, to sp^3 carbon induced by the covalent modification of graphene sheets. The latter disrupts the p-conjugated network and also impoverished the electronic structure of graphene.

4. Mechanism of the exfoliation/functionalization process

A mechanism of electrochemical exfoliation and functionalization is proposed below and consists in two main consecutive steps (Figure 5). The first one is the formation of graphene sheets, which involves water oxidation and intercalation of sulfate cations in the oxidized graphite electrode [92]. Briefly, when a high positive voltage is applied between the graphite electrode and the negative electrode, hydroxyl radicals generated by oxidation of water at the anode react at active edge sites [6,7,93,94]. At the resulting oxidized sites, the intercalation of SO_4^{2-} anions caused the exfoliation and production of graphene sheets. Secondly, in the presence of diazonium ions in the electrolyte, these diazonium ions are spontaneously reduced by the freshly exfoliated graphene sheets. The graphene sheets act as reducing agent for diazonium ions, as previously reported for the spontaneous modification of various carbons including graphene [29,47,48,60,66]. The lower yield for the formation of EG-AQ relative to EG mentioned above could be due to the fact that diazonium ions act as scavengers of oxygen and hydroxyl radicals, resulting in a smaller concentration of oxidized carbon sites [27].

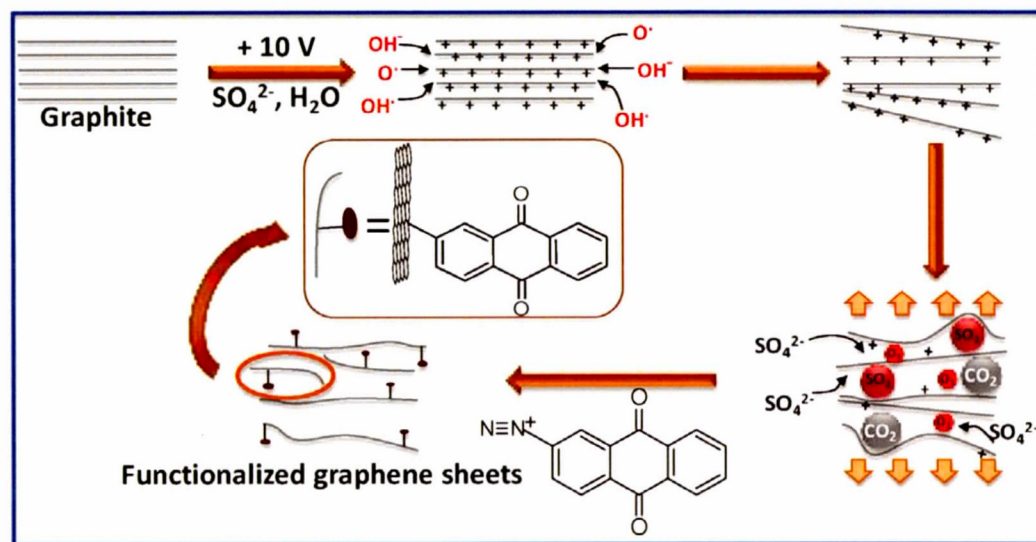


Figure 5 Main steps of the mechanism of electrochemical exfoliation/functionalization of graphene sheets. (A colour version of this figure can be viewed online)

A related but conceptually different process to modify graphene with a one-pot approach involves the reaction of already expanded graphene with CO_2 to obtain carboxylated graphene [95]. In that study, expanded graphene was obtained by electrochemical reductive charging of multilayered graphene in the presence of large tetrabutylammonium cations in the electrolyte [95]. In addition to the data presented above, control experiments performed to confirm the exfoliation and grafting process are presented and discussed below. Firstly, the electrochemical exfoliation and reaction with diazonium ions were carried out in two steps, as previously reported (see Table 1) [22]. In this experiment, graphene sheets were firstly produced in 0.1 M H_2SO_4 . Following electrochemical exfoliation for 1 h, a diazonium ions solution was added to the electrochemical cell and left to react at open circuit under continuous

stirring for 1 h. In this case, grafting of a much smaller amount of anthraquinone molecules was observed by TGA (Fig. 4g) and electrochemistry (Table 1). This indicates that the reaction of diazonium ions is more favorable with freshly produced graphene sheets. Interestingly, it has been demonstrated that the electrochemical activity of graphene is strongly affected by exposure to oxygen, water and other chemicals, which lead to modification of graphene and decrease of electron transfer activity [96,97]. Another possible cause is that in the two-step process, the graphene sheets have aggregated, yielding a lower accessible surface area for chemical grafting. Secondly, even if strong evidence for grafting of quinone molecules was obtained above, anthraquinone is known to strongly adsorb on carbon surfaces [65,98,99]. In order to rule out a possible adsorption of anthraquinone on graphene sheets, the electrochemical exfoliation was performed in the presence of anthraquinone (instead of in situ generated diazonium ions) in the 0.1 M H₂SO₄ solution. Analysis of the resulting electrochemically exfoliated materials, under the form of a composite electrode and as carried out in Fig. 4h, by cyclic voltammetry shows only the presence of a small amount 0.01 wt% of anthraquinone molecules on the graphene sheets. Thirdly, when 2-aminoanthraquinone was added to the electrolyte, the electrochemical exfoliation of graphite did not occurred. The lack of exfoliation is presumably due the formation of a polyaniline derivative of anthraquinone resulting from the oxidation of the monomer when the high positive potential is applied to the graphite electrode. In this case, the resulting polyaniline layer prevents the electrochemical exfoliation of graphite. Furthermore, this result indirectly demonstrates that the diazotization of 2-aminoanthraquinone, in the presence of tertbutylnitrite, is complete.

5. Conclusions

One-pot synthesis of anthraquinone modified graphene sheets was achieved during the electrochemical oxidative exfoliation of graphite in the presence of in situ generated anthraquinone diazonium cations in 0.1 M H₂SO₄. Modification of the exfoliated graphene sheets occurred by their spontaneous reduction of diazonium ions present in the electrolyte. This method is conceptually different from previous approaches based on electrochemical reductive exfoliation of a carbon-based electrode and subsequent addition a diazonium ions solution to the mixture containing electrochemically exfoliated graphene sheets [22,58]. It allows a more rapid functionalization of graphene sheets relative to the method based on reaction of diazonium ions with pre-exfoliated graphene sheets. The presence of anthraquinone molecules on the graphene sheets was demonstrated by AFM, FTIR, XPS, SEM, TEM, HRTEM, TGA and Raman spectroscopy. Evidence for the covalent grafting of the anthraquinone groups was provided by electronic conductivity measurements, thermogravimetric analysis, Raman spectroscopy and electrochemistry. The observation of a difference in the anthraquinone molecules loading by TGA and electrochemistry (Table 1) is intriguing and requires further investigation. Functionalized graphene sheets show a better dispersibility and a larger BET specific surface area than unmodified exfoliated graphene sheets due to the presence of grafted molecules that prevent restacking and aggregation of graphene sheets. Future works will focus on getting a better understanding of the electrochemical exfoliation/functionalization one-pot process. For example, it will be interesting to investigate the effect of the concentration of diazonium ions, the role of radical traps of reactive species involved in the exfoliation process [27,100] and the grafting step [101]. This will allow a control of the quality of the graphene sheets and the loading of anthraquinone or other grafted molecules. To this end, useful information will be

obtained by monitoring the actual electrode potential by using a three-electrode configuration. In addition, it will be relevant to determine the effect of the anode electrode potential on the chemical stability of the diazonium ions. Finally, this one-pot electrochemical exfoliation and functionalization method can be also used to generate other functionalized graphene sheet materials and the results will be reported elsewhere in due course.

6. Acknowledgements

This work was financially supported by the Natural Sciences and Engineering Research Council of Canada (NSERC). This research benefited from the use of the research infrastructure of NanoQAM, which is also acknowledged.

7. References

- [1] K.S. Novoselov, A.K. Geim, S. V Morozov, D. Jiang, Y. Zhang, S. V Dubonos, et al., Electric field effect in atomically thin carbon films., *Science*. 306 (2004) 666–669.
- [2] A.A. Balandin, S. Ghosh, W. Bao, I. Calizo, D. Teweldebrhan, F. Miao, et al., Superior thermal conductivity of single-layer graphene., *Nano Lett.* 8 (2008) 902–907.
- [3] M.D. Stoller, S. Park, Y. Zhu, J. An, R.S. Ruoff, Graphene-based ultracapacitors., *Nano Lett.* 8 (2008) 3498–3502.

- [4] C. Lee, X. Wei, J.W. Kysar, J. Hone, Measurement of the elastic properties and intrinsic strength of monolayer graphene., *Science*. 321 (2008) 385–358.
- [5] G.-H. Lee, R.C. Cooper, S.J. An, S. Lee, A. van der Zande, N. Petrone, et al., High-strength chemical-vapor-deposited graphene and grain boundaries., *Science*. 340 (2013) 1073–1076.
- [6] K. Parvez, Z.-S. Wu, R. Li, X. Liu, R. Graf, X. Feng, et al., Exfoliation of graphite into graphene in aqueous solutions of inorganic salts., *J. Am. Chem. Soc.* 136 (2014) 6083–6091.
- [7] K. Parvez, R. Li, S.R. Puniredd, Y. Hernandez, F. Hinkel, S. Wang, et al., Electrochemically exfoliated graphene as solution-processable, highly conductive electrodes for organic electronics., *ACS Nano*. 7 (2013) 3598–3606.
- [8] D. Wu, F. Zhang, H. Liang, X. Feng, Nanocomposites and macroscopic materials: assembly of chemically modified graphene sheets, *Chem. Soc. Rev.* 41 (2012) 6160–6177.
- [9] Z.-S. Wu, K. Parvez, X. Feng, K. Müllen, Graphene-based in-plane micro-supercapacitors with high power and energy densities., *Nat. Commun.* 4 (2013) 2487–3487.
- [10] A. Guermoune, T. Chari, F. Popescu, S.S. Sabri, J. Guillemette, H.S. Skulason, et al., Chemical vapor deposition synthesis of graphene on copper with methanol, ethanol, and propanol precursors, *Carbon*. 49 (2011) 4204–4210.

- [11] I. Forbeaux, J. Themlin, J. Debever, Heteroepitaxial graphite on 6 H - SiC(0001) : Interface formation through conduction-band electronic structure, *Phys. Rev. B.* 58 (1998) 396–406.
- [12] P.W. Sutter, J.-I. Flege, E.A. Sutter, Epitaxial graphene on ruthenium., *Nat. Mater.* 7 (2008) 406–411.
- [13] W.S. Hummers, R.E. Offeman, Preparation of Graphitic Oxide, *J. Am. Chem. Soc.* 80 (1958) 1339–1339.
- [14] D.R. Dreyer, S. Park, C.W. Bielawski, R.S. Ruoff, The chemistry of graphene oxide., *Chem. Soc. Rev.* 39 (2010) 228–240.
- [15] H. Li, Y. Wang, Y. Shi, J. Li, L.H. Yang, H. Ying, Large scale synthesized sulphonated reduced graphene oxide: a high performance material for electrochemical capacitor, *RSC Adv.* 35 (2013) 14839–15492.
- [16] A.B. Bourlinos, K. Safarova, K. Siskova, R. Zbořil, The production of chemically converted graphenes from graphite fluoride, *Carbon.* 50 (2012) 1425–1428.
- [17] A.K. Das, M. Srivastav, R.K. Layek, M.E. Uddin, D. Jung, N.H. Kim, et al., Iodide-mediated room temperature reduction of graphene oxide: a rapid chemical route for the synthesis of a bifunctional electrocatalyst, *J. Mater. Chem. A.* 2 (2014) 1332–1340.
- [18] W. Chen, L. Yan, Preparation of graphene by a low-temperature thermal reduction at atmosphere pressure., *Nanoscale.* 2 (2010) 559–563.

- [19] T. Kuila, A.K. Mishra, P. Khanra, N.H. Kim, J.H. Lee, Recent advances in the efficient reduction of graphene oxide and its application as energy storage electrode materials., *Nanoscale*. 5 (2013) 52–71.
- [20] Y. Shao, J. Wang, H. Wu, J. Liu, I.A. Aksay, Y. Lin, Graphene based electrochemical sensors and biosensors: A review, *Electroanalysis*. 22 (2010) 1027–1036.
- [21] J. Wang, K.K. Manga, Q. Bao, K.P. Loh, High-Yield Synthesis of Few-Layer Graphene Flakes through Electrolyte, *J. Am. Chem. Soc.* 133 (2011) 8888–8891.
- [22] Y.L. Zhong, T.M. Swager, Enhanced Electrochemical Expansion of Graphite for in Situ Electrochemical Functionalization, *J. Am. Chem. Soc.* 134 (2012) 17896–17899.
- [23] Y. Hernandez, V. Nicolosi, M. Lotya, F.M. Blighe, Z. Sun, S. De, et al., High-yield production of graphene by liquid-phase exfoliation of graphite., *Nat. Nanotechnol.* 3 (2008) 563–568.
- [24] G. Wang, B. Wang, J. Park, Y. Wang, B. Sun, J. Yao, Highly efficient and large-scale synthesis of graphene by electrolytic exfoliation, *Carbon*. 47 (2009) 3242–3246.
- [25] A.M. Abdelkader, A.J. Cooper, R.A.W. Dryfe, I.A. Kinloch, How to get between the sheets: a review of recent works on the electrochemical exfoliation of graphene materials from bulk graphite, *Nanoscale*. 7 (2015) 6944–6956.

- [26] M. Lotya, Y. Hernandez, P.J. King, R.J. Smith, V. Nicolosi, L.S. Karlsson, et al., Liquid Phase Production of Graphene by Exfoliation of Graphite in Surfactant / Water Solutions, *J. Am. Chem. Soc.* 131 (2009) 3611–3620.
- [27] J.M. Munuera, J.I. Paredes, S. Villar-Rodil, M. Ayán-Varela, A. Martínez-Alonso, J.M.D. Tascon, Electrolytic exfoliation of graphite in water with multifunctional electrolytes: en route towards high quality, oxide-free graphene flakes, *Nanoscale*. 8 (2016) 2982–2998.
- [28] E. Demory, K. Devaraj, A. Orthaber, P.J. Gates, L.T. Pilarski, Boryl (Hetero)aryne Precursors as Versatile Arylation Reagents: Synthesis through C-H Activation and Orthogonal Reactivity, *Angew. Chem. Int. Ed.* 54 (2015) 11765–11769.
- [29] G.L.C. Paulus, Q.H. Wang, M.S. Strano, Covalent electron transfer chemistry of graphene with diazonium salts, *Acc. Chem. Res.* 46 (2013) 160–170.
- [30] V. Georgakilas, M. Otyepka, A.B. Bourlinos, V. Chandra, N. Kim, K.C. Kemp, et al., Functionalization of graphene: covalent and non-covalent approaches, derivatives and applications., *Chem. Rev.* 112 (2012) 6156–6214.
- [31] P.T. Yin, S. Shah, M. Chhowalla, K.-B. Lee, Design, Synthesis, and Characterization of Graphene–Nanoparticle Hybrid Materials for Bioapplications, *Chem. Rev.* 115 (2015) 2483–2531.
- [32] E. Bekyarova, M.E. Itkis, P. Ramesh, C. Berger, M. Sprinkle, W.A. De Heer, et al., Chemical modification of epitaxial graphene: Spontaneous grafting of aryl groups, *J. Am. Chem. Soc.* 131 (2009) 1336–1337.

- [33] Z. Jin, J.R. Lomeda, B.K. Price, W. Lu, Y. Zhu, J.M. Tour, Mechanically assisted exfoliation and functionalization of thermally converted graphene sheets, *Chem. Mater.* 21 (2009) 3045–3047.
- [34] J.R. Lomeda, C.D. Doyle, D. V Kosynkin, W.-F. Hwang, J.M. Tour, Diazonium functionalization of surfactant-wrapped chemically converted graphene sheets., *J. Am. Chem. Soc.* 130 (2008) 16201–16206.
- [35] Z. Liu, S.P. Lau, F. Yan, Functionalized graphene and other two-dimensional materials for photovoltaic devices : device design and processing, *Chem. Soc. Rev.* 44 (2015) 5638–5679.
- [36] H. Lim, J.S. Lee, H.J. Shin, H.S. Shin, H.C. Choi, Spatially resolved spontaneous reactivity of diazonium salt on edge and basal plane of graphene without surfactant and its doping effect, *Langmuir*. 26 (2010) 12278–12284.
- [37] Z. Jin, T.P. McNicholas, C.J. Shih, Q.H. Wang, G.L.C. Paulus, A.J. Hilmer, et al., Click chemistry on solution-dispersed graphene and monolayer CVD graphene, *Chem. Mater.* 23 (2011) 3362–3370.
- [38] P.A. Brooksby, A.K. Farquhar, H.M. Dykstra, M.R. Waterland, A.J. Downard, Quantum Capacitance of Aryldiazonium Modi fi ed Large Area Few- Layer Graphene Electrodes, *J. Phys. Chem. C.* 119 (2015) 25778–25785.
- [39] Y.I. Zhang, L. Zhang, C. Zhou, Graphene and Related Applications, *Acc. Chem. Res.* 46 (2013) 2329–2339.
- [40] J. Li, G. Wang, W. Zhang, G. Jin, M. Zhang, X. Jiang, et al., chemically stable , electrically conductive, and biologically active substrate, *J. Mater. Chem. B Mater. Biol. Med.* 3 (2015) 1544–1555.

- [41] D. Bélanger, J. Pinson, Electrografting: a powerful method for surface modification., *Chem. Soc. Rev.* 40 (2011) 3995–4048.
- [42] A. Mesnage, X. Lefe, P. Je, G. Deniau, S. Palacin, Spontaneous Grafting of Diazonium Salts : Chemical Mechanism on Metallic Surfaces, *Langmuir*. 28 (2012) 11767–11778.
- [43] Z. Zha, L. Xu, Z. Wang, X. Li, Q. Pan, P. Hu, et al., 3D Graphene Functionalized by Covalent Organic Framework Thin Film as Capacitive Electrode in Alkaline Media, *ACS Appl. Mater. Interfaces*. 7 (2015) 17837–17843.
- [44] J. Greenwood, T.H. Phan, Y. Fujita, Z. Li, O. Ivasenko, H. Uji-i, et al., Covalent Modification of Graphene and Graphite Using Diazonium Chemistry : Tunable Grafting and, *ACS Nano*. 9 (2015) 5520–5535.
- [45] G. Dubey, R. Urcuyo, S. Abb, G. Rinke, M. Burghard, S. Rauschenbach, et al., Chemical Modification of Graphene via Hyperthermal Molecular Reaction, *J. Am. Chem. Soc.* 136 (2014) 13482–13485.
- [46] Y. Li, L. Galmiche, P. Audebert, F. Miomandre, G. Louarn, M. Bozlar, et al., Functionalization of Graphene Oxide by Tetrazine Derivatives: A Versatile Approach toward Covalent Bridges between Graphene, *Chem. Mater.* 27 (2015) 4298–4310.
- [47] G. Pognon, T. Brousse, D. Bélanger, Effect of molecular grafting on the pore size distribution and the double layer capacitance of activated carbon for electrochemical double layer capacitors, *Carbon*. 49 (2011) 1340–1348.

- [48] A. Le Comte, G. Pognon, T. Brousse, D. Bélanger, Determination of the Quinone-loading of a Modified Carbon Powder-based Electrode for Electrochemical Capacitor, *Electrochemistry*. 81 (2013) 873–876.
- [49] M. Weissmann, O. Crosnier, T. Brousse, D. Bélanger, Electrochemical study of anthraquinone groups, grafted by the diazonium chemistry, in different aqueous media-relevance for the development of aqueous hybrid electrochemical capacitor, *Electrochim. Acta*. 82 (2012) 250–256.
- [50] E. Lebègue, T. Brousse, J. Gaubicher, R. Retoux, C. Cougnon, Toward fully organic rechargeable charge storage devices based on carbon electrodes grafted with redox molecules, *J. Mater. Chem. A*. 2 (2014) 8599–8602.
- [51] E. Lebègue, T. Brousse, J. Gaubicher, C. Cougnon, Chemical functionalization of activated carbon through radical and diradical intermediates, *Electrochim. Commun.* 34 (2013) 14–17.
- [52] A. Le Comte, T. Brousse, D. Bélanger, Simpler and greener grafting method for improving the stability of anthraquinone-modified carbon electrode in alkaline media, *Electrochim. Acta*. 137 (2014) 447–453.
- [53] S. Brunauer, L.S. Deming, W.E. Deming, E. Teller, On a theory of the van der Waals adsorption of gases, *J. Am. Chem. Soc.* 62 (1940) 1723–1732.
- [54] S. Brunauer, P.H. Emmett, E. Teller, Adsorption of Gases in Multimolecular Layers, *J. Am. Chem. Soc.* 60 (1938) 309–319.

- [55] V. Chabot, B. Kim, B. Sloper, C. Tzoganakis, A. Yu, High yield production and purification of few layer graphene by gum arabic assisted physical sonication., *Sci. Rep.* 3 (2013) 1–7.
- [56] Y. Zhu, M.D. Stoller, W. Cai, A. Velamakanni, R.D. Piner, D. Chen, et al., Exfoliation of graphite oxide in propylene carbonate and thermal reduction of the resulting graphene oxide platelets, *ACS Nano.* 4 (2010) 1227–1233.
- [57] Y. Wang, X. Tong, X. Guo, Y. Wang, G. Jin, X. Guo, Large scale production of highly-qualified graphene by ultrasonic exfoliation of expanded graphite under the promotion of (NH₄)₂CO₃ decomposition, *Nanotechnology.* 24 (2013) 1–5.
- [58] Y.R. Leroux, J.F. Bergamini, S. Ababou, J.C. Le Breton, P. Hapiot, Synthesis of functionalized few-layer graphene through fast electrochemical expansion of graphite, *J. Electroanal. Chem.* 753 (2014) 42–46.
- [59] J.K. Kariuki, M.T. McDermott, Nucleation and growth of functionalized aryl films on graphite electrodes, *Langmuir.* 15 (1999) 6534–6540.
- [60] M. Toupin, D. Bélanger, Spontaneous functionalization of carbon black by reaction with 4-nitrophenyldiazonium cations., *Langmuir.* 24 (2008) 1910–1917.
- [61] M. Enterría, J.L. Figueiredo, Nanostructured mesoporous carbons: Tuning texture and surface chemistry, *Carbon.* 108 (2016) 79–108.
- [62] A.M. Dimiev, G. Ceriotti, A. Metzger, N.D. Kim, J.M. Tour, Chemical Mass Production of Graphene Nanoplatelets in ~100% Yield, *ACS Nano.* 10 (2015) 274–279.

- [63] Q. Wu, Y. Sun, H. Bai, G. Shi, High-performance supercapacitor electrodes based on graphene hydrogels modified with 2-aminoanthraquinone moieties., *Phys. Chem. Chem. Phys.* 13 (2011) 11193–11198.
- [64] Y. Xu, H. Bai, G. Lu, C. Li, G. Shi, Flexible graphene films via the filtration of water-soluble noncovalent functionalized graphene sheets, *J. Am. Chem. Soc.* 130 (2008) 5856–5857.
- [65] A. Le Comte, D. Chhin, A. Gagnon, R. Retoux, T. Brousse, D. Bélanger, Spontaneous grafting of 9,10-phenanthrenequinone on porous carbon as active electrode material in electrochemical capacitor in alkaline electrolyte, *J. Mater. Chem. A*. 3 (2015) 6146–6156.
- [66] J. Lyskawa, A. Grondein, D. Bélanger, Chemical modifications of carbon powders with aminophenyl and cyanophenyl groups and a study of their reactivity, *Carbon*. 48 (2010) 1271–1278.
- [67] D.B. Ossonon, M. Weissmann, D. Bélanger, Electrochemical modification of carbon electrode with benzylphosphonic groups, *Electrochim. Acta*. 122 (2014) 210–217.
- [68] C. Saby, B. Ortiz, G.Y. Champagne, D. Bélanger, Electrochemical Modification of Glassy Carbon Electrode Using Aromatic Diazonium Salts . 1 . Blocking Effect of 4-Nitrophenyl and 4-Carboxyphenyl Groups, *Langmuir*. 7463 (1997) 6805–6813.
- [69] A.C. Ferrari, J.C. Meyer, V. Scardaci, C. Casiraghi, M. Lazzeri, F. Mauri, et al., Raman Spectrum of Graphene and Graphene Layers, *Phys. Rev. Lett.* 97 (2006) 187401–187405.

- [70] A.C. Ferrari, D.M. Basko, Raman spectroscopy as a versatile tool for studying the properties of graphene., *Nat. Nanotechnol.* 8 (2013) 235–246.
- [71] Z. Sun, Z. Yan, J. Yao, E. Beitler, Y. Zhu, J.M. Tour, Growth of graphene from solid carbon sources., *Nature*. 468 (2010) 549–552.
- [72] H. Wang, Y. Wang, X. Cao, M. Feng, G. Lan, The thermal stability of graphene in air investigated by Raman spectroscopy, *J. Raman Spectrosc.* 44 (2013) 1018–1021.
- [73] C. Mattevi, H. Kim, M. Chhowalla, A review of chemical vapour deposition of graphene on copper, *J. Mater. Chem.* 21 (2011) 3324–3334.
- [74] C.-Y. Su, A.-Y. Lu, Y. Xu, F.-R. Chen, A.N. Khlobystov, L.-J. Li, High-quality thin graphene films from fast electrochemical exfoliation., *ACS Nano*. 5 (2011) 2332–2339.
- [75] A.C. Ferrari, J. Robertson, Interpretation of Raman spectra of disordered and amorphous carbon, *Phys. Rev. B*. 61 (2000) 14095–14107.
- [76] J.L. Bahr, J. Yang, D. V. Kosynkin, M.J. Bronikowski, R.E. Smalley, J.M. Tour, Functionalization of carbon nanotubes by electrochemical reduction of aryl diazonium salts: A bucky paper electrode, *J. Am. Chem. Soc.* 123 (2001) 6536–6542.
- [77] Y. Yang, S. Qiu, X. Xie, X. Wang, R.K.Y. Li, A facile, green, and tunable method to functionalize carbon nanotubes with water-soluble azo initiators by one-step free radical addition, *Appl. Surf. Sci.* 256 (2010) 3286–3292.

- [78] L. Buglione, E.L.K. Chng, A. Ambrosi, Z. Sofer, M. Pumera, Graphene materials preparation methods have dramatic influence upon their capacitance, *Electrochim. Commun.* 14 (2012) 5–8.
- [79] H. Zhou, F. Yu, H. Yang, C. Qiu, M. Chen, L. Hu, et al., Layer-dependent morphologies and charge transfer of Pd on n-layer graphenes., *Chem. Commun.* 47 (2011) 9408–9410.
- [80] I. Calizo, D. Teweldebrhan, W. Bao, F. Miao, C.N. Lau, A.A. Balandin, Spectroscopic raman nanometrology of graphene and graphene multilayers on arbitrary substrates, *J. Phys. Conf. Ser.* 109 (2008) 012008.
- [81] D.B. Farmer, G.M. Roksana, V. Perebeinos, Y.M. Lin, G.S. Tuievski, J.C. Tsang, et al., Chemical doping and electron-hole conduction asymmetry in graphene devices, *Nano Lett.* 9 (2009) 388–392.
- [82] S. Eissa, G.C. Jimenez, F. Mahvash, A. Guermoune, C. Tlili, T. Szkopek, et al., Functionalized CVD Monolayer Graphene for Label-Free Impedimetric Biosensing, *Nano Res.* 8 (2015) 1698–1709.
- [83] G.K. Ramesha, N.S. Sampath, Electrochemical reduction of oriented Graphene oxide films: An in situ Raman spectroelectrochemical study, *J. Phys. Chem. C.* 113 (2009) 7985–7989.
- [84] R. Sharma, J.H. Baik, C.J. Perera, M.S. Strano, Anomalously large reactivity of single graphene layers and edges toward electron transfer chemistries, *Nano Lett.* 10 (2010) 398–405.

- [85] M. Kullapere, J.M. Seinberg, U. Mäeorg, G. Maia, D.J. Schiffrin, K. Tammeveski, Electroreduction of oxygen on glassy carbon electrodes modified with in situ generated anthraquinone diazonium cations, *Electrochim. Acta.* 54 (2009) 1961–1969.
- [86] A. Ambrosi, C.K. Chua, A. Bonanni, M. Pumera, Electrochemistry of graphene and related materials., *Chem. Rev.* 114 (2014) 7150–7188.
- [87] A. Jaffe, A. Saldivar Valdes, H.I. Karunadasa, Quinone-Functionalized Carbon Black Cathodes for Lithium Batteries with High Power Densities, *Chem. Mater.* 27 (2015) 3568–3571.
- [88] J. Yan, Q. Wang, T. Wei, Z. Fan, Recent advances in design and fabrication of electrochemical supercapacitors with high energy densities, *Adv. Energy Mater.* 4 (2014) 1300816–1300859.
- [89] S. Baranton, D. Bélanger, Electrochemical derivatization of carbon surface by reduction of in situ generated diazonium cations., *J Phys. Chem. B.* 109 (2005) 24406–24410.
- [90] V. Volman, Y. Zhu, A.R.O. Raji, B. Genorio, W. Lu, C. Xiang, et al., Radio-frequency-transparent, electrically conductive graphene nanoribbon thin films as deicing heating layers, *ACS Appl. Mater. Interfaces.* 6 (2014) 298–304.
- [91] J. Han, X. Wang, Y. Qiu, J. Zhu, P. Hu, Infrared-transparent films based on conductive graphene network fabrics for electromagnetic shielding, *Carbon.* 87 (2015) 206–214.
- [92] K. Kinoshita, Carbon-Electrochemical and Physicochemical Properties., in: Wiley, New York, 1988: p. 533.

- [93] C.A. Martínez-Huitle, S. Ferro, Electrochemical oxidation of organic pollutants for the wastewater treatment: direct and indirect processes., *Chem. Soc. Rev.* 35 (2006) 1324–1340.
- [94] M. Rueffer, D. Bejan, N.J. Bunce, Graphite: An active or an inactive anode?, *Electrochim. Acta.* 56 (2011) 2246–2253.
- [95] E. Bjerglund, M. Kongsfelt, K. Shimizu, B. Bror, E. Jensen, L. Koefoed, et al., Controlled Electrochemical Carboxylation of Graphene To Create a Versatile Chemical Platform for Further Functionalization, *Langmuir.* 30 (2014) 6622–6628.
- [96] M. Velicky, D.F. Bradley, A.J. Cooper, E.W. Hill, I.A. Kinloch, A. Mishchenko, et al., Electron Transfer Kinetics on Mono- and Multilayer Graphene, *ACS Nano.* 8 (2014) 10089–10100.
- [97] R. Chen, N. Nioradze, P. Santhosh, Z. Li, S.P. Surwade, G.J. Shenoy, et al., Ultrafast Electron Transfer Kinetics of Graphene Grown by Chemical Vapor Deposition, *Angew. Chemie - Int. Ed.* 54 (2015) 15134–15137.
- [98] A.P. Brown, F.C. Anson, Cyclic and differential pulse voltammetric behavior of reactants confined to the electrode surface, *Anal. Chem.* 49 (1977) 1589–1595.
- [99] D.M. Anjos, J.K. McDonough, E. Perre, G.M. Brown, S.H. Overbury, Y. Gogotsi, et al., Pseudocapacitance and performance stability of quinone-coated carbon onions, *Nano Energy.* 2 (2013) 702–712.

- [100] S. Yang, S. Brüller, Z.-S. Wu, Z. Liu, K. Parvez, R. Dong, et al., Organic Radical-Assisted Electrochemical Exfoliation for the Scalable Production of High-Quality Graphene, *J. Am. Chem. Soc.* 137 (2015) 13927–13932.
- [101] T. Menanteau, C. Benoît, T. Breton, C. Cougnon, Enhancing the performance of a diazonium-modified carbon supercapacitor by controlling the grafting process, *Electrochim. Commun.* 63 (2016) 70–73.

8. Electronic Supplementary information

Experimental section: In situ electrochemical grafting with Nafion membrane

To rule out any effect associated with the electrochemical reduction of diazonium ions at the negative electrode and subsequent side reaction that might contribute to the presence of anthraquinone derived products with the functionalized graphene sheets, the electrochemical exfoliation was carried out in the same conditions as described in the Experimental section but with a Nafion (Nafion 117 obtained from Dupont, thickness 178 μm). The membrane was pretreated by boiling successively in H_2O_2 (3% v/v), H_2O , H_2SO_4 (0.5 M), and H_2O for 1 h and stored in 1 M HCl membrane. In this case, the loading of anthraquinone on the electrochemically exfoliate graphene sheets was found to be similar as a loading of about 1.2 wt. % of anthraquinone was determined. Please note that in the two-compartment configuration, the experimental conditions differ slightly as the actual potential at the positive electrode might differ due to the ohmic drop associated with the Nafion membrane.

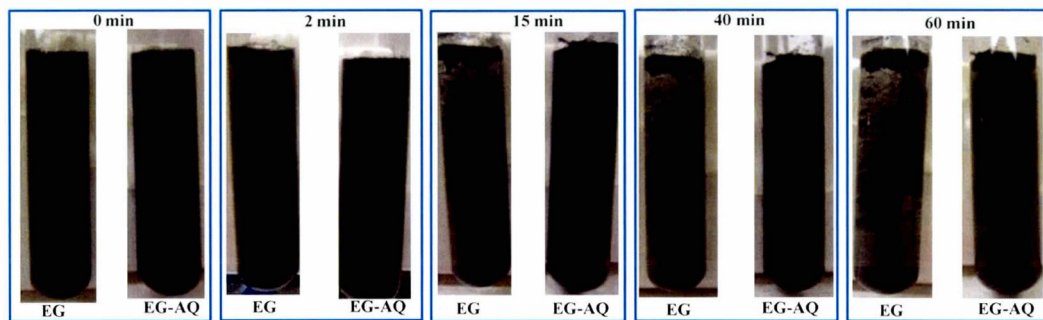


Figure S1 Optical photographs of unmodified (EG) and modified (EG-AQ) graphene dispersed at 0.5mg mL^{-1} in water by bath sonication immediately after preparation (0 min) and after 2, 15, 40 and 60 min.

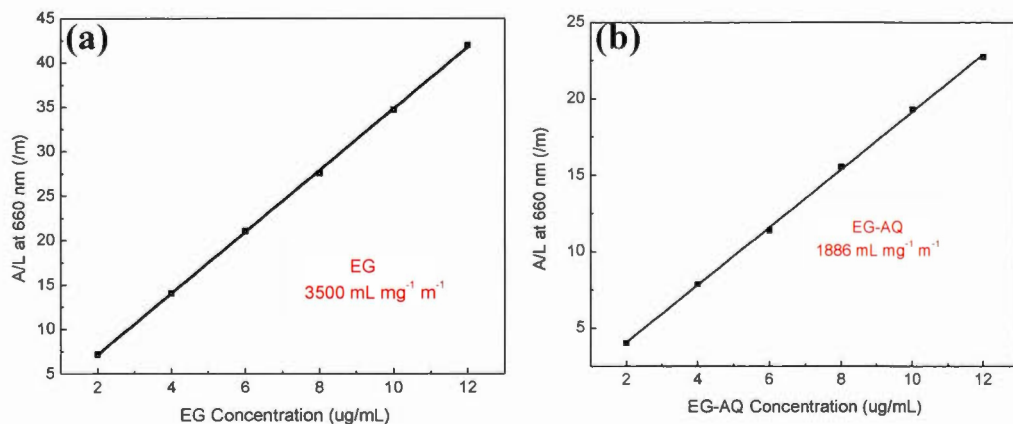


Figure S2 Plot of A/L (absorbance/path length (600 nm)) vs. exfoliated graphene concentration : (a) EG and (b) EG-AQ.

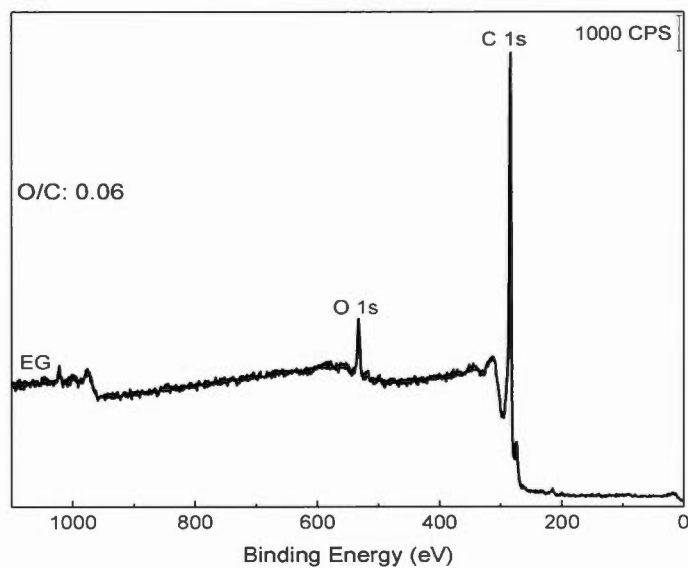


Figure S3 XPS survey spectrum of EG.

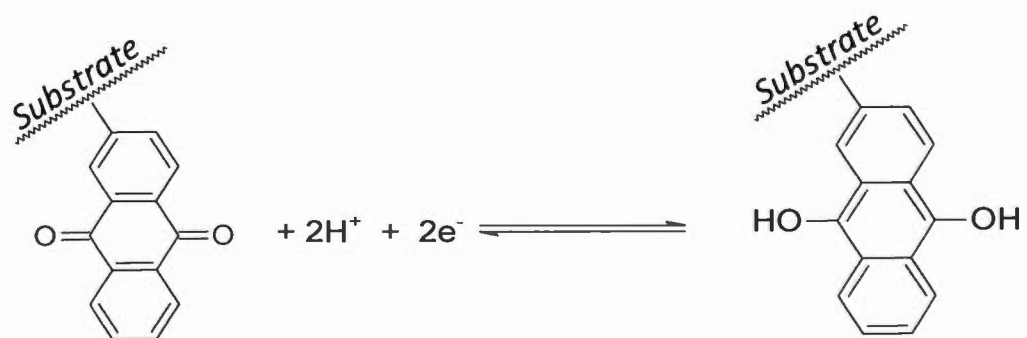


Figure S4 Redox reaction of covalently bound anthraquinone in acid electrolyte.

CHAPITRE III

A ONE-STEP METHOD TO DECORATE GRAPHENE SHEETS WITH METAL NANOPARTICLES DURING THE ELECTROCHEMICAL EXFOLIATION OF GRAPHITE

Résumé de l'article 3

La présente étude vise à fonctionnaliser le graphène de manière non-covalente par des nanoparticules métalliques, comparativement au chapitre précédent où nous nous sommes intéressés à la fonctionnalisation organique et covalente des feuillets de graphène durant l'exfoliation électrochimique du graphite. Cette approche a permis de synthétiser, sans l'ajout d'un agent réducteur, différents types de nanocomposites à base de graphène et d'argent, d'or et des deux métaux. La synthèse est réalisée en une seule étape, dans un milieu contenant le précurseur métallique. Les images TEM obtenues ont permis d'évaluer la taille des nanoparticules sphériques et les données XPS et l'analyse ICP ont confirmé la présence des métaux sur la surface des feuillets de graphène. La spectroscopie Raman a permis d'évaluer la qualité et les propriétés électriques des nanomatériaux de graphène. La performance électrocatalytique des nanocomposites préparés pour la réaction de réduction de l'oxygène en milieu alcalin a été évaluée par voltammetrie cyclique.

Contribution des auteurs:

Benjamin Diby Ossonon

L'auteur principal a effectué toutes les expériences au laboratoire. Il a également écrit l'article en faisant les figures et les recherches bibliographiques appropriées. Benjamin a participé à la correction de l'article à soumettre

Daniel Bélanger

Le co-auteur a supervisé le projet de recherche et les expériences en laboratoire, il a donné de nombreuses idées, des pistes de réflexion et des directives. Il a également participé à la rédaction et aux corrections de l'article.

Article 3. A One-Step Method to Decorate Graphene Sheets with Metal Nanoparticles During the Electrochemical Exfoliation of Graphite.

B. D Ossonon and D. Bélanger

Département Chimie, Université du Québec à Montréal, CP8888, Succ. Centre Ville, Montréal, Québec, Canada H3C 3P8

Abstract

A simple method was developed to prepare graphene-metal nanoparticles composites during the electrochemical exfoliation of graphite in the presence of metal compounds (AgNO_3 , HAuCl_4 or a mixture of AgNO_3 and HAuCl_4 salt in 0.1 M H_2SO_4). In these conditions, the freshly exfoliated graphene sheets (EG) spontaneously reduce the metal ions to generate graphene decorated sheets with Ag, Au and Ag-Au nanoparticles. The characterization of the resulting graphene-metal materials by transmission electron microscopy coupled with energy dispersive x-ray spectroscopy, X-ray diffraction, X-ray photoelectron spectroscopy, thermogravimetric analysis and inductively coupled plasma-optical emission spectroscopy confirmed the presence of metal nanoparticles on graphene sheets. The electrocatalytic activity of these materials for the oxygen reduction reaction in alkaline media was investigated and it was found that the EG-Ag/Au bimetallic nanocomposites, with a low loading of nanoparticle exhibited the best performance.

1 **Introduction**

Nanoscience, nanotechnology and nanomaterials are currently in full swing and are cross-cutting areas between physics, chemistry, electronics and many other fields.^{1,2} Graphene-nanoparticles hybrid structures have received enormous attention

because of their structural and electronic properties,^{3–5} but also for their many technological applications.^{6–9} In the past decades, considerable efforts have already been deployed to synthesize graphene-based hybrid nanomaterials, and develop their applications in fuel cell,^{10–12} electrochemical sensing,^{13,14} biomedical diagnosis,^{6,14} energy storage and conversion.^{1,6,14–16}

Graphene, with its planar sp² structure, good electronic conductivity, high corrosion resistance and large surface area remains an ideal substrate to support metallic nanoparticles.^{17–21} Among existing techniques to prepare graphene/metals hybrid nanocomposites, chemical deposition methods using graphene oxide, reduced graphene oxide or graphene already synthesized as a substrate is well-known.^{22–26} But, these procedures require more often toxic chemicals and stabilizers or surfactants to avoid aggregation.^{24,27–29} In addition, more time is needed to prepare the final composite materials because the procedure takes place in several steps.^{11,30–32} More specifically, these traditional methods show several disadvantages. Firstly, the chemical oxidation of graphite that produces graphene oxide disrupts the aromatic system within the basal planes, which dramatically degrades the electrical properties of graphene.³³ Although partial restoration of the graphitic structure is accomplished by thermal or chemical reduction, the structural defects of reduced graphene oxide cannot be fully repaired. Secondly, the chemical functionalization of graphene with metal nanoparticles usually requires high temperature.^{34,35} Since the growth of metal

nanoparticles is preferentially done on the edges of the graphene due to electrostatic forces and also on the defective sites, this could lead to the non-uniform distribution of metal nanoparticles on graphene.^{36,37} To address these issues, electrochemical methods appeared to be an attractive to prepare graphene/metal nanocomposites. Indeed, several types of metal nanoparticles have been electrochemically deposited on graphene surface by two-step processes.^{5,31,38–44}

Here, we report a simple one-step method to decorate electrochemically exfoliated graphene sheets (EG) by silver, gold, gold-silver nanoparticles without using any reducing and capping agents. Thus, EG-Ag, EG-Au and EG-Ag_x/Au_y nanocomposites were produced during the electrochemical exfoliation of graphite in acid media in the presence of the corresponding metal ions in the exfoliation electrolyte. The metallic nanoparticles were formed *in situ* by spontaneous reduction of the metallic ions by the freshly electrochemically exfoliated graphene sheets. The various nanocomposites were characterized by scanning/transmission electron microscopy coupled with energy dispersive X-ray spectroscopy, X-ray diffraction, X-ray photoelectron spectroscopy and thermogravimetric analysis. The graphene nanocomposites electrocatalytic activity for the oxygen reduction reaction in alkaline electrolyte was also investigated.

2 Experimental

2.1 Materials and chemicals

Graphite foil (natural graphite, 0.5 mm thick, 99.8%) was obtained from Alfa Aesar. The crystallite size of graphite, determined from the Scherrer equation from the 002 peak of the X-ray diffraction pattern is 16 nm.⁴⁵ All reagents were obtained

from Aldrich and were used without further purification. Nanopure water ($18.2\text{ M}\Omega\text{ cm}$) obtained from a Milli-Q water purification system was used to prepare all aqueous solutions and to wash the samples.

2.2 Synthesis of graphene sheets

Few layers graphene were synthesized according to our previous work by electrochemical exfoliation of a graphite foil in $0.1\text{ M H}_2\text{SO}_4$ but in a two-compartment cell.⁴⁶

2.3 Synthesis of graphene-Ag, graphene-Au and graphene-Ag/Au

The electrochemical synthesis of graphene nanocomposites was carried out in a two-compartment-electrode cell, separated by a Nafion membrane (Nafion® 117 membrane, $178\text{ }\mu\text{m}$) to isolate the negative and positive electrode compartments (Supporting Information, Figure S1). Each electrochemical synthesis of hybrid materials was performed at room temperature of 10 V for 1 h using a DC power supply system. Graphite foil ($5\text{ cm} \times 2\text{ cm}$ and thickness = 0.05 cm) was used as positive and a Pt mesh as negative electrodes. The membrane was subjected to a pretreatment procedure using the following sequence: boiling in 3% H_2O_2 for 90 min , followed by boiling in Nanopure water during 60 min . Then, the membrane was boiled in $0.5\text{ M H}_2\text{SO}_4$ for 60 min , and finally, it was boiled during rinsing and washing in Nanopure water for 60 min .⁴⁷ For the synthesis of graphene-Ag (EG-Ag) and graphene-Au (EG-Au) hybrids, the electrolytes consisted of $0.1\text{ M H}_2\text{SO}_4$ with 1 mM AgNO_3 and $1\text{ mM HAuCl}_4 \cdot 3\text{H}_2\text{O}$, respectively. To obtain the graphene-Ag/Au hybrid, the $0.1\text{ M H}_2\text{SO}_4$ electrolyte also contained 0.5 mM AgNO_3 and $0.5\text{ mM HAuCl}_4 \cdot 3\text{H}_2\text{O}$. Electrolytes with higher equimolar concentrations (1 , 5 and 10 mM) were also used. Please note that in the text, the hybrid catalysts are identified by using

the initial concentration of the metal salts (example: EG-Ag_{0.5}/Au_{0.5}) instead of their actual metal content. The graphene suspensions were collected by vacuum filtration and washed several times with Nanopure water (18.2 MΩ cm) obtained from a Milli-Q water purification system. Then, all samples were heat-treated under a mixture of helium (95%) and hydrogen (5%) gas at 300 °C for 1 hour.

2.4 Characterization techniques

Transmission Electron Microscopy (TEM) analyses were carried out using JEOL JEM-2100 electron microscope, operating at 200 keV with a bright field. For TEM characterization, graphene nanocomposites (EG-Ag, EG-Au and EG-Ag_{0.5}/Au_{0.5}) were dispersed in ethanol and homogenized with an ultrasonic bath. The dispersion is finally deposited onto a lacy carbon coated 230-mesh copper TEM micro-grid and dried in ambient air prior to electron microscopy analysis. The morphological studies of graphene nanocomposites (EG-Ag_{0.5}/Au_{0.5}, EG-Ag₁/Au₁, EG-Ag₅/Au₅, and EG-Ag₁₀/Au₁₀) were also performed with a scanning electron microscope (SEM) JSM-840A equipped with a field emission gun (FEG). XPS data have been collected with the spectrophotometer PHI 5600-ci (Physical Electronics, Eden Prairie, MN, USA). The excitation source used for survey spectra was by Al (1486.6 eV) X-rays at 300 W and for core level spectra, by Mg Kα (1253.6 eV) X-rays at 150 W. The analyses were performed without charge compensation at an angle of 45° with the surface. The detector aperture was set at 5 and the surface area analyzed was 0.016 cm². Thermogravimetric analysis was carried out with a thermogravimetric analyzer (TA Instruments TGA (Q500) / Discovery MS). Samples of typically 2 mg were placed in Pt pans and heated from 30 to 900°C with a temperature ramp of 5°C/min, under flowing air. Raman spectroscopy measurements were performed using a micro-Raman system (UHTS300) with excitation from an argon ion laser beam (532 nm) at low power level of 2 mW. X-ray diffraction (XRD)

data were collected on a rotating anode X-ray diffraction (Bruker, D8 Advance) at $2\theta = 20\text{--}80^\circ$, using monochromatic Cu K α radiation ($\lambda = 1.54060 \text{ \AA}$) operated at 40.0 kV/40.0 mA and controlled by DIFFRAC.EVA Data Collector software. Scherrer equation ($D=0.9\lambda/(\beta.\cos\theta)$, where λ is the wavelength of X-ray = 1.54056 \AA , θ is the Bragg's diffraction angle, and β is the half-peak width of the X-ray diffraction lines) was used to estimate particle sizes. Dynamic Light Scattering (DLS) measurements were made with a Malvern Zetasizer NanoS90, using a 632.8 nm HeNe laser at power level of 4 mW and operated in backscatter mode at an angle of 90° . Graphene nanocomposites (1 mg/mL) were dispersed in ethanol, using ultrasonication bath and the resulting suspensions were filtered through a polytetrafluoroethylene (PTFE) membrane filter with $0.20 \mu\text{m}$ pore size. Samples (the filtrate) were equilibrated to 25°C for 120 s prior to measurement in quartz cuvettes having 10 mm path length. Value for solvent ethanol viscosity at 25°C , as provided by the solvent supplier, was entered into the software. An automatic measurement duration setting was used, with automatic measurement positioning and automatic attenuation. The content of Ag, Au and Ag/Au in the graphene matrix (EG-Ag, EG-Au and EG- $\text{Ag}_{0.5}/\text{Au}_{0.5}$) was determined by ICP-OES (Agilent Technologie, 5100). Sample for ICP analysis was prepared by accurately weighing 5 mg of graphene nanocomposite into a volumetric flask (100 mL), followed by addition of 10 mL aqua regia ($\text{HNO}_3 + 3 \text{ HCl}$). Each dispersion was heat-stirred (50°C) for 1 hour. Then, the suspension was continuously stirred overnight at room temperature and finally diluted with Nanopure water before being filtrated.

2.5 Electrochemical measurements

Electrochemical measurements were performed at room temperature with a conventional three-electrode system. Glassy carbon (GC) electrodes used as support,

were polished with 1 μm alumina powder on a micro-cloth. Then, GC electrodes were thoroughly cleaned ultrasonically with Nanopure water for 10 min, rinsed with ethanol for 5 min and dried under N_2 flow. Graphene metal nanocomposites suspensions (5 mg/mL) were prepared using DMF (dimethylformamide) as solvent. A drop (10 μL) of the suspension was deposited onto the surface of GC electrode. Finally, the electrocatalyst-coated GC electrode was dried at 60 °C for 1 hour prior to the electrochemical measurements. The conventional three-electrode system was composed of a modified glass carbon electrode as working electrode, a platinum mesh (2 cm^2) as auxiliary electrode placed approximately at 20 mm of the working electrode, and an Hg/HgO (1 M KOH) reference electrode. All potentials are referred to Hg/HgO reference electrode. Cyclic voltammetry was carried out using a potentiostat electrochemical interface SI480 (Solartron Instruments) controlled with DC Corrware software (Scribner Associates, version 2.8d). Cyclic voltammograms were recorded in N_2 - and O_2 -saturated 0.1 M KOH electrolyte solutions with modified glassy carbon electrodes, at a scan rate of 10 mV s⁻¹ between - 0.8 and 0 V (vs Hg/HgO).

3 Results and discussion

3.1 Mechanism of the formation of metal nanoparticles on electrochemically exfoliated graphene sheets

Metal nanoparticles are formed during the electrochemical exfoliation of graphite in one pot involving two consecutive processes, as illustrated in Figure 1. Firstly, the graphite electrode is electrochemically oxidized by applying 10 V. This leads to the rapid formation of electrochemically exfoliated graphene sheets in the electrolyte.^{46,48–50} Secondly, these freshly exfoliated graphene sheets spontaneously

reduced metallic ions present in the electrolyte to form the corresponding metal nanoparticles on the graphene sheets. This is in agreement with the observation of the spontaneous reduction of Ag (I)^{30,51} and Au (III)⁵²⁻⁵⁴ on carbon substrates such as carbon nanotubes, graphene oxide, reduced graphene oxide and graphene.^{20,55,56}

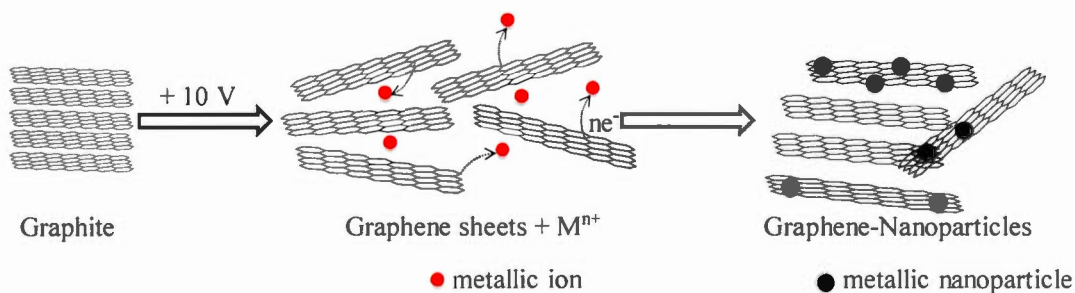


Figure 1. Schematic of the formation of EG-metal nanoparticles hybrids.

3.2 Characterization of graphene nanocomposites

The morphology and structure of the resulting EG metal composites were investigated by SEM, TEM, EDX and DLS. DLS measurements (Supporting Information, Figure S4) show the wide size distribution of the electrochemically exfoliated graphene sheets. Despite that a cut-off filter of 200 nm was used to prepare the samples, the presence of particles with size larger than 200 nm demonstrates the aggregation of the graphene sheets. The fraction of particles larger than 200 nm seems smaller for the monometallic graphene hybrids. Thus, restacking of the graphene sheets seems to be somewhat prevented for the Ag_{0.5}/Au_{0.5} graphene hybrid. The presence of metal particles is clearly seen on the SEM micrographs presented in Supporting Information (Figure S3). TEM images (left hand side of Figure 2) of the as-synthesized EG-Ag (Figure 2A), EG-Au (Figure 2B) and EG-Ag_{0.5}/Au_{0.5} (Figure

2C) nanocomposites show that the surface of graphene sheets is decorated with spherical nanoparticles of different sizes. From TEM images, the particle size of metallic nanoparticles was estimated and the histograms are presented in Figure 2 (center). The average diameter of Au, Ag and $\text{Ag}_{0.5}/\text{Au}_{0.5}$ particles on graphene sheets is about 8, 12 and 9 nm, respectively. In addition, the EG- $\text{Ag}_{0.5}/\text{Au}_{0.5}$ sample contains particles of different shape and some of them show larger size (Supporting Information, Figure S4). This is due to a merging effect of the metal nanoparticles on the surface of graphene during the synthesis process.⁵⁷⁻⁵⁹ The energy-dispersive X-ray spectra (EDX) confirm the elemental of graphene nanocomposites (EG-Ag, EG-Au and EG- $\text{Ag}_{0.5}/\text{Au}_{0.5}$), as shown in Figure 2 (right hand side). The Au, Ag and C peaks indicate the presence of nanoparticles of Ag and Au on graphene sheets (Figure 2A and B). Moreover, the corresponding EDX analysis for EG- $\text{Ag}_{0.5}/\text{Au}_{0.5}$ nanocomposites revealed the presence of Ag and Au on the graphene sheets (Figure 2C).

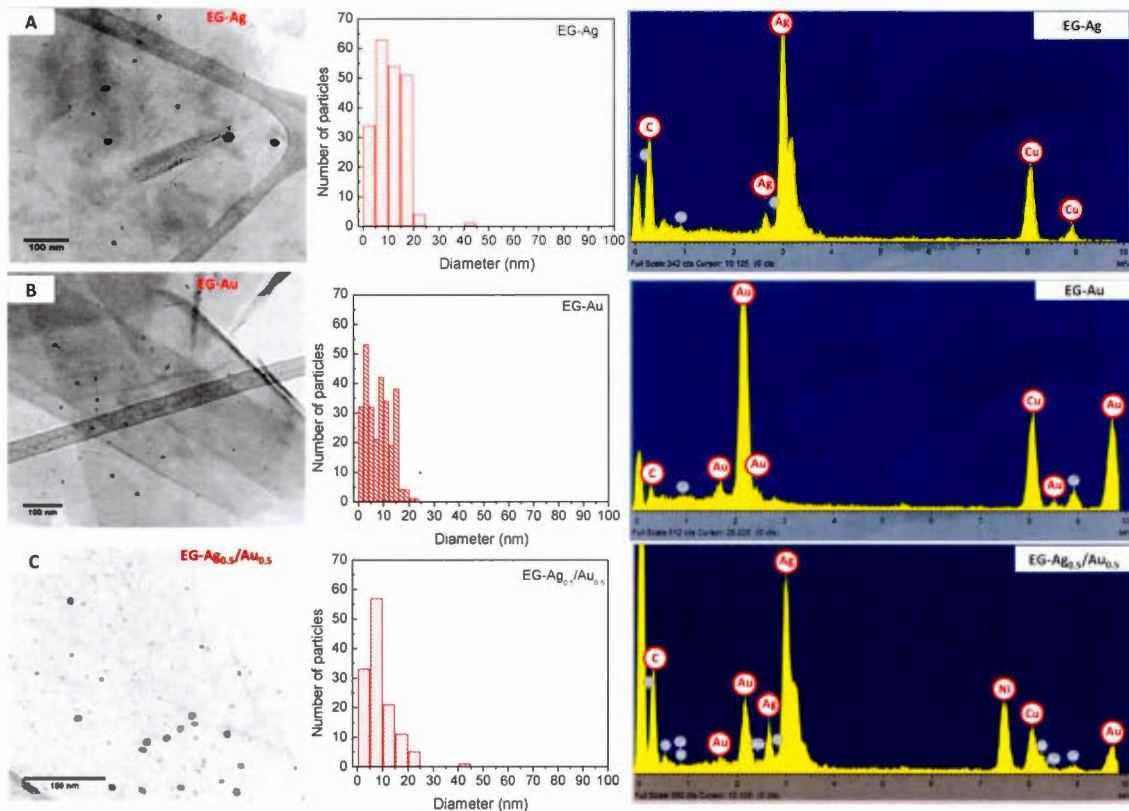


Figure 2. TEM images (left hand side) of graphene nanocomposites A (EG-Ag), B (EG-Au) and C (EG-Ag_{0.5}/Au_{0.5}), histogram for the metal particles (center) and EDX profile (right hand side). The Cu and Ni peaks are attributed to the substrates

3.3 Thermogravimetric analysis

Thermogravimetric analysis (TGA) was used to evaluate the thermal stability of graphene materials and to estimate the weight % of nanoparticles loaded on the graphene sheets. Figure 3 exhibits weight profiles of graphene nanocomposites as a function of temperature under air atmosphere. All samples show a good thermal

stability up to 450 °C. Above about 500 °C, the significant weight loss was mostly caused by the decomposition of the graphene skeleton.^{60,61} Such a temperature suggests that the hybrid materials contain very few surface defects.^{46,60–62}

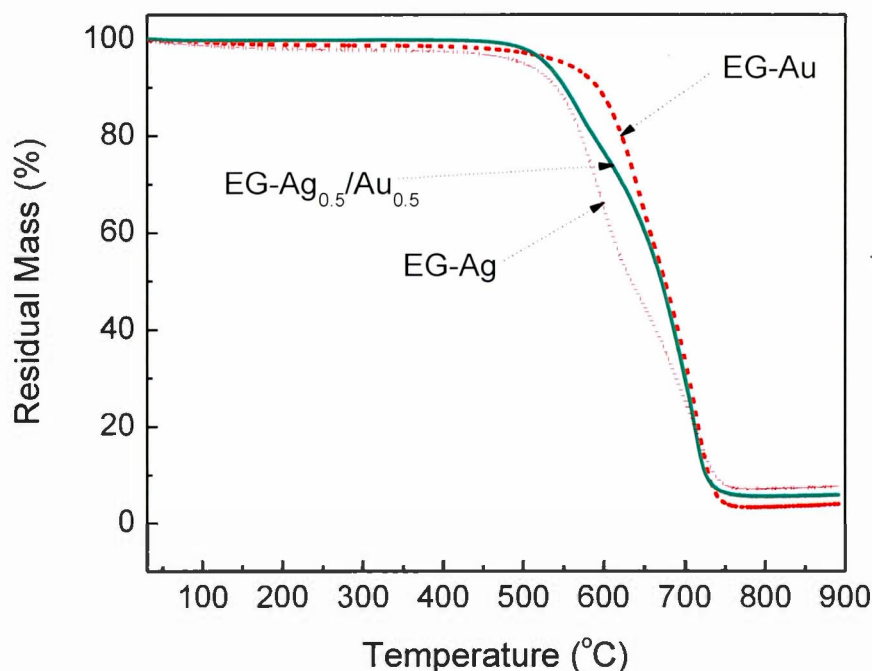


Figure 3. TGA profiles of graphene-AgNPs (EG-Ag), graphene-AuNPs (EG-Au) and graphene-Ag/Au nanocomposites (EG-Ag_{0.5}/Au_{0.5}) recorded with a temperature ramp of 5 °C/min under air.

The mass percentage (wt.%) of Ag and Au nanoparticles in EG-Ag, EG-Au and in nanocomposite EG-Ag_{0.5}/Au_{0.5} are determined to be 7.2, 4.0 and 6.0 wt.%, respectively (Figure 3). Since the measurements were performed in air, metal oxides are present at the end presumably as AgO and Au₂O₃. Table 1 includes the metal content of each sample by taking into account that these oxides are formed. When the

concentration of the metallic ions in the electrolyte was varied from 0.5 to 10 mM, the loading of the metal nanoparticles in EG-Ag/Au composites was found to be in the range of 6.0–24.0 wt.% (Supporting Information, Figure S5). A shift of the degradation of graphene sheets in EG-Ag/Au nanocomposites to lower temperature occurs when the metal content of the nanoparticles in the hybrid materials increased (Supporting Information, Figure S5). The lower degradation temperature could be due to the catalytic effect of the metal nanoparticles for graphene burn-off. This catalytic effect increases with a higher loading of Ag/Au on the graphene flakes. It also possible that the graphene flakes are less aggregated relative to the single metal materials or lower loading of metal nanoparticles.^{46,62} The presence of a larger loading of nanoparticles could prevent the exfoliated graphene sheets from aggregating.

3.4 ICP analysis

ICP analysis of the materials was performed to evaluate their metal content (see Table 1). This method is expected to yield a better accuracy than TGA. Table 1 shows that a similar metal content of about 5 wt.% was determined for the single metal graphene hybrids. In the case of the bimetallic hybrids, the incorporation of the metals is clearly less efficient. Using a total Ag and Au metal complexes salt concentration of 1 mM afforded a smaller metal content (3.2 wt.%) on the graphene sheets in comparison to the single metal hybrids. The reason for the observation of this phenomenon is unclear at the moment. Increasing both metal salts up to equimolar concentration of 10 mM in the electrolyte led to an increase of the Au content but, surprisingly, the loading of Ag nanoparticles on graphene sheets tend toward a limiting value. This phenomena is probably due to galvanic replacement reaction that is occurring during the electrochemical exfoliation process.^{63,64}

Presumably, in addition to the spontaneous reduction of metallic ions by electrochemically exfoliated graphene sheets, due to the difference in their redox potential, the freshly formed Ag nanoparticles can be oxidized by the Au metallic complex to form metallic gold and soluble Ag species. This galvanic displacement reaction might explain the formation of the larger nanoparticles that are observed by TEM.

Table 1. Results of TGA and ICP analysis of EG/metal hybrids

Sample	Metal loading (wt.%)	
	TGA	ICP
Ag	7.2	5.3 ± 1.4
Au	4.0	4.8 ± 1.0
Ag _{0.5} /Au _{0.5}	6.0	Ag Au 2.0 ± 0.1 1.2 ± 0.1
Ag ₁ /Au ₁	12.3	5.3 ± 0.1 3.0 ± 0.1

Ag_5/Au_5	18	5.8 ± 0.1	15.4 ± 0.3
$\text{Ag}_{10}/\text{Au}_{10}$	24	6.5 ± 0.1	19.5 ± 0.3

3.5 X-ray diffraction (XRD)

The crystal structure of the graphene sheets (EG) was determined and compared to pristine natural graphite by X-ray diffraction (XRD) (Figure 4A). The XRD pattern of EG, when dried at room temperature (RT) overnight displays a weak and broad (002) peak at around 25.4° , corresponding to a d-spacing of about 0.349 nm. After thermal annealing at 300°C , the (002) peak shifted to 25.8° and becomes more pronounced and sharper. The layer-to-layer distance slightly reduced to 0.344 nm. The XRD results clearly indicate that thermal annealing led to the restacking of graphene sheets. It is worthy to note that the d-spacing of the resulting graphene at 300°C is slightly greater than that in pristine natural graphite (0.333 nm) (Figure 4A).⁶⁵⁻⁶⁷ On the other hand, the (002) peak of the exfoliated graphene (Figure 4A) at 25.8° compared to 26.7° of graphite position peak indicates that exfoliation of graphite layers occurred without noticeable basal plane distortion and lattice extension, as it can be seen in graphene oxide or reduced graphene oxide containing more defects.⁶⁸⁻⁷⁰ Furthermore, the crystalline nature of the metals in graphene–Ag (EG-Ag), graphene–Au (EG-Au) and graphene–Ag/Au (EG- $\text{Ag}_{0.5}/\text{Au}_{0.5}$) nanocomposites was investigated. XRD patterns of EG-Ag and EG-Ag (Figure 4B) show all of the major peaks of Ag and Au practically superposable at ca. 38° (111), 44.2° (200), 64.3° (220) and 77.4° (311) because of the similarity of their lattice

parameters (0.4080 nm for Au and 0.4086 nm for Ag).⁷¹⁻⁷³ As can be observed in Figure 4B, the XRD pattern of EG-Ag_{0.5}/Au_{0.5} displayed four characteristic (111), (200), (220) and (311) peaks, respectively located at 38.15°, 44.3°, 64.43° and 77.5° indicating a face-centered cubic structure of bimetallic Au-Ag.^{27,72,74} For all nanocomposites (graphene-NPs), the peak corresponding to the (111) plane is the most intense with a sharp reflection (Figure 4B), indicating that the (111) plane is the predominant orientation and confirm that Ag, Au and the bimetallic Au-Ag nanoparticles exist in the crystalline state on the graphene sheets.^{27,71,75,76}

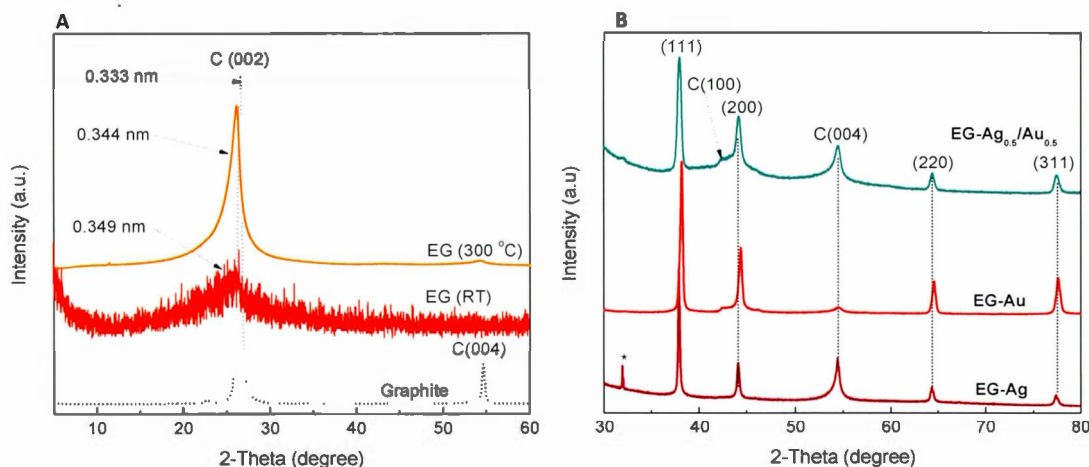


Figure 4. XRD patterns of (A) graphite and graphene (EG) samples at various temperature and (B) EG-Ag, EG-Au and EG-Ag_{0.5}/Au_{0.5} nanocomposites.

The mean size as-synthesized of Ag, Au and Ag/Au nanoparticles are estimated from the (111) plane diffraction peak at $2\theta \approx 38.1^\circ$ by the Scherrer equation⁴⁵ and is 20 ± 3 , 10 ± 4 and 18 ± 2 nm in the matrix of graphene sheets, respectively. However, the average size of nanoparticle calculated by Scherrer formula are somewhat larger than the values observed with transmission electron

microscopy (TEM) analysis (Figure 2). This discrepancy could be attributed to the aggregation of nanoparticles with various shapes on graphene surface, as see in Figure S4.⁷⁷

3.6 X-ray Photoelectron Spectroscopy (XPS)

XPS was used to determine the metal content of the nanocomposites and the electronic properties of the metals. The survey spectrum of the EG-Ag_{0.5}/Au_{0.5} sample presented in Figure 5A, shows the presence of the Ag 3d and Au 4f peaks at 369 and 85 eV⁷⁸ in addition to the C 1s and O 1s peaks at 284 and 530 eV. The latter are only present on the spectrum of the unmodified graphene (Supporting Information, Figure S6). In comparison of the survey spectrum of the EG-Ag_{0.5}/Au_{0.5} sample, XPS survey spectra of EG-Ag and EG-Au show the Ag3d and Au4f peaks, respectively, that confirmed the functionalization of graphene sheets with monometallic species (Supporting Information, Figure S6). The Au 4f and Ag 3d core level spectra were also measured for the metal-containing samples. Figure 4B shows the Au 4f core level spectrum of the Au nanoparticles supported on the exfoliated graphene sheets,^{26,79–82} with the Au 4f_{7/2} and Au 4f_{5/2} peaks at binding energies of 88.4 and 84.7 eV. Their position is in agreement with the characteristic peaks for metallic Au⁰.^{79,83–86} The Ag3d core level spectrum of EG-Ag composite presented in Figure 5C shows two peaks at 368.2 (Ag 3d_{5/2}) and 374.2 eV (Ag 3d_{3/2}) that are attributed to metallic Ag⁰.^{87,88}

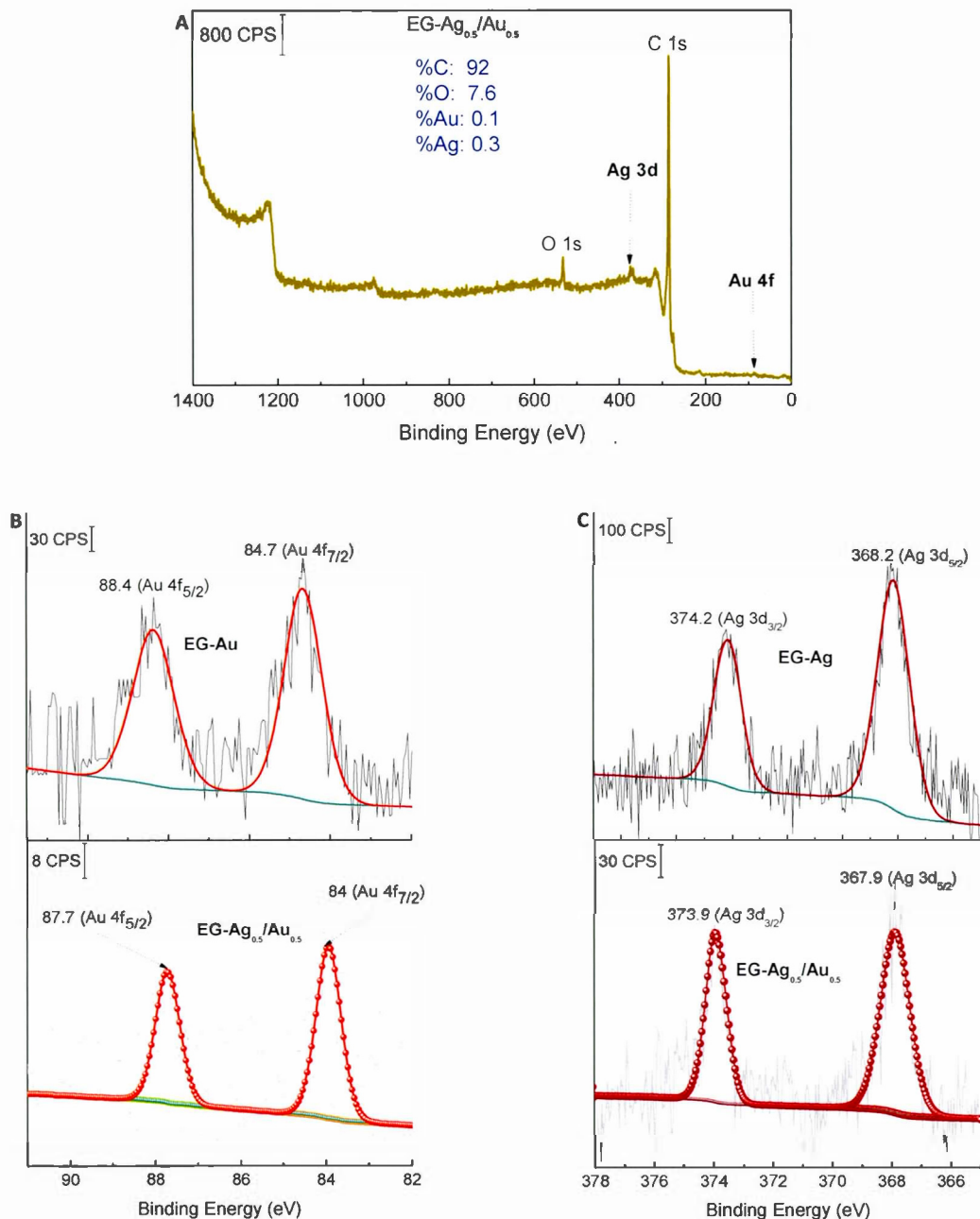


Figure 5. XPS (A) survey spectrum of EG-Ag_{0.5}/Au_{0.5}, and core level spectra of (B) EG-Au and EG-Ag/Au and (C) EG-Ag and EG-Ag_{0.5}/Au_{0.5} nanocomposites.

The Au $4f$ peaks on EG-Ag_{0.5}/Au_{0.5} bimetallic nanocomposites observed at 87.7 and 84 eV, are shifted toward lower energies by ~ 0.7 eV relatively to EG-Au sample (Figure 5B).^{21,79,89} Due to the higher electron affinity of gold with respect of silver, partial electron transfer from Ag to Au atoms can cause a shift of the Au $4f$ peaks towards lower binding energies.^{86,90} Close examination of the Ag $3d$ core level spectrum of EG-Ag_{0.5}/Au_{0.5} sample reveals, as well, a slight shift (0.3 eV) of the Ag $3d_{5/2}$ and $3d_{3/2}$ peaks to lower binding energy values (Ag $3d_{5/2}$, 373.9 eV and $3d_{3/2}$, 367.9 eV) compared to those of the monometallic silver sample (EG-Ag). This is an abnormal observation, because a shift to lower binding energy for one component should be accompanied by a corresponding shift to higher binding energy for the second metal.^{81,86,88} However, the slight negative shift could arise from the electron transfer from the exfoliated graphene sheets, less oxidized and more reactive, to the Ag atoms in Ag–Au^{20,91} which further confirms that the Au-Ag nanoparticles are strongly interacting with the graphene sheets. It should be pointed out that since the work function of graphene (4.3 – 4.48 eV)^{91–93} is lower than that of Ag (4.72 ± 0.2 eV),⁸⁸ electron transfer could occur from the graphene sheets to Ag nanoparticles.^{93,94}

3.7 Raman spectroscopy

Raman spectroscopy is a very useful technique that can provide information about graphene quality.⁹⁵ It was used to probe the structural changes of the graphene-based nanocomposites during the electrochemical exfoliation process in presence of metal ions in the electrolyte. As shown in Figure 6, Raman spectra of exfoliated graphene (EG) and functionalized-exfoliated graphene with nanoparticles exhibit 3 characteristic D, G and 2D peaks at around 1335, 1565 and 2665 cm⁻¹, respectively.^{96,97} The prominent G peak can be assigned to the first-order scattering of E_{2g} vibration mode and the D peak to the breathing mode of k-point photons of A_{1g}

symmetry.^{97,98} Its activity is due to some defects or anomalies in the graphene lattice such as edge defects, functional groups, or structural disorders, while the 2D-band around 2665 cm^{-1} is related to a second-order Raman process.^{96,97,99}

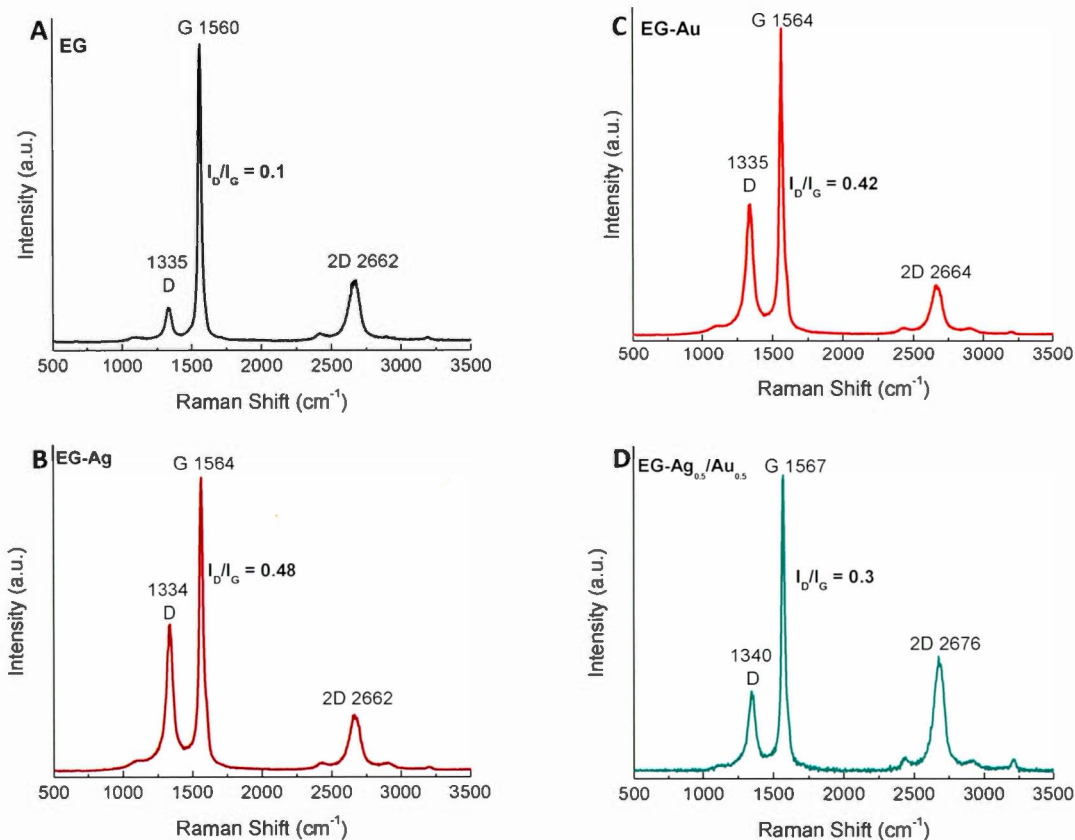


Figure 6. Raman spectra of (A) EG, (B) EG-Ag, (C) EG-Au and (D) EG-Ag_{0.5}/Au_{0.5} nanocomposites.

Generally, the relative intensity ratio of the D and G bands (I_D/I_G) depends strongly on the degree of disorder in the graphitic material and increases when defects are introduced into the graphene structure. As shown in Figure 6, the I_D/I_G ratios of

graphene nanocomposites (EG-Ag, EG-Au and EG- $\text{Ag}_{0.5}/\text{Au}_{0.5}$) are calculated to be 0.48, 0.42, and 0.30, respectively, which are higher than that of undecorated-graphene sheets (0.1).⁴⁶ This shows that the spontaneous reduction of metallic ions on graphene sheets and subsequent nucleation of Au and Ag NPs on graphene sheets introduces few defects into the graphene structure. The increase of I_D/I_G could also come from oxygen functional groups introduced during the spontaneous reduction of the metallic ions, which causes disorder at the graphene edges.¹⁰⁰ The insertion of oxygen groups during exfoliation can also be confirmed by X-ray photoelectron spectroscopy (Supporting Information, Table S1). In addition, the slight shift to the higher vibration frequencies ($\sim 4 \text{ cm}^{-1}$) of the G band that can be noticed for graphene metal composites confirm the functionalization of graphene sheets. The shape and position of the 2D-band evaluate with the number of graphene sheets.^{101,102} Then, it can be deduced from Figure 6 that the number of layers of graphene in the nanomaterials (EG, EG-Ag, EG-Au and EG- $\text{Ag}_{0.5}/\text{Au}_{0.5}$) varies between 1 and 3 layers.¹⁰³ Figure S7, in Supporting Information shows that the I_D/I_G ratio increases with the concentration of nanoparticles in the composite, which suggests that more defects are created with higher ion metallic concentration in the electrolyte used for the electrochemical exfoliation.

3.8 Electrocatalytic behavior for O_2 reduction

Cyclic voltammetry measurements in a conventional three-electrode system were performed to investigate the electrocatalytic activity of the prepared catalyst (EG-Ag, EG-Au and EG- Ag_x/Au_x , $x = 0.5, 1, 5$ and 10) towards the oxygen reduction reaction at room temperature in alkaline electrolyte. Figure 6 presents the cyclic voltammograms of the catalysts in O_2 and N_2 -saturated 0.1 M KOH solution. Figure 7A exhibits a cathodic wave for oxygen reduction with an onset potential of -0.20 V

and a peak potential of -0.51 V for the EG-Ag_{0.5}/Au_{0.5} nanocomposite-modified glassy carbon electrode. The intensity of the peak current for oxygen reduction follows the order: EG-Ag < EG-Au < EG-Ag_{0.5}/Au_{0.5}. The higher electrochemical performance for the electrochemical reduction of oxygen in an alkaline medium observed with EG-Ag_{0.5}/Au_{0.5} electrocatalyst in comparison to the EG-Ag and EG-Au monometallic electrocatalysts might be due to a difference in electrochemically active surface area (ECSA). Also, the lesser aggregation of the graphene sheets for EG-Ag_{0.5}/Au_{0.5}, as determined by DLS, might be as well contribute to the observed difference of electrocatalytic activity. In others words, the observed high electrocatalytic effect of O₂ reduction could be attributed to the alloy effect between Ag and Au and the presence of Ag and Au nanoparticles in the graphene matrix, which increases the stability of EG-Ag_{0.5}/Au_{0.5} catalyst against poisoning effects.^{105–108} The EG-Ag_{0.5}/Au_{0.5} catalyst was also evaluated in N₂-saturated 0.1 M KOH solution (Figure 7B, dashed curve). It can be clearly seen that the cathodic peak is not observed, confirming that the reduction waves observed on Figures 7A and B are due to oxygen reduction on the EG-Ag, EG-Au and EG-Ag_{0.5}/Au_{0.5} electrocatalysts.

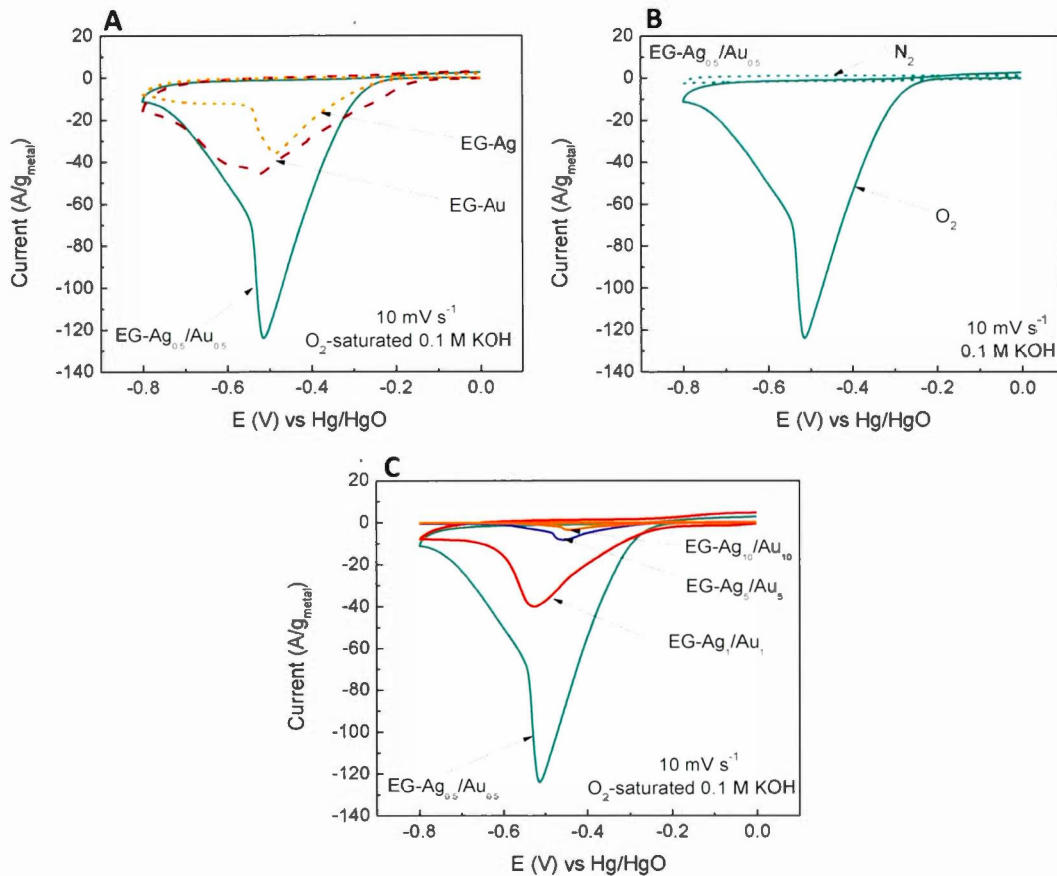


Figure 7. Cyclic voltammograms of EG-Ag, EG-Au and EG-Ag_{0.5}/Au_{0.5} in (A) O₂ and (B) N₂-saturated, (C) Cyclic voltammograms of EG-Ag_x/Au_x ($x = 0.5, 1, 5$ and 10) catalysts in O₂-saturated 0.1 M KOH solution. Scan rate is 10 mV s⁻¹.

Figure 7C shows that the current intensity of the cathodic peak for the ORR gradually decreased with the increase of the loading of Ag/Au. This is consistent with the larger particles on the graphene sheets surface, as seen in the SEM images (Supporting Information, Figure S3).

4 Conclusion

In this present study, we demonstrated that graphene sheets can be spontaneously decorated by metallic nanoparticles during the electrochemical exfoliation of graphite without any reducing or capping agents, using electrochemical method. The method employed for the synthesis of EG-Ag, EG-Au and EG-Ag/Au nanocomposites is environmentally friendly and easy to perform. EG-Ag_{0.5}/Au_{0.5} exhibits relatively high electrocatalytic activity for O₂ reduction in terms of reduction peak potential, peak current and the onset potential. Finally, additional work is required to optimize the process for the formation of graphene-metal nanocomposites.

5 Acknowledgements

This work was financially supported by the Natural Sciences and Engineering Research Council of Canada (NSERC). This research also benefited from the use of the research infrastructure of NanoQAM, which is also acknowledged.

6 References

- (1) Abdelkader, A. M.; Cooper, A. J.; Dryfe, R. A. W.; Kinloch, I. A. How to Get between the Sheets: A Review of Recent Works on the Electrochemical Exfoliation of Graphene Materials from Bulk Graphite. *Nanoscale* **2015**, *7*, 6944–6956.
- (2) Dresselhaus, M. S.; Jorio, A.; Hofmann, M.; Dresselhaus, G.; Saito, R. Perspectives on Carbon Nanotubes and Graphene Raman Spectroscopy. *Nano Lett.* **2010**, *10*, 751–758.
- (3) Mattevi, C.; Eda, G.; Agnoli, S.; Miller, S.; Mkhoyan, K. A.; Celik, O.; Mastrogiovanni, D.; Cranazzi, C.; Carfunkel, E.; Chhowalla, M. Evolution of Electrical, Chemical, and Structural Properties of Transparent and Conducting Chemically Derived Graphene Thin Films. *Adv. Funct. Mater.* **2009**, *19*, 2577–2583.
- (4) Karlický, F.; Zboží, R. Band Gaps and Structural Properties of Graphene Halides and Their Derivates: A Hybrid Functional Study with Localized Orbital Basis Sets. *J. Chem. Phys.* **2012**, *137*, 1–7.
- (5) Lopes, J. H.; Ye, S.; Gostick, J. T.; Barralet, J. E.; Merle, G. Electrocatalytic Oxygen Reduction Performance of Silver Nanoparticle Decorated Electrochemically Exfoliated Graphene. *Langmuir* **2015**, *31*, 9718–9727.
- (6) Online, V. A.; Nguyen, K. T.; Zhao, Y. Nanoscale Biological and Electronic Applications. *Nanoscale* **2014**, *6*, 6245–6266.
- (7) Fabbro, A.; Scaini, D.; Leon, V.; Vázquez, E.; Cellot, G.; Privitera, G.; Lombardi, L.; Torrisi, F.; Tomarchio, F.; Bonaccorso, F.; *et al.* Graphene-Based Interfaces Do Not Alter Target Nerve Cells. *ACS Nano* **2015**, *10*, 615–623.
- (8) Hernandez, Y.; Nicolosi, V.; Lotya, M.; Blighe, F. M.; Sun, Z.; De, S.; McGovern, I. T.; Holland, B.; Byrne, M.; Gun'Ko, Y. K.; *et al.* High-Yield Production of Graphene by Liquid-Phase Exfoliation of Graphite. *Nat. Nanotechnol.* **2008**, *3*, 563–568.
- (9) Hu, W.; Peng, C.; Luo, W.; Lv, M.; Li, X.; Li, D.; Huang, Q.; Fan, C. Graphene-Based Antibacterial Paper. *ACS Nano* **2010**, *4*, 4317–4323.

- (10) Chen, D.; Li, C.; Liu, H.; Ye, F.; Yang, J. Core-Shell Au@Pd Nanoparticles with Enhanced Catalytic Activity for Oxygen Reduction Reaction via Core-Shell Au@Ag/Pd Constructions. *Sci. Rep.* **2015**, *5*, 11949.
- (11) Lu, J.; Li, Y.; Li, S.; Jiang, S. P. Self-Assembled Platinum Nanoparticles on Sulfonic Acid-Grafted Graphene as Effective Electrocatalysts for Methanol Oxidation in Direct Methanol Fuel Cells. *Sci. Rep.* **2016**, *6*, 21530–21542.
- (12) Nethravathi, C.; Anumol, E. A.; Rajamathi, M.; Ravishankar, N. Highly Dispersed Ultrafine Pt and PtRu Nanoparticles on Graphene: Formation Mechanism and Electrocatalytic Activity. *Nanoscale* **2011**, *3*, 569–571.
- (13) Alkilany, A. M.; Lohse, S. E.; Murphy, C. J. The Gold Standard: Gold Nanoparticle Libraries to Understand the Nano-Bio Interface. *Acc. Chem. Res.* **2013**, *46*, 650–661.
- (14) Shao, Y.; Wang, J.; Wu, H.; Liu, J.; Aksay, I. A.; Lin, Y. Graphene Based Electrochemical Sensors and Biosensors: A Review. *Electroanalysis* **2010**, *22*, 1027–1036.
- (15) Sutter, P. W.; Flege, J.-I.; Sutter, E. A. Epitaxial Graphene on Ruthenium. *Nat. Mater.* **2008**, *7*, 406–411.
- (16) Wang, H.; Lu, S.; Chen, Y.; Han, L.; Zhou, J.; Wu, X.; Qin, W. Graphene/Co 9 S 8 Nanocomposite Paper as a Binder-Free and Free-Standing Anode for Lithium-Ion Batteries. *J. Mater. Chem. A* **2015**, *3*, 23677–23683.
- (17) Castro Neto, A. H.; Guinea, F.; Peres, N. M. R.; Novoselov, K. S.; Geim, A. K. The Electronic Properties of Graphene. *Rev. Mod. Phys.* **2009**, *81*, 109–162.
- (18) Geim, A. K.; Novoselov, K. S. The Rise of Graphene. *Nat. Mater.* **2007**, *6*, 183–191.
- (19) Qaseem, A.; Chen, F.; Wu, X.; Johnston, R. L. Pt-Free Silver Nanoalloy Electrocatalysts for Oxygen Reduction Reaction in Alkaline Media. *Catal. Sci. Technol.* **2016**, *6*, 3317–3340.
- (20) Wu, T.; Ma, J.; Wang, X.; Liu, Y.; Xu, H.; Gao, J.; Wang, W.; Liu, Y.; Yan, J. Graphene Oxide Supported Au-Ag Alloy Nanoparticles with Different Shapes and Their High Catalytic Activities. *Nanotechnology* **2013**, *24*, 125301–125311.

- (21) Fujigaya, T.; Kim, C.; Hamasaki, Y.; Nakashima, N. Growth and Deposition of Au Nanoclusters on Polymer-Wrapped Graphene and Their Oxygen Reduction Activity. *Sci. Rep.* **2016**, *6*, 21314–21324.
- (22) Goncalves, G.; Marques, P. A. A. P.; Granadeiro, C. M.; Nogueira, H. I. S.; Singh, M. K.; Grácio, J. Surface Modification of Graphene Nanosheets with Gold Nanoparticles: The Role of Oxygen Moieties at Graphene Surface on Gold Nucleation and Growth. *Chem. Mater.* **2009**, *21*, 4796–4802.
- (23) Govindhan, M.; Chen, A. Simultaneous Synthesis of Gold Nanoparticle/graphene Nanocomposite for Enhanced Oxygen Reduction Reaction. *J. Power Sources* **2015**, *274*, 928–936.
- (24) Ayán-Varela, M.; Paredes, J. I.; Guardia, L.; Villar-Rodil, S.; Munuera, J. M.; Díaz-González, M.; Fernández-Sánchez, C.; Martínez-Alonso, A.; Tascón, J. M. D. Achieving Extremely Concentrated Aqueous Dispersions of Graphene Flakes and Catalytically Efficient Graphene-Metal Nanoparticle Hybrids with Flavin Mononucleotide as a High-Performance Stabilizer. *ACS Appl. Mater. Interfaces* **2015**, *7*, 10293–10307.
- (25) Liu, K.; Liu, L.; Luo, Y.; Jia, D. One-Step Synthesis of Metal Nanoparticle Decorated Graphene by Liquid Phase Exfoliation. *J. Mater. Chem.* **2012**, *22*, 20342.
- (26) Yang, M.-Q.; Pan, X.; Zhang, N.; Xu, Y.-J. A Facile One-Step Way to Anchor Noble Metal (Au, Ag, Pd) Nanoparticles on a Reduced Graphene Oxide Mat with Catalytic Activity for Selective Reduction of Nitroaromatic Compounds. *CrystEngComm* **2013**, *15*, 6819–6828.
- (27) Zhang, Y.; Gao, G.; Qian, Q.; Cui, D. Chloroplasts-Mediated Biosynthesis of Nanoscale Au-Ag Alloy for 2-Butanone Assay Based on Electrochemical Sensor. *Nanoscale Res. Lett.* **2012**, *7*, 475–482.
- (28) Singh, V.; Joung, D.; Zhai, L.; Das, S.; Khondaker, S. I.; Seal, S. Graphene Based Materials: Past, Present and Future. *Prog. Mater. Sci.* **2011**, *56*, 1178–1271.

- (29) Munuera, J. M.; Paredes, J. I.; Villar-Rodil, S.; Ayán-Varela, M.; Martínez-Alonso, A.; Tascon, J. M. D. Electrolytic Exfoliation of Graphite in Water with Multifunctional Electrolytes: En Route towards High Quality, Oxide-Free Graphene Flakes. *Nanoscale* **2016**, *8*, 2982–2998.
- (30) Yang, Y.-K.; He, C.-E.; He, W.-J.; Yu, L.-J.; Peng, R.-G.; Xie, X.-L.; Wang, X.-B.; Mai, Y.-W. Reduction of Silver Nanoparticles onto Graphene Oxide Nanosheets with N,N-Dimethylformamide and SERS Activities of GO/Ag Composites. *J. Nanopart. Res.* **2011**, *13*, 5571–5581.
- (31) Benvidi, A.; Dehghani-Firouzabadi, A.; Mazloum-Ardakani, M.; Mirjalili, B.-B. F.; Zare, R. Electrochemical Deposition of Gold Nanoparticles on Reduced Graphene Oxide Modified Glassy Carbon Electrode for Simultaneous Determination of Levodopa, Uric Acid and Folic Acid. *J. Electroanal. Chem.* **2015**, *736*, 22–29.
- (32) Xu, S.; Ye, L.; Li, Z.; Wang, Y.; Lei, F.; Lin, S. Facile Synthesis of Bimetallic Pt-Ag/Graphene Composite and Its Electro-Photo-Synergistic Catalytic Properties for Methanol Oxidation. *Catalysts* **2016**, *6*, 144–156.
- (33) Bai, H.; Li, C.; Shi, G. Functional Composite Materials Based on Chemically Converted Graphene. *Adv. Mater.* **2011**, *23*, 1089–1115.
- (34) Wu, D.; Zhang, F.; Liang, H.; Feng, X. Nanocomposites and Macroscopic Materials: Assembly of Chemically Modified Graphene Sheets. *Chem. Soc. Rev.* **2012**, *41*, 6160–6177.
- (35) Gao, R.; Hu, N.; Yang, Z.; Zhu, Q.; Chai, J.; Su, Y.; Zhang, L.; Zhang, Y. Paper-like Graphene-Ag Composite Films with Enhanced Mechanical and Electrical Properties. *Nanoscale Res. Lett.* **2013**, *8*, 32–40.
- (36) Wang, X.; Sun, G.; Routh, P.; Kim, D.-H.; Huang, W.; Chen, P. Heteroatom-Doped Graphene Materials: Syntheses, Properties and Applications. *Chem. Soc. Rev.* **2014**, *43*, 7067–7098.
- (37) Sharma, R.; Baik, J. H.; Perera, C. J.; Strano, M. S. Anomalously Large Reactivity of Single Graphene Layers and Edges toward Electron Transfer Chemistries. *Nano Lett.* **2010**, *10*, 398–405.

- (38) Hu, Y.; Lu, L.; Liu, J.; Chen, W. Direct Growth of Size-Controlled Gold Nanoparticles on Reduced Graphene Oxide Film from Bulk Gold by Tuning Electric Field: Effective Methodology and Substrate for Surface Enhanced Raman Scattering Study. *J. Mater. Chem.* **2012**, *22*, 11994–12000.
- (39) Raj, M. A.; John, S. A. Assembly of Gold Nanoparticles on Graphene Film via Electroless Deposition: Spontaneous Reduction of Au³⁺ Ions by Graphene Film. *RSC Adv.* **2015**, *5*, 4964–4971.
- (40) Yu, Z. Electrodeposition of Gold Nanoparticles on Electrochemically Reduced Graphene Oxide for High Performance Supercapacitor Electrode Materials. *Int. J. Electrochem. Sci.* **2016**, *11*, 3643–3650.
- (41) Jing, Y.; Lin, E.; Su, X.; Liu, Y.; Li, H.; Yuan, X.; Ping, L.; Fan, Y. Electrodeposition of Au Nanoparticles on Poly(diallyldimethylammonium Chloride) Functionalized Reduced Graphene Oxide Sheets for Voltammetric Determination of Nicotine in Tobacco Products and Anti-Smoking Pharmaceuticals. *RSC Adv.* **2016**, *6*, 26247–26253.
- (42) Qin, Q.; Bai, X.; Hua, Z. Electrochemical Synthesis of Well-Dispersed CdTe Nanoparticles on Reduced Graphene Oxide and Its Photoelectrochemical Sensing of Catechol. *J. Electrochem. Soc.* **2017**, *164*, H241–H249.
- (43) Sivaprasad, M.; Y. Sreedhar, N.; R. Jayapal, M.; Yang, L.; Ni, H. Two Step Electrochemical Deposition Of Palladium And Polyaniline On Graphene Dispersed Glassy Carbon Electrode For Electrochemical Analysis Of Pesticide. *Adv. Mater. Lett.* **2016**, *8*, 30–36.
- (44) Moradi Golsheikh, A.; Huang, N. M.; Lim, H. N.; Zakaria, R.; Yin, C. Y. One-Step Electrodeposition Synthesis of Silver-Nanoparticle-Decorated Graphene on Indium-Tin-Oxide for Enzymeless Hydrogen Peroxide Detection. *Carbon N. Y.* **2013**, *62*, 405–412.
- (45) Monshi, A.; Foroughi, M. R.; Monshi, M. R. Modified Scherrer Equation to Estimate More Accurately Nano-Crystallite Size Using XRD. *World J. Nano Sci. Eng.* **2012**, *2*, 154–160.
- (46) Ossonon, B. D.; Bélanger, D. Functionalization of Graphene Sheets by the Diazonium Chemistry during Electrochemical Exfoliation of Graphite. *Carbon.* **2017**, *111*, 83–93.

- (47) Rajendra Prasad, K.; Munichandraiah, N. Electrooxidation of Methanol on Polyaniline without Dispersed Catalyst Particles. *J. Power Sources* **2002**, *103*, 300–304.
- (48) Parvez, K.; Wu, Z.-S.; Li, R.; Liu, X.; Graf, R.; Feng, X.; Müllen, K. Exfoliation of Graphite into Graphene in Aqueous Solutions of Inorganic Salts. *J. Am. Chem. Soc.* **2014**, *136*, 6083–6091.
- (49) Eredia, M.; Bertolazzi, S.; Leydecker, T.; El Garah, M.; Janica, I.; Melinte, G.; Ersen, O.; Ciesielski, A.; Samori, P. Morphology and Electronic Properties of Electrochemically Exfoliated Graphene. *J. Phys. Chem. Lett.* **2017**, *8*, 3347–3355.
- (50) Munuera, J. M.; Paredes, J. I.; Enterría, M.; Pagán, A.; Villar-Rodil, S.; Pereira, M. F. R.; Martins, J. I.; Figueiredo, J. L.; Cenis, J. L.; Martínez-Alonso, A.; *et al.* Electrochemical Exfoliation of Graphite in Aqueous Sodium Halide Electrolytes toward Low Oxygen Content Graphene for Energy and Environmental Applications. *ACS Appl. Mater. Interfaces* **2017**, *9*, 24085–24099.
- (51) Kim, Y.-K.; Ok, G.; Choi, S.-W.; Jang, H.; Min, D.-H. The Interfacing Structural Effect of Ag/graphene Oxide Nanohybrid Films on Surface Enhanced Raman Scattering. *Nanoscale* **2017**, *9*, 5872–5878.
- (52) Song, J.; Xu, L.; Xing, R.; Li, Q.; Zhou, C.; Liu, D.; Song, H. Synthesis of Au/Graphene Oxide Composites for Selective and Sensitive Electrochemical Detection of Ascorbic Acid. *Sci. Rep.* **2015**, *4*, 7515–7522.
- (53) Yin, H.; Tang, H.; Wang, D.; Gao, Y.; Tang, Z. Facile Synthesis of Surfactant-Free Au Cluster/graphene Hybrids for High-Performance Oxygen Reduction Reaction. *ACS Nano* **2012**, *6*, 8288–8297.
- (54) Wang, L.; Tang, Z.; Yan, W.; Yang, H.; Wang, Q.; Chen, S. Porous Carbon-Supported Gold Nanoparticles for Oxygen Reduction Reaction: Effects of Nanoparticle Size. *ACS Appl. Mater. Interfaces* **2016**, *8*, 20635–20641.
- (55) Yuan, W.; Gu, Y.; Li, L. Applied Surface Science Green Synthesis of Graphene / Ag Nanocomposites. *Appl. Surf. Sci.* **2012**, *261*, 753–758.
- (56) Han, J. W.; Kim, J. Reduced Graphene Oxide – Silver Nanoparticle Nanocomposite : A Potential Anticancer Nanotherapy. *Int. J. Nanomedecine* **2015**, *10*, 6257–6276.

- (57) Grouchko, M.; Roitman, P.; Zhu, X.; Popov, I.; Kamyshny, A.; Su, H.; Magdassi, S. Merging of Metal Nanoparticles Driven by Selective Wettability of Silver Nanostructures. *Nat. Commun.* **2014**, *5*, 2994–3000.
- (58) Thanh, N. T. K.; Maclean, N.; Mahiddine, S. Mechanisms of Nucleation and Growth of Nanoparticles in Solution. *Chem. Rev.* **2014**, *114*, 7610–7630.
- (59) Wang, J.; Chen, S.; Cui, K.; Li, D.; Chen, D. Approach and Coalescence of Gold Nanoparticles Driven by Surface Thermodynamic Fluctuations and Atomic Interaction Forces. *ACS Nano* **2016**, *10*, 2893–2902.
- (60) Shang, N. G.; Papakonstantinou, P.; Sharma, S.; Lubarsky, G.; Li, M.; Mcneill, D. W.; Quinn, A. J.; Zhou, W.; Blackley, R. Controllable Selective Exfoliation of High-Quality Graphene Nanosheets and Nanodots by Ionic Liquid Assisted Grinding. *Chem. Commun.* **2012**, *48*, 1877–1879.
- (61) Chen, H.; Müller, M. B.; Gilmore, K. J.; Wallace, G. G.; Li, D. Mechanically Strong, Electrically Conductive, and Biocompatible Graphene Paper. *Adv. Mater.* **2008**, *20*, 3557–3561.
- (62) Nan, H. Y.; Ni, Z. H.; Wang, J.; Zafar, Z.; Shi, Z. X.; Wang, Y. Y. The Thermal Stability of Graphene in Air Investigated by Raman Spectroscopy. *J. Raman Spectrosc.* **2013**, *44*, 1018–1021.
- (63) El Mel, A. A.; Chettab, M.; Gautron, E.; Chauvin, A.; Humbert, B.; Mevellec, J. Y.; Delacote, C.; Thiry, D.; Stephan, N.; Ding, J.; *et al.* Galvanic Replacement Reaction: A Route to Highly Ordered Bimetallic Nanotubes. *J. Phys. Chem. C* **2016**, *120*, 17652–17659.
- (64) Ghosh, T.; Kabiraj, D.; Satpati, B. Substrate Decomposition in Galvanic Displacement Reaction: Contrast between Gold and Silver Nanoparticle Formation. In *AIP Conference Proceedings*; 2015; p. 80040.
- (65) Guan, J.; Chen, X.; Wei, T.; Liu, F.; Wang, S.; Yang, Q.; Lu, Y.; Yang, S. Directly Bonded Hybrid of Graphene Nanoplatelets and Fullerene: Facile Solid-State Mechanochemical Synthesis and Application as Carbon-Based Electrocatalyst for Oxygen Reduction Reaction. *J. Mater. Chem. A* **2015**, *3*, 4139–4146.

- (66) Abdelkader, A. M.; Patten, H. V.; Li, Z.; Chen, Y.; Kinloch, I. A. Electrochemical Exfoliation of Graphite in Quaternary Ammonium-Based Deep Eutectic Solvents: A Route for the Mass Production of Graphene. *Nanoscale* **2015**, *7*, 11386–11392.
- (67) Kumar, M. P.; Shanthini, S.; Srivastava, C. Electrochemical Exfoliation of Graphite for Producing Graphene Using Saccharin. *RSC Adv.* **2015**, *5*, 53865–53869.
- (68) Alam, S. N.; Sharma, N.; Kumar, L. Synthesis of Graphene Oxide (GO) by Modified Hummers Method and Its Thermal Reduction to Obtain Reduced Graphene Oxide (rGO)*. *Graphene* **2017**, *6*, 1–18.
- (69) Park, S.; An, J.; Potts, J. R.; Velamakanni, A.; Murali, S.; Ruoff, R. S. Hydrazine-Reduction of Graphite- and Graphene Oxide. *Carbon N. Y.* **2011**, *49*, 3019–3023.
- (70) Yu, P.; Tian, Z.; Lowe, S. E.; Song, J.; Ma, Z.; Wang, X.; Han, Z. J.; Bao, Q.; Simon, G. P.; Li, D.; et al. Mechanically-Assisted Electrochemical Production of Graphene Oxide. *Chem. Mater.* **2016**, *28*, 8429–8438.
- (71) Sun, S.; Wu, P. Competitive Surface-Enhanced Raman Scattering Effects in Noble Metal Nanoparticle-Decorated Graphene Sheets. *Phys. Chem. Chem. Phys.* **2011**, *13*, 21116–21120.
- (72) Zhao, D.; Yu, Y.; Xu, C. A Sensitive Electrochemical Immunosensor for the Detection of Human Chorionic Gonadotropin Based on a Hierarchical Nanoporous AuAg Alloy. *RSC Adv.* **2016**, *6*, 87–93.
- (73) Tsuji, M.; Matsunaga, M.; Kumagai, H.; Ogino, M.; Hikino, S.; Yoshida, Y.; Ishizaki, T. Synthesis of Au@Ag@Cu Trimetallic Nanocrystals Using Three-Step Reduction. *CrystEngComm* **2013**, *15*, 1345–1351.
- (74) Pogacean, F.; Biris, A. R.; Coros, M.; Lazar, M. D.; Watanabe, F.; Kannarpady, G. K.; Al Said, S. A. F.; Biris, A. S.; Pruneanu, S. Direct Electrochemical Oxidation of S-Captopril Using Gold Electrodes Modified with Graphene-AuAg Nanocomposites. *Int. J. Nanomedicine* **2014**, *9*, 1111–1125.
- (75) Yang, J.; Sargent, E. H.; Kelley, S. O.; Ying, J. Y. A General Phase-Transfer Protocol for Metal Ions and Its Application in Nanocrystal Synthesis. *Nat. Mater.* **2009**, *8*, 683–689.

- (76) Yang, S.; Yue, W.; Zhu, J.; Ren, Y.; Yang, X. Graphene-Based Mesoporous SnO₂ with Enhanced Electrochemical Performance for Lithium-Ion Batteries. *Adv. Funct. Mater.* **2013**, *23*, 3570–3576.
- (77) Borchert, H.; Shevchenko, E. V.; Robert, A.; Mekis, I.; Kornowski, A.; Grüberl, G.; Weller, H. Determination of Nanocrystal Sizes: A Comparison of TEM, SAXS, and XRD Studies of Highly Monodisperse CoPt₃ Particles. *Langmuir* **2005**, *21*, 1931–1936.
- (78) Gopalakrishnan, R.; Loganathan, B.; Raghu, K. Green Synthesis of Au–Ag Bimetallic Nanocomposites Using Silybum Marianum Seed Extract and Their Application as a Catalyst. *RSC Adv.* **2015**, *5*, 31691–31699.
- (79) Song, Y.; Liu, K.; Chen, S. AgAu Bimetallic Janus Nanoparticles and Their Electrocatalytic Activity for Oxygen Reduction in Alkaline Media. *Langmuir* **2012**, *28*, 17143–17152.
- (80) Li, F.; Yang, H.; Shan, C.; Zhang, Q.; Han, D.; Ivaska, A.; Niu, L. The Synthesis of Perylene-Coated Graphene Sheets Decorated with Au Nanoparticles and Its Electrocatalysis toward Oxygen Reduction. *J. Mater. Chem.* **2009**, *19*, 4022–4025.
- (81) Wang, A.; Liu, J.; Lin, S. D.; Lin, T.; Mou, C. A Novel Efficient Au – Ag Alloy Catalyst System : Preparation , Activity , and Characterization. *J. Catal.* **2005**, *233*, 186–197.
- (82) Barreca, D. Silica-Supported Ag-Au Bimetallic Nanosystems by XPS. *Surf. Sci. Spectra* **2007**, *13*, 1–8.
- (83) Luo, Z.; Yuan, X.; Yu, Y.; Zhang, Q.; Leong, D. T.; Lee, J. Y.; Xie, J. From Aggregation-Induced Emission of Au(I)-Thiolate Complexes to Ultrabright Au(0)@Au(I)-Thiolate Core-Shell Nanoclusters. *J. Am. Chem. Soc.* **2012**, *134*, 16662–16670.
- (84) Ge, X.; Sumboja, A.; Wuu, D.; An, T.; Li, B.; Goh, F. W. T.; Hor, T. S. A.; Zong, Y.; Liu, Z. Oxygen Reduction in Alkaline Media: From Mechanisms to Recent Advances of Catalysts. *ACS Catal.* **2015**, *5*, 4643–4667.

- (85) Jaramillo, T. F.; Baeck, S.-H. H.; Cuenya, B. R.; McFarland, E. W. Catalytic Activity of Supported Au Nanoparticles Deposited from Block Copolymer Micelles. *J. Am. Chem. Soc.* **2003**, *125*, 7148–7149.
- (86) Chimentão, R. J.; Cota, I.; Dafinov, A.; Medina, F.; Fuente, J. L. G. de la; Fierro, J. L. G.; Sueiras, J. E.; Cesteros, Y.; Salagre, P. Synthesis of Silver-Gold Alloy Nanoparticles by a Phase-Transfer System. *J. Mater. Res.* **2006**, *21*, 105–111.
- (87) Ge, L.; Han, C.; Liu, J.; Li, Y. Enhanced Visible Light Photocatalytic Activity of Novel Polymeric G-C₃N₄ Loaded with Ag Nanoparticles. *Appl. Catal. A Gen.* **2011**, *409*–*410*, 215–222.
- (88) Tjeng, L. H.; Meinders, M. B. J.; Elp, J. Van; Ghijsen, J.; Sawatzky, G. A.; Johnson, R. L. Electronic Structure of Ag₂O. *Phys. Rev. B* **1990**, *41*, 3190–3199.
- (89) Hu, P.; Song, Y.; Chen, L.; Chen, S. Electrocatalytic Activity of Alkyne-Functionalized AgAu Alloy Nanoparticles for Oxygen Reduction in Alkaline Media. *Nanoscale* **2015**, *7*, 9627–9636.
- (90) Pauling, L. The Nature of the Chemical Bond. In *The Journal of Chemical Physics*; Press), (Cornell University, Ed.; New York, 1960; p. 93.
- (91) Li, J.; Liu, C.; Liu, Y. Au/graphene Hydrogel: Synthesis, Characterization and Its Use for Catalytic Reduction of 4-Nitrophenol. *J. Mater. Chem.* **2012**, *22*, 8426–8430.
- (92) Organic, S. M. H.; Park, J.; Lee, W. H.; Huh, S.; Sim, S. H.; Kim, S. Bin; Cho, K.; Hong, B. H.; Kim, K. S. Work-Function Engineering of Graphene Electrodes by Self-Assembled Monolayers for High-Performance Organic Field-Effect Transistors. *J. Phys. Chem. Lett.* **2011**, *2*, 841–845.
- (93) Giovannetti, G.; Khomyakov, P. A.; Brocks, G.; Karpan, V. M.; Van Den Brink, J.; Kelly, P. J. Doping Graphene with Metal Contacts. *Phys. Rev. Lett.* **2008**, *101*, 026803–026807.
- (94) Li, X.; Tay, B. K.; Li, J.; Tan, D.; Tan, C. W.; Liang, K. Mildly Reduced Graphene Oxide-Ag Nanoparticle Hybrid Films for Surface-Enhanced Raman Scattering. *Nanoscale Res. Lett.* **2012**, *7*, 205–213.

- (95) Ferrari, A. C.; Robertson, J. Interpretation of Raman Spectra of Disordered and Amorphous Carbon. *Phys. Rev. B* **2000**, *61*, 14095–14107.
- (96) Ferrari, A. C.; Basko, D. M. Raman Spectroscopy as a Versatile Tool for Studying the Properties of Graphene. *Nat. Nanotechnol.* **2013**, *8*, 235–246.
- (97) Ferrari, A. C. Raman Spectroscopy of Graphene and Graphite: Disorder, Electron-Phonon Coupling, Doping and Nonadiabatic Effects. *Solid State Commun.* **2007**, *143*, 47–57.
- (98) Pimenta, M. A.; Dresselhaus, G.; Dresselhaus, M. S.; Cançado, L. G.; Jorio, A.; Saito, R. Studying Disorder in Graphite-Based Systems by Raman Spectroscopy. *Phys. Chem. Chem. Phys.* **2007**, *9*, 1276–1291.
- (99) Ferrari, A. C.; Meyer, J. C.; Scardaci, V.; Casiraghi, C.; Lazzeri, M.; Mauri, F.; Piscanec, S.; Jiang, D.; Novoselov, K. S.; Roth, S.; *et al.* Raman Spectrum of Graphene and Graphene Layers. *Phys. Rev. Lett.* **2006**, *97*, 187401–187405.
- (100) Yu, P.; Lowe, S. E.; Simon, G. P.; Zhong, Y. L. Electrochemical Exfoliation of Graphite and Production of Functional Graphene. *Curr. Opin. Colloid Interface Sci.* **2015**, *20*, 329–338.
- (101) Song, L.; Ci, L.; Lu, H.; Sorokin, P. B.; Jin, C.; Ni, J.; Kvashnin, A. G.; Kvashnin, D. G.; Lou, J.; Yakobson, B. I.; *et al.* Large Scale Growth and Characterization of Atomic Hexagonal Boron Nitride Layers. *Nano Lett.* **2010**, *10*, 3209–3215.
- (102) Guermoune, A.; Chari, T.; Popescu, F.; Sabri, S. S.; Guillemette, J.; Skulason, H. S.; Szkopek, T.; Siaj, M. Chemical Vapor Deposition Synthesis of Graphene on Copper with Methanol, Ethanol, and Propanol Precursors. *Carbon*. **2011**, *49*, 4204–4210.
- (103) Malard, L. M.; Pimenta, M. A.; Dresselhaus, G.; Dresselhaus, M. S. Raman Spectroscopy in Graphene. *Phys. Rep.* **2009**, *473*, 51–87.
- (104) Song, J. M.; Chen, W. T.; Hsieh, K. H.; Kao, T. H.; Chen, I. G.; Chiu, S. J.; Lee, H. Y. An in Situ Study on the Coalescence of Monolayer-Protected Au-Ag Nanoparticle Deposits upon Heating. *Nanoscale Res Lett* **2014**, *9*, 438–449.

- (105) Cai, B.; Wen, D.; Liu, W.; Herrmann, A. K.; Benad, A.; Eychmüller, A. Function-Led Design of Aerogels: Self-Assembly of Alloyed PdNi Hollow Nanospheres for Efficient Electrocatalysis. *Angew. Chemie - Int. Ed.* **2015**, *54*, 13101–13105.
- (106) Hu, C.; Zhai, X.; Zhao, Y.; Bian, K.; Zhang, J.; Qu, L.; Zhang, H.; Luo, H. Small-Sized PdCu Nanocapsules on 3D Graphene for High-Performance Ethanol Oxidation. *Nanoscale* **2014**, *6*, 2768–2775.
- (107) Wu, G.; More, K. L.; Johnston, C. M.; Zelenay, P. High-Performance Electrocatalysts for Oxygen Reduction Derived from Polyaniline, Iron, and Cobalt. *Science*. **2011**, *332*, 443–447.
- (108) Dong, Y.; Deng, Y.; Zeng, J.; Song, H.; Liao, S. A High-Performance Composite ORR Catalyst Based on the Synergy between Binary Transition Metal Nitride and Nitrogen-Doped Reduced Graphene Oxide. *J. Mater. Chem. A* **2017**, *5*, 5829–5837.

7 Electronic Supplementary information

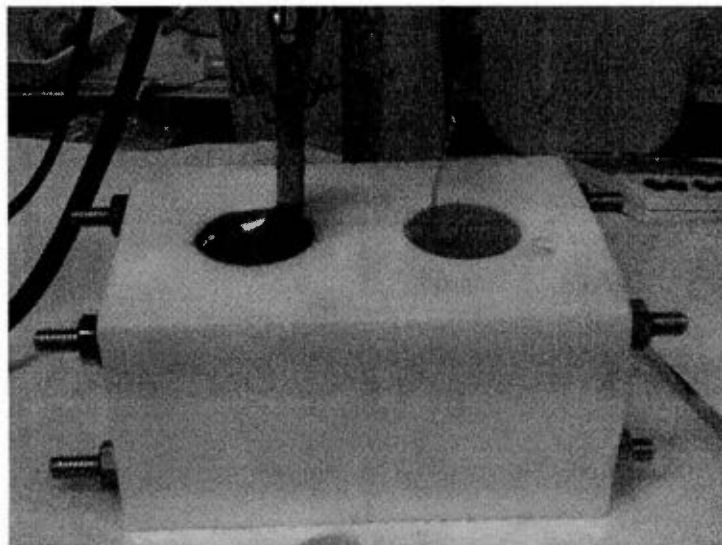


Figure S1. Photograph of typical electrochemical cell for graphene nanocomposites synthesis.

7.1 Dynamic light scattering

Dynamic light scattering (DLS) was employed to obtain a rough measure of the lateral size distributions of EG-Ag, EG-Au and EG-Ag₁/Au₁. The graphene suspensions were filtered (0.20 µm) before measurements because of the instrument is limited when the particle size becomes large. In the prepared sample, it was observed that graphene sheets have a wide size distribution, but the majority of them were dispersed within a narrow range, as shown in Figure S2. The average of graphene filtered size from the histogram was found to be 200 nm.

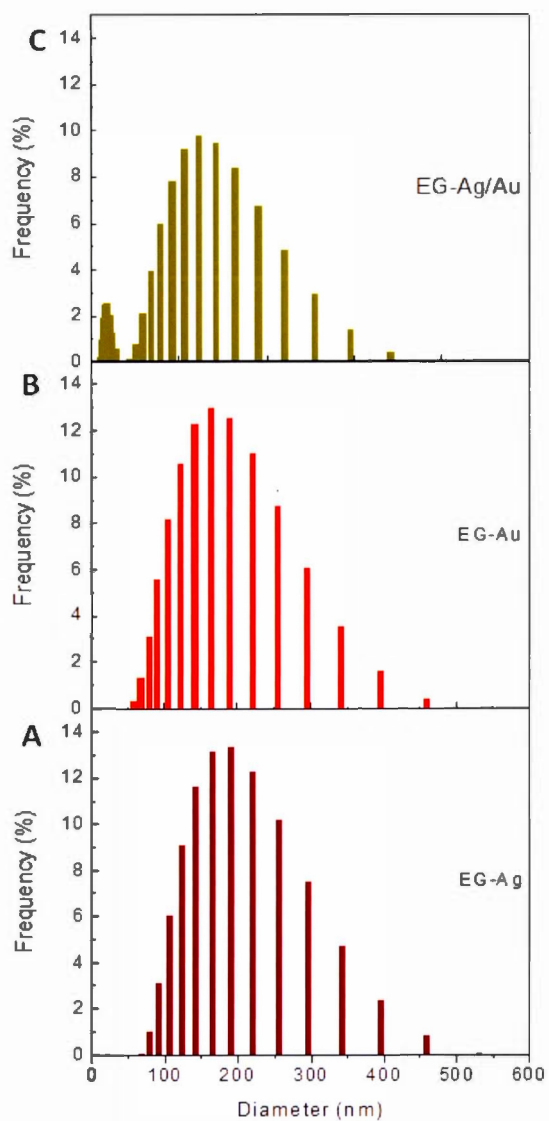


Figure S2. DLS of (A) EG-Ag, (B) EG-Au and (C) EG-Ag/Au.

7.2 Morphology characterization

The morphology of graphene and hybrid graphene materials was determined by SEM analysis. Figure S3A shows as-exfoliated, flexible and almost transparent images of graphene sheets, suggesting that the graphene layers are very thin. After nanoparticles graphene functionalization, Figures S3(B-E) clarify the morphology and exhibited the dispersion of Au and Ag nanoparticles on EG surface, which were absents on graphene sheets. From these microscopic images, it can be seen spherical Ag and Au NPs dispersed on graphene surface with variable diameters, increasing with nanoparticle concentration up to 500 nm because of aggregation.

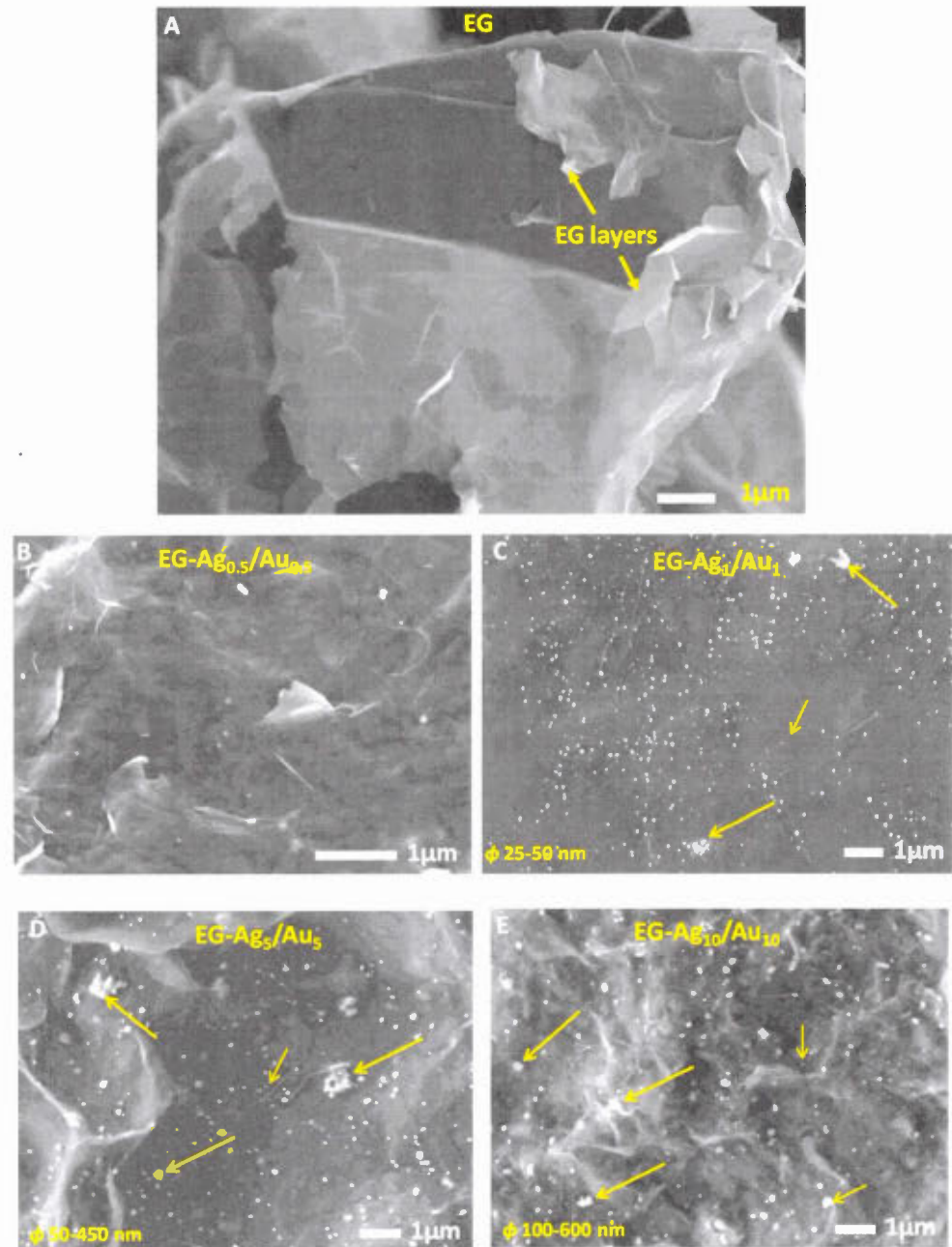


Figure S3. SEM images of (A) EG, (B) EG-Ag_{0.5}/Au_{0.5}, (C) EG-Ag₁/Au₁, (D) EG-Ag₅/Au₅, and (E) EG-Ag₁₀/Au₁₀

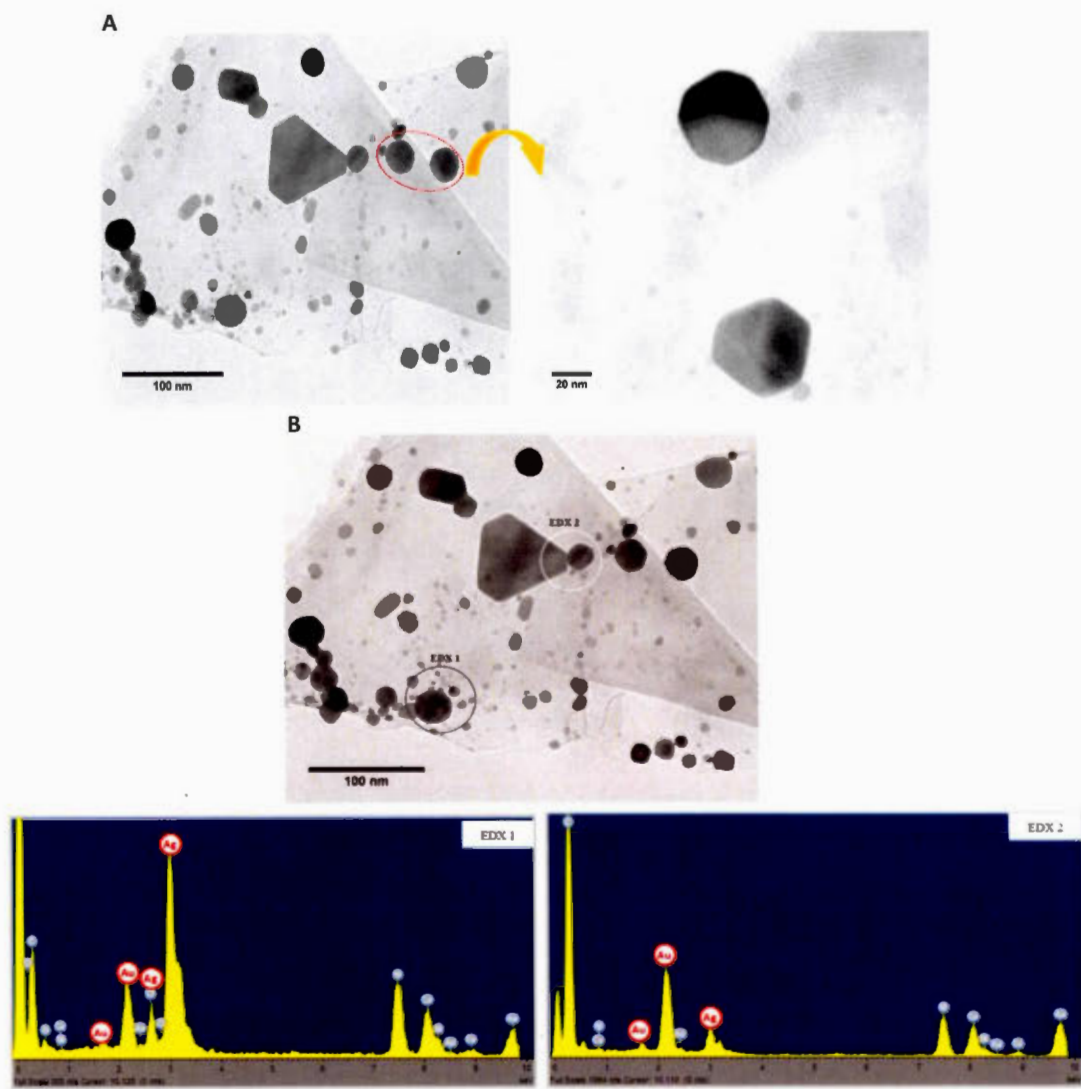


Figure S4. TEM images at different magnifications of $\text{EG}-\text{Ag}_{0.5}/\text{Au}_{0.5}$ and EDX spectra.

7.3 Thermogravimetric analysis

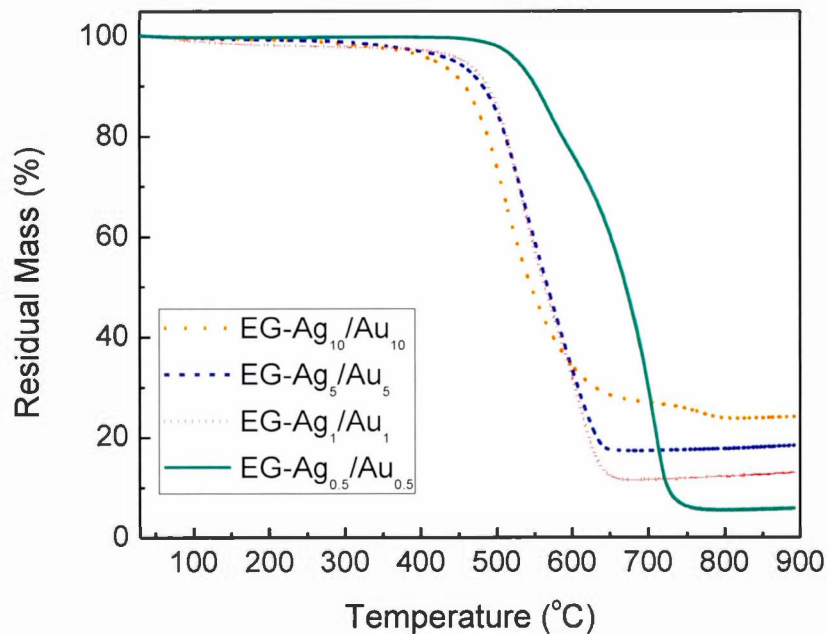


Figure S5. TGA profiles of graphene-Ag/Au nanocomposites with different metal concentrations (EG-Ag_{0.5}/Au_{0.5}, EG-Ag₁/Au₁, EG-Ag₅/Au₅, and EG-Ag₁₀/Au₁₀) recorded with a temperature ramp of 5 °C/min under air.

7.4 XPS analysis

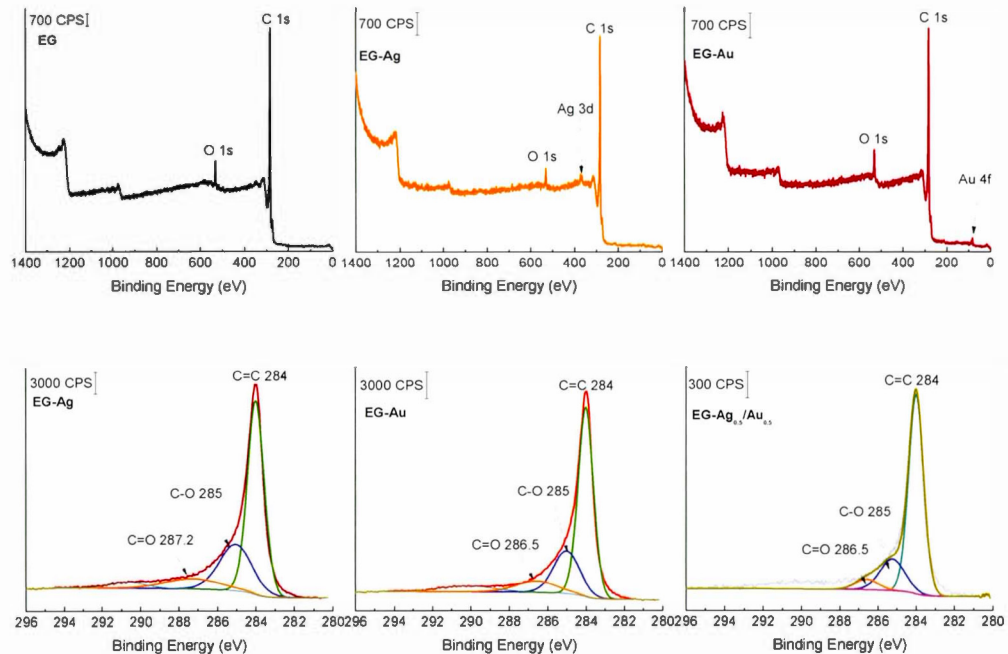


Figure S6. XPS survey spectrum of EG, EG-Ag and EG-Au, and C 1s level of EG-Ag, EG-Au and EG-Ag_{0.5}/Au_{0.5}

Table S1. XPS elements concentration (at.%) of the surface graphene nanocomposites samples.

Atomic concentrations (at. %)	%C	%O	%Ag	%Au
EG-Ag	90.7	4.7	1.1	nd
EG-Au	93	5.9	nd	0.6
EG-Ag_{0.5}/Au_{0.5}	92.8	6.7	0.1	0.4

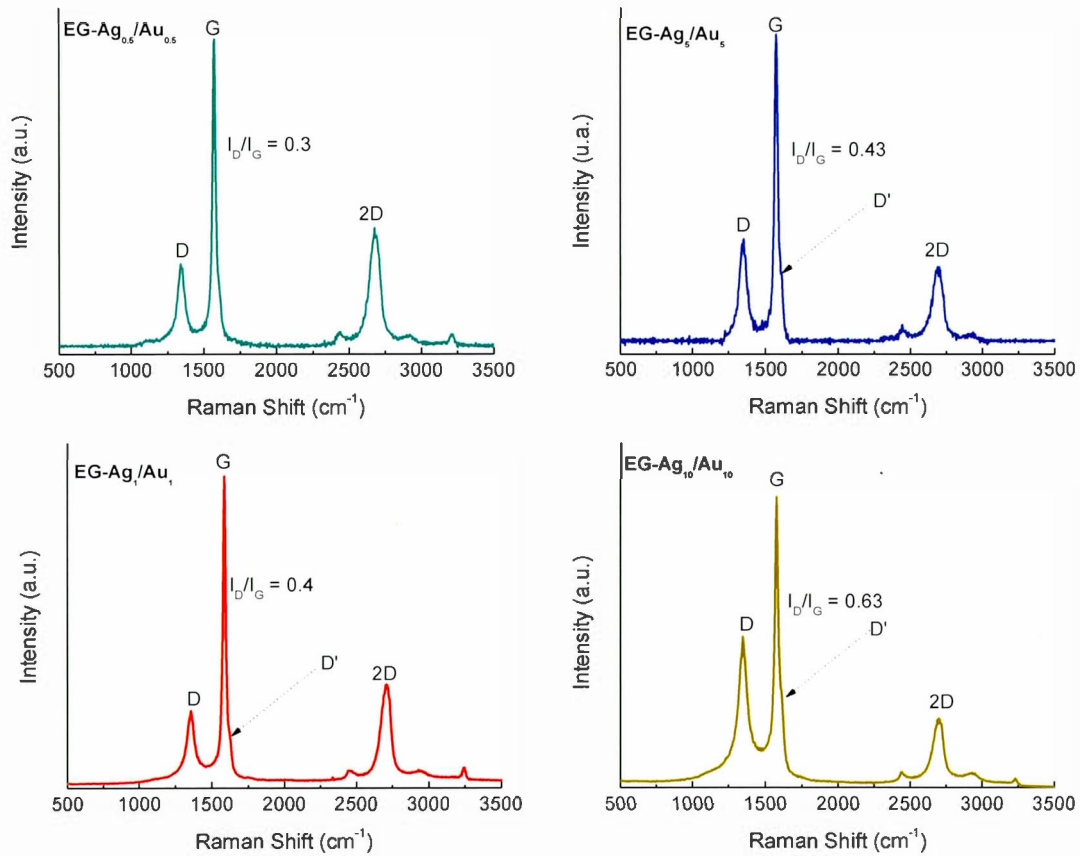


Figure S7. Raman spectra of EG-Ag_x/Au_x nanocomposites ($x = 0.5, 1, 5$ and 10).

CONCLUSIONS ET PERSPECTIVES

Depuis la découverte du graphène en 2004, un grand nombre d'applications potentielles ont été déjà proposées pour ce matériau, allant des capteurs, des films conducteurs transparents et flexibles, des catalyseurs jusqu'aux supercondensateurs électrochimiques et aux batteries. Néanmoins, il reste évidemment un effort colossal à déployer dans le but d'étudier, de comprendre et de façonner les propriétés du graphène afin de le rendre encore plus attrayant. Ce qui ouvre la voie à plusieurs défis.

Cette thèse a essentiellement porté sur la préparation et la caractérisation des matériaux à base de graphène, en se basant soit sur des méthodes préexistantes avec amélioration ou modification de certains paramètres, soit sur de nouvelles approches adoptées pour synthétiser le graphène et ses dérivés. Pour atteindre cet objectif, deux principales voies de synthèse ont été explorées: la fonctionnalisation covalente avec des molécules organiques par réaction spontanée et la modification non-covalente des feuillets de graphène par des nanoparticules métalliques lors de l'exfoliation électrochimique du graphite.

Dans l'article 1, qui constitue le chapitre I de cette thèse, nous nous sommes focalisés sur la fonctionnalisation et l'analyse de l'oxyde de graphène réduit (RGO), obtenu à partir de l'oxyde de graphène. La modification chimique et spontanée du matériau par réduction d'ions aryle diazonium a été choisie dans cette étude pour attacher des groupements sulfophényles de manière covalente à la surface de RGO. Des analyses par spectroscopie du photoélectron-X, UV-visible-proche infrarouge, spectroscopie Raman et analyse thermogravimétrique ont permis de déterminer la nature des groupements fonctionnels présents sur le RGO et de confirmer la présence

des groupements sulfophényles sur le RGO modifié (SRGO). La fonctionnalisation covalente qui entraîne une modification de surface des feuillets de graphène par la conversion des carbones sp² en carbone sp³ a été démontrée par spectroscopie Raman, analyse de la bande optique et mesure de conductivité.

Les travaux futurs pour ce projet pourraient consister à faire une étude comparative de ces poudres (RGO et SRGO) comme matériaux d'électrode dans les capteurs chimiques, les piles à combustible à membrane échangeuse de protons, les supercondensateurs électrochimiques et dans les batteries dans le but d'observer leur performance électrochimique. Les groupements sulfophényles, greffés à la surface du RGO sont thermiquement stables. Ils ont une conductivité protonique élevée et sont capables d'accroître la sensibilité des électrodes et ainsi que leur sélectivité face à certains ions tels que Na⁺, H⁺, Li⁺ etc... Ces groupements peuvent notamment servir de supports catalytiques pour le platine pour préparer des électrocatalyseurs pour l'oxydation du méthanol dans les piles à combustible au méthanol direct (DMFC, de l'anglais direct-methanol fuel cell).

À la suite du premier article, l'objectif a été de proposer une méthode améliorée pour produire une nouvelle variété de graphène. Le chapitre II, dédié à cette étude décrit une approche innovante permettant de fonctionnaliser spontanément le graphène lors de sa synthèse. Cette méthode, comportant une seule étape est opposée à celle utilisée dans le chapitre précédent pour fonctionnaliser le RGO à partir des cations diazonium. À partir des résultats expérimentaux obtenus et des observations faites, il a été permis de proposer un mécanisme de fonctionnalisation unique, lié à la réactivité élevée des feuillets de graphène une fois détachés de l'électrode de graphite. Les feuillets de graphène, étant moins passivés dans ces conditions permettent un transfert d'électron plus rapide pour réduire les cations anthraquinone (AQ) diazonium présents dans le milieu réactionnel. Le matériau

modifié (EG-AQ) qui comprend un lien covalent entre le graphène et la molécule organique a démontré une surface BET plus élevée que celui non modifié (EG). Ces résultats intéressants qui contrastent avec les observations habituelles dans le cas d'une modification d'un carbone par la chimie du diazonium ont donné lieu au deuxième article (*cf. chapitre II*) publié dans le journal Carbon. Cette étude ouvre la voie à la fonctionnalisation avec d'autres molécules.

Les travaux futurs pour ce projet, dont une première partie est en cours de réalisation, pourraient consister à varier la concentration des cations diazonium dans le milieu réactionnel afin de varier le taux de greffage des molécules d'anthraquinone. Un autre aspect important à envisager dans cette étude serait de déterminer le potentiel réel d'exfoliation dans différents milieux (0.1 M H₂SO₄ et 0.1 M H₂SO₄ + cations diazonium) par un système à trois électrodes par voltammetrie cyclique. La nature des gaz générés lors de l'exfoliation de l'électrode de graphite pourrait être déterminée par chromatographie en phase gazeuse couplée à la spectroscopie de masse. Certains paramètres tels que le potentiel d'exfoliation, l'effet de la température et le temps de réaction pourraient être étudiés en vue de mieux comprendre le processus d'exfoliation électrochimique impliquant un greffage de molécules. La seconde phase de cette étude est d'analyser et de comprendre la différence obtenue par TGA et par voltammetrie cyclique, quant à la quantité d'anthraquinone greffée. Une étude comparative de l'activité électrocatalytique des matériaux synthétisés (EG et EG-AQ), pour la réaction de réduction de l'oxygène pourrait être effectuée.

Dans le dernier chapitre, une synthèse simple et rapide a permis la préparation de matériaux hybrides graphène-nanoparticules métalliques. La combinaison des résultats expérimentaux obtenus lors de cette étude a permis de conclure que l'exfoliation électrochimique est un procédé approprié pour déposer des

nanoparticules métalliques sur des feuillets de graphène sans l'ajout d'agent réducteur. La caractérisation microstructurale des systèmes EG-Ag et EG-Au par microscopie électronique en transmission a montré la présence de nanoparticules sphériques sur les feuillets du graphène. Alors que l'échantillon EG-Ag_{0,5}/Au_{0,5} montre la présence de nanoparticules de tailles variables, phénomène dû à la fusion des nanoparticules métalliques à la surface du graphène au cours de la préparation. Ce dernier nanomatériau montre de bonnes propriétés électrocatalytiques pour la réaction de réduction de l'oxygène en milieu KOH.

Néanmoins, il serait encore intéressant de poursuivre l'étude de ces systèmes graphène-Ag (EG-Ag), graphène-Au (Eg-Au) et graphène-Ag/Au (EG-Ag/Au) en variant certains paramètres de synthèse tels que le temps d'exfoliation, la température et le temps de recuit des poudres et la concentration des précurseurs métalliques. Cette étude supplémentaire nécessite d'être réalisée afin d'étudier l'effet de la taille des nanoparticules ainsi que leur nature dans le but de tester la performance électrochimique de chacun des nanomatériaux pour la réaction de réduction de l'oxygène.

Une des principales perspectives de ces travaux est de préparer des matériaux hybrides, composés de graphène électrochimiquement exfolié et de nanoparticules d'autres métaux tel que le platine à partir de la méthode précédemment décrite. L'activité électrocatalytique de ce matériau pour la réaction de réduction de l'oxygène pourrait être évaluée. Comme électrocatalyseur pour la réaction d'oxydation du méthanol, un matériau bi-fonctionnel à base de Pt et Ru sur le graphène (EG-Pt/Ru) pourrait être étudié.

Au cours de ce projet de doctorat, les approches développées ont permis de préparer des matériaux composites à base de graphène avec différentes propriétés liées à la fonctionnalisation des feuillets de graphène. L'optimisation de certains

procédés existants a permis de préparer du graphène de haute qualité qui peut être utilisé comme additif ou support conducteur dans certaines applications. Ces travaux ouvrent plusieurs champs de recherche dans le domaine du graphène.

RÉFÉRENCES

- [1] A.H. Castro Neto, F. Guinea, N.M.R. Peres, K.S. Novoselov, A.K. Geim, The electronic properties of graphene, *Rev. Mod. Phys.* 81 (2009) 109–162.
- [2] K. Singh, A. Ohlan, S.K. Dhawan, Polymer-Graphene Nanocomposites: Preparation, Characterization, Properties, and Applications, in: *Nanocomposites - New Trends Dev.*, 2012: pp. 37–71.
- [3] R.M. Hazen, R.T. Downs, A.P. Jones, L. Kah, Carbon Mineralogy and Crystal Chemistry, *Carbon in Earth.* 75 (2013) 7–46.
- [4] R.M. Hazen, C.M. Schiffries, Why Deep Carbon?, *Rev. Mineral. Geochemistry.* 75 (2013) 1–6.
- [5] I.S.I. Web, S. This, H. Press, M. Science, N. York, A. Nw, Graphene : Status and Prospects, 1530 (2014) 1530–1535.
- [6] S. Sorella, Y. Otsuka, S. Yunoki, Absence of a spin liquid phase in the Hubbard model on the honeycomb lattice., *Sci. Rep.* 2 (2012) 992–996.
- [7] U.K. Sur, Graphene: A Rising Star on the Horizon of Materials Science, *Int. J. Electrochem.* 2012 (2012) 1–12.
- [8] A.K. Geim, K.S. Novoselov, The rise of graphene, *Nat. Mater.* 6 (2007) 183–191.
- [9] H.W. Kroto, J.R. Heath, S.C. O'Brien, R.F. Curl, R.E. Smalley, C 60: buckminsterfullerene, *Nature.* 318 (1985) 162–163.

- [10] Sumio Iijima, Helical microtubules of graphitic carbon, *Nature*. 354 (1991) 56–58.
- [11] P.R. Wallace, The band theory of graphite, *Phys. Rev.* 71 (1947) 622–634.
- [12] V. Singh, D. Joung, L. Zhai, S. Das, S.I. Khondaker, S. Seal, Graphene based materials: Past, present and future, *Prog. Mater. Sci.* 56 (2011) 1178–1271.
- [13] R. Peierls, Quelques propriétés typiques des corps solides, *Ann. I.H.Poincare*. 5 (1935) 177–222.
- [14] L. D. Landau, Zur Theorie der phasenumwandlungen II, *Phys. Zeitschrift Der Sowjetunion*. 11 (1937) 26 – 35.
- [15] K.S. Novoselov, A.K. Geim, S. V Morozov, D. Jiang, Y. Zhang, S. V Dubonos, et al., Electric field effect in atomically thin carbon films., *Science*. 306 (2004) 666–669.
- [16] Nobelprize.org., The Nobel Prize in Physics 2010: Graphene – the perfect atomic lattice, *Hyomen Kagaku*. 31 (2010) 682–682.
- [17] M.D. Stoller, S. Park, Y. Zhu, J. An, R.S. Ruoff, Graphene-based ultracapacitors., *Nano Lett.* 8 (2008) 3498–3502.
- [18] F. Li, Y. Wang, D. Wang, F. Wei, Characterization of single-wall carbon nanotubes by N₂ adsorption, *Carbon*. 42 (2004) 2375–2383.
- [19] A. Peigney, C. Laurent, E. Flahaut, R.R. Bacsa, A. Rousset, Specific surface area of carbon nanotubes and bundles of carbon nanotubes, *Carbon*. 39 (2001) 507–514.

- [20] A. Yella, H.-W. Lee, H.N. Tsao, C. Yi, A.K. Chandiran, M.K. Nazeeruddin, et al., Porphyrin-sensitized solar cells with cobalt (II/III)-based redox electrolyte exceed 12 percent efficiency., *Science*. 334 (2011) 629–634.
- [21] K.A. Kini, Surface Area of Active Carbon and Carbon Black by the B.E.T. Method Using Argon, Carbon Dioxide, Methanol, Krypton, and Xenon, *J. Phys. Chem.* 68 (1964) 1962–1963.
- [22] M. Toupin, D. Bélanger, Spontaneous functionalization of carbon black by reaction with 4-nitrophenyldiazonium cations., *Langmuir*. 24 (2008) 1910–1917.
- [23] T. Menanteau, C. Benoît, T. Breton, C. Cougnon, Enhancing the performance of a diazonium-modified carbon supercapacitor by controlling the grafting process, *Electrochim. Commun.* 63 (2016) 70–73.
- [24] G. Pognon, T. Brousse, D. Bélanger, Effect of molecular grafting on the pore size distribution and the double layer capacitance of activated carbon for electrochemical double layer capacitors, *Carbon*. 49 (2011) 1340–1348.
- [25] S. Lee, K. Lee, C.-H. Liu, Z. Zhong, Homogeneous bilayer graphene film based flexible transparent conductor, *Nanoscale*. 4 (2012) 639–644.
- [26] M.-S. Lee, J. Kim, J. Park, J.-U. Park, Studies on the mechanical stretchability of transparent conductive film based on graphene-metal nanowire structures, *Nanoscale Res. Lett.* 10 (2015) 27–36.

- [27] B.D. Ossonon, D. Bélanger, Functionalization of graphene sheets by the diazonium chemistry during electrochemical exfoliation of graphite, *Carbon.* 111 (2017) 83–93.
- [28] S. Stankovich, D.A. Dikin, G.H.B. Dommett, K.M. Kohlhaas, E.J. Zimney, E.A. Stach, et al., Graphene-based composite materials, *Nature.* 442 (2006) 282–286.
- [29] G.-H. Lee, R.C. Cooper, S.J. An, S. Lee, A. van der Zande, N. Petrone, et al., High-strength chemical-vapor-deposited graphene and grain boundaries., *Science (80-).* 340 (2013) 1073–1076.
- [30] R.R. Nair, P. Blake, A.N. Grigorenko, K.S. Novoselov, T.J. Booth, T. Stauber, et al., Fine Structure Constant Defines Visual Transparency of Graphene, *Science (80-).* 320 (2008) 1308–1309.
- [31] K.S. Kim, Y. Zhao, H. Jang, S.Y. Lee, J.M. Kim, K.S. Kim, et al., Large-scale pattern growth of graphene films for stretchable transparent electrodes, *Nature.* 457 (2008) 706–710.
- [32] F. Bonaccorso, Z. Sun, T. Hasan, A.C. Ferrari, Graphene Photonics and Optoelectronics, *Nat. Photonics.* 4 (2010) 611–622.
- [33] T.H.E. Royal, S. Academy, O.F. Sciences, Graphene, R. Swedish Acad. Sci. 50005 (2010) 0–10.
- [34] A.A. Balandin, S. Ghosh, W. Bao, I. Calizo, D. Teweldebrhan, F. Miao, et al., Superior thermal conductivity of single-layer graphene., *Nano Lett.* 8 (2008) 902–907.

- [35] C. Mattevi, G. Eda, S. Agnoli, S. Miller, K.A. Mkhoyan, O. Celik, et al., Evolution of electrical, chemical, and structural properties of transparent and conducting chemically derived graphene thin films, *Adv. Funct. Mater.* 19 (2009) 2577–2583.
- [36] T. Ihn, J. Güttinger, F. Molitor, S. Schnez, E. Schurtenberger, A. Jacobsen, et al., Graphene single-electron transistors, *Mater. Today.* 13 (2010) 44–50.
- [37] C. Mattevi, H. Kim, M. Chhowalla, A review of chemical vapour deposition of graphene on copper, *J. Mater. Chem.* 21 (2011) 3324–3334.
- [38] J.K. Wasie, R.B. Kaner, Graphene, a promising transparent conductor, *Mater. Today.* 13 (2010) 52–59.
- [39] W. Choi, I. Lahiri, R. Seelaboyina, Y.S. Kang, Synthesis of Graphene and Its Applications: A Review, *Crit. Rev. Solid State Mater. Sci.* 35 (2010) 52–71.
- [40] V.S. Channu, R. Bobba, R. Holze, Graphite and graphene oxide electrodes for lithium ion batteries, *Colloids Surfaces A Physicochem. Eng. Asp.* 436 (2013) 245–251.
- [41] D. Wei, L. Grande, V. Chundi, R. White, C. Bower, P. Andrew, et al., Graphene from electrochemical exfoliation and its direct applications in enhanced energy storage devices, *Chem. Commun.* 48 (2012) 1239–1241.
- [42] H. Kim, K.-Y. Park, J. Hong, K. Kang, All-graphene-battery: bridging the gap between supercapacitors and lithium ion batteries., *Sci. Rep.* 4 (2014) 5278–5282.

- [43] J. Yang, S. Gunasekaran, V.H. Pham, T. Gebre, J.H. Dickerson, Y. Chen, et al., Covalent bulk functionalization of graphene, *Carbon N. Y.* 3 (2013) 573–580.
- [44] E.S. Cho, A.M. Ruminski, S. Aloni, Y.-S. Liu, J. Guo, J.J. Urban, Graphene oxide/metal nanocrystal multilaminates as the atomic limit for safe and selective hydrogen storage., *Nat. Commun.* 7 (2016) 10804.
- [45] E. Malic, T. Winzer, F. Wendler, A. Knorr, Review on carrier multiplication in graphene, *Phys. Status Solidi.* 253 (2016) 2303–2310.
- [46] J.C. Johannsen, S. Ulstrup, A. Crepaldi, F. Cilento, M. Zacchigna, J.A. Miwa, et al., Tunable carrier multiplication and cooling in graphene, *Nano Lett.* 15 (2015) 326–331.
- [47] X. Gan, R. Lv, J. Bai, Z. Zhang, J. Wei, Z.-H. Huang, et al., Efficient photovoltaic conversion of graphene–carbon nanotube hybrid films grown from solid precursors, *2D Mater.* 2 (2015) 1–7.
- [48] I.A. Baburin, A. Klechikov, G. Mercier, A. Talyzin, G. Seifert, Hydrogen adsorption by perforated graphene, *Int. J. Hydrogen Energy.* 40 (2015) 6594–6599.
- [49] A.G. Klechikov, G. Mercier, P. Merino, S. Blanco, C. Merino, A. V. Talyzin, Hydrogen storage in bulk graphene-related materials, *Microporous Mesoporous Mater.* 210 (2015) 46–51.

- [50] K. Hu, X. Xie, T. Szkopek, M. Cerruti, Understanding Hydrothermally Reduced Graphene Oxide Hydrogels: From Reaction Products to Hydrogel Properties, *Chem. Mater.* 28 (2016) 1756–1768.
- [51] D.C.B. Alves, R. Silva, D. Voiry, T. Asefa, M. Chhowalla, Copper nanoparticles stabilized by reduced graphene oxide for CO₂ reduction reaction, *Mater. Renew. Sustain. Energy.* 4 (2015).
- [52] T.S. Sreeprasad, T. Pradeep, Graphene for Environmental and Biological Applications, *Int. J. Mod. Phys. B.* 26 (2012) 1242001–1240026.
- [53] S. Porada, R. Zhao, A. van der Wal, V. Presser, P.M. Biesheuvel, Review on the science and technology of water desalination by capacitive deionization, *Prog. Mater. Sci.* 58 (2013) 1388–1442.
- [54] S. De, J.N. Coleman, Are there fundamental limitations on the sheet resistance and transmittance of thin graphene films?, *ACS Nano.* 4 (2010) 2713–2720.
- [55] Y. Shao, J. Wang, H. Wu, J. Liu, I.A. Aksay, Y. Lin, Graphene based electrochemical sensors and biosensors: A review, *Electroanalysis.* 22 (2010) 1027–1036.
- [56] P.T. Yin, T.-H. Kim, J.-W. Choi, K.-B. Lee, Prospects for graphene-nanoparticle-based hybrid sensors., *Phys. Chem. Chem. Phys.* 15 (2013) 12785–12799.
- [57] J.H. Seol, I. Jo, A.L. Moore, L. Lindsay, Z.H. Aitken, M.T. Pettes, et al., Two-dimensional phonon transport in supported graphene., *Science (80-.).* 328 (2010) 213–236.

- [58] V. Smejkal, E. Gruber, R.A. Wilhelm, A. Hierzenberger, B.C. Bayer, K. Andrey, et al., Ultrafast electronic response of graphene to a strong and localized electric field, *Nat. Commun.* 7 (2016) 13948.
- [59] S. Ichinokura, K. Sugawara, A. Takayama, T. Takahashi, S. Hasegawa, Superconducting Calcium-Intercalated Bilayer Graphene, *ACS Nano.* 10 (2016) 2761–2765.
- [60] T. Monetta, A. Acuesta, F. Bellucci, Graphene/Epoxy Coating as Multifunctional Material for Aircraft Structures, *Aerospace.* 2 (2015) 423–434.
- [61] W. Zhang, M. Yi, Z. Shen, X. Zhao, X. Zhang, S. Ma, Graphene-reinforced epoxy resin with enhanced atomic oxygen erosion resistance, *J. Mater. Sci.* 48 (2013) 2416–2423.
- [62] Z. Zhang, W. Zhang, D. Li, Y. Sun, Z. Wang, C. Hou, et al., Mechanical and anticorrosive properties of graphene/epoxy resin composites coating prepared by in-situ method, *Int. J. Mol. Sci.* 16 (2015) 2239–2251.
- [63] X. Huang, X. Qi, F. Boey, H. Zhang, Graphene-based composites, *Chem. Soc. Rev.* 41 (2012) 666–686.
- [64] B. Shen, W. Zhai, D. Lu, J. Wang, W. Zheng, Ultrasonication-assisted direct functionalization of graphene with macromolecules, *RSC Adv.* 2 (2012) 4713–4719.
- [65] M. Fang, K. Wang, H. Lu, Y. Yang, S. Nutt, Covalent polymer functionalization of graphene nanosheets and mechanical properties of composites, *J. Mater. Chem.* 19 (2009) 7098–7105.

- [66] Vorbeck, Composite Materials, (2017). <https://vorbeck.com/pages/products-composites> (accessed November 10, 2017).
- [67] Q. Li, N. Mahmood, J. Zhu, Y. Hou, S. Sun, Graphene and its composites with nanoparticles for electrochemical energy applications, *Nano Today.* 9 (2014) 668–683.
- [68] H. Yin, H. Tang, D. Wang, Y. Gao, Z. Tang, Facile synthesis of surfactant-free Au cluster/graphene hybrids for high-performance oxygen reduction reaction, *ACS Nano.* 6 (2012) 8288–8297.
- [69] R. Fang, S. Zhao, S. Pei, X. Qian, P.X. Hou, H.M. Cheng, et al., Toward More Reliable Lithium-Sulfur Batteries: An All-Graphene Cathode Structure, *ACS Nano.* 10 (2016) 8676–8682.
- [70] L. David, R. Bhandavat, U. Barrera, G. Singh, electrode for long-cycle lithium-ion batteries, *Nat. Commun.* 7 (2016) 10998–11008.
- [71] N. Kim, C. Oh, J. Kim, J.-S. Kim, E.D. Jeong, J.-S. Bae, et al., High Performance Li-Ion Battery Anodes Based on Silicon-Graphene Self-Assemblies, *J. Electrochem. Soc.* 164 (2017) 6075–6083.
- [72] H.J. Yoon, D.H. Jun, J.H. Yang, Z. Zhou, S.S. Yang, M.M.C. Cheng, Carbon dioxide gas sensor using a graphene sheet, *Sensors Actuators, B Chem.* 157 (2011) 310–313.
- [73] R. Pearce, T. Iakimov, M. Andersson, L. Hultman, A.L. Spetz, R. Yakimova, Epitaxially grown graphene based gas sensors for ultra sensitive NO₂ detection, *Sensors Actuators, B Chem.* 155 (2011) 451–455.

- [74] N. Wang, M. Lin, H. Dai, H. Ma, Functionalized gold nanoparticles/reduced graphene oxide nanocomposites for ultrasensitive electrochemical sensing of mercury ions based on thymine-mercury-thymine structure, *Biosens. Bioelectron.* 79 (2016) 320–326.
- [75] H. Bai, C. Li, G. Shi, Functional composite materials based on chemically converted graphene, *Adv. Mater.* 23 (2011) 1089–1115.
- [76] Y. Liu, X. Dong, P. Chen, Biological and chemical sensors based on graphene materials, *Chem Soc Rev.* 41 (2012) 2283–2307.
- [77] C. Wu, Q. Cheng, K. Wu, G. Wu, Q. Li, Graphene prepared by one-pot solvent exfoliation as a highly sensitive platform for electrochemical sensing, *Anal. Chim. Acta.* 825 (2014) 26–33.
- [78] L. Gao, J. Xie, X. Ma, M. Li, L. Yu, DNA@Mn₃(PO₄)₂ Nanoparticles Supported with Graphene Oxide as Photoelectrodes for Photoelectrocatalysis, *Nanoscale Res. Lett.* 12 (2017) 17–25.
- [79] B.H. Nguyen, V.H. Nguyen, Promising applications of graphene and graphene-based nanostructures, *Adv. Nat. Sci. Nanosci. Nanotechnol.* 7 (2016) 023002–023017.
- [80] D. Akinwande, L. Tao, Q. Yu, X. Lou, P. Peng, D. Kuzum, Large-Area Graphene Electrodes: Using CVD to facilitate applications in commercial touchscreens, flexible nanoelectronics, and neural interfaces., *IEEE Nanotechnol. Mag.* 9 (2015) 6–14.

- [81] S. POULTER, Bendable smartphones are coming! Devices with screens made from graphene are so flexible they can be worn like a BRACELET, (2016). <http://www.dailymail.co.uk/sciencetech/article-3607191/Bendable-smartphones-coming-Devices-screens-graphene-flexible-worn-like-BRACELET.html> (accessed April 28, 2017).
- [82] J.A. Garrido, Graphene points to improved retinal implants, (2014). <http://optics.org/news/5/9/52> (accessed January 22, 2017).
- [83] S.M.H. Organic, J. Park, W.H. Lee, S. Huh, S.H. Sim, S. Bin Kim, et al., Work-Function Engineering of Graphene Electrodes by Self-Assembled Monolayers for High-Performance Organic Field-Effect Transistors, *J. Phys. Chem. Lett.* 2 (2011) 841–845.
- [84] J. a Torres, R.B. Kaner, Graphene synthesis: Graphene closer to fruition., *Nat. Mater.* 13 (2014) 328–329.
- [85] A. Bendali, L.H. Hess, M. Seifert, V. Forster, A.F. Stephan, J.A. Garrido, et al., Purified Neurons can Survive on Peptide-Free Graphene Layers, *Adv. Healthc. Mater.* 2 (2013) 929–933.
- [86] L. Tisza, L. Landau, L. Onsager, R.P. Feynman, C.J. Gorter, V.L. Ginzburg, et al., Transformation Optics Using Graphene, *Science*. 332 (2011) 1291–1294.
- [87] J.R. Miller, P. Simon, Electrochemical Capacitors for, *Science* (80-.). 321 (2008) 651–652.
- [88] Z.-S. Wu, K. Parvez, X. Feng, K. Müllen, Graphene-based in-plane micro-supercapacitors with high power and energy densities., *Nat. Commun.* 4 (2013) 2487–3487.

- [89] J.M. Chem, K. Jost, Y. Gogotsi, Textile energy storage in perspective, *J. Mater. Chem. A.* 2 (2014) 10776–10787.
- [90] M. Moussa, M.F. El-kady, Z. Zhao, Recent progress and performance evaluation for polyaniline / graphene nanocomposites as supercapacitor electrodes, *Nanotechnology*. 27 (2016) 42001–42021.
- [91] H. Ji, X. Zhao, Z. Qiao, J. Jung, Y. Zhu, Y. Lu, et al., Capacitance of carbon-based electrical double-layer capacitors., *Nat. Commun.* 5 (2014) 3317–3324.
- [92] E. Radvanyi, E. Radvanyi, E. De Vito, W. Porcher, J. Danet, P. Desbois, et al., *Materials Chemistry A Materials for energy and sustainability*, 1 (2013) 9315–9546.
- [93] D. Ghosh, S. Giri, T. Basu, M. Mandal, C.K. Das, α MnMoO₄/graphene hybrid composite: high energy density supercapacitor electrode material, *Dalt. Trans.* 43 (2014) 11067–11076.
- [94] J. Ji, L.L. Zhang, H. Ji, Y. Li, X. Zhao, X. Bai, et al., Nanoporous Ni(OH)₂ thin film on 3d ultrathin-graphite foam for asymmetric supercapacitor, *ACS Nano.* 7 (2013) 6237–6243.
- [95] I.H. Son, J. Hwan Park, S. Kwon, S. Park, M.H. Rümmeli, A. Bachmatiuk, et al., Silicon carbide-free graphene growth on silicon for lithium-ion battery with high volumetric energy density., *Nat. Commun.* 6 (2015) 7393–7401.
- [96] P. Lian, X. Zhu, S. Liang, Z. Li, W. Yang, H. Wang, Large reversible capacity of high quality graphene sheets as an anode material for lithium-ion batteries, *Electrochim. Acta*. 55 (2010) 3909–3914. doi:10.1016/j.electacta.2010.02.025.

- [97] J.M. Tarascon, M. Armand, review article Issues and challenges facing rechargeable lithium batteries, *Nat. 4.* 14 (2001) 359–367..
- [98] M.F. El-Kady, Y. Shao, R.B. Kaner, Graphene for batteries, supercapacitors and beyond, *Nat. Rev. Mater.* 1 (2016) 16033–16047.
- [99] R. Raccichini, A. Varzi, S. Passerini, B. Scrosati, The role of graphene for electrochemical energy storage., *Nat. Mater.* 14 (2015) 271–279.
- [100] Q. Tang, X. Wang, P. Yang, B. He, A Solar Cell That Is Triggered by Sun and Rain, *Angew. Chem. Int. Ed.* 55 (2016) 5243–5246.
- [101] H.W. Zheng, X. Liang, Y.H. Yu, K. Wang, X.A. Zhang, B.Q. Men, et al., Bi₅FeTi₃O₁₅ nanofibers/graphene nanocomposites as an effective counter electrode for dye-sensitized solar cells, *Nanoscale Res. Lett.* 12 (2017).
- [102] H. Yuana, Q. Jiaoa, J. Liua, X. Liua, H. Yanga, Y. Zhaoa, et al., Ultrathin-walled Co₉S₈ nanotube/reduced graphene oxide composite as an efficient electrocatalyst for the reduction of triiodide, *J. Power Sources.* 336 (2016) 132–142.
- [103] J. Yin, X. Li, J. Yu, Z. Zhang, J. Zhou, W. Guo, Generating electricity by moving a droplet of ionic liquid along graphene, *Nat Nanotechnol.* 9 (2014) 378–383.
- [104] J. Lao, Y. He, X. Li, F. Wu, T. Yang, M. Zhu, et al., Flow-induced voltage generation in graphene network, *Nano Res.* 8 (2015) 2467–2473.

- [105] U. Bach, D. Lupo, P. Comte, J.E. Moser, F. Weissortel, J. Salbeck, et al., Solid-state dye-sensitized mesoporous TiO₂ solar cells with high photon-to-electron conversion efficiencies, *Nature*. 395 (1998) 583–585.
- [106] J. Wang, L.K. Wu, J.H. Zhou, J.M. Hu, J.Q. Zhang, C.N. Cao, Construction of a novel painting system using electrodeposited SiO₂ film as the pretreatment layer, *Corros. Sci.* 68 (2013) 57–65.
- [107] M. Ates, A review on conducting polymer coatings for corrosion protection, *J. Adhes. Sci. Technol.* 30 (2016) 1510–1536.
- [108] M.J. Nine, M.A. Cole, L. Johnson, D.N.H. Tran, D. Losic, Robust Superhydrophobic Graphene-Based Composite Coatings with Self-Cleaning and Corrosion Barrier Properties, *ACS Appl. Mater. Interfaces*. 7 (2015) 28482–28493.
- [109] Y. Su, V.G. Kravets, S.L. Wong, J. Waters, A.K. Geim, R.R. Nair, Impermeable barrier films and protective coatings based on reduced graphene oxide., *Nat. Commun.* 5 (2014) 4843–4848.
- [110] K.C. Chang, M.H. Hsu, H.I. Lu, M.C. Lai, P.J. Liu, C.H. Hsu, et al., Room-temperature cured hydrophobic epoxy/graphene composites as corrosion inhibitor for cold-rolled steel, *Carbon*. 66 (2014) 144–153.
- [111] W. Do Diamond, Mass production of high quality graphene: Juin, 28. (2012). <http://www.nanowerk.com/spotlight/spotid=25744.php> (accessed January 23, 2017).

- [112] A. Ambrosi, C.K. Chua, A. Bonanni, M. Pumera, Electrochemistry of graphene and related materials., *Chem. Rev.* 114 (2014) 7150–7188.
- [113] W. Norimatsu, M. Kusunoki, Epitaxial graphene on SiC{0001}: advances and perspectives, *Phys. Chem. Chem. Phys.* 16 (2014) 3501–3511.
- [114] A. Guermoune, T. Chari, F. Popescu, S.S. Sabri, J. Guillemette, H.S. Skulason, et al., Chemical vapor deposition synthesis of graphene on copper with methanol, ethanol, and propanol precursors, *Carbon N. Y.* 49 (2011) 4204–4210.
- [115] K. Parvez, S. Yang, X. Feng, K. Müllen, Exfoliation of graphene via wet chemical routes, *Synth. Met.* 210 (2015) 123–132.
- [116] U. Khan, A. O'Neill, M. Lotya, S. De, J.N. Coleman, High-concentration solvent exfoliation of graphene, *Small.* 6 (2010) 864–871.
- [117] M. Cai, D. Thorpe, D.H. Adamson, H.C. Schniepp, Methods of graphite exfoliation, *J. Mater. Chem.* 22 (2012) 24992–25002.
- [118] Y.L. Zhong, T.M. Swager, Enhanced Electrochemical Expansion of Graphite for in Situ Electrochemical Functionalization, *J. Am. Chem. Soc.* 134 (2012) 17896–17899.
- [119] G. Krishnaiah, V. Varma, United States (12) Patent Application Publication (10) Pub. No.: US 2012/0128570 A1, 12, 2012.
- [120] R. Van Noorden, Production: Beyond sticky tape, *Nature.* 483 (2012) S32–S33.

- [121] N. Mishra, J. Boeckl, N. Motta, F. Iacopi, Graphene growth on silicon carbide: A review, *Phys. Status Solidi A.* 213 (2016) 2277–2289.
- [122] D.V. Badami, X-Ray studies of graphite formed by decomposing silicon carbide, *Carbon.* 3 (1965) 53–54.
- [123] J. Hass, F. Varchon, J.E. Millan-Otoya, M. Sprinkle, N. Sharma, W.A. De Heer, et al., Why multilayer graphene on 4H-SiC(0001) behaves like a single sheet of graphene, *Phys. Rev. Lett.* 100 (2008) 125504–125508.
- [124] H. Fukidome, Y. Kawai, H. Handa, H. Hibino, H. Miyashita, M. Kotsugi, et al., Site-selective epitaxy of graphene on si wafers, *Proc. IEEE.* 101 (2013) 1557–1566.
- [125] M.H. Oliveira, T. Schumann, F. Fromm, R. Koch, M. Ostler, M. Ramsteiner, et al., Formation of high-quality quasi-free-standing bilayer graphene on SiC(0 0 1) by oxygen intercalation upon annealing in air, *Carbon N. Y.* 52 (2013) 83–89.
- [126] X. Li, W. Cai, J. An, S. Kim, J. Nah, D. Yang, et al., Large-area synthesis of high-quality and uniform graphene films on copper foils., *Science (80-.).* 324 (2009) 1312–1314.
- [127] Z. Sun, Z. Yan, J. Yao, E. Beitler, Y. Zhu, J.M. Tour, Growth of graphene from solid carbon sources., *Nature.* 468 (2010) 549–552.
- [128] R. Chen, N. Nioradze, P. Santhosh, Z. Li, S.P. Surwade, G.J. Shenoy, et al., Ultrafast Electron Transfer Kinetics of Graphene Grown by Chemical Vapor Deposition, *Angew. Chemie - Int. Ed.* 54 (2015) 15134–15137.

- [129] C.C. Chen, C.J. Kuo, C. Da Liao, C.F. Chang, C.A. Tseng, C.R. Liu, et al., Growth of Large-Area Graphene Single Crystals in Confined Reaction Space with Diffusion-Driven Chemical Vapor Deposition, *Chem. Mater.* 27 (2015) 6249–6258.
- [130] N.W. Nicholas, L.M. Connors, F. Ding, B.I. Yakobson, H.K. Schmidt, R.H. Hauge, Templatized growth of graphenic materials., *Nanotechnology*. 20 (2009) 245607–245613.
- [131] H. Ago, Y. Ito, N. Mizuta, K. Yoshida, B. Hu, C.M. Orofeo, et al., Epitaxial chemical vapor deposition growth of single-layer graphene over cobalt film crystallized on sapphire, *ACS Nano*. 4 (2010) 7407–7414.
- [132] H.C. Lee, W.-W. Liu, S.-P. Chai, A.R. Mohamed, C.W. Lai, C.-S. Khe, et al., Synthesis of Single-layer Graphene: A Review of Recent Development, *Procedia Chem.* 19 (2016) 916–921.
- [133] I. Pasternak, M. Wesolowski, I. Jozwik, M. Lukosius, G. Lupina, P. Dabrowski, et al., Graphene growth on Ge(100)/Si(100) substrates by CVD method, *Sci. Rep.* 6 (2016) 21773–21780.
- [134] M. Huang, Y. Zhang, C. Wang, J.-G. Ren, Q.-H. Wu, Q.-B. Li, Growth of graphene films on Cu catalyst in hydrogen plasma using polymethylmethacrylate as carbon source, *Catal. Today*. 256 (2015) 209–214.
- [135] Y.I. Zhang, L. Zhang, C. Zhou, Graphene and Related Applications, *Acc. Chem. Res.* 46 (2013) 2329–2339.
- [136] H. Shu, X.-M. Tao, F. Ding, What are the active carbon species during graphene chemical vapor deposition growth?, *Nanoscale*. 7 (2015) 1627–1634.

- [137] L. Banszerus, M. Schmitz, S. Engels, J. Dauber, M. Oellers, F. Haupt, et al., Ultrahigh-mobility graphene devices from chemical vapor deposition on reusable copper, *Sci. Adv.* 1 (2015) 1500222–1500228.
- [138] M. Lotya, Y. Hernandez, P.J. King, R.J. Smith, V. Nicolosi, L.S. Karlsson, et al., Liquid Phase Production of Graphene by Exfoliation of Graphite in Surfactant / Water Solutions, *J. Am. Chem. Soc.* 131 (2009) 3611–3620.
- [139] Y. Hernandez, V. Nicolosi, M. Lotya, F.M. Blighe, Z. Sun, S. De, et al., High-yield production of graphene by liquid-phase exfoliation of graphite., *Nat. Nanotechnol.* 3 (2008) 563–568.
- [140] P. May, U. Khan, J.M. Hughes, J.N. Coleman, Role of solubility parameters in understanding the steric stabilization of exfoliated two-dimensional nanosheets by adsorbed polymers, *J. Phys. Chem. C.* 116 (2012) 11393–11400.
- [141] J.M. Munuera, J.I. Paredes, S. Villar-Rodil, M. Ayán-Varela, A. Martínez-Alonso, J.M.D. Tascon, Electrolytic exfoliation of graphite in water with multifunctional electrolytes: en route towards high quality, oxide-free graphene flakes, *Nanoscale.* 8 (2016) 2982–2998.
- [142] A.B. Bourlinos, V. Georgakilas, R. Zboril, T.A. Sterioti, A.K. Stubos, Liquid-Phase Exfoliation of Graphite Towards Solubilized Graphenes, *Small.* 5 (2009) 1841–1845.
- [143] J. Wang, K.K. Manga, Q. Bao, K.P. Loh, High-Yield Synthesis of Few-Layer Graphene Flakes through Electrolyte, *J. Am. Chem. Soc.* 133 (2011) 8888–8891.

- [144] Y. Wang, X. Tong, X. Guo, Y. Wang, G. Jin, X. Guo, Large scale production of highly-qualified graphene by ultrasonic exfoliation of expanded graphite under the promotion of $(\text{NH}_4)_2\text{CO}_3$ decomposition., *Nanotechnology*. 24 (2013) 475602–475607.
- [145] M. Cao, N. Wang, L. Wang, Y. Zhang, Y. Chen, Z. Xie, et al., Direct exfoliation of graphite into graphene in aqueous solutions of amphiphilic peptides, *J. Mater. Chem. B*. 4 (2016) 152–161.
- [146] S. Haar, M. Bruna, J.X. Lian, F. Tomarchio, Y. Olivier, R. Mazzaro, et al., Liquid-Phase Exfoliation of Graphite into Single- and Few-Layer Graphene with α -Functionalized Alkanes, *J. Phys. Chem. Lett.* 7 (2016) 2714–2721.
- [147] A.M. Dimiev, G. Ceriotti, A. Metzger, N.D. Kim, J.M. Tour, Chemical Mass Production of Graphene Nanoplatelets in ~100% Yield, *ACS Nano*. 10 (2015) 274–279.
- [148] R.S. Park, S.; Ruoff, Chemical methods for the production of graphenes, *Nat. Nanotechnol.* 4 (2009) 217–224.
- [149] M.P. Lavin-Lopez, J.L. Valverde, L. Sanchez-Silva, A. Romero, Solvent-Based Exfoliation via Sonication of Graphitic Materials for Graphene Manufacture, *Ind. Eng. Chem. Res.* 55 (2016) 845–855.
- [150] S. Lin, L. Dong, J. Zhang, H. Lu, Room-Temperature Intercalation and ~1000-Fold Chemical Expansion for Scalable Preparation of High-Quality Graphene, *Chem. Mater.* 28 (2016) 2138–2146.
- [151] R. Narayan, S.O. Kim, Surfactant mediated liquid phase exfoliation of graphene, *Nano Converg.* 2 (2015) 20–39.

- [152] A.A. Green, M.C. Hersam, Solution phase production of graphene with controlled thickness via density differentiation, *Nano Lett.* 9 (2009) 4031–4036.
- [153] B. Puangbuppha, P. Limsuwan, P. Asanithi, Non-chemically functionalized graphene exfoliated from graphite in water using ultrasonic treatment, *Procedia Eng.* 32 (2012) 1094–1099.
- [154] J.T. Han, J.I. Jang, H. Kim, J.Y. Hwang, H.K. Yoo, J.S. Woo, et al., Extremely efficient liquid exfoliation and dispersion of layered materials by unusual acoustic cavitation, *Sci Rep.* 4 (2014) 5133–5140.
- [155] C.E. Hamilton, J.R. Lomeda, Z. Sun, J.M. Tour, A.R. Barron, High-yield organic dispersions of unfunctionalized graphene, *Nano Lett.* 9 (2009) 3460–3462.
- [156] H. Feng, R. Cheng, X. Zhao, X. Duan, J. Li, A low-temperature method to produce highly reduced graphene oxide., *Nat. Commun.* 4 (2013) 1539–1546.
- [157] S. You, S.M. Luzan, T. Szabó, A. V. Talyzin, Effect of synthesis method on solvation and exfoliation of graphite oxide, *Carbon N. Y.* 52 (2013) 171–180.
- [158] S. Pei, H.M. Cheng, The reduction of graphene oxide, *Carbon N. Y.* 50 (2012) 3210–3228.
- [159] S. Park, J. An, J.R. Potts, A. Velamakanni, S. Murali, R.S. Ruoff, Hydrazine-reduction of graphite- and graphene oxide, *Carbon N. Y.* 49 (2011) 3019–3023.

- [160] S. Some, Y. Kim, Y. Yoon, H. Yoo, S. Lee, Y. Park, et al., High-quality reduced graphene oxide by a dual-function chemical reduction and healing process., *Sci. Rep.* 3 (2013) 1929–1934.
- [161] G.K. Ramesha, N.S. Sampath, Electrochemical reduction of oriented Graphene oxide films: An *in situ* Raman spectroelectrochemical study, *J. Phys. Chem. C.* 113 (2009) 7985–7989.
- [162] X. Mao, F. Guo, E.H. Yan, G.C. Rutledge, T.A. Hatton, Remarkably High Heterogeneous Electron Transfer Activity of Carbon-Nanotube-Supported Reduced Graphene Oxide, *Chem. Mater.* 28 (2016) 7422–7432.
- [163] S.J. An, Y. Zhu, S.H. Lee, M.D. Stoller, T. Emilsson, S. Park, et al., Thin film fabrication and simultaneous anodic reduction of deposited graphene oxide platelets by electrophoretic deposition, *J. Phys. Chem. Lett.* 1 (2010) 1259–1263.
- [164] W.S. Hummers, R.E. Offeman, Preparation of Graphitic Oxide, *J. Am. Chem. Soc.* 80 (1958) 1339–1339.
- [165] D.C. Marcano, D. V Kosynkin, J.M. Berlin, A. Sinitskii, Z. Sun, A. Slesarev, et al., Improved synthesis of graphene oxide., *ACS Nano.* 4 (2010) 4806–4814.
- [166] T. Kuila, A.K. Mishra, P. Khanra, N.H. Kim, J.H. Lee, Recent advances in the efficient reduction of graphene oxide and its application as energy storage electrode materials., *Nanoscale.* 5 (2013) 52–71.
- [167] B.C. Brodie, On the Atomic Weight of Graphite, *Philos. Trans. R. Soc. London.* 149 (1859) 249–259.

- [168] H.L. Poh, F. Šaněk, A. Ambrosi, G. Zhao, Z. Sofer, M. Pumera, Graphenes prepared by Staudenmaier, Hofmann and Hummers methods with consequent thermal exfoliation exhibit very different electrochemical properties, *Nanoscale*. 4 (2012) 3515–3522.
- [169] C. Hontoria-Lucas, A.J. López-Peinado, J. de D. López-González, M.L. Rojas-Cervantes, R.M. Martín-Aranda, Study of oxygen-containing groups in a series of graphite oxides: Physical and chemical characterization, *Carbon*. 33 (1995) 1585–1592.
- [170] J. Chen, B. Yao, C. Li, G. Shi, An improved Hummers method for eco-friendly synthesis of graphene oxide, *Carbon*. 64 (2013) 225–229.
- [171] H. Yaren, H. Mollaoglu, B. Kurt, A. Korkmaz, S. Oter, T. Topal, et al., Lung toxicity of nitrogen mustard may be mediated by nitric oxide and peroxynitrite in rats, *Res. Vet. Sci.* 83 (2007) 116–122.
- [172] C. Fu, G. Zhao, H. Zhang, S. Li, Evaluation and Characterization of Reduced Graphene Oxide Nanosheets as Anode Materials for Lithium-Ion Batteries, *Int. J. Electrochem. Sci.* 8 (2013) 6269–6280.
- [173] B.M. Ganesh, A.M. Isloor, A.F. Ismail, Enhanced hydrophilicity and salt rejection study of graphene oxide-polysulfone mixed matrix membrane, *Desalination*. 313 (2013) 199–207.
- [174] S.N. Alam, N. Sharma, L. Kumar, Synthesis of Graphene Oxide (GO) by Modified Hummers Method and Its Thermal Reduction to Obtain Reduced Graphene Oxide (rGO)*, *Graphene*. 6 (2017) 1–18.

- [175] J. Zhang, H. Yang, G. Shen, P. Cheng, J. Zhang, S. Guo, Reduction of graphene oxide via L-ascorbic acid., *Chem. Commun.* 46 (2010) 1112–1114.
- [176] S. Stankovich, D. a. Dikin, R.D. Piner, K. a. Kohlhaas, A. Kleinhammes, Y. Jia, et al., Synthesis of graphene-based nanosheets via chemical reduction of exfoliated graphite oxide, *Carbon*. 45 (2007) 1558–1565.
- [177] A.K. Das, M. Srivastav, R.K. Layek, M.E. Uddin, D. Jung, N.H. Kim, et al., Iodide-mediated room temperature reduction of graphene oxide: a rapid chemical route for the synthesis of a bifunctional electrocatalyst, *J. Mater. Chem. A*. 2 (2014) 1332–1340.
- [178] H.J. Shin, K.K. Kim, A. Benayad, S.M. Yoon, H.K. Park, I.S. Jung, et al., Efficient reduction of graphite oxide by sodium borohydride and its effect on electrical conductance, *Adv. Funct. Mater.* 19 (2009) 1987–1992.
- [179] G. Wang, J. Yang, J. Park, X. Gou, B. Wang, H. Liu, et al., Facile synthesis and characterization of graphene nanosheets, *J. Phys. Chem. B*. 112 (2008) 8192–8195.
- [180] X. Fan, W. Peng, Y. Li, X. Li, S. Wang, G. Zhang, et al., Deoxygenation of Exfoliated Graphite Oxide under Alkaline Conditions: A Green Route to Graphene Preparation, *Adv. Mater.* 20 (2008) 4490–4493.
- [181] Y. Wang, Z.X. Shi, J. Yin, Facile synthesis of soluble graphene via a green reduction of graphene oxide in tea solution and its biocomposites, *ACS Appl. Mater. Interfaces*. 3 (2011) 1127–1133.

- [182] C.Y. Su, Y. Xu, W. Zhang, J. Zhao, A. Liu, X. Tang, et al., Highly efficient restoration of graphitic structure in graphene oxide using alcohol vapors, *ACS Nano.* 4 (2010) 5285–5292.
- [183] M. Mohandoss, S. Sen Gupta, A. Nelleri, T. Pradeep, S.M. Maliyekkal, Solar mediated reduction of graphene oxide, *RSC Adv.* 7 (2017) 957–963.
- [184] Y. Zhu, M.D. Stoller, W. Cai, A. Velamakanni, R.D. Piner, D. Chen, et al., Exfoliation of graphite oxide in propylene carbonate and thermal reduction of the resulting graphene oxide platelets, *ACS Nano.* 4 (2010) 1227–1233.
- [185] X. Li, H. Wang, J.T. Robinson, H. Sanchez, G. Diankov, H. Dai, Simultaneous Nitrogen Doping and Reduction of Graphene Oxide, *J. Am. Chem. Soc.* 131 (2009) 15939–15944.
- [186] X. Wang, L. Zhi, K. Müllen, Transparent, conductive graphene electrodes for dye-sensitized solar cells, *Nano Lett.* 8 (2008) 323–327.
- [187] B. Zhao, P. Liu, Y. Jiang, D. Pan, H. Tao, J. Song, et al., Supercapacitor performances of thermally reduced graphene oxide, *J. Power Sources.* 198 (2012) 423–427.
- [188] L. Sun, Z. Yi, J. Lin, F. Liang, Y. Wu, Z. Cao, et al., Fast and Energy Efficient Synthesis of ZnO@RGO and its Application in Ni-Zn Secondary Battery, *J. Phys. Chem. C.* 120 (2016) 12337–12343.
- [189] C.T.J. Low, F.C. Walsh, M.H. Chakrabarti, M.A. Hashim, M.A. Hussain, Electrochemical approaches to the production of graphene flakes and their potential applications, *Carbon.* 54 (2013) 1 –2 1.

- [190] K. Parvez, Z.-S. Wu, R. Li, X. Liu, R. Graf, X. Feng, et al., Exfoliation of graphite into graphene in aqueous solutions of inorganic salts., *J. Am. Chem. Soc.* 136 (2014) 6083–6091.
- [191] K. Parvez, R. Li, S.R. Puniredd, Y. Hernandez, F. Hinkel, S. Wang, et al., Electrochemically exfoliated graphene as solution-processable, highly conductive electrodes for organic electronics., *ACS Nano.* 7 (2013) 3598–3606.
- [192] S. Yang, S. Brüller, Z.-S. Wu, Z. Liu, K. Parvez, R. Dong, et al., Organic Radical-Assisted Electrochemical Exfoliation for the Scalable Production of High-Quality Graphene, *J. Am. Chem. Soc.* 137 (2015) 13927–13932.
- [193] Z.Y. Xia, S. Pezzini, E. Treossi, G. Giambastiani, F. Corticelli, V. Morandi, et al., The exfoliation of graphene in liquids by electrochemical, chemical, and sonication-assisted techniques: A nanoscale study, *Adv. Funct. Mater.* 23 (2013) 4684–4693.
- [194] T. Electrochemical, The Electrochemical Graphite Intercalation Formation of Compound in r-Butyrolactone Yoshiyuki Takada and Rokuro Fujii In the case of the electrochemical preparation of the intercalation compound , one of the advan- tages is that the reaction process can b, *Tanso.* 1985 (1985) 110–113.
- [195] H. Takenaka, M. Kawaguchi, M. Lerner, N. Bartlett, Synthesis and characterization of graphite fluorides by electrochemical fluorination in aqueous and anhydrous hydrogen fluoride, *J. Chem. Soc. Chem. Commun.* (1987) 1431–1432.

- [196] M. Inagaki, N. Iwashita, Z.D. Wang, Y. Maeda, Electrochemical synthesis of graphite intercalation compounds with nickel and hydroxides, *Synth. Met.* 26 (1988) 41–47.
- [197] Electrochemical production of graphite salts using a three-dimensional electrode of graphite particles, *Electrochim. Acta* 27 (1982) 1247–1252.
- [198] P. Yu, S.E. Lowe, G.P. Simon, Y.L. Zhong, Electrochemical exfoliation of graphite and production of functional graphene, *Curr. Opin. Colloid Interface Sci.* 20 (2015) 329–338.
- [199] J. Liu, H. Yang, S.G. Zhen, C.K. Poh, A. Chaurasia, J. Luo, et al., RSC Advances A green approach to the synthesis of high-quality graphene oxide flakes via electrochemical exfoliation of pencil core, *RSC Adv.* 3 (2013) 11745–11750.
- [200] C.-Y. Su, A.-Y. Lu, Y. Xu, F.-R. Chen, A.N. Khlobystov, L.-J. Li, High-quality thin graphene films from fast electrochemical exfoliation., *ACS Nano.* 5 (2011) 2332–2339.
- [201] N. Liu, F. Luo, H. Wu, Y. Liu, C. Zhang, J. Chen, One-Step Ionic-Liquid-Assisted Electrochemical Synthesis of Ionic-Liquid-Functionalized Graphene Sheets Directly from Graphite, *Adv. Funct. Mater.* 18 (2008) 1518–1525.
- [202] Z. Xia, F. Leonardi, M. Gobbi, Y. Liu, V. Bellani, A. Liscio, et al., Electrochemical Functionalization of Graphene at the Nanoscale with Self-Assembling Diazonium Salts, *ACS Nano.* 10 (2016) 7125–7134.

- [203] <https://cambridgenanosystems.com/> (accessed November 10, 2017).
- [204] B. Gurzeda, T. Buchwald, M. Nocuń, A. Bąkowicz, P. Krawczyk, Graphene material preparation through thermal treatment of graphite oxide electrochemically synthesized in aqueous sulfuric acid, *RSC Adv.* 7 (2017) 19904–19911.
- [205] K.S. Sivudu, Y. Mahajan, Mass production of high quality graphene: (2012). <https://www.nanowerk.com/spotlight/spotid=25744.php> (accessed November 10, 2017).
- [206] X. Ji, Y. Xu, W. Zhang, L. Cui, J. Liu, Review of functionalization, structure and properties of graphene/polymer composite fibers, *Compos. Part A Appl. Sci. Manuf.* 87 (2016) 29–45.
- [207] M. Garcia-hernandez, J. Coleman, Materials science of graphene : a flagship perspective, *2D Mater.* 3 (2016) 010401–010414.
- [208] C.A. Hunter, K.R. Lawson, J. Perkins, C.J. Urch, Aromatic interactions, *J. Chem. Soc.* 2 (2001) 651–669.
- [209] K.E. Riley, M. Pitonak, P. Jurecka, P. Hobza, Stabilization and structure calculations for noncovalent interactions in extended molecular systems based on wave function and density functional theories, *Chem. Rev.* 110 (2010) 5023–5063.
- [210] S. Bose, T. Kuila, A.K. Mishra, N.H. Kim, J.H. Lee, Preparation of non-covalently functionalized graphene using 9-anthracene carboxylic acid., *Nanotechnology*. 22 (2011) 405603–405610.

- [211] M. Dubeck, L. Mitas, P. Jurecka, Noncovalent Interactions by Quantum Monte Carlo, *Chem. Rev.* 116 (2016) 5188–5215.
- [212] Y. Xu, H. Bai, G. Lu, C. Li, G. Shi, Flexible graphene films via the filtration of water-soluble noncovalent functionalized graphene sheets, *J. Am. Chem. Soc.* 130 (2008) 5856–5857.
- [213] Y. Xu, B. Hua, G. Lu, Flexible Graphene Films via the Filtration of Water-Soluble Noncovalent Functionalized Graphene Sheets, *J. Am. Chem. Soc.* 130 (2008) 5856–5857.
- [214] H. Bai, Y. Xu, L. Zhao, C. Li, G. Shi, Non-covalent functionalization of graphene sheets by sulfonated polyaniline., *Chem. Commun.* 4 (2009) 1667–1669.
- [215] A. Benvidi, A. Dehghani-Firouzabadi, M. Mazloum-Ardakani, B.-B.F. Mirjalili, R. Zare, Electrochemical deposition of gold nanoparticles on reduced graphene oxide modified glassy carbon electrode for simultaneous determination of levodopa, uric acid and folic acid, *J. Electroanal. Chem.* 736 (2015) 22–29.
- [216] S.J. Li, J.M. Du, J. Chen, N.N. Mao, M.J. Zhang, H. Pang, Electrodeposition of cobalt oxide nanoparticles on reduced graphene oxide: A two-dimensional hybrid for enzyme-free glucose sensing, *J. Solid State Electrochem.* 18 (2014) 1049–1056.
- [217] M. Govindhan, A. Chen, Simultaneous synthesis of gold nanoparticle/graphene nanocomposite for enhanced oxygen reduction reaction, *J. Power Sources.* 274 (2015) 928–936.

- [218] D. Wu, F. Zhang, H. Liang, X. Feng, Nanocomposites and macroscopic materials: assembly of chemically modified graphene sheets, *Chem. Soc. Rev.* 41 (2012) 6160–6177.
- [219] M.A. Raj, S.A. John, Assembly of gold nanoparticles on graphene film via electroless deposition: spontaneous reduction of Au³⁺ ions by graphene film, *RSC Adv.* 5 (2015) 4964–4971.
- [220] T.M. Paronyan, A.K. Thapa, A. Sherehiy, J.B. Jasinski, J.S.D. Jangam, A. Hérold, et al., Incommensurate Graphene Foam as a High Capacity Lithium Intercalation Anode, *Sci. Rep.* 7 (2017) 39944–39955.
- [221] M.S. El-Deab, T. Okajima, T. Ohsaka, Electrochemical Reduction of Oxygen on Gold Nanoparticle-Electrodeposited Glassy Carbon Electrodes, *J. Electrochem. Soc.* 150 (2003) A851–A857.
- [222] Z. Yu, Electrodeposition of Gold Nanoparticles on Electrochemically Reduced Graphene Oxide for High Performance Supercapacitor Electrode Materials, *Int. J. Electrochem. Sci.* 11 (2016) 3643–3650.
- [223] P.T. Yin, S. Shah, M. Chhowalla, K.-B. Lee, Design, Synthesis, and Characterization of Graphene–Nanoparticle Hybrid Materials for Bioapplications, *Chem. Rev.* 115 (2015) 2483–2531.
- [224] V. Georgakilas, M. Otyepka, A.B. Bourlinos, V. Chandra, N. Kim, K.C. Kemp, et al., Functionalization of graphene: covalent and non-covalent approaches, derivatives and applications., *Chem. Rev.* 112 (2012) 6156–6214.

- [225] S. Yang, X. Feng, S. Ivanovici, K. M??llen, Fabrication of graphene-encapsulated oxide nanoparticles: Towards high-performance anode materials for lithium storage, *Angew. Chemie - Int. Ed.* 49 (2010) 8408–8411.
- [226] J.R. Lomeda, C.D. Doyle, D. V Kosynkin, W.-F. Hwang, J.M. Tour, Diazonium functionalization of surfactant-wrapped chemically converted graphene sheets., *J. Am. Chem. Soc.* 130 (2008) 16201–16206.
- [227] Y. Li, L. Galmiche, P. Audebert, F. Miomandre, G. Louarn, M. Bozlar, et al., Functionalization of Graphene Oxide by Tetrazine Derivatives: A Versatile Approach toward Covalent Bridges between Graphene, *Chem. Mater.* 27 (2015) 4298–4310.
- [228] V. V. Shunaev, O.E. Glukhova, Topology Influence on the Process of Graphene Functionalization by Epoxy and Hydroxyl Groups, *J. Phys. Chem. C.* 120 (2016) 4145–4149.
- [229] C.K. Chua, M. Pumera, The reduction of graphene oxide with hydrazine: elucidating its reductive capability based on a reaction-model approach, *Chem. Commun.* 52 (2016) 72–75.
- [230] T. Breton, D. Bélanger, Modification of carbon electrode with aryl groups having an aliphatic amine by electrochemical reduction of in situ generated diazonium cations., *Langmuir*. 24 (2008) 8711–8718.
- [231] D.B. Ossonon, M. Weissmann, D. Bélanger, Electrochemical modification of carbon electrode with benzylphosphonic groups, *Electrochim. Acta*. 122 (2014) 210–217.

- [232] D. Bélanger, J. Pinson, Electrografting: a powerful method for surface modification., *Chem. Soc. Rev.* 40 (2011) 3995–4048.
- [233] B. Desalegn, T. Brousse, D. Be, Advances on the use of diazonium chemistry for functionalization of materials used in energy storage systems, *Carbon.* 92 (2015) 362–381.
- [234] A. Sinitskii, A. Dimiev, D.A. Corley, A.A. Fursina, D. V. Kosynkin, J.M. Tour, Kinetics of diazonium functionalization of chemically converted graphene nanoribbons, *ACS Nano.* 4 (2010) 1949–1954.
- [235] G.L.C. Paulus, Q.H. Wang, M.S. Strano, Covalent electron transfer chemistry of graphene with diazonium salts, *Acc. Chem. Res.* 46 (2013) 160–170.
- [236] Z. Jin, J.R. Lomeda, B.K. Price, W. Lu, Y. Zhu, J.M. Tour, Mechanically assisted exfoliation and functionalization of thermally converted graphene sheets, *Chem. Mater.* 21 (2009) 3045–3047.
- [237] J. Greenwood, T.H. Phan, Y. Fujita, Z. Li, O. Ivasenko, H. Uji-i, et al., Covalent Modification of Graphene and Graphite Using Diazonium Chemistry : Tunable Grafting and, *ACS Nano.* 9 (2015) 5520–5535.
- [238] F. Lipp-bregolin, P. Jussieu, F.- Paris, Evidence for Charge Transfer at the Interface between Hybrid Phosphomolybdate and Epitaxial Graphene, *Langmuir.* 32 (2016) 774–4783.
- [239] A.C. Ferrari, D.M. Basko, Raman spectroscopy as a versatile tool for studying the properties of graphene., *Nat. Nanotechnol.* 8 (2013) 235–246.

- [240] S. Niyogi, E. Bekyarova, M.E. Itkis, H. Zhang, J. Hicks, M. Sprinkle, et al., Spectroscopy of Covalently Functionalized Graphene, *Nano Lett.* 10 (2010) 4061–4066.
- [241] Q.H. Wang, Z. Jin, K.K. Kim, A.J. Hilmer, G.L.C. Paulus, C.-J. Shih, et al., Understanding and controlling the substrate effect on graphene electron-transfer chemistry via reactivity imprint lithography., *Nat. Chem.* 4 (2012) 724–732.
- [242] R. Sharma, N. Nair, M. Strano, Structure– Reactivity Relationships for Graphene Nanoribbons, *J. Phys. Chem.* 113 (2009) 14771–14777.
- [243] R. Sharma, J.H. Baik, C.J. Perera, M.S. Strano, Anomalously large reactivity of single graphene layers and edges toward electron transfer chemistries, *Nano Lett.* 10 (2010) 398–405.
- [244] J. Paier, M. Marsman, K. Hummer, G. Kresse, I.C. Gerber, J.G. Angyán, Screened hybrid density functionals applied to solids, *J. Chem. Phys.* 124 (2006) 154709–154722.
- [245] N. Nair, W.J. Kim, M.L. Usrey, M.S. Strano, A structure-reactivity relationship for single walled carbon nanotubes reacting with 4-hydroxybenzene diazonium salt, *J. Am. Chem. Soc.* 129 (2007) 3946–3954.
- [246] A. Cohen, Y. Yang, Q.L. Yan, A. Shlomovich, N. Petrutik, L. Burstein, et al., Highly Thermostable and Insensitive Energetic Hybrid Coordination Polymers Based on Graphene Oxide-Cu(II) Complex, *Chem. Mater.* 28 (2016) 6118–6126.

- [247] A.K. Farquhar, C.M. Fitchett, H.M. Dykstra, M.R. Waterland, P.A. Brooksby, A.J. Downard, Diels – Alder Reaction of Anthranilic Acids: A Versatile Route to Dense Monolayers on Flat Edge and Basal Plane Graphitic Carbon Substrates, *ACS Appl. Mater. Interfaces.* 8 (2016) 23389–23395.
- [248] J. Li, M. Li, L. Zhou, S. Lang, H. Lu, D. Wang, et al., Click and Patterned Functionalization of Graphene by Diels – Alder Reaction, *J. Am. Chem. Soc.* 138 (2016) 7448–7451.
- [249] X. Zhou, Y. Li, G. Ma, Q. Ma, Z. Lei, One-step solid-state synthesis of sulfur-reduced graphene oxide composite for lithium-sulfur batteries, *J. Alloys Compd.* 685 (2016) 216–221.
- [250] Q. Li, Y. Chen, J. He, F. Fu, J. Lin, W. Zhang, Three-dimensional VS₄/graphene hierarchical architecture as high-capacity anode for lithium-ion batteries, *J. Alloys Compd.* 685 (2016) 294–299.
- [251] A. Ambrosi, C.K. Chua, B. Khezri, Z. Sofer, R.D. Webster, M. Pumera, Chemically reduced graphene contains inherent metallic impurities present in parent natural and synthetic graphite, *Proc. Natl. Acad. Sci.* 109 (2012) 12899–12904.
- [252] S. Pei, J. Zhao, J. Du, W. Ren, H.M. Cheng, Direct reduction of graphene oxide films into highly conductive and flexible graphene films by hydrohalic acids, *Carbon.* 48 (2010) 4466–4474.
- [253] J. Park, S.B. Jo, Y.J. Yu, Y. Kim, J.W. Yang, W.H. Lee, et al., Single-gate bandgap opening of bilayer graphene by dual molecular doping, *Adv. Mater.* 24 (2012) 407–411.

- [254] S. Umrao, S. Abraham, F. Theil, S. Pandey, V. Ciobota, P.K. Shukla, et al., A possible mechanism for the emergence of an additional band gap due to a Ti–O–C bond in the TiO_2 –graphene hybrid system for enhanced photodegradation of methylene blue under visible light, *RSC Adv.* 4 (2014) 59890–59901.
- [255] L. Song, L. Ci, H. Lu, P.B. Sorokin, C. Jin, J. Ni, et al., Large scale growth and characterization of atomic hexagonal boron nitride layers, *Nano Lett.* 10 (2010) 3209–3215.
- [256] M. Saranya, R. Ramachandran, P. Kollu, S.K. Jeong, A.N. Grace, A template-free facile approach for the synthesis of CuS–rGO nanocomposites towards enhanced photocatalytic reduction of organic contaminants and textile effluents, *RSC Adv.* 5 (2015) 15831–15840.
- [257] Y.N. Singhbabu, K.K. Sahu, D. Dadhich, a K. Pramanick, T. Mishra, R.K. Sahu, Capsule-embedded reduced graphene oxide: synthesis, mechanism and electrical properties, *J. Mater. Chem. C.* 1 (2013) 958–966.
- [258] X. Li, H. Zhu, J. Wei, K. Wang, E. Xu, Z. Li, et al., Determination of band gaps of self-assembled carbon nanotube films using Tauc/Davis-Mott model, *Appl. Phys. A Mater. Sci. Process.* 97 (2009) 341–344.
- [259] J. Landers, G.Y. Gor, A. V. Neimark, Density functional theory methods for characterization of porous materials, *Colloids Surfaces A Physicochem. Eng. Asp.* 437 (2013) 3–32.
- [260] D.S. Yu, T. Kuila, N.H. Kim, P. Khanra, J.H. Lee, Effects of covalent surface modifications on the electrical and electrochemical properties of graphene using sodium 4-aminoazobenzene-4- sulfonate, *Carbon.* 54 (2013) 310–322.

- [261] G. Wang, B. Wang, J. Park, Y. Wang, B. Sun, J. Yao, Highly efficient and large-scale synthesis of graphene by electrolytic exfoliation, *Carbon.* 47 (2009) 3242–3246.
- [262] Y. Wang, X. Tong, X. Guo, Y. Wang, G. Jin, X. Guo, Large scale production of highly-qualified graphene by ultrasonic exfoliation of expanded graphite under the promotion of (NH₄)₂CO₃ decomposition, *Nanotechnology.* 24 (2013) 1–5.
- [263] S. Umrao, S. Abraham, F. Theil, S. Pandey, V. Ciobota, P.K. Shukla, et al., A possible mechanism for the emergence of an additional band gap due to a Ti–O–C bond in the TiO₂ –graphene hybrid system for enhanced photodegradation of methylene blue under visible light, *RSC Adv.* 4 (2014) 59890–59901.
- [264] A. Mathkar, D. Tozier, P. Cox, P. Ong, C. Galande, K. Balakrishnan, et al., Controlled, stepwise reduction and band gap manipulation of graphene oxide, *J. Phys. Chem. Lett.* 3 (2012) 986–991.
- [265] J.M. Englert, C. Dotzer, G. Yang, M. Schmid, C. Papp, J.M. Gottfried, et al., Covalent bulk functionalization of graphene, *Nat. Chem.* 3 (2011) 279–286.
- [266] K.T. Shruthi, M.S. Kumar, A. Pratap, N. Chandrasekaran, Graphene oxide aided structural tailoring of 3D N-doped amorphous carbon network for enhanced energy storage, *RSC Adv.* 5 (2015) 93423–93432.
- [267] Y. Gao, D. Ma, C. Wang, J. Guan, X. Bao, Reduced graphene oxide as a catalyst for hydrogenation of nitrobenzene at room temperature, *Chem. Commun.* 47 (2011) 2432–2434.

- [268] S. Brunauer, L.S. Deming, W.E. Deming, E. Teller, On a theory of the van der Waals adsorption of gases, *J. Am. Chem. Soc.* 62 (1940) 1723–1732.
- [269] A. Gambou-Bosca, D. Belanger, Chemical Mapping and Electrochemical Performance of Manganese Dioxide/Activated Carbon Based Composite Electrode for Asymmetric Electrochemical Capacitor, *J. Electrochem. Soc.* 162 (2015) A5115–A5123.
- [270] K.S.W. Sing, R.T. Williams, Physisorption hysteresis loops and the characterization of nanoporous materials, *Adsorpt. Sci. Technol.* 22 (2004) 773–782.
- [271] T. Ohkubo, J. Miyawaki, K. Kaneko, R. Ryoo, N.A. Seaton, Adsorption properties of templated mesoporous carbon (CMK-1) for nitrogen and supercritical methane - Experiment and GCMC simulation, *J. Phys. Chem. B.* 106 (2002) 6523–6528.
- [272] R.F. Bruinsma, P.G. De Gennes, J.B. Freund, D. Levine, A route to high surface area, porosity and inclusion of large molecules in crystals Hee, *Nature.* 427 (2004) 523–527.
- [273] D.R. Dreyer, S. Park, C.W. Bielawski, R.S. Ruoff, The chemistry of graphene oxide, *Chem. Soc. Rev.* 39 (2010) 228–240.
- [274] C. Moreno-Castilla, M.A. Ferro-Garcia, J.P. Joly, I. Bautista-Toledo, F. Carrasco-Marín, J. Rivera-Utrilla, Activated carbon surface modifications by nitric acid, hydrogen peroxide, and ammonium peroxydisulfate treatments, *Langmuir.* 11 (1995) 4386–4392.

- [275] A. Le Comte, D. Chhin, A. Gagnon, R. Retoux, T. Brousse, D. Bélanger, Spontaneous grafting of 9,10-phenanthrenequinone on porous carbon as active electrode material in electrochemical capacitor in alkaline electrolyte, *J. Mater. Chem. A.* 3 (2015) 6146–6156.
- [276] H. Li, Y. Wang, Y. Shi, J. Li, L.H. Yanga, H. Ying, Large scale synthesized sulphonated reduced graphene oxide: a high performance material for electrochemical capacitor, *RSC Adv.* 35 (2013) 14839–15492.
- [277] D.D. Jiang, Q. Yao, M.A. McKinney, C.A. Wilkie, TGA/FTIR studies on the thermal degradation of some polymeric sulfonic and phosphonic acids and their sodium salts, *Polym. Degrad. Stab.* 63 (1999) 423–434.
- [278] J. Lu, Y. Li, S. Li, S.P. Jiang, Self-assembled platinum nanoparticles on sulfonic acid-grafted graphene as effective electrocatalysts for methanol oxidation in direct methanol fuel cells, *Sci. Rep.* 6 (2016) 21530–21542.
- [279] D.H. Johnston, D.F. Shriver, Vibrational Study of the Trifluoromethanesulfonate Anion: Unambiguous Assignment of the Asymmetric Stretching Modes, *Inorg. Chem.* 32 (1993) 1045–1047.
- [280] A.C. Ferrari, J. Robertson, Interpretation of Raman spectra of disordered and amorphous carbon, *Phys. Rev. B.* 61 (2000) 14095–14107.
- [281] A.C. Ferrari, J.C. Meyer, V. Scardaci, C. Casiraghi, M. Lazzeri, F. Mauri, et al., Raman Spectrum of Graphene and Graphene Layers, *Phys. Rev. Lett.* 97 (2006) 187401–187405.

- [282] W. Gao, M. Majumder, L.B. Alemany, T.N. Narayanan, M.A. Ibarra, B.K. Pradhan, et al., Engineered graphite oxide materials for application in water purification., *ACS Appl. Mater. Interfaces.* 3 (2011) 1821–1826.
- [283] M.A. Pimenta, G. Dresselhaus, M.S. Dresselhaus, L.G. Cançado, A. Jorio, R. Saito, Studying disorder in graphite-based systems by Raman spectroscopy., *Phys. Chem. Chem. Phys.* 9 (2007) 1276–1291.
- [284] W. Chen, L. Yan, Preparation of graphene by a low-temperature thermal reduction at atmosphere pressure., *Nanoscale.* 2 (2010) 559–563.
- [285] Y. Wang, D.C. Alsmeyer, R.L. McCreery, *of Observed Spectra, Carbon N. Y.* 2 (1990) 557–563.
- [286] K.N. Kudin, B. Ozbas, H.C. Schniepp, R.K. Prud'homme, I.A. Aksay, R. Car, Raman spectra of graphite oxide and functionalized graphene sheets., *Nano Lett.* 8 (2008) 36–41.
- [287] G. Wei, M. Yan, R. Dong, D. Wang, X. Zhou, J. Chen, et al., Covalent modification of reduced graphene oxide by means of diazonium chemistry and use as a drug-delivery system., *Chem. Eur. J.* 18 (2012) 14708–14716.
- [288] H. Lim, J.S. Lee, H.J. Shin, H.S. Shin, H.C. Choi, Spatially resolved spontaneous reactivity of diazonium salt on edge and basal plane of graphene without surfactant and its doping effect, *Langmuir.* 26 (2010) 12278–12284.
- [289] M.S. Dresselhaus, A. Jorio, M. Hofmann, G. Dresselhaus, R. Saito, Perspectives on carbon nanotubes and graphene Raman spectroscopy, *Nano Lett.* 10 (2010) 751–758.

- [290] A. Ganguly, S. Sharma, P. Papakonstantinou, J. Hamilton, Probing the Thermal Deoxygenation of Graphene Oxide using High Resolution In Situ X-Ray based Spectroscopies, *J. Phys. Chem.* 115 (2011) 17009–17019.
- [291] Z. Jin, T.P. McNicholas, C.J. Shih, Q.H. Wang, G.L.C. Paulus, A.J. Hilmer, et al., Click chemistry on solution-dispersed graphene and monolayer CVD graphene, *Chem. Mater.* 23 (2011) 3362–3370.
- [292] C. Singh, A.K. Mishra, A. Paul, Highly conducting reduced graphene synthesis via low temperature chemically assisted exfoliation and energy storage application, *J. Mater. Chem. A.* 3 (2015) 18557–18563.
- [293] J. Wang, T. Zhou, H. Deng, F. Chen, K. Wang, Q. Zhang, et al., An environmentally friendly and fast approach to prepare reduced graphite oxide with water and organic solvents solubility., *Colloids Surf. B. Biointerfaces.* 101 (2013) 171–176.
- [294] J. Guan, X. Chen, T. Wei, F. Liu, S. Wang, Q. Yang, et al., Directly bonded hybrid of graphene nanoplatelets and fullerene: facile solid-state mechanochemical synthesis and application as carbon-based electrocatalyst for oxygen reduction reaction, *J. Mater. Chem. A.* 3 (2015) 4139–4146.
- [295] G. Gao, D. Liu, S. Tang, C. Huang, M. He, Y. Guo, et al., Heat-Initiated Chemical Functionalization of Graphene, *Sci. Rep.* 6 (2016) 1–8.
- [296] S. Baranton, D. Bélanger, Electrochemical derivatization of carbon surface by reduction of in situ generated diazonium cations., *J Phys. Chem. B.* 109 (2005) 24406–24410.

- [297] E. Lebègue, T. Brousse, J. Gaubicher, C. Cougnon, Spontaneous arylation of activated carbon from aminobenzene organic acids as source of diazonium ions in mild conditions, *Electrochim. Acta.* 88 (2013) 680–687.
- [298] F. Hauquier, N. Debou, S. Palacin, B. Jousselme, Amino functionalized thin films prepared from Gabriel synthesis applied on electrografted diazonium salts, *J. Electroanal. Chem.* 677–680 (2012) 127–132.
- [299] J. Lyskawa, A. Grondein, D. Bélanger, Chemical modifications of carbon powders with aminophenyl and cyanophenyl groups and a study of their reactivity, *Carbon.* 48 (2010) 1271–1278.
- [300] M. Toupin, D. Bélangeer, Thermal Stability Study of Aryl Modified Carbon Black by in Situ Generated Diazonium Salt, *J. Phys. Chem. C.* 111 (2007) 5394–5401.
- [301] L. Madec, K.A. Seid, J.-C. Badot, B. Humbert, P. Moreau, O. Dubrunfaut, et al., Redirected charge transport arising from diazonium grafting of carbon coated LiFePO₄, *Phys. Chem. Chem. Phys.* 16 (2014) 22745–22753.
- [302] C. Saby, B. Ortiz, G.Y. Champagne, D. Bélanger, Electrochemical Modification of Glassy Carbon Electrode Using Aromatic Diazonium Salts . 1 . Blocking Effect of 4-Nitrophenyl and 4-Carboxyphenyl Groups, *Langmuir.* 7463 (1997) 6805–6813.
- [303] T.S. Sreeprasad, S.M. Maliyekkal, K.P. Lisha, T. Pradeep, Reduced graphene oxide-metal/metal oxide composites: facile synthesis and application in water purification., *J. Hazard. Mater.* 186 (2011) 921–931.

- [304] S. Park, K.-S. Lee, G. Bozoklu, W. Cai, S.T. Nguyen, R.S. Ruoff, Graphene oxide papers modified by divalent ions-enhancing mechanical properties via chemical cross-linking., *ACS Nano.* 2 (2008) 572–578.
- [305] S. Eigler, C. Dotzer, A. Hirsch, M. Enzelberger, P. Müller, Formation and decomposition of CO₂ intercalated graphene oxide, *Chem. Mater.* 24 (2012) 1276–1282.
- [306] A. Mesnage, X. Lefe, P. Je, G. Deniau, S. Palacin, Spontaneous Grafting of Diazonium Salts : Chemical Mechanism on Metallic Surfaces, *Langmuir.* 28 (2012) 11767–11778.
- [307] J. Marwan, T. Addou, D. Bélanger, Functionalization of Glassy Carbon Electrodes with Metal-Based Species, *Chem. Mater.* 17 (2005) 2395–2403.
- [308] A.L. Gui, G. Liu, M. Chockalingam, G. Le Saux, J.B. Harper, J.J. Gooding, A Comparative Study of Modifying Gold and Carbon Electrode with 4-Sulfophenyl Diazonium Salt, *Electroanalysis.* 22 (2010) 1283–1289.
- [309] A.Y. Romanchuk, A.S. Slesarev, S.N. Kalmykov, D. V Kosynkin, J.M. Tour, Graphene oxide for effective radionuclide removal., *Phys. Chem. Chem. Phys.* 15 (2013) 2321–2327.
- [310] H. Dai, Z. Xu, X. Yang, Water Permeation and Ion Rejection in Layer-by-Layer Stacked Graphene Oxide Nanochannels: A Molecular Dynamics Simulation, *J. Phys. Chem. C.* 120 (2016) 22585–22596.

- [311] V. Shubina, L. Gallet, S. Ababou-Girard, V. Gaudefroy, T. Chaussadent, F. Farças, et al., The influence of biosurfactant adsorption on the physicochemical behaviour of carbon steel surfaces using contact angle measurements and X-ray photoelectron spectroscopy, *Appl. Surf. Sci.* 351 (2015) 1174–1183.
- [312] A. Ganguly, S. Sharma, P. Papakonstantinou, J. Hamilton, Probing the thermal deoxygenation of graphene oxide using high-resolution *in situ* X-ray-based spectroscopies, *J. Phys. Chem. C.* 115 (2011) 17009–17019.
- [313] Y. Ishii, D. Yang, A. Velamakanni, S.J. An, M. Stoller, Structural Characterization of C-Labeled Graphite Oxide, *Science*. 321 (2008) 1815–1818.
- [314] T. Szabo, O. Berkesi, P. Forgo, K. Josepovits, Y. Sanakis, D. Petridis, et al., Evolution of surface functional groups in a series of progressively oxidized graphite oxides, *Chem. Mater.* 18 (2006) 2740–2749.
- [315] G. Gunasekaran, L.R. Chauhan, Eco friendly inhibitor for corrosion inhibition of mild steel in phosphoric acid medium, *Electrochim. Acta*. 49 (2004) 4387–4395.
- [316] Y. Xiong, Y. Xie, Z. Li, C. Wu, Growth of well-aligned γ -MnO₂ monocristalline nanowires through a coordination-polymer-precursor route, *Chem. - A Eur. J.* 9 (2003) 1645–1651.
- [317] A. Buchsteiner, A. Lerf, J. Pieper, Water dynamics in graphite oxide investigated with neutron scattering, *J. Phys. Chem. B.* 110 (2006) 22328–22338.

- [318] L.B. Casabianca, M.A. Shaibat, W.W. Cai, S. Park, R. Piner, R.S. Ruoff, et al., NMR-based structural modeling of graphite oxide using multidimensional ^{13}C solid-state NMR and ab initio chemical shift calculations, *J. Am. Chem. Soc.* 132 (2010) 5672–5676.
- [319] C. Zhao, H. Gao, C. Chen, H. Wu, Reduction of graphene oxide in Li-ion batteries, *J. Mater. Chem. A.* 3 (2015) 18360–18364.
- [320] A.M. Abdelkader, A.J. Cooper, R.A.W. Dryfe, I.A. Kinloch, How to get between the sheets: a review of recent works on the electrochemical exfoliation of graphene materials from bulk graphite, *Nanoscale.* 7 (2015) 6944–6956.
- [321] F. Karlický, R. Zbožná, Band gaps and structural properties of graphene halides and their derivates : A hybrid functional study with localized orbital basis sets, *J. Chem. Phys.* 137 (2012) 1–7.
- [322] J.H. Lopes, S. Ye, J.T. Gostick, J.E. Barralet, G. Merle, Electrocatalytic Oxygen Reduction Performance of Silver Nanoparticle Decorated Electrochemically Exfoliated Graphene, *Langmuir.* 31 (2015) 9718–9727.
- [323] V.A. Online, K.T. Nguyen, Y. Zhao, Nanoscale biological and electronic applications, *Nanoscale.* 6 (2014) 6245–6266.
- [324] A. Fabbro, D. Scaini, V. Leon, E. Vázquez, G. Cellot, G. Privitera, et al., Graphene-Based Interfaces do not Alter Target Nerve Cells, *ACS Nano.* 10 (2015) 615–623.
- [325] W. Hu, C. Peng, W. Luo, M. Lv, X. Li, D. Li, et al., Graphene-based antibacterial paper., *ACS Nano.* 4 (2010) 4317–4323.

- [326] D. Chen, C. Li, H. Liu, F. Ye, J. Yang, Core-shell Au@Pd nanoparticles with enhanced catalytic activity for oxygen reduction reaction via core-shell Au@Ag/Pd constructions., *Sci. Rep.* 5 (2015) 11949.
- [327] C. Nethravathi, E.A. Anumol, M. Rajamathi, N. Ravishankar, Highly dispersed ultrafine Pt and PtRu nanoparticles on graphene: formation mechanism and electrocatalytic activity, *Nanoscale*. 3 (2011) 569–571.
- [328] A.M. Alkilany, S.E. Lohse, C.J. Murphy, The gold standard: Gold nanoparticle libraries to understand the nano-bio interface, *Acc. Chem. Res.* 46 (2013) 650–661.
- [329] P.W. Sutter, J.-I. Flege, E.A. Sutter, Epitaxial graphene on ruthenium., *Nat. Mater.* 7 (2008) 406–411.
- [330] H. Wang, S. Lu, Y. Chen, L. Han, J. Zhou, X. Wu, et al., Graphene/Co 9 S 8 nanocomposite paper as a binder-free and free-standing anode for lithium-ion batteries, *J. Mater. Chem. A*. 3 (2015) 23677–23683.
- [331] A. Qaseem, F. Chen, X. Wu, R.L. Johnston, Pt-free silver nanoalloy electrocatalysts for oxygen reduction reaction in alkaline media, *Catal. Sci. Technol.* 6 (2016) 3317–3340.
- [332] T. Wu, J. Ma, X. Wang, Y. Liu, H. Xu, J. Gao, et al., Graphene oxide supported Au-Ag alloy nanoparticles with different shapes and their high catalytic activities., *Nanotechnology*. 24 (2013) 125301–125311.

- [333] T. Fujigaya, C. Kim, Y. Hamasaki, N. Nakashima, Growth and Deposition of Au Nanoclusters on Polymer-wrapped Graphene and Their Oxygen Reduction Activity, *Sci. Rep.* 6 (2016) 21314–21324.
- [334] G. Goncalves, P.A.A.P. Marques, C.M. Granadeiro, H.I.S. Nogueira, M.K. Singh, J. Grácio, Surface modification of graphene nanosheets with gold nanoparticles: The role of oxygen moieties at graphene surface on gold nucleation and growth, *Chem. Mater.* 21 (2009) 4796–4802.
- [335] M. Ayán-Varela, J.I. Paredes, L. Guardia, S. Villar-Rodil, J.M. Munuera, M. Díaz-González, et al., Achieving extremely concentrated aqueous dispersions of graphene flakes and catalytically efficient graphene-metal nanoparticle hybrids with flavin mononucleotide as a high-performance stabilizer, *ACS Appl. Mater. Interfaces.* 7 (2015) 10293–10307.
- [336] K. Liu, L. Liu, Y. Luo, D. Jia, One-step synthesis of metal nanoparticle decorated graphene by liquid phase exfoliation, *J. Mater. Chem.* 22 (2012) 20342.
- [337] M.-Q. Yang, X. Pan, N. Zhang, Y.-J. Xu, A facile one-step way to anchor noble metal (Au, Ag, Pd) nanoparticles on a reduced graphene oxide mat with catalytic activity for selective reduction of nitroaromatic compounds, *CrystEngComm.* 15 (2013) 6819–6828.
- [338] Y. Zhang, G. Gao, Q. Qian, D. Cui, Chloroplasts-mediated biosynthesis of nanoscale Au-Ag alloy for 2-butanone assay based on electrochemical sensor., *Nanoscale Res. Lett.* 7 (2012) 475–482. doi:10.1186/1556-276X-7-475.

- [339] Y.-K. Yang, C.-E. He, W.-J. He, L.-J. Yu, R.-G. Peng, X.-L. Xie, et al., Reduction of silver nanoparticles onto graphene oxide nanosheets with N,N-dimethylformamide and SERS activities of GO/Ag composites, *J. Nanopart. Res.* 13 (2011) 5571–5581.
- [340] S. Xu, L. Ye, Z. Li, Y. Wang, F. Lei, S. Lin, Facile Synthesis of Bimetallic Pt-Ag/Graphene Composite and Its Electro-Photo-Synergistic Catalytic Properties for Methanol Oxidation, *Catalysts.* 6 (2016) 144–156.
- [341] R. Gao, N. Hu, Z. Yang, Q. Zhu, J. Chai, Y. Su, et al., Paper-like graphene-Ag composite films with enhanced mechanical and electrical properties., *Nanoscale Res. Lett.* 8 (2013) 32–40.
- [342] X. Wang, G. Sun, P. Routh, D.-H. Kim, W. Huang, P. Chen, Heteroatom-doped graphene materials: syntheses, properties and applications., *Chem. Soc. Rev.* 43 (2014) 7067–7098.
- [343] Y. Hu, L. Lu, J. Liu, W. Chen, Direct growth of size-controlled gold nanoparticles on reduced graphene oxide film from bulk gold by tuning electric field: effective methodology and substrate for surface enhanced Raman scattering study, *J. Mater. Chem.* 22 (2012) 11994–12000.
- [344] Y. Jing, E. Lin, X. Su, Y. Liu, H. Li, X. Yuan, et al., Electrodeposition of Au nanoparticles on poly(diallyldimethylammonium chloride) functionalized reduced graphene oxide sheets for voltammetric determination of nicotine in tobacco products and anti-smoking pharmaceuticals, *RSC Adv.* 6 (2016) 26247–26253.

- [345] Q. Qin, X. Bai, Z. Hua, Electrochemical Synthesis of Well-Dispersed CdTe Nanoparticles on Reduced Graphene Oxide and Its Photoelectrochemical Sensing of Catechol, *J. Electrochem. Soc.* 164 (2017) H241–H249.
- [346] M. Sivaprasad, N. Y. Sreedhar, M. R. Jayapal, L. Yang, H. Ni, Two Step Electrochemical Deposition Of Palladium And Polyaniline On Graphene Dispersed Glassy Carbon electrode For Electrochemical Analysis Of Pesticide, *Adv. Mater. Lett.* 8 (2016) 30–36.
- [347] A. Moradi Golsheikh, N.M. Huang, H.N. Lim, R. Zakaria, C.Y. Yin, One-step electrodeposition synthesis of silver-nanoparticle-decorated graphene on indium-tin-oxide for enzymeless hydrogen peroxide detection, *Carbon.* 62 (2013) 405–412.
- [348] A. Monshi, M.R. Foroughi, M.R. Monshi, Modified Scherrer Equation to Estimate More Accurately Nano-Crystallite Size Using XRD, *World J. Nano Sci. Eng.* 2 (2012) 154–160.
- [349] K. Rajendra Prasad, N. Munichandraiah, Electrooxidation of methanol on polyaniline without dispersed catalyst particles, *J. Power Sources.* 103 (2002) 300–304.
- [350] M. Eredia, S. Bertolazzi, T. Leydecker, M. El Garah, I. Janica, G. Melinte, et al., Morphology and Electronic Properties of Electrochemically Exfoliated Graphene, *J. Phys. Chem. Lett.* 8 (2017) 3347–3355.

- [351] J.M. Munuera, J.I. Paredes, M. Enterría, A. Pagán, S. Villar-Rodil, M.F.R. Pereira, et al., Electrochemical Exfoliation of Graphite in Aqueous Sodium Halide Electrolytes toward Low Oxygen Content Graphene for Energy and Environmental Applications, *ACS Appl. Mater. Interfaces.* 9 (2017) 24085–24099.
- [352] Y.-K. Kim, G. Ok, S.-W. Choi, H. Jang, D.-H. Min, The interfacing structural effect of Ag/graphene oxide nanohybrid films on surface enhanced Raman scattering, *Nanoscale.* 9 (2017) 5872–5878.
- [353] J. Song, L. Xu, R. Xing, Q. Li, C. Zhou, D. Liu, et al., Synthesis of Au/Graphene Oxide Composites for Selective and Sensitive Electrochemical Detection of Ascorbic Acid, *Sci. Rep.* 4 (2015) 7515–7522.
- [354] L. Wang, Z. Tang, W. Yan, H. Yang, Q. Wang, S. Chen, Porous Carbon-Supported Gold Nanoparticles for Oxygen Reduction Reaction: Effects of Nanoparticle Size, *ACS Appl. Mater. Interfaces.* 8 (2016) 20635–20641.
- [355] W. Yuan, Y. Gu, L. Li, Applied Surface Science Green synthesis of graphene / Ag nanocomposites, *Appl. Surf. Sci.* 261 (2012) 753–758.
- [356] J.W. Han, J. Kim, Reduced graphene oxide – silver nanoparticle nanocomposite : a potential anticancer nanotherapy, *Int. J. Nanomedicine.* 10 (2015) 6257–6276.
- [357] M. Grouchko, P. Roitman, X. Zhu, I. Popov, A. Kamyshny, H. Su, et al., Merging of metal nanoparticles driven by selective wettability of silver nanostructures., *Nat. Commun.* 5 (2014) 2994–3000.

- [358] N.T.K. Thanh, N. Maclean, S. Mahiddine, Mechanisms of nucleation and growth of nanoparticles in solution, *Chem. Rev.* 114 (2014) 7610–7630.
- [359] J. Wang, S. Chen, K. Cui, D. Li, D. Chen, Approach and Coalescence of Gold Nanoparticles Driven by Surface Thermodynamic Fluctuations and Atomic Interaction Forces, *ACS Nano.* 10 (2016) 2893–2902.
- [360] N.G. Shang, P. Papakonstantinou, S. Sharma, G. Lubarsky, M. Li, D.W. Mcneill, et al., Controllable selective exfoliation of high-quality graphene nanosheets and nanodots by ionic liquid assisted grindingw, *Chem. Commun.* 48 (2012) 1877–1879.
- [361] H. Chen, M.B. Müller, K.J. Gilmore, G.G. Wallace, D. Li, Mechanically strong, electrically conductive, and biocompatible graphene paper, *Adv. Mater.* 20 (2008) 3557–3561.
- [362] H.Y. Nan, Z.H. Ni, J. Wang, Z. Zafar, Z.X. Shi, Y.Y. Wang, The thermal stability of graphene in air investigated by Raman spectroscopy, *J. Raman Spectrosc.* 44 (2013) 1018–1021.
- [363] A.A. El Mel, M. Chettab, E. Gautron, A. Chauvin, B. Humbert, J.Y. Mevellec, et al., Galvanic Replacement Reaction: A Route to Highly Ordered Bimetallic Nanotubes, *J. Phys. Chem. C.* 120 (2016) 17652–17659.
- [364] T. Ghosh, D. Kabiraj, B. Satpati, Substrate decomposition in galvanic displacement reaction: Contrast between gold and silver nanoparticle formation, in: *AIP Conf. Proc.*, 2015: p. 80040.

- [365] A.M. Abdelkader, H. V Patten, Z. Li, Y. Chen, I.A. Kinloch, Electrochemical exfoliation of graphite in quaternary ammonium-based deep eutectic solvents: A route for the mass production of graphane, *Nanoscale*. 7 (2015) 11386–11392.
- [366] M.P. Kumar, S. Shanthini, C. Srivastava, Electrochemical Exfoliation of Graphite for Producing Graphene Using Saccharin, *RSC Adv.* 5 (2015) 53865–53869.
- [367] P. Yu, Z. Tian, S.E. Lowe, J. Song, Z. Ma, X. Wang, et al., Mechanically-assisted electrochemical production of graphene oxide, *Chem. Mater.* 28 (2016) 8429–8438.
- [368] S. Sun, P. Wu, Competitive surface-enhanced Raman scattering effects in noble metal nanoparticle-decorated graphene sheets., *Phys. Chem. Chem. Phys.* 13 (2011) 21116–21120. doi:10.1039/c1cp22727k.
- [369] D. Zhao, Y. Yu, C. Xu, A sensitive electrochemical immunosensor for the detection of human chorionic gonadotropin based on a hierarchical nanoporous AuAg alloy, *RSC Adv.* 6 (2016) 87–93.
- [370] M. Tsuji, M. Matsunaga, H. Kumagai, M. Ogino, S. Hikino, Y. Yoshida, et al., Synthesis of Au@Ag@Cu trimetallic nanocrystals using three-step reduction, *CrystEngComm.* 15 (2013) 1345–1351.
- [371] F. Pogacean, A.R. Biris, M. Coros, M.D. Lazar, F. Watanabe, G.K. Kannarpady, et al., Direct electrochemical oxidation of S-captopril using gold electrodes modified with graphene-AuAg nanocomposites, *Int. J. Nanomedicine*. 9 (2014) 1111–1125.

- [372] J. Yang, E.H. Sargent, S.O. Kelley, J.Y. Ying, A general phase-transfer protocol for metal ions and its application in nanocrystal synthesis., *Nat. Mater.* 8 (2009) 683–689.
- [373] S. Yang, W. Yue, J. Zhu, Y. Ren, X. Yang, Graphene-based mesoporous SnO₂ with enhanced electrochemical performance for lithium-ion batteries, *Adv. Funct. Mater.* 23 (2013) 3570–3576.
- [374] H. Borchert, E. V. Shevchenko, A. Robert, I. Mekis, A. Kornowski, G. Grübel, et al., Determination of nanocrystal sizes: A comparison of TEM, SAXS, and XRD studies of highly monodisperse CoPt₃ particles, *Langmuir*. 21 (2005) 1931–1936.
- [375] R. Gopalakrishnan, B. Loganathan, K. Raghu, Green synthesis of Au–Ag bimetallic nanocomposites using *Silybum marianum* seed extract and their application as a catalyst, *RSC Adv.* 5 (2015) 31691–31699.
- [376] Y. Song, K. Liu, S. Chen, AgAu bimetallic janus nanoparticles and their electrocatalytic activity for oxygen reduction in alkaline media, *Langmuir*. 28 (2012) 17143–17152.
- [377] F. Li, H. Yang, C. Shan, Q. Zhang, D. Han, A. Ivaska, et al., The synthesis of perylene-coated graphene sheets decorated with Au nanoparticles and its electrocatalysis toward oxygen reduction, *J. Mater. Chem.* 19 (2009) 4022–4025.
- [378] A. Wang, J. Liu, S.D. Lin, T. Lin, C. Mou, A novel efficient Au – Ag alloy catalyst system : preparation , activity , and characterization, *J. Catal.* 233 (2005) 186–197.

- [379] D. Barreca, Silica-supported Ag-Au Bimetallic Nanosystems by XPS, *Surf. Sci. Spectra.* 13 (2007) 1–8.
- [380] Z. Luo, X. Yuan, Y. Yu, Q. Zhang, D.T. Leong, J.Y. Lee, et al., From aggregation-induced emission of Au(I)-thiolate complexes to ultrabright Au(0)@Au(I)-thiolate core-shell nanoclusters, *J. Am. Chem. Soc.* 134 (2012) 16662–16670.
- [381] X. Ge, A. Sumboja, D. Wuu, T. An, B. Li, F.W.T. Goh, et al., Oxygen Reduction in Alkaline Media: From Mechanisms to Recent Advances of Catalysts, *ACS Catal.* 5 (2015) 4643–4667.
- [382] T.F. Jaramillo, S.-H.H. Baeck, B.R. Cuenya, E.W. McFarland, Catalytic activity of supported Au nanoparticles deposited from block copolymer micelles., *J. Am. Chem. Soc.* 125 (2003) 7148–7149.
- [383] R.J. Chimentão, I. Cota, A. Dafinov, F. Medina, J.L.G. de la Fuente, J.L.G. Fierro, et al., Synthesis of silver-gold alloy nanoparticles by a phase-transfer system, *J. Mater. Res.* 21 (2006) 105–111.
- [384] L. Ge, C. Han, J. Liu, Y. Li, Enhanced visible light photocatalytic activity of novel polymeric g-C₃N₄ loaded with Ag nanoparticles, *Appl. Catal. A Gen.* 409–410 (2011) 215–222.
- [385] L.H. Tjeng, M.B.J. Meinders, J. Van Elp, J. Ghijssen, G.A. Sawatzky, R.L. Johnson, Electronic structure of Ag₂O, *Phys. Rev. B.* 41 (1990) 3190–3199.

- [386] P. Hu, Y. Song, L. Chen, S. Chen, Electrocatalytic activity of alkyne-functionalized AgAu alloy nanoparticles for oxygen reduction in alkaline media, *Nanoscale*. 7 (2015) 9627–9636.
- [387] L. Pauling, *The Nature of the Chemical Bond*, in: (Cornell University Press) (Ed.), *J. Chem. Phys.*, Third, New York, 1960: p. 93.
- [388] J. Li, C. Liu, Y. Liu, Au/graphene hydrogel: synthesis, characterization and its use for catalytic reduction of 4-nitrophenol, *J. Mater. Chem.* 22 (2012) 8426–8430.
- [389] G. Giovannetti, P.A. Khomyakov, G. Brocks, V.M. Karpan, J. Van Den Brink, P.J. Kelly, Doping graphene with metal contacts, *Phys. Rev. Lett.* 101 (2008) 026803–026807.
- [390] X. Li, B.K. Tay, J. Li, D. Tan, C.W. Tan, K. Liang, Mildly reduced graphene oxide-Ag nanoparticle hybrid films for surface-enhanced Raman scattering., *Nanoscale Res. Lett.* 7 (2012) 205–213.
- [391] A.C. Ferrari, Raman spectroscopy of graphene and graphite: Disorder, electron-phonon coupling, doping and nonadiabatic effects, *Solid State Commun.* 143 (2007) 47–57.
- [392] L.M. Malard, M.A. Pimenta, G. Dresselhaus, M.S. Dresselhaus, Raman spectroscopy in graphene, *Phys. Rep.* 473 (2009) 51–87.
- [393] B. Cai, D. Wen, W. Liu, A.K. Herrmann, A. Benad, A. Eychmüller, Function-Led Design of Aerogels: Self-Assembly of Alloyed PdNi Hollow Nanospheres for Efficient Electrocatalysis, *Angew. Chemie - Int. Ed.* 54 (2015) 13101–13105.

- [394] C. Hu, X. Zhai, Y. Zhao, K. Bian, J. Zhang, L. Qu, et al., Small-sized PdCu nanocapsules on 3D graphene for high-performance ethanol oxidation, *Nanoscale*. 6 (2014) 2768–2775.
- [395] G. Wu, K.L. More, C.M. Johnston, P. Zelenay, High-Performance Electrocatalysts for Oxygen Reduction Derived from Polyaniline, Iron, and Cobalt, *Science* (80-.). 332 (2011) 443–447.
- [396] Y. Dong, Y. Deng, J. Zeng, H. Song, S. Liao, A high-performance composite ORR catalyst based on the synergy between binary transition metal nitride and nitrogen-doped reduced graphene oxide, *J. Mater. Chem. A*. 5 (2017) 5829–5837.